



UNIVERSITA' DEGLI STUDI DI NAPOLI FEDERICO II

FACOLTÀ DI SCIENZE MM. FF .NN.

**DOTTORATO DI RICERCA IN SCIENZE DELLA TERRA
XXIII CICLO**

**HYDROLOGICAL AND STABILITY MODELLING OF INITIAL LANDSLIDES
TRIGGERING DEBRIS FLOWS IN ASH-FALL DEPOSITS COVERING
HILLSLOPES SURROUNDING SOMMA-VESUVIUS (SOUTHERN ITALY).**

Candidato:

Dott.ssa Elisabetta Napolitano

Tutor:

Prof. Pantaleone De Vita

Co-Tutor:

Jonathan Godt

Coordinatore del Dottorato:

Prof. Maria Boni

Anno Accademico 2010/2011

Abstract

Rainfall-induced debris flows involving ash-fall pyroclastic deposits covering steep mountain slopes that surround the Somma-Vesuvius volcano, are natural events representing the main cause of risk for urban settlements located at footslopes. The presented research was based on the review of the wide scientific literature and was aimed to the improvement of some crucial aspects regarding the initiation of debris flows by means of field and laboratory experimental methods and modelling applied in representative sample areas of the Sarno Mountain Range, where deadly flow-like landslides initiated on May 5th - 6th 1998.

Detailed stratigraphic and topographic surveys carried out in three representative initiation areas led to recognise that, depending on the slope angle, ash-fall pyroclastic deposits are discontinuously distributed along slopes, showing a total thickness that varies from a maximum value recognisable in the slope angle range lower than 30° up to be negligible for slope angle values greater than 50°, thus being strongly related to bedrock morphology itself. This distribution influences stratigraphical setting of ash-fall pyroclastic mantle leading to a downward thinning up to pinch out of pyroclastic horizons. Three fundamental quantitative engineering geological models were identified, in which the most part of the initial landslides occurred in May 1998 can be classified: i) knickpoints, characterised by a downward progressive thinning of pyroclastic mantle; ii) rocky scarps, identified as causing an abrupt interruption of pyroclastic mantle; iii) road cuts in pyroclastic mantle, whereas they occur in a critical slope angle range.

Coupled geotechnical and saturated/unsaturated hydraulic characterisations of pyroclastic soils, led to the hydro-mechanical modelling of slope stability in the initiation areas. Results demonstrated that initial instabilities of pyroclastic mantle can occur without a hydraulic contribution from the carbonate bedrock, therefore critical increase of pore pressure derives from the infiltration and throughflow processes. Finally, the hydro-mechanical modelling of slope stability permitted the deterministic definition of intensity/duration hydrological thresholds.

Extended abstract (in Italian)

Le instabilità che coinvolgono i depositi di origine piroclastica che ricoprono i versanti perivesuviani circostanti la Piana Campana sono fenomeni franosi superficiali unici in Italia e rari in tutto il resto del mondo. Essi sono molto rilevanti in Campania poiché costituiscono la principale fonte di rischio per i numerosi insediamenti urbani localizzati nelle fasce pedemontane. Inoltre, per la loro catastrofica natura e complessità, le instabilità delle coltri piroclastiche sono di grande interesse per la comunità scientifica nazionale che si occupa di suscettibilità e di rischio a franare.

Questa tesi di dottorato è parte dell'ampio ed articolato scenario di attività di ricerca scientifica che è stata intrapresa, con rinnovata energia, dopo i tragici eventi del 5 e 6 maggio del 1998 che colpirono i centri abitati circostanti i Monti di Sarno, con l'obiettivo di migliorare la comprensione dei meccanismi di innesco e di propagazione delle frane e con la finalità di valutare la suscettibilità ad esse connessa.

Il punto di partenza di questo lavoro di tesi è stata la consapevolezza che allo stato attuale non esiste un'univoca interpretazione e comprensione dettagliata dei meccanismi di innesco di questo particolare tipo di frane, il cui approfondimento è di fondamentale importanza per l'ottimizzazione dei criteri per la redazione di carte della suscettibilità e per la programmazione di eventuali opere di difesa attiva sui versanti. La rilevanza di questi problemi ha portato a concentrare la ricerca su un approccio innovativo volto a comprendere i meccanismi di innesco i cui risultati potrebbero consentire la progettazione di uno specifico modello distribuito per la valutazione della suscettibilità a franare.

Partendo da un'attenta analisi dei dati e dei modelli noti in letteratura, nonché dalle osservazioni di campo, è stato possibile fare riferimento ad un modello evolutivo delle frane nel quale sono riconoscibili fino a tre successivi differenti stadi evolutivi: 1) *debris slide (soil slip)*; 2) *debris avalanche* (Hungar *et alii*, 2001); 3) *debris flow* (Hungar *et alii*, 2001). Da ciò consegue che le frane, nello stadio intermedio o finale, in cui assumono la reologia di un fluido (*debris avalanche* e *debris flow*), sono innescate da una piccola frana iniziale (*debris slide – soil slip*), pertanto esse sono definibili “*landslide triggered debris flow*” (Jakob & Hungar, 2005).

In considerazione delle dimensioni delle frane iniziali, spesso di ordine decametrico, l'obiettivo della ricerca si è concentrato sulla realizzazione di indagini dettagliate nelle zone di innesco consistite in indagini stratigrafiche e nella caratterizzazione idraulica e meccanica degli orizzonti piroclastici, mediante prove di laboratorio. I modelli geologico - tecnici ricostruiti possono essere

considerati come un primo tentativo di definire quantitativamente le frane iniziali a scala di dettaglio. Essi estendono ed approfondiscono quelli concettuali già noti in letteratura riguardanti l'influenza delle condizioni morfologiche del versante sulla suscettibilità a franare delle coltri piroclastiche. Tra i fattori naturali erano già stati identificati da diversi ricercatori il brusco aumento dell'angolo di pendio, connesso a discontinuità naturali del substrato roccioso, e la conseguente interruzione della continuità della coltre piroclastica, come l'interruzione artificiale della continuità della coltre ad opera di tagli stradali. In generale, considerando il ruolo dei fattori morfologici naturali, lo spessore e la geometria degli orizzonti piroclastici è fortemente legata alla variazione dell'angolo di pendio, che, nel caso di progressivo aumento verso valle, comporta una riduzione dello spessore totale della copertura e la terminazione verso valle (*pinch-out*) degli orizzonti piroclastici, fino a valori di angolo di pendio approssimativamente pari a circa 50°. Oltre questo valore, lo spessore della copertura diventa trascurabile.

Dopo l'osservazione e l'analisi critica della maggior parte delle frane iniziali che si sono innescate nel maggio 1998 nei Monti di Sarno, sono stati considerati tre casi rappresentativi: in corrispondenza di *knickpoint*; al disopra di cornici morfologiche; a monte di tagli artificiali nelle coperture piroclastiche.

Sulla base della ricostruzione dei modelli geologico-tecnici delle tre frane iniziali ritenute rappresentative, sono state effettuate la modellazione numerica agli elementi finiti dei processi idrologici che hanno luogo all'interno della copertura piroclastica e la successiva analisi di stabilità. La modellazione idrologica del pendio è stata effettuata mediante il modello alle differenze finite VS2DTI, applicato sui modelli fisici di dettaglio delle tre frane rappresentative. Essa ha permesso di comprendere i processi idrologici che si instaurano all'interno delle coperture piroclastiche e le caratteristiche delle piogge che determinano l'instabilità.

I risultati di questa modellazione indicano che il flusso insaturo che attraversa gli strati costituenti la copertura tende a concentrarsi, con un incremento delle pressioni di poro, fino al raggiungimento della saturazione, laddove la sezione idraulica si restringe per riduzione di spessore della coltre piroclastica e gli orizzonti di lapilli pomicei si chiudono. Questo fenomeno si osserva per tutti i casi di studio presi in considerazione. In particolare, dalle simulazioni idrologiche, al momento della rottura, appare chiaro che il flusso d'acqua con prevalente componente orizzontale, e prossimo alle condizioni di saturazione, si concentra in un ristretto intervallo (5 ÷ 10 m), in corrispondenza del restringimento della sezione idraulica, ed in particolare laddove gli orizzonti di lapilli pomicei (orizzonti C) hanno una soluzione di continuità verso valle. Anche nel caso del taglio

stradale, la concentrazione del flusso avviene in un intervallo di distanza ridotto, a monte della scarpata. Queste osservazioni sono congruenti con le piccole dimensioni delle frane iniziali.

Questi risultati possono essere considerati di grande rilevanza per la comprensione delle questioni riguardanti la suscettibilità delle frane iniziali perché rivelano il ruolo cruciale svolto dalle variazioni a piccola scala, sia dello spessore della coltre di origine piroclastica (negli ordini di grandezza di $10^0 \div 10^{-1}$ m) che della morfologia dei versanti (negli ordini di grandezza di $10^1 \div 10^0$ m) i quali non possono essere semplificati come costanti e valutati dalle normali carte topografiche (scala 1:5.000). Di conseguenza, i risultati acquisiti dovrebbero essere considerati ed implementati di uno specifico modello per la valutazione della suscettibilità da frana iniziale, su base distribuita.

Inoltre, i risultati ottenuti, se paragonati ai precedenti modelli noti in letteratura, portano ad un avanzamento nella comprensione dei meccanismi di innesco, evidenziando l'esistenza di condizioni idrogeologiche che consentono la formazione di un flusso insaturo/saturo all'interno delle coperture piroclastiche, sufficiente per l'innesco di frane nei pressi di discontinuità morfologiche naturali e artificiali. L'innesco delle frane iniziali è quindi possibile anche senza l'apporto di eventuali flussi derivanti dal substrato carbonatico.

La chiara relazione di causa-effetto tra l'infiltrazione derivante da piogge e l'accadimento delle frane iniziali ha fornito un ulteriore obiettivo dell'attività di ricerca, identificato nella ricostruzione, su base deterministica, di soglie idrologiche di intensità/durata. Le soglie intensità/durata ricavate con la suddetta metodologia, possono essere considerate come un tentativo di superare o testare le incertezze del classico approccio empirico basato su dati pluviometrici spesso registrati in settori distanti dalle zone di innesco delle frane e/o alle basse altitudini. Questi fattori possono, infatti, condizionare l'affidabilità di tali soglie, soprattutto nelle zone montane, dove la variabilità spaziale è elevata, soprattutto per eventi di pioggia di breve durata / elevata intensità.

A tale scopo è stata effettuata la modellizzazione idrologica di versante con tassi di infiltrazione costante (5 mm/h; 10 mm/h, 20 mm/h e 40 mm/h), considerando come condizione iniziale la distribuzione di pressione di poro all'interno della copertura piroclastica, normalmente esistente durante la stagione invernale (5 kPa \div 15 kPa). Dalla contemporanea analisi di stabilità del pendio è stato possibile identificare le durate critiche delle piogge che ne determinano la rottura. Le soglie di intensità/durata così ottenute sono ovviamente dipendenti dai parametri meccanici utilizzati (c' e ϕ'). Al fine di tener conto dell'effetto della variabilità dei suddetti parametri meccanici sui valori di soglia, è stata effettuata un'analisi di sensitività, basata sull'analisi statistica dei valori ricavati da prove di laboratorio.

Alcune incertezze sulla definizione delle soglie idrologiche deterministiche, esistono e sono legate soprattutto alla valutazione dei parametri di resistenza al taglio. Sulla base di questo assunto, ulteriori ricerche dovrebbero concentrarsi sulla realizzazione, in campo, delle misure della resistenza a taglio al fine di determinare la stessa su volumi di terreno non disturbati, rappresentativi anche di macrostrutture, altrimenti non valutabili mediante prove di laboratorio standard.

Index

| | |
|---|-----|
| Abstract..... | 2 |
| Extended abstract (in Italian) | 3 |
| Index | 7 |
| Introduction..... | 9 |
| Chapter 1 | 11 |
| Geological setting of the study area..... | 11 |
| 1.1 Geological setting of southern Apennines..... | 11 |
| 1.2 Evolution of the Campanian Plain and the Somma-Vesuvius volcano | 14 |
| 1.3 Geology of the Sarno mountain ranges | 15 |
| 1.4 Main plinian eruptions of the Somma-Vesuvius | 17 |
| 1.4.1 The Sarno eruption (17 k-year) | 17 |
| 1.4.2 The Ottaviano eruption (8 k-year) | 17 |
| 1.4.3 The Avellino eruption (3.7 k-year) | 19 |
| 1.4.4 The 79 AD eruption | 22 |
| 1.4.5 The 472 AD eruption | 24 |
| 1.4.6 The 1631 eruption..... | 25 |
| 1.5 Distribution of ash-fall pyroclastic deposits along mountain slopes..... | 27 |
| 1.6 The climate in Campania region..... | 31 |
| Chapter 2..... | 33 |
| Instability conditions of Ash-Fall pyroclastic soils mantling peri – vesuvian hillslopes: a review of the scientific literature | 33 |
| 2.1. Landslides phenomena and their classification | 33 |
| 2.1.1 Classification of landslide phenomena..... | 35 |
| 2.1.2. Landslides types on peri-vesuvian hillslopes | 51 |
| 2.3 Landslide mobility | 64 |
| 2.4 The cause-effect relationship between heavy rainfalls and landslide initiation | 66 |
| 2.4.1 Hillslope conceptual hydrogeological models..... | 72 |
| 2.5 Special hydraulic and mechanical properties of andosols..... | 76 |
| 2.6 Geotechnical models..... | 77 |
| 2.6.1 Pore pressure regime in pyroclastic mantle and stability analysis | 81 |
| 2.6.2 Geotechnical modelling of landslide initiation..... | 88 |
| Chapter 3 | 90 |
| Objectives and methods of the research..... | 90 |
| 3.1 Objectives and phases of the research..... | 90 |
| 3.2 Identification of representative sample sites | 95 |
| 3.3 Engineering geological characterization of pyroclastic cover mantling pizzo d'alvano massif: field methodologies | 98 |
| 3.3.1 Topographical surveys | 98 |
| 3.3.2 Stratigraphical characterization | 100 |

| | |
|---|-----|
| 3.3.3 Undisturbed sampling for characterization of physical and mechanical properties of pyroclastic horizons | 104 |
| 3.3.4 Field tests for hydraulic conductivity measurement | 107 |
| 3.4 Laboratory methodologies for the characterization of pyroclastic soils | 111 |
| 3.4.1 Physical characterization of pyroclastic soils | 111 |
| 3.4.2 USCS classification for investigated soils..... | 114 |
| 3.4.3 Characterization of mechanical properties | 116 |
| 3.5 Characterization of unsaturated pyroclastic soils hydraulic properties | 119 |
| 3.5.1 Soil water characteristic curve models..... | 122 |
| 3.5.2 Instrumentations for testing..... | 124 |
| 3.6 Characterization of the soils hydraulic behaviour in the saturated domain..... | 128 |
| 3.6.1 Constant head permeameter | 130 |
| 3.7 VS2DTI: finite difference hydrological model for variably saturated porous media | 133 |
| 3.7.1 Numerical solutions | 136 |
| 3.8 Finite slope stability analysis..... | 137 |
| Chapter 4..... | 141 |
| Engineering–geological characterization of pyroclastic cover: results..... | 141 |
| 4.1 Results from stratigraphical analysis | 141 |
| 4.2 Laboratory characterization of the physical index and mechanical properties of pyroclastic mantle.. | 145 |
| 4.3 Hydraulic characterization of pyroclastic soil horizons | 152 |
| 4.3.1 Results from field and laboratory tests for saturated hydraulic conductivity measurement..... | 152 |
| 4.3.2 Unsaturated hydraulic characterization from “Tempe cells” | 158 |
| 4.4. Engineering geological models of initial landslides | 162 |
| 4.5 Distribution of ash-fall pyroclastic soils on slopes in the study areas | 168 |
| Chapter 5..... | 172 |
| Hydrological modeling and slope stability analysis: results | 172 |
| 5.1 Hydrological modelling of the initial landslides through VS2DTI..... | 172 |
| 5.1.2 Results of hydrological modeling | 177 |
| 5.2 Stability modeling of initial landslides | 181 |
| 5.3. Setting of the hydro-mechanical model | 181 |
| 5.4 Deterministic hydrological thresholds | 189 |
| Chapter 6..... | 192 |
| Conclusions | 192 |
| 6.1 Relevance of the topics | 192 |
| 6.2 Concluding remarks of main results and open issues | 193 |
| Acknowledgments | 196 |
| References..... | 197 |

Introduction

The problem of the rapid to extremely rapid debris flows, i.e. the slope movements in which the unstable mass of unsorted and non-plastic soils, constituted of residual, colluvial as well as volcanic deposits, moves as a viscous fluid (Hungri et al., 2001), recurred in recent years with extreme spatial variability in the Campania region, causing high damage and loss of lives in urban settlements located at the footslope of the mountain ranges that surround the Somma-Vesuvius.

In this part of the peri-Vesuvian area, debris flows involve ash-fall pyroclastic soils and, due to the high altitude and slope steepness, they can move downhill with high mobility covering on most occasions long distances and then stopping hundreds of meters or even some kilometers away from the source. The May 5th - 6th 1998 landslides that affected the Sarno Mountain Range causing the invasion of the flows into urban settlements and the loss of 162 lives, are the most representative events within this framework. This type of landslides may propagate with high speed downstream and increase their volume with complex mechanisms. It is clear how, due to their characteristics, these landslides result in a high destructive power, impacting on buildings and infrastructures and harming human lives. On the basis of field observations, these phenomena can be considered as “landslide triggered debris flows” (*sensu* Hungri & Jacob, 2006), namely flow-like landslides caused by an initial landslide that often involves small volume of pyroclastic soils.

The research carried out in this thesis can be considered as included into the wide and complex framework of research activities carried out by many national research teams that regarded different aspects of the pyroclastic debris flow hazard and susceptibility analysis. This research has had a great boost after the events of May 1998. In this context the specific aim of the doctorate research can be summarized in the following key points.

- A. Improvement of the understanding of the triggering mechanisms acquiring new geological and geotechnical data by means of field surveys and laboratory testings. The models known in literature, allowed to focus open issues and to plan a specific and innovative approach to the study of the initial failure mechanisms. This allowed to advance the existing triggering models, whose comprehension is fundamental if considering that the whole flow-like landslide, often with a magnitude of thousands and hundreds of thousands of cubic meters, can be triggered by a very small initial landslide. In such a view, surveys and measurements were carried out at a detailed scale within the initial landslide areas with the purpose to reconstruct detailed engineering-geological models of the initial landslides.

- B. Saturated and unsaturated hydraulic as well as mechanical characterizations of pyroclastic soils involved in the initial landslides. In order to achieve this hydro-mechanical characterization a significant number of field and laboratory tests were carried out.
- C. Hydrological and stability modeling of initial landslides by means of finite differences numerical models simulating the effects of extreme rainfall events.
- D. Definition of hydrological thresholds for triggering of initial landslides through a deterministic approach (Godt and McKenna, 2008) based on the reconstruction of detailed engineering geological models and hydrological and stability modelling.

The significance of these problems led to focus the research on an innovative approach aimed at understanding the triggering mechanisms that would then permit the design of a specific model for the assessment of distributed landslide susceptibility.

Chapter 1

Geological setting of the study area

1.1 Geological setting of southern Apennines

The Southern Apennines orogenic belt is part of the central Mediterranean and consists of a stack of thrust resulting from the deformation of different Mesozoic-Cenozoic domains (Figure 1.1) which are the result of Cretaceous-Quaternary convergence between the African and European plates (Channell et al., 1979, Dewey et al., 1989).

In the central and western Mediterranean, the convergence between Africa and Europe is accompanied by the formation of deep extensional basins locally characterized by the formation of oceanic crust. Here, the tectonic evolution of the region was deeply influenced by Adria, a tectonic domain formed by Mesozoic carbonate of platform, basin deposits and Cenozoic sedimentary rocks deposited on continental crust with African affinity (Argand, 1924).

On a narrower scale, the strain field on the Adria margins shows the substantial variability in the style of deformation. This might be due in part to the interaction between crustal blocks detached from their base during the tectonic transport towards the European continental margin.

Although compression dominated in the Mesozoic and Cenozoic deformation, combined extensional and compressive events resulted in lengthening and shortening that affected the western margin of Adria.

The Apennine-Maghreb orogen form a curved area around the eastern and southern margins of the Tyrrhenian extensional basin. The deformation that affected Adria reflects the deformation pattern that began in the late Mesozoic and Tertiary. The size of Adria was heavily modified over time by compressive strain fields that developed along the eastern, northern and western edge of paleo-tectonic domain. The rocks from the Adriatic plate were detached from their lithospheric basement and transferred to the orogenic system. This mass transfer was also accompanied by crustal detachment, where the mantle and perhaps the lower crust were separated from their coverage and subducted under the orogen. In the southern Apennines, contraction affected the external areas and extension that affected the internal areas. This produced a complex spatial and temporal pattern of vertical and horizontal displacements of which only the most recent episodes are

be described below.

From the late Miocene to the Middle Pleistocene migration of the compression front occurred which was not accompanied by lifting of the front and the mountain range, remained below sea level (Ferranti & Oldow, 2005). In southern Italy, the strain evolved during the collision between Europe and Africa when Cenozoic rocks were stripped from the western margin of Adria (Argand 1924, Channel et al., 1979) and incorporated into the Apennine as a thrust belt (D'Argenio et al., 1975).

The extension that affected the internal sector caused crust stretching and the local formation of oceanic crust in the Tyrrhenian basin. The deformation from the Miocene to Pleistocene was marked by the combined action of contraction and distension of the hinterland, advancing towards the Apulian sector of the Adriatic foreland (Patacca et al., 1990).

In the Southern Apennines, progressive development of compressive and extensional structures is recorded in three tectonic areas: hinterland, thrust belt and Apulian foreland. The formation of compressive structures in the front began in mid-late Miocene (Patacca et al., 1990) and continued during the Pliocene up to the Pleistocene affecting Mesozoic-Cenozoic basinal rocks transported toward the NE to the western edge of the Apulian foreland.

The southern Apennines consists of stacked thrusts forming a complex system of duplex tectonically transported onto the South West margin of the Apulian foreland (Cinque et al., 1993).

The deeper tectonic units underlying the basal thrusts and consisting of Mesozoic-Tertiary carbonates of shallow marine deposits, were stratigraphically overlapped to Messinian and Pliocene marine deposits. The basal thrusts come mainly from relatively deep basinal domains originally located between shallow water carbonate platforms, of which the eastern (inner platform Apula) is represented by the buried thrusts. Finally, thrusts coming from the inner domain, stacked before the formation of the Tyrrhenian sea and formed units higher than the duplex system.

The last orogenic transport of the northern sector (Molise - Sannita) belongs to the Pliocene whereas in the southern sector (Campanian-Lucanian) it belongs to the lower Pleistocene.

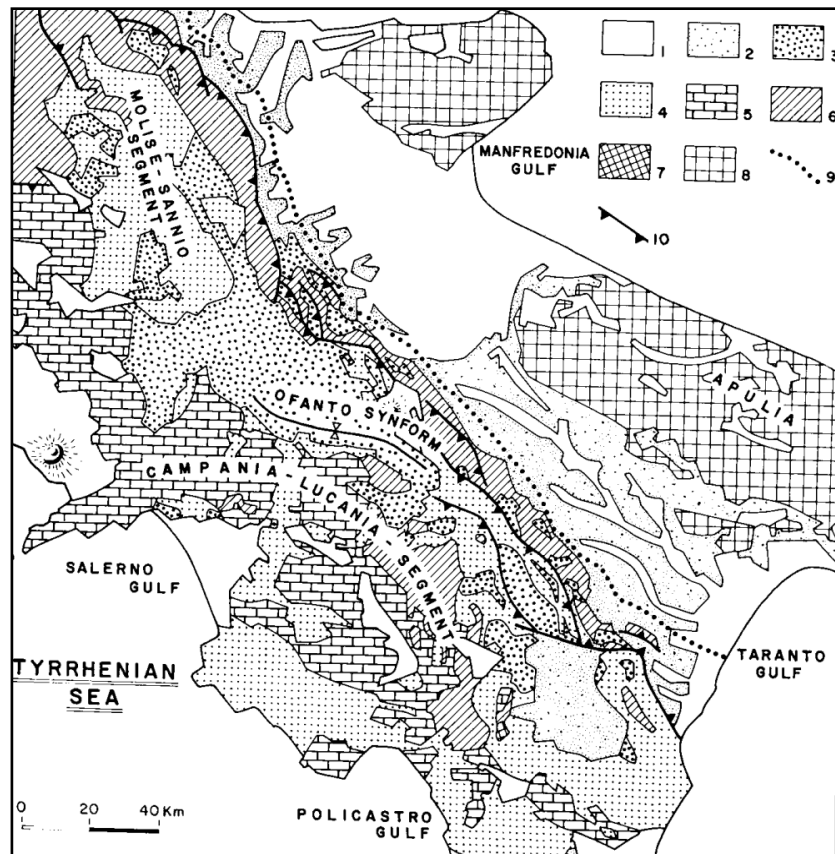


Figure 1.1: Simplified tectonic framework of the Southern Apennines: 1) continental deposits and middle Holocene - Pleistocene; Quaternary volcanoes; 2) late Pliocene deposits - lower Pleistocene marine and continental deposits; 3) clastic deposits of the upper Tortonian - Pliocene Upper accumulated in piggy back basins, on top of advancing thrusts; 4) Apennine thrusts arising from the internal palaeogeographic domains, originally placed on the edge of the plate and the European system of western carbonate platforms. These include Mesozoic - Tertiary basinal sequences and ophiolites that (Penninic thrusts, and Ligurid Sicilid), in second order pre - Alpine crystalline rocks (Calabrian thrusts), Mesozoic and Tertiary metamorphosed and not metamorphosed limestone sequences (San Donato and Verbicaro units) and clastic deposits from lower Miocene, related to piggyback basins (the formation of Albidona); 5) thrusts resulting from external carbonate platforms and from marginal areas, these include Mesozoic - Tertiary carbonate rocks from both shallow and deep sea; flysch deposits from upper Tortonian - Messinian; 6) Apennine thrusts from basal domains, originally located between the western and eastern Platforms: they include Lagonegro-Molise Tertiary units (Frosolone, Agnone, Serra Palazzo and Daunia). The top of the Molise sequence consists of silico-clastic Messinian deposits; 7) Unit of Mount Alps; 8) Carbonate Mesozoic - Tertiary of the Apulian foreland; 9) frontal ramps of the Apennines thrusts; 10) thrusts out of sequence. (Cinque et al., 1993).

The Tyrrhenian margin of the Apennine was dissected during the Pleistocene by normal faults oriented NW/SE (Apennine fault system) that caused vertical displacement towards the Tyrrhenian Sea. Anti - Apennine normal system faults dissect the whole mountain range and cause, from the Tyrrhenian coast to the Apulian foreland, horizontal dislocations (Cinque et al., 1993). Frontal ramps of the Campanian-Lucanian sector lie directly on the deposits of Upper Pliocene - Pleistocene located at the top of the Apulian carbonates. The external sector of the Apennines form a wide synclinal along the Adriatic edge of the Apennines. The axial field is mainly formed by Miocene stacked thrusts that were transported during Pliocene onto the Eastern platform.

1.2 Evolution of the Campanian Plain and the Somma-Vesuvius volcano

The study area is located on the Tyrrhenian coast of the Campania region where major Plio-Quaternary faults related to the extension of the Tyrrhenian Sea gave rise to the "Campanian Graben".

The ridges bordering the carbonate Campanian Plain belong to the massive Sorrento-Lattari of Partenio, Caserta, Pizzo D'Alvano and M. Maggiore groups. These reliefs consist of 1500 m of Mesozoic limestone and dolomites series that only locally preserve Mio-Pliocene terrigenous complex on the massifs and have greater thickness on the Plain, where they reach a depth of 1000-2000 m.

These massifs are morphologically complex since they have very steep slopes resulting from the erosion of fault scarps and are the result of major Pleistocene extensional tectonic phases. As observed for the regional tectonic contexts of the Southern Apennines, massifs formed as consequence of the uplift phase, were displaced by complex fault systems. This mechanism caused subsidence phenomena leading to the formation of semi-graben systems giving rise, in this context, to the formation of the "Campanian Graben" at whose center the Somma-Vesuvius system is located.

The dislocation that involved the Campanian Plain began about two million years ago, at the end of the Pleistocene and throughout the Quaternary when the lifting phase of the Apennine Mountains started. This volcano started its eruptive history after the Campanian ignimbrite eruption following which it is possible to reconstruct the evolutionary stages that led to the formation of its characteristic bicuspid shape.

After the great ignimbrite eruption, a predominantly effusive phase began and a large volcanic cone formed followed in turn, (after about 10,000 year), by a first explosive eruption dated about 25 k-year (Rolandi, 2001). For a certain period, the volcano probably returned to its previous eruptive style, i.e. predominantly effusive, and for about 17 k-year there were a series of a strongly explosive eruptions: Sarno (17 k-year), Novelle (15 k-year), Ottaviano (8 k-year).

These Plinian eruptions were interspersed with periods in which the eruptive style was mainly explosive. Thereafter, about 3.5 k-years B.P., the fifth explosive eruption took place, (Avellino eruption), with a strong interaction between magma and groundwater. These phenomenon led to the formation of "base surge", i.e. a high speed flow of fragmented and solidified magma and water vapor which generated overpressures capable of causing the demolition of the western portion of the volcano that, in turn, led to the formation of a volcanic caldera. The volcano formed by this mechanism continued its activity in the form of weak explosive activity for about 800 years. Three

main eruptive phases took place with the last eruption occurring 2.7 k-year B.P. following which there was a stasis phase culminating in the 79 AD eruption. Moreover, the less energetic eruptions were confined between two Plinian eruptions, (Avellino and the 79 AD eruptions).

As regarding interplinian activity, only the protostoric eruptions will be described. Ancient chronicles report the absence of a volcanic cone in the caldera of the Somma (Rolandi, 2001). After the 472 AD eruption, also very destructive, the Medieval interplinian activity (472 AD - 1139 AD), mostly mildly explosive-effusive, determines the formation inside the caldera of the Somma: the Vesuvius eruptive center (Rolandi et al., 2004).

1.3 Geology of the Sarno mountain ranges

The ridges in peri-Vesuvian area are characterized by Mesozoic platform carbonate sequences belonging to the Unit of Picentini-Taburno Mountain and are covered by late ash-fall pyroclastic deposits. The study area is a carbonate ridge belonging to the Sarno Mountain Ranges culminating in the Relief of Pizzo D'Alvano which rises to 1,133 m above sea level and is located in the south-eastern sector of the Campanian Plain bounded on the west by Nola Plain, on the south by the Sarno River Plain and to the north by the Lauro valley.

The structure consists of a sequence of dolomitic limestone alternating with Lower Cretaceous microcrystalline and detritic limestone and Upper Cretaceous gray limestones, white and crystalline, whose passage is marked by a marly-conglomerate level with orbitolinae which is dislocated at different altitudes from direct fault systems affecting the carbonate series.

The most recent deposits mainly consist of continental debris and pyroclastic deposits covering both the Campanian plain and carbonate ridges. Here, pyroclastic cover is a few meters thick and is linked with the main eruptions of the Pleistocene-Holocene eruptive centers of the island of Ischia (from 150 k-year to 1302 AD), the Phlegrean Fields (from 39 k-year to 1538 AD) and Mount Somma-Vesuvius (from 25 k-year to 1944).

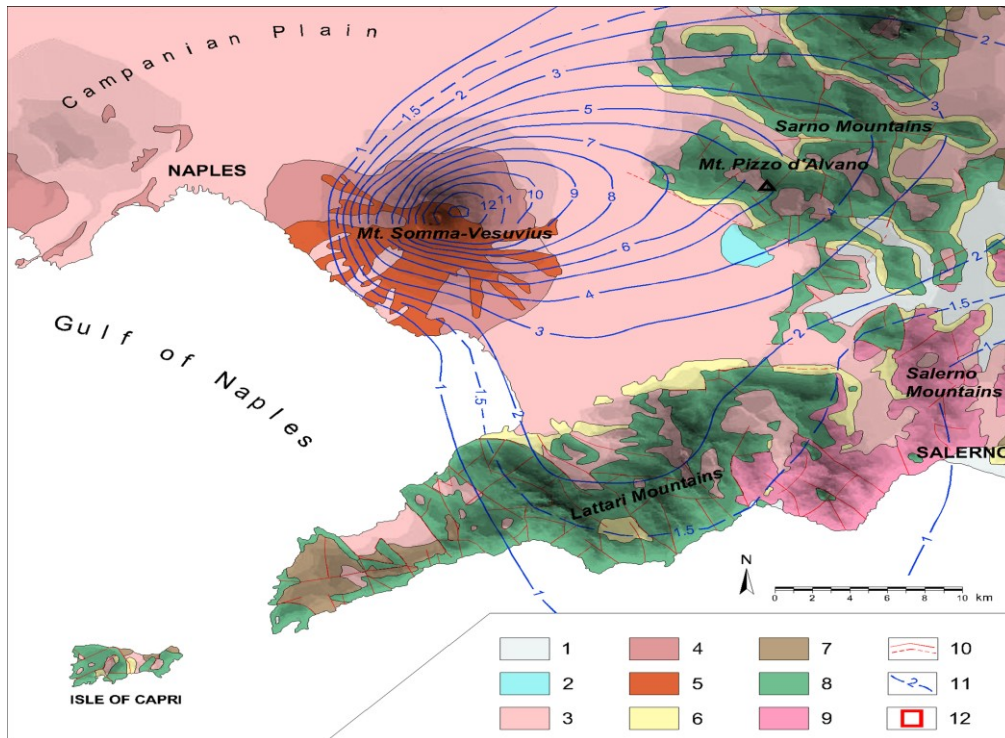


Figure 1.2: Geological sketch of peri-Vesuvian area: 1) Eruption of Sarno: 17 k-year (Rolandi et al., 2000); 2) Eruption of Ottaviano: 8 k-year (Rolandi et al., 1993a); 3) Eruption of Avellino: 3.5 k-year (Rolandi et al., 1993b); 4) Eruption of 79 A.D. (Lirer et al., 1973); 5) Eruption of 472 A.D. (Rolandi et al., 2004); 6) Eruption of 1631 A.D.: (Rosi et al., 1993); 7) Miocenic flysch; 8) middle Giurassic limestone; 9) dolomitic limestones and limestones of lower Triassic – Middle Giurassic; 10) outcropping and buried faults; 11) total isopachs of main eruptions of Somma-Vesuvius system.

A complete pyroclastic sequence was identified at the foothills of the Sarno Mountain (Rolandi et al., 2000), whose oldest products were attributed to the APC (Ancient Pyroclastic Complex) and mainly consist of Campanian Ignimbrite flow deposits dated at about 39 k-year and other products of the eruptions of Phlegrean Fields and the Ischia island. The most recent pyroclastic deposits belong to Recent Pyroclastic Complex (RPC), coming from the Mount Somma eruptions: Sarno, dated 17 k-year (Rolandi et al, 2000), Ottaviano, dated 8 k-year (Rolandi et al, 1993a), Avellino, dated 3.76 k-year (Rolandi et al, 1993b). Products of RPC are also historical eruptions of Vesuvius: 79 AD (Rolandi et al, 2007), 472 AD (Rolandi et al, 2004) and 1631 AD (Rosi et al, 1993) and also the subsequent eruptions, of minor importance for the volume of erupted material, the last of which occurred in 1944.

1.4 Main plinian eruptions of the Somma-Vesuvius

1.4.1 The Sarno eruption (17 k-year)

The eruption of basal pumice, also known as “Sarno eruption” (Rolandi et al., 2000), has a succession of deposits made up, from the bottom up of:

- plinian fall deposits with subordinate surge deposits;
- a series of volcanic landslides (lahars) and fall deposits, flow and surge highly enriched in lithic components.

The eruption *vent* was located, on the basis of the reconstruction of isopach and ballistic trajectories, in an eccentric position compared to the Somma’s caldera which is in the western sector at 1-2.5 km from the current cone of Vesuvius. The large volumes of tephra erupted indicates that the eruption of basal pumice was the strongest explosive event which occurred in the last 20 k-year. Indeed, the ash fall deposits covered an area of 2,600 km² within the isopach of 20 cm with a volume of 4.4 km³. The main fallout deposit were spread eastward maintaining a thickness of about 6.5 m at 10 km from the volcano. The composition of the plinian fall ranges from white trachytic pumice (SiO₂: 63 wt %) to dark latitic scoria (SiO₂: 53.7 wt%), together with a decreasing amount of the clast vesiculation (from 80 to 45%, respectively). This compositional variation reflects a chemically-zoned magmatic camera that fed the eruption.

1.4.2 The Ottaviano eruption (8 k-year)

The Ottaviano eruption was one of the most violent volcanic events in the history of the Somma volcano.

On the slopes of the Monte Somma the deposits of the Ottaviano formation are located between the fallout pyroclastic deposits of two Phlegrean Fields eruptions which occurred, respectively, 9.800 and 4.400 k-year B.P. The Ottaviano formation consists mainly of fallout deposits, located on the north-east flank, of flow deposits all over the western and eastern side and of deposits of typical surge depositional mechanisms.

Stratigraphic correlations of the Ottaviano formation (Rolandi et al., 1993a), were made by referring to two markers that is the Avellino formation (3.7 k-year) and Main Pumice formation (9 k-year), respectively located on top and bottom of the sequence (Figure 1.3). All the analyzed sequences, (Rolandi et al., 1993a) end up with a pyroclastic flow deposit and are well represented in the Ottaviano cross section (Rolandi et al., 1993a). The stratigraphic sequence located in Lagno

1.4 Main plinian eruptions of the Somma-Vesuvius

Amendolare represents the flow deposits consisting of a lower, middle and upper flow units. The fallout products of this eruption, mainly consist of pumice layers, representing the products of a single explosive phase. The different dispersal axes are related to the changes in physical conditions during the eruption (Figure 1.4). Individual isopach maps for each level show an elliptical distribution with its main axis oriented eastward and its dispersion axis East-North-East (Figure 1.3). In conclusion, it can be argued that the analysis of the sequences described allowed the reconstruction of the eruptive event that was defined as sub-plinian. The presence of highly vesicular pumices indicates a high fragmentation of magma and the low presence of crystals within the pumice also suggests a high concentration of gas within the magma chamber. This evidence suggests that the Ottaviano eruption was mainly magmatic (Rolandi et al., 1993a).

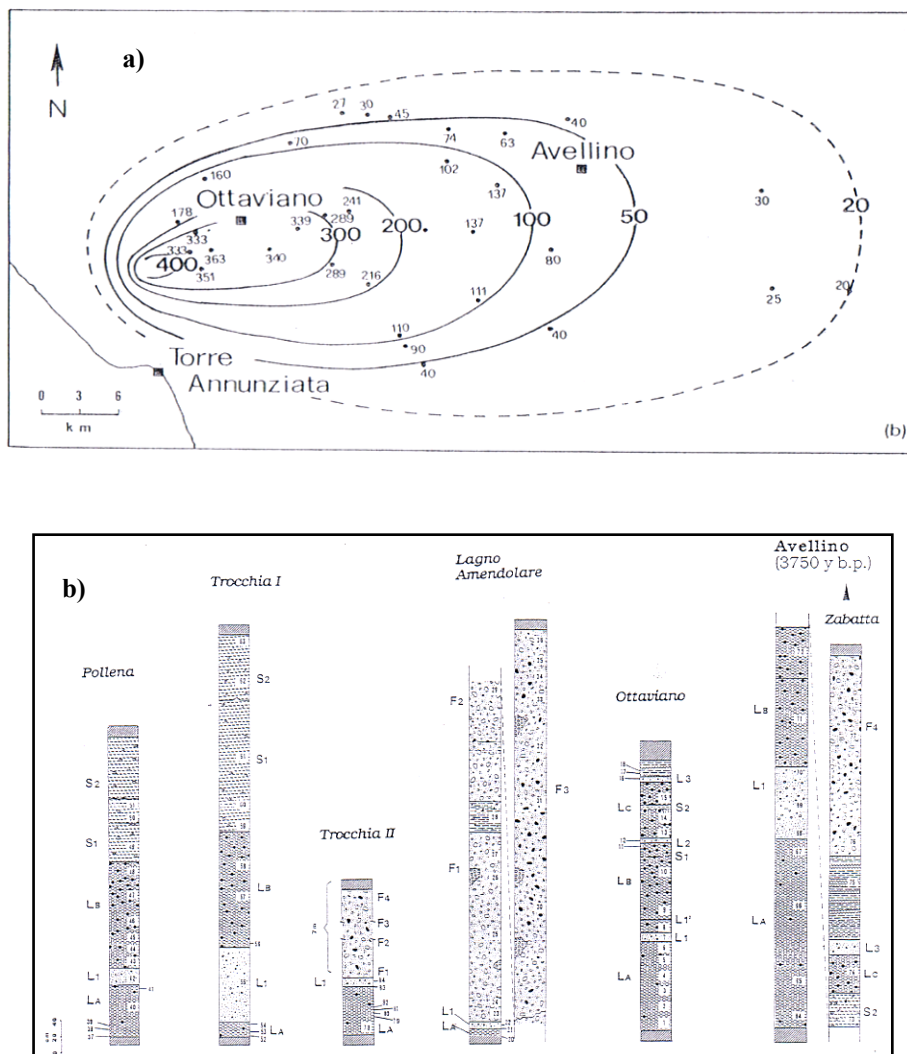


Figure 1.3: Ottaviano eruption: direction of distribution of pyroclastic deposits(a) and correlation between stratigraphic sequences investigated in the area (b) (Rolandi et al., 1993a).

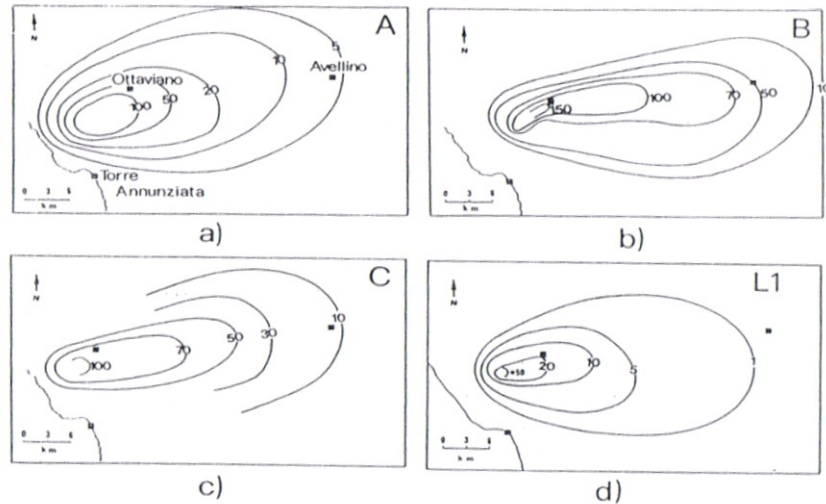


Figure 1.4: isopach map for the Ottaviano eruption deposits, the thickness is total. (Rolandi et al., 1993a)

1.4.3 The Avellino eruption (3.7 k-year)

It is considered as the major Plinian eruption of the Somma-Vesuvius that gave rise to a complex sequence characterized by pyroclastic units made of pyroclastic flow and pyroclastic surge.

A typical section of the Avellino eruption is located in Lagno Trocchia, on the western side of the volcano (Rolandi et al., 1993b). It is mostly made up of thinly laminated ashy layers with a uniform layer of white pumice lapilli, a thin layer of white pumice, a massive layer of gray pumiceous lapilli, with reverse grading (coarsening up) until it becomes a thin layer of consolidated cineritic layers. The whole unit is very rich in lithic elements. The sequence continues with a layer of well graded and glassy ash alternating with a thinner level, still ashy and with wavy lamination (Figure 1.5).

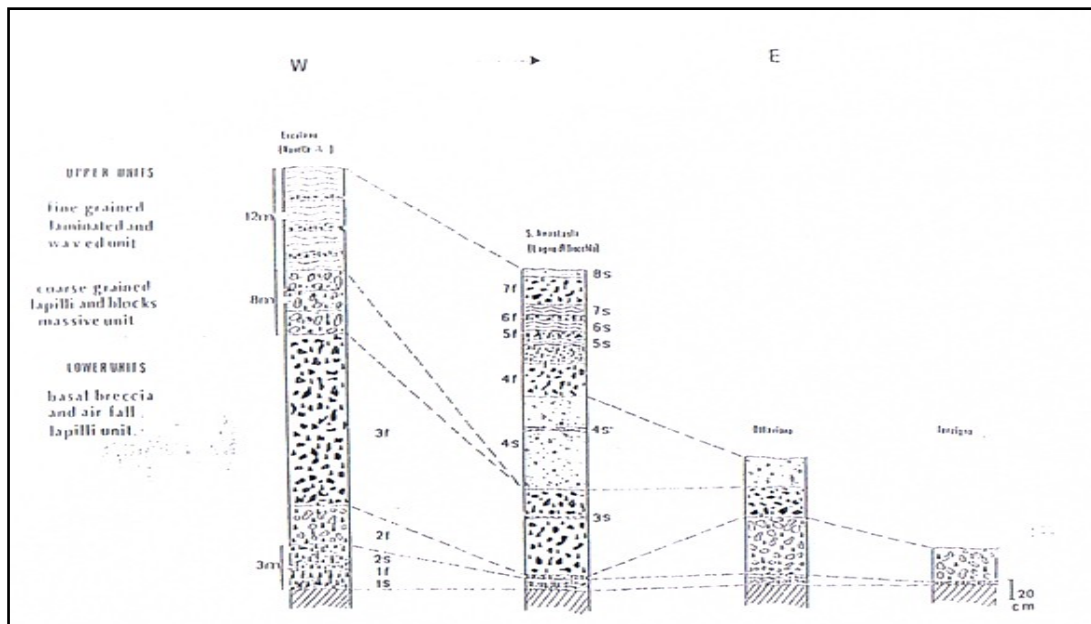


Figure 1.5: correlation of pyroclastic deposits of Avellino eruption, between the stratigraphic sections located in the North sector of Somma - Vesuvius (Rolandi et al., 1993b).

Based on the description of the typical sequence and on stratigraphic correlations made by the Authors, it is possible to define two main units:

- the lower unit of basal breccia and coarse fallout unit represented by coarse lapilli
- the higher unit of fine and laminated ash and lapilli and coarse massive blocks.

Stratigraphic analysis carried out by the Authors shows a different distribution of the main volcanic units (Figure 1.6). It is possible to observe a variation in the orientation of the dispersion axes; the basal breccia has a less widespread dispersion axis towards the east.

The white pumiceous lapilli level, on the other hand, has a dispersion axis oriented ENE and finally, the gray pumice unit, which is the main and more widespread event, has a dispersion axis towards NNE (Rolandi et al, 1993b). In general, the direction of isopach elongation is ENE.

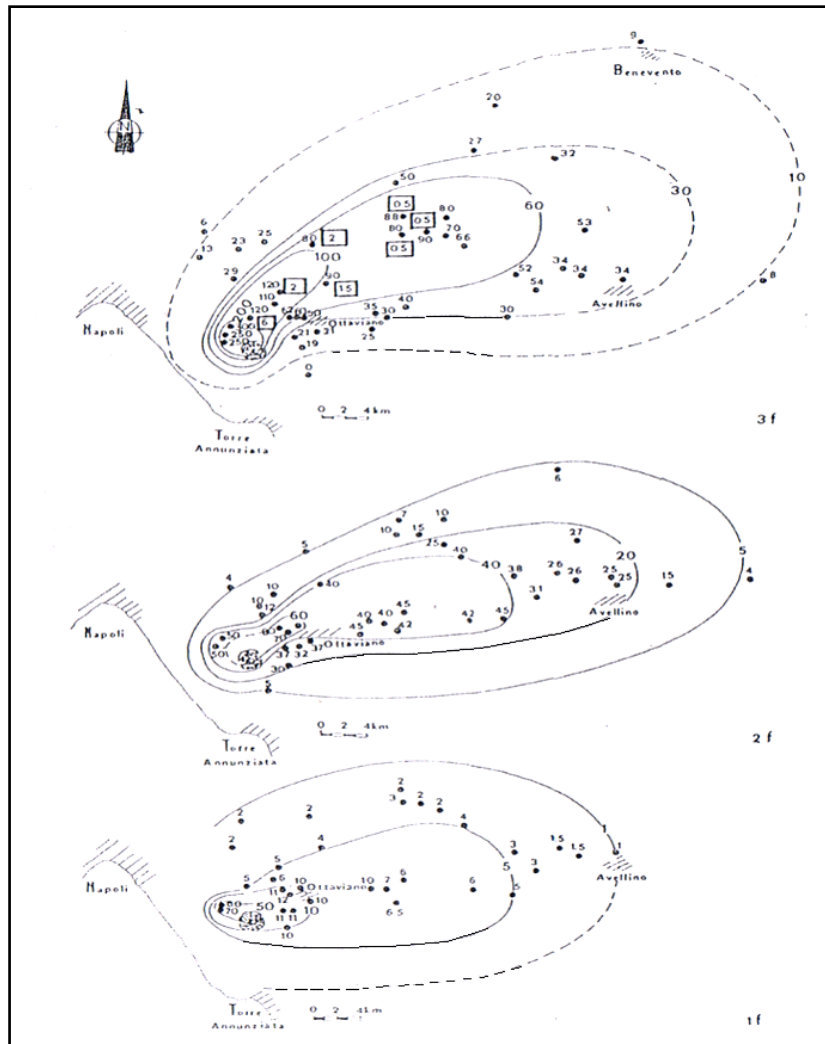


Figure 1.6: isopach map of the ash-fall units of the Avellino formation. The three main levels fall eruption are represented: the basal 1f, 2f member of white pumice and gray pumice member 3f (Rolandi et al., 1993b).

The isopach map of deposits shows a dispersion axis predominantly oriented towards NNE. Finally, the careful analysis of Avellino eruption shows, according to the authors, a close analogy with the 79 AD eruption. Both eruptions show evidence of a compositionally zoned magma with upward increments in gas concentration and initial interaction, although limited, between magma - groundwater with volatile-rich magma at the top. Such a mechanism gives rise to basal levels and is followed by major plinian episodes mainly characterized by magma release interrupted by limited hydromagmatic events.

1.4.4 The 79 AD eruption

The 79 AD plinian eruption produced pyroclastic deposits by fall mechanisms (tephra) consisting of white pumice at the bottom and gray pumice in the upper part, which was then followed by a change in the eruption dynamics. The sequence is interrupted by typical deposits that are the result of pyroclastic flows and pyroclastic surge mechanisms due to a collapse of the Plinian column. The dispersion axis of this eruption, oriented SE, is considered by the authors to be unusual probably because of the wind direction and speed (relatively high) and the height reached by the Plinian column, that is the main factor affecting the distribution of tephra (Rolandi et al., 2007).

The eruption of 79 AD, with its different eruptive mechanisms, and mainly consisting of fallout deposits, surge, pyroclastic flow and ashy levels is one of the most studied Plinian events.

Stratigraphic correlations of markers levels allowed to recognize the typical pyroclastic sequence of this eruption, whose stratigraphy is often complicated by lateral and vertical variations in texture of layers (Figure 1.7). The type section of the 79 AD eruption is characterized by white pumice fallout deposited only in the ESE sector in the towns of Terzigno Pozzelle and Pompei (Lirer et al., 1993). An important marker that indicates the beginning of the deposition of gray pumice is widely spread in Pompei, Villa Regina, Oplonti (Lirer et al., 1993). The transition from magmatic to hydromagmatic activity (the asterisk in figure 1.7) suddenly takes place in the sequences without a transition.

The main stages of the eruption may be summarized as follows (Figure 1.8): ash fall deposition and early stages of deposition of fallout pumice (A), final deposition of the white pumice and of the surge deposits (B), first deposition of the gray pumice and of pyroclastic flows (C), final deposition of gray pumice resulting from pyroclastic flow deposits (D), deposition of hydromagmatic products (E) (Lirer et al., 1993).

1.4 Main plinian eruptions of the Somma-Vesuvius

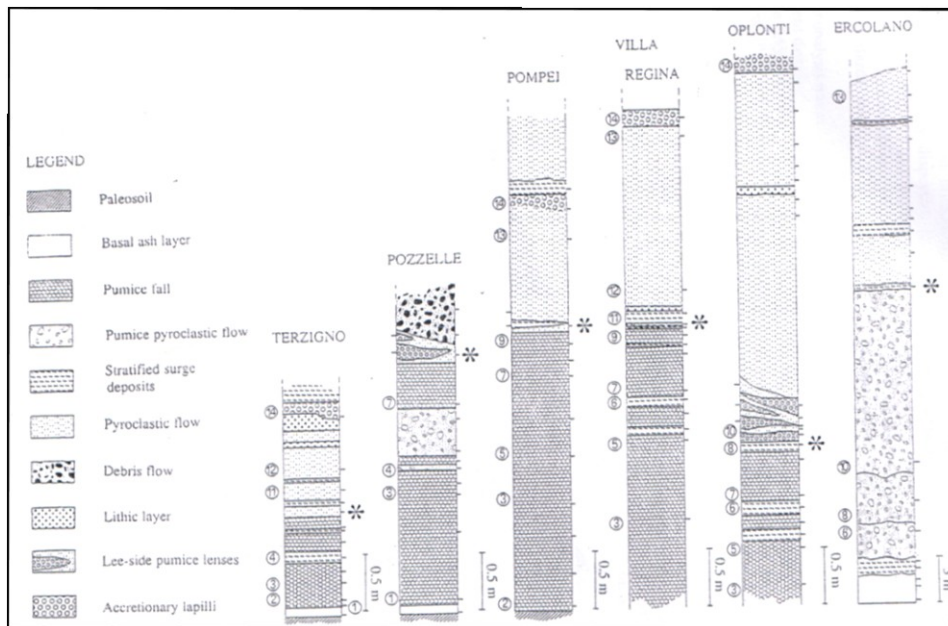


Figure 1.7: stratigraphic correlations made deposits of the 79 AD deposits (Lirer et al., 1993).

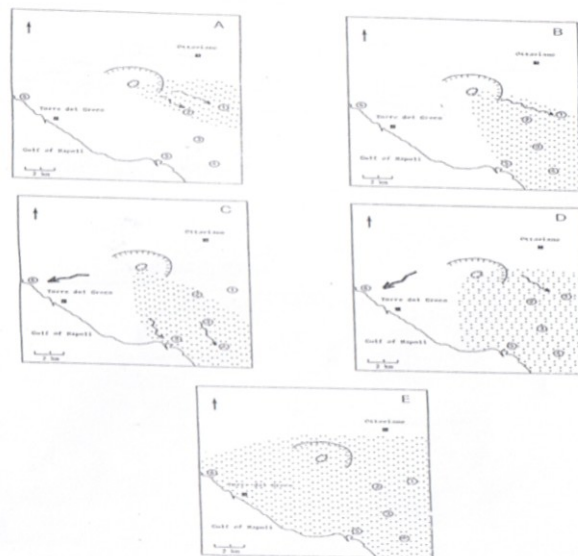


Figure 1.8: chronological reconstruction and spatial phase of the 79 AD Eruption (Lirer et al., 1993)

1.4.5 The 472 AD eruption

The 472 AD explosive eruption began from the caldera of the Mount Somma. The stratigraphy of pyroclastic deposits suggests a complex series of events that can be grouped into four main phases:

- Small magmatic explosion resulting in well-vesicular pumice layers (L_a) dispersed in a N-NE direction and representing the opening phase of the vent.
- The fallout deposits divided into L_b and L_{max} levels and scattered, respectively, towards the N-NE and NE-SE sectors. The latter are mainly phreato-magmatic because of the influence of groundwater and of its interaction with the magma within the system chamber - magma conduit.
- The rising pressure due to strong interaction between magma and water is the main cause of the formation of debris flows of the third stage (Rolandi et al., 2004).
- The fourth phase is the final activity that produced surge deposits rich in lapilli and ash fallout which are closely related to the phreato-magmatic activity. The typical stratigraphic section was found in Somma Vesuviana (Rolandi et al., 2004).

The typical stratigraphy of this eruption is shown in Figure 1.9. It indicates that prolonged phases characterized by intense convective columns, were alternated with small explosions (Rolandi et al., 2004), whose products were dispersed in a N-NE direction.

There was also an evolution to highly hydromagmatic processes that produced a very dense column rich in lithic elements; the collapse of the column was responsible for the formation of debris flow. The increased interaction with water also caused the development of base surge deposits with the formation of laminated structures representing the final stage of the powerful freatomagmatic phase.

According to the Authors, the presence of lithic elements consisting of lava fragments indicates that the 472 AD eruption mainly consisted of hydromagmatic processes and it was classified by the Authors as Plinian.

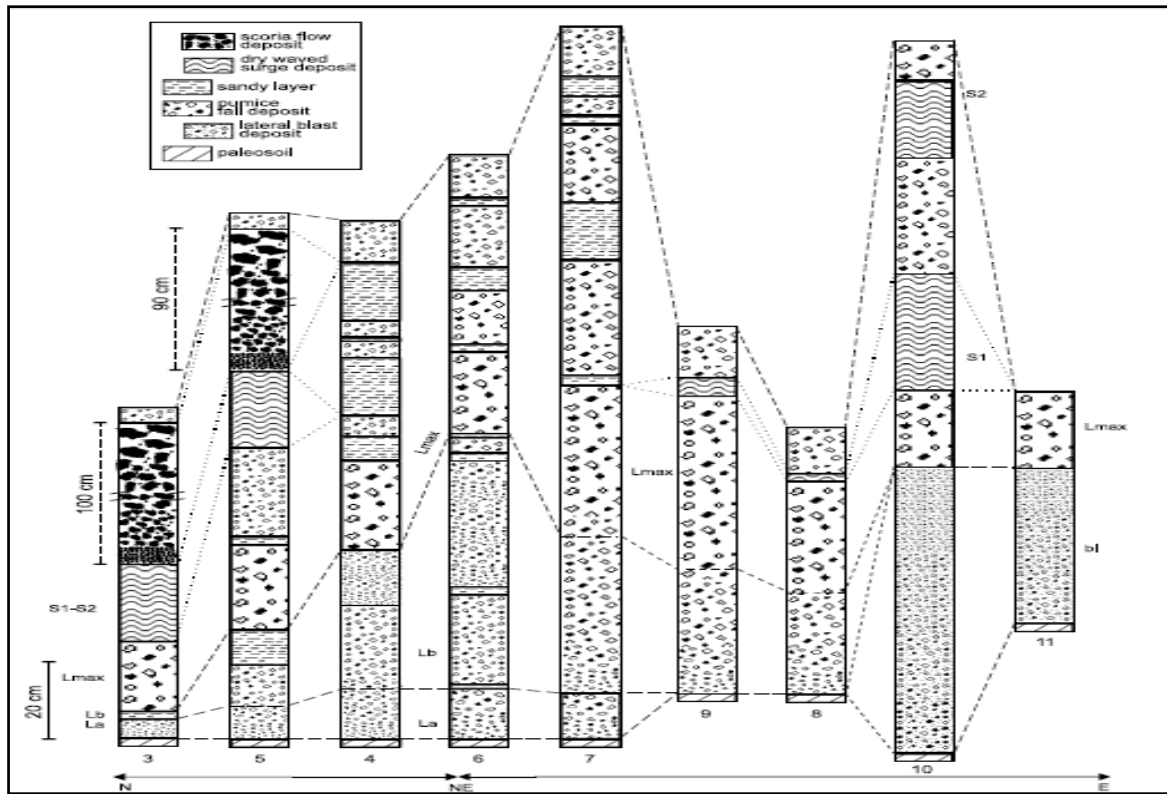


Figure 1.9: stratigraphic correlations for deposits of the 472 AD eruption, along a transect located in the proximal area of the volcanic complex (Rolandi et al., 2004).

1.4.6 The 1631 eruption

The reconstruction of the stratigraphy of the 1631 eruption was performed in the proximal area of the volcano and revealed the presence of fallout deposits, pyroclastic flows, lavas and only subordinately surge deposits.

The ash-fall products of 1631 are placed on the eruption representing the last phase of medieval explosive activity. A good example of the eruption products outcrops in the eastern sector of the volcano where the basal levels consist of small white pumice. The intermediate level consists of pumice-rich crystals and the upper level is a scoriaceous coarser and dark gray layer topped by a thin ash layer deposited during the same eruption. The gradual color change within the deposit obviously reflects a change in the mineralogical and chemical composition of pumice and glass (Rolandi et al., 1993). The dispersion axes of these levels are toward NE with gradual thinning in this direction. The pyroclastic flows seem to be discontinuous in the southern sector but also outcrop in the NW side of Mount Somma. The type section of the flow deposits can be divided into three units. The basal unit is a dark gray pumice and lithic elements and at the top it has an erosion

surface consisting of a horizontal massive gray horizon that marks the transition to the upper unit. In a quarry in the town of Lagno Amendolare a surge deposit with a limited areal distribution outcrops (Rolandi et al., 1993). The emission of lava during the eruption is well documented although its existence is controversial (Rolandi et al., 1993). The pyroclastic flow deposits are dominated by an epiclastic deposit whose type section consists of two units containing elements of stone blocks and variable lithology (Rolandi et al., 1993). The origin of this deposit was associated by the Authors to the strong explosive eruption that caused the destruction of the peak of Vesuvius.

Finally, from the stratigraphic reconstruction it is possible to guess that an initial explosive eruption took place producing a strong convective column (Rolandi et al., 1993). Afterwards, according to the authors, a change in eruptive style occurred with the start of a phreatomagmatic phase. In the last stage the magma intrudes into the system of lateral fractures and produces a spectacular effusive phase (Rolandi et al., 1993).

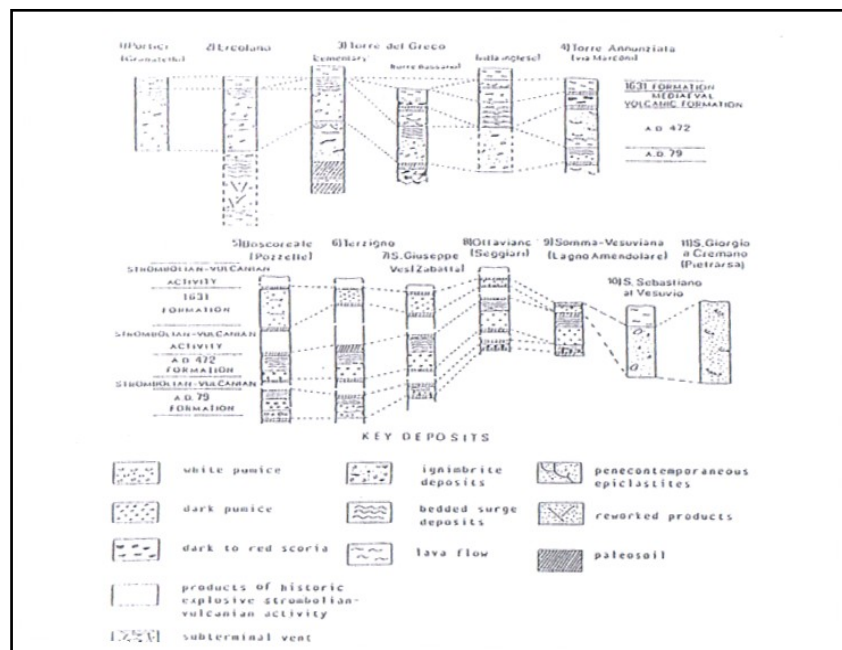


Figure 1.10: stratigraphic sections and correlations of the 1631 eruption deposits in proximal system Somma - Vesuvius. (Rolandi et al., 1993).

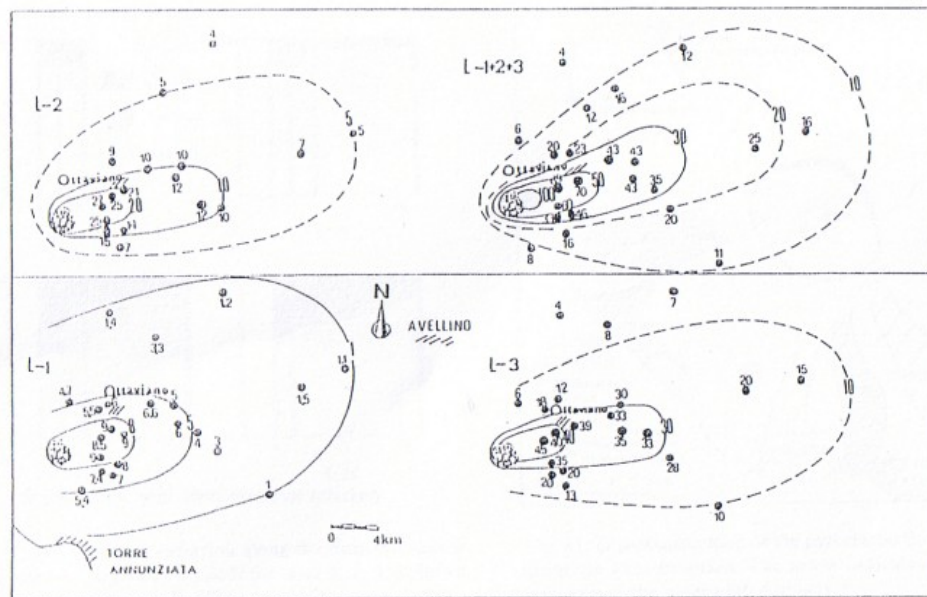


Figure 1.11: dispersion axes identified for the fall deposits by the 1631 eruption, the thickness of isopach are in cm. (Rolandi et al., 1993)

1.5 Distribution of ash-fall pyroclastic deposits along mountain slopes

The pyroclastic deposits mantling carbonate ridges of the Sarno mountain ranges were emplaced after the main morphogenetic stages, starting from 40 k-year B.P. and are the result of the most important eruptive phases of the Somma-Vesuvius system and subordinately of the Phlegrean Fields. After depositions, these deposits were subjected to denudational processes by erosion and by gravitational mass-movements phenomena. Actually their thickness essentially depends on slope angle and often reflects an incomplete volcanoclastic sequence. On the other hand, more complete sequences are present in the Campanian Plain, depending on the distance from the vent, the orientation of the dispersion axis and the lateral variability induced by erosion and deposition in the hydrographic network.

A reference volcanoclastic series was identified in the western foot of the Sarno Mountains, where the oldest pyroclastic deposits were ascribed to the Ancient Pyroclastic Complex (APC) primarily consisting of pyroclastic flow deposits of the Campanian Ignimbrite (39 k-year) and other products coming from Phlegrean Fields and from Ischia island. More recent deposits were ascribed to Recent Pyroclastic Complex (RPC) comprising one of the Mount Somma eruptions, including Codola (25 k-year) (Rolandi et al., 2000), Sarno, dated 17 k-year (Rolandi et al., 2000), Ottaviano, dated 8 k-year (Rolandi et al., 1993a) and Avellino, dated 3.76 k-year (Rolandi et al., 1993b). The RPC also includes the products of the middle age (historical) eruptions of Vesuvius: 79 AD (Lirer et

al., 1973), 472 AD (Rolandi et al., 2004) and 1631 AD (Rosi et al., 1993), and the subsequent ones, characterized by smaller erupted volumes, the last of which occurred in 1944.

In order to understand the distribution and thickness of the pyroclastic mantle along slopes, a total isopach map of the main eruptions of the Somma-Vesuvius volcanic complex (Figure 1.12) was achieved by means of the algebraic sum of numerical maps of thickness, and of geostatistic interpolation based on data available in literature (De Vita et al., 2006). It is possible to observe that the RPC gets the maximum theoretical thickness with values ranging from 4 to 7 m on Sarno Mountains, and variable values of about 2 m on Lattari Mountains.

The total isopach thickness (S_t) results from ash-fall deposition mechanisms, giving rise to a stratification parallel to the slope (Fisher, 1985). It is fundamental to point out that real thickness of ash-fall deposits (S), measured on an inclined plane (i.e. slope) as the length orthogonal to the plane of the slope, is a function of slope angle (α) and of the theoretical thickness of ash-fall deposits (S_t), up to the limit case of vertical slope where there is no deposition, according to the relation

$$S = S_t \cdot \cos(\alpha)$$

This relationship accounts for the theoretical distribution of ash-fall pyroclastic deposits along slopes expressed in terms of real thickness.

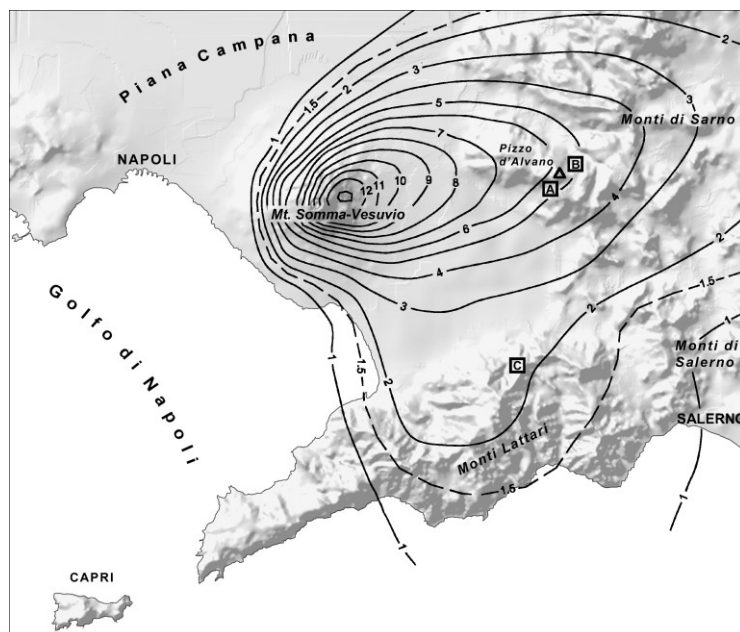


Figure 1.12: total isopach map concerning RPC derived by the algebraic sum of isopachs of the eruptions of Codola (25 k-years), Sarno (17 k-years); Ottaviano (8 k-years); Avellino (3.7 k-years); 79 AC; 472 AC; 1631 A.D.) (De Vita et al., 2006a).

With the aim to verify such relationship a series of field surveys were carried out in different morphological conditions along the mountain slopes of the Sarno and Lattari mountain ranges (De Vita et al., 2006a; 2006b).

The total isopachs that indicatively indicates the maximum theoretical thickness of ash-fall deposits was verified with field measurements only in the most conservative areas of slopes. Here morphological conditions led to a negligible erosion and secondary depositional processes, such as: secondary order morphological divides and gently inclined slopes. Instead, for all those areas with greater slope angle, the real thickness of ash-fall pyroclastic deposits was measured as reduced respect to the theoretical values derived from the previous equation (Figure 1.13).

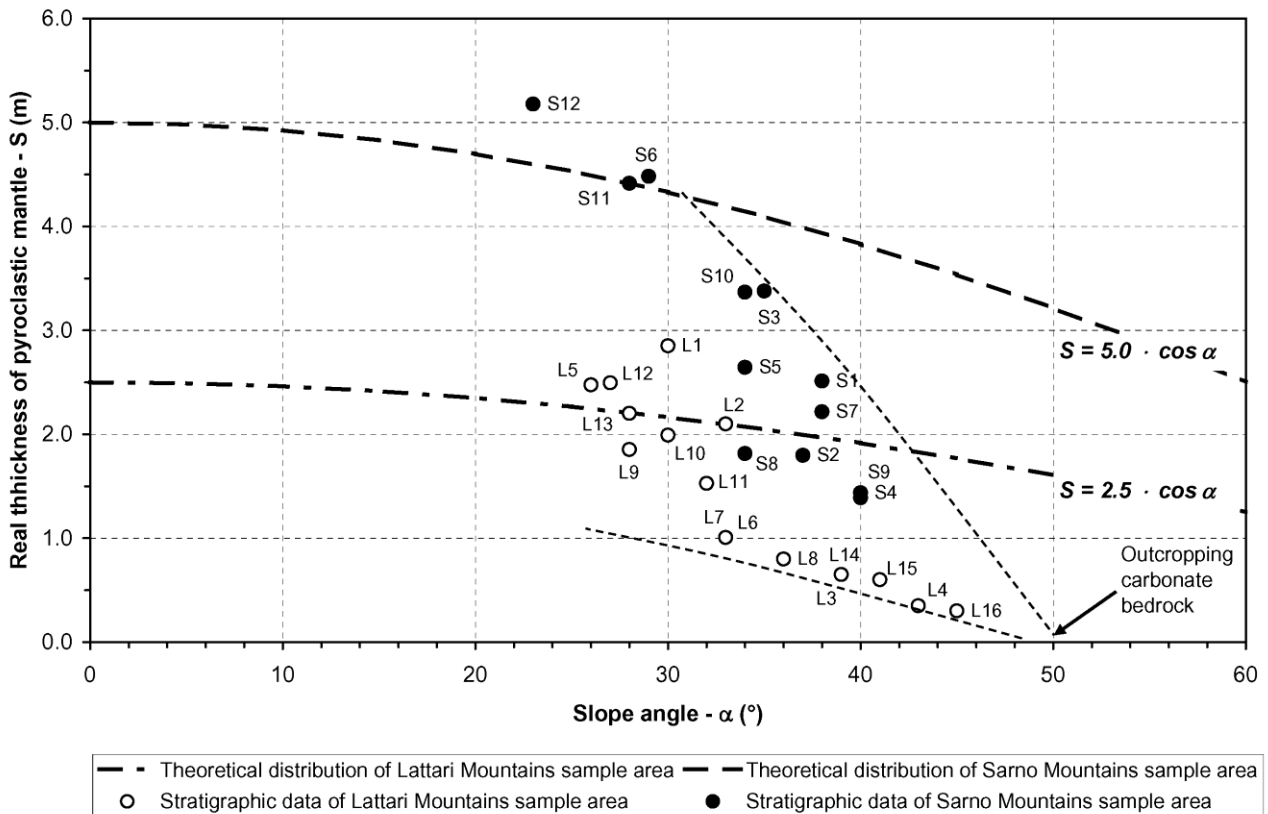


Figure 1.13: Theoretical (curves) and real (data points) distribution of ash-fall pyroclastic deposits along slopes of the Sarno and Lattari mountain ranges (De Vita et al., 2006b), expressed in terms of real thickness. It is possible to point out the divergence of real thickness data from the theoretical distribution for slope angle values greater than 30°. The pyroclastic mantle become negligible for slope angle values greater than 50° (outcropping of the carbonate bedrock).

Following field investigations, carried out in order to estimate the thickness of the pyroclastic mantle it was possible to reconstruct the stratigraphy of the volcanoclastic series in sample areas of the Sarno Mountains located in the NE sector of Pizzo D'Alvano (Figure 1.14). Here, complete volcanoclastic series were observed depending on the slope angle values.

The use of the pedological nomenclature of the main soil horizons (Soil Survey Staff, 1998; Terribile et al., 2000) combined with the lithostratigraphic methods, allowed to recognize different depositional episodes alternated with pedogenic deposits. From a lithostratigraphic point of view, the sequence can be related taking into account the C horizons features to the succession of Ottaviano eruptions (Cb horizon) and Avellino (C horizon). In this succession, Bb horizons can be considered as the result of pedogenic processes that acted on pyroclastic materials in primary deposition.

The investigations carried out in less conservative areas (characterized by a greater slope angle), show lower thickness and incomplete sequences, highlighting the existence of a single horizon C until the complete absence, the welding of the basal horizons B with Bb. The latter may also be classified as Andosols (USDA, 1998), because they are pedogenetic products on volcanoclastic deposits (Figure 1.14).

The relationship between slope angle and thickness of pyroclastic layers decreases as angle α increases (Figure 1.13). The maximum value of real thickness is found for slope angle of about 30°. Over this value, the real thickness progressively reduces to zero, for slope angles of approximately 50° (De Vita et al., 2006a).

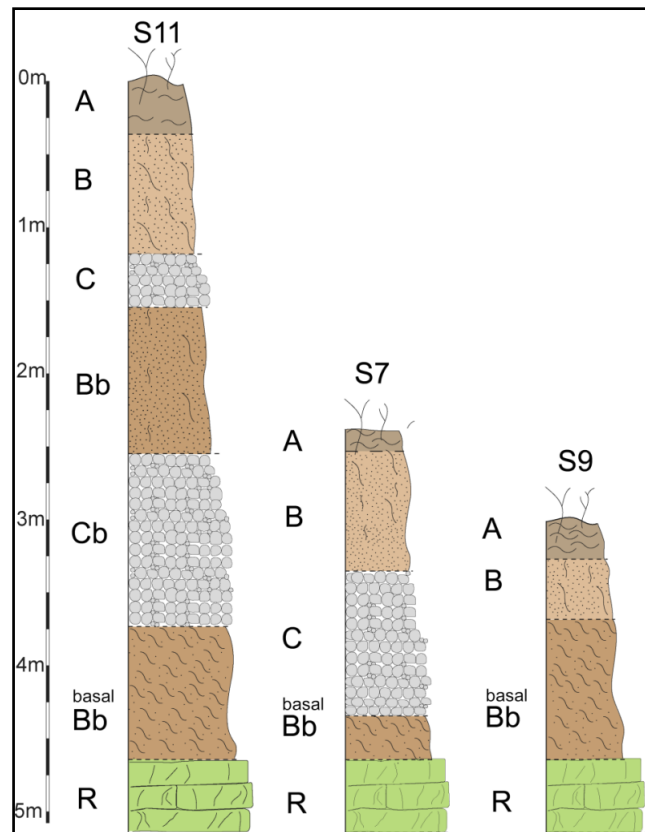


Figure 1.14: representative stratigraphical columns (real thicknesses) derived from exploration trenches carried out in the sample area of Sarno Mountain in different slope angle conditions: S11 → 28°; S7 → 38°; S9 → 40°. Soil horizons: A horizon, classified as organic soil (Pt); B horizon, characterized by pumiceous lapilli, variable in grain size from coarse to fine ash, subject to pedogenesis processes and classified as sand with silt (SM); C horizon, consisting of pumiceous lapilli, angular and little altered, with greatest size up to 30 mm, variable from lapilli to coarse ash, classified as clean gravel and sand well graded (GW or GP); Bb horizon that is a paleosol, corresponding to a buried B horizon by subsequent depositional event and, classified as sand with silt (MS); Cb horizon, representing a buried C horizon, consisting variable in grain size from pumiceous lapilli to coarse ash, classified as the C horizon (GW or GP); Bb basal horizon, corresponding to a residual pyroclastic deposit subject to intense pedogenetic processes, representative of the previous eruptions' products, also classified as sand with silt (SM); R horizon, corresponding to the limestone bedrock. (De Vita et al., 2006b).

1.6 The climate in Campania region

The Campania Region is 13.578 km² wide, with the exception of the insular area, and it extends in a relatively narrow belt of latitude (40 ° N - 41 ° N) and a relatively wide range of latitude, varying from sea level to 2.050 m above sea level (Mount Miletto). The distribution of bands of altitude is characterized by the prevalence of areas at low altitude, in fact, the average altitude is 440 m above sea level.

The Campanian climate is generally homogeneous, and is attributable to the Mediterranean climate, temperate winters and wet or poorly wet summers. The climate is generally homogeneous,

but variable at a local scale, particularly in function of the varied orographic pattern, which allows the division into two zones: the coastal sector, represented by wide floodplains, and inner sector which includes the Apenninic massifs.

From analysis of data from air temperature and rain gauge stations managed by Hydrographic and Tidal National Service (*Servizio Idrografico e Mareografico Nazionale*), it is possible to state that rainfall are directly related to the height and that this relationship varies spatially in a complex orographic territory. In fact, the different exposition of the slopes of the massifs to the wet air currents mainly coming from West, determines a subdivision of rainfall in different pluviometric sub-zones.

In particular, in Campania two sub-zones were individuated: the first comprehends all the mountain slopes overlooking the Tyrrhenian Sea, culminating in the higher watersheds that are affected by wet air currents coming from the sea; the second is represented by areas overshadowed by reliefs, with respect to the airflow coming from the sea. In a such a way, the different distribution of precipitations in Campania region can be justified. It explicates in a higher concentration of areas exposed to of wet air currents coming from from the sea. The first climatic zone, comprehending the Campanian Plain, the Sele plain and the smaller coastal plains, the climatic conditions are much less influenced by the proximity of the sea and therefore, as elsewhere in the Mediterranean area, they are characterized by mild winters and hot summers, relatively dry.

The first rains begin when there is a deficit in soil water content, that is at the beginning of the wet season. Such rains have the effect to increase soil moisture and, therefore, the same amount of rain falling on the ground during the wet season, makes the soil being close to saturation and then leach into deeper levels of the pyroclastic mantle and into the bedrock, or to move downslope as surface runoff or lateral flow (throughflow).

Moreover, the soil moisture accumulated during the antecedent precipitations and the onset of wet season have an important effect on how a new precipitation event interacts with the slope. In particular the lack of soil moisture must be satisfied before the pore pressures becomes positive, thus creating slope instability.

Chapter 2

Instability conditions of Ash-Fall pyroclastic soils mantling peri – vesuvian hillslopes: a review of the scientific literature

2.1. Landslides phenomena and their classification

The term landslide denotes “the movement of a mass of rock, debris or earth down a slope” (Cruden, 1991) primarily controlled by the force of gravity. The term landslide refers to all the phenomena of shallow or deep, rapid or slow mass movement of rock or soil caused mainly by the forces of gravity (Varnes, 1978; Cruden & Varnes, 1996). Gravitational slope phenomena play a major role in the morphological evolution of the slopes because they represent one of main processes of erosion. The volumes involved in the landslide can vary from a few dm^3 to million m^3 . Landslide phenomena occurring in a given area can be due to the combination of several unfavorable factors as regards the stability of a slope. It is clear that the determination and control of these factors may be useful in order to avoid the recurrence of events that harm lives and infrastructures.

Natural disasters recorded in the State Archives in which instability phenomena involves pyroclastic cover can be easily recognized and they highlight a marked occurrence/repetition of debris flows in mountain slopes surrounding the Somma-Vesuvius volcano since the first half of the XVII Century. The first evidence derives from historical sources such as literary works, paintings and documents stored in the parish archives. Other information can be found in the CNR archives such as the AVI Project (Guzzetti et al., 1994) and documents preserved in the State Archives of Salerno where it is possible to examine surveys carried out in order to deal with the emergencies (Cascini & Sorbino, 2002). The analysis of known disasters in the area of the Sarno and Lattari Mountains demonstrates a high level of mortality due to debris flows. The historical sequences of debris flow events, known from different chronicles sources can be shown both as single or distributed phenomena together with the number of victims and main eruptions of the Vesuvius in time (Figures 2.1a and 2.1b).

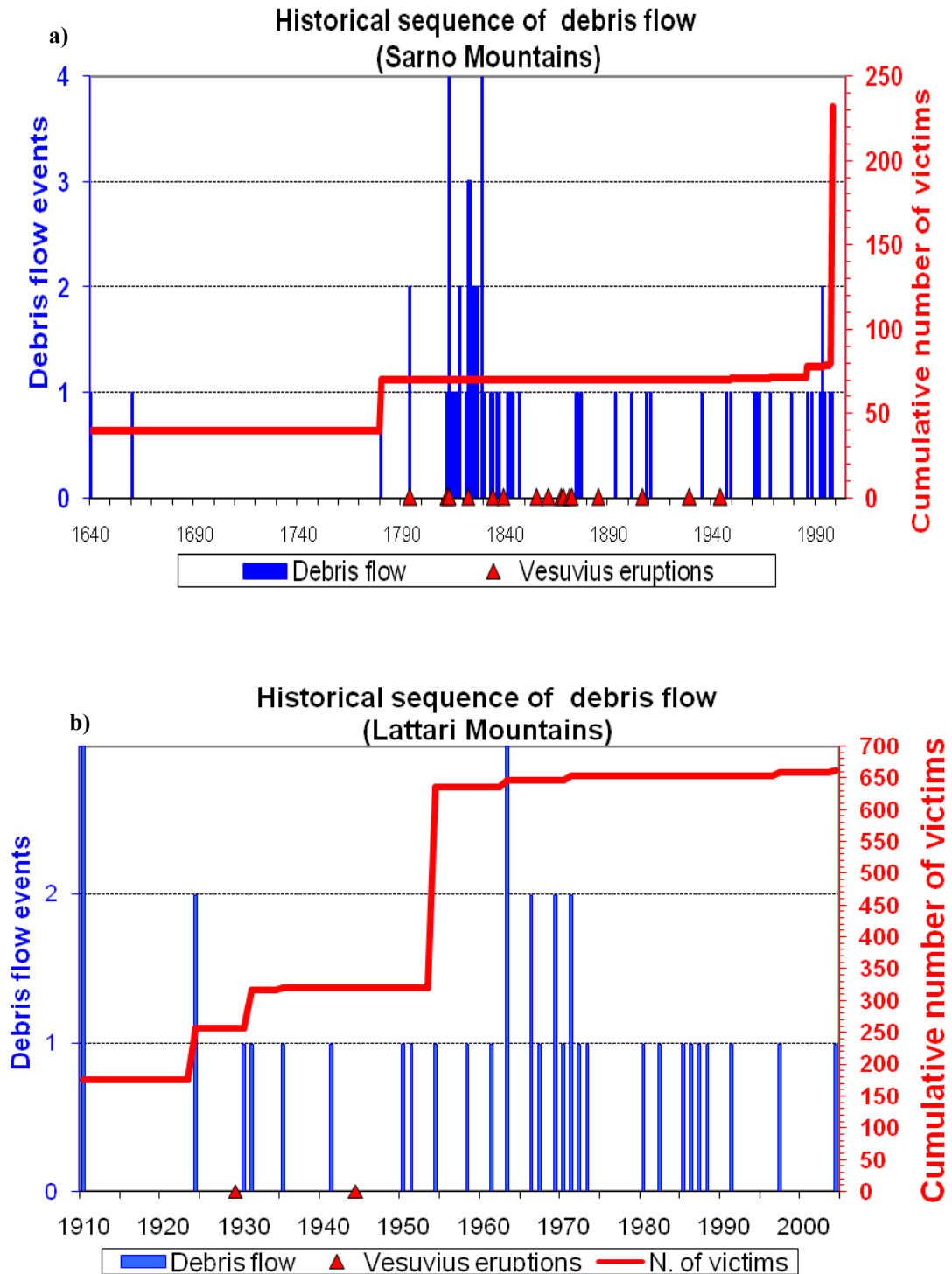


Figure 2.1: historical series of debris flow events, concerning the Sarno (a) and Lattari (b) Mountains, known by historical chronicles.

The abovementioned figures show the high level of risk due to this type of event, especially if one considers a whole series of events which occurred on both the Sarno and Lattari Mountains and

which show a tendency to increase in the last six hundred years. If one considers the number of deaths caused by debris flow (Figure 2.2) the significance of these catastrophic events and the need to reduce the risk becomes clear. This, in turn, demonstrates the importance of understanding well the predisposing and triggering factors and the need to stabilize slopes historically affected by landslides and those potentially affected.

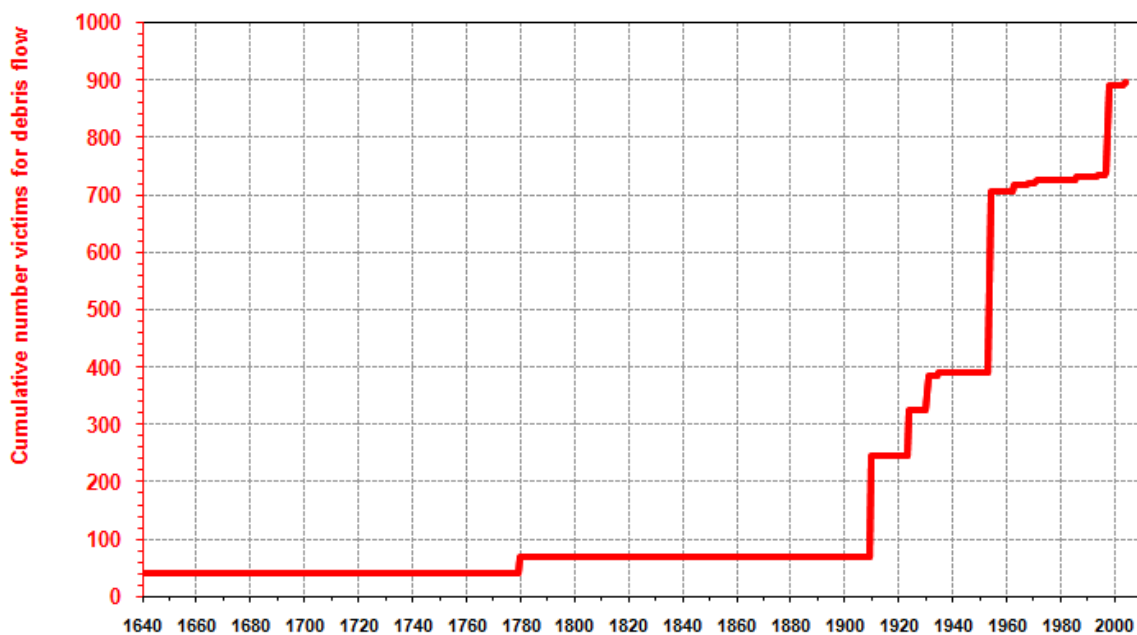


Figure 2.2: cumulative curve, representing number of victims in the Lattari and Sarno Mountains.

2.1.1 Classification of landslide phenomena

Many classifications for landslides were proposed in literature (Sharpe, 1938; Varnes, 1978; Sassa, 1985; Pierson & Costa, 1987; Hutchinson, 1988; Cruden & Varnes, 1996; Hungr et al., 2001) based fundamentally on the type of mechanisms (e.g. slide or flow) and on the type of materials involved (e.g. earth or debris, etc.) rather than on the causes or on geotechnical characteristics. The type of mechanism was considered the principal character of a landslide that can also be recognized by means of a geomorphological analysis, that provides a practical means of identifying and classifying landslides. Thus, a basic discrimination does not concern the nature of the geological materials involved such as cohesive or loose rocks because their physical and mechanical properties can vary significantly. Furthermore, the type of movement, among other characteristics, leads to an easier reading since it is based on the interpretation of morphological characteristics of landslides.

It is necessary at this point to describe the main distinctive morphological and geometric features characterizing a landslide taking into account a cross section of a slope. To better understand the different parts of a landslide, the following nomenclature as proposed by (Working Party on World Landslide Inventory) (1993b) and confirmed by Cruden & Varnes, (1996), can be considered (Figure 2.3). These elements can be defined as:

Crown: is the uppermost sector of the landslide of undisplaced material is adjacent to highest part of main scarp.

Main scarp: is the first vertical scarp in the downstream direction which identifies the nearly undisturbed area around the top part of the landslide, and it is caused by movement of displaced material

Top: highest contact area between the undisturbed material and main scarp

Head: is the upper part of landslide along contact between displaced material and main scarp.

Minor scarp: steep surface produced by relative movements of the displaced material.

Main body: part of displaced material overlying the surface of rupture between main scarp and toe of surface of rupture.

Foot: part of a landslide that moved beyond the toe of surface of rupture and overlies the original ground surface.

Tip: is the portion of material that is moved downstream of the lower edge of the fracture surface.

Toe: is the lower and most distant point from main scarp. It is usually curved.

Surface of rupture: forms or formed the lower boundary of displaced material.

Toe of surface of rupture: intersection between lower part of surface of rupture and the original ground surface.

Surface of separation: is a sector of the original ground surface, now overlain by the foot of the landslide.

Zone of depletion: area within which the displaced material lies below the original ground surface.

Zone of accumulation: area of a landslide within which the displaced material lies above the original ground surface.

Depletion: volume bounded by main scarp, depleted mass and original ground surface.

Depleted mass: volume of displaced material that overlies surface of rupture, but underlies original ground surface.

Accumulation: volume of displaced material lying above original ground surface.

Flanks: undisturbed soil located laterally to the failure surface.

Transverse cracks: due to longitudinal movement of the material and the progressive loss of water from the soil mobilized; they may represent a sign for the evaluation of dormancy or the resumption of the landslide phenomenon.

Area of longitudinal cracks: a morphologically depressed area where runoff water and stagnant groundwater form ephemeral ponds. Here the landslide material due to the different rates of mobilization, proceeds downward resulting in longitudinal fractures between different edges.

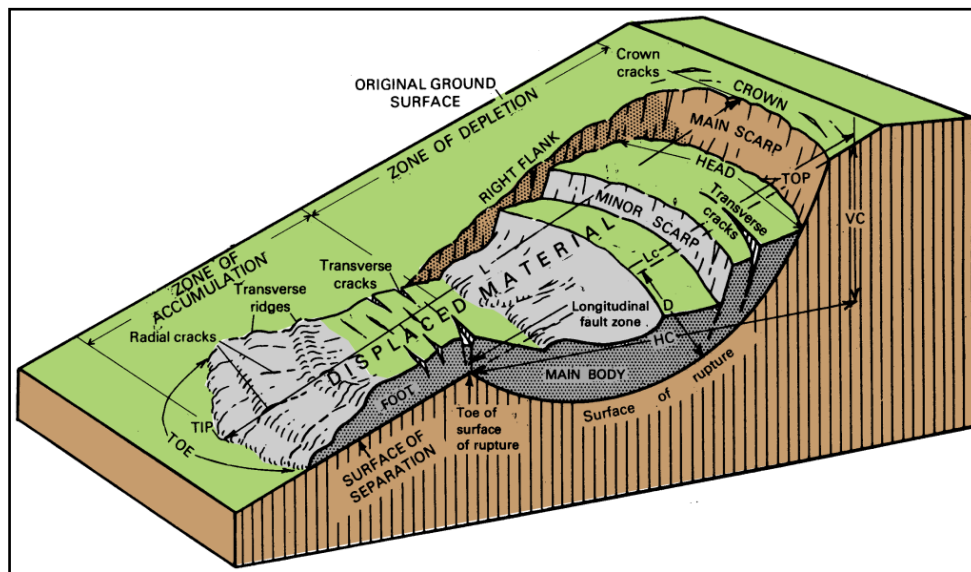


Figure 2.3: simplified cross-section of a landslide (Varnes, 1978).

Landslide phenomena occur in a given area due to the combination of several unfavorable causal factors. It is clear that the determination and control of these factors may be useful to avoid recurrence of the events that cause harm to lives and infrastructures. Following Varnes's (1978) distinction regarding causal factors of a landslide, it is possible to distinguish three main processes:

- Increase in shear stress
- Contribution to low shear strength
- Reduction of material shear strength

As regarding risk, many factors have to be monitored: natural, anthropogenic and geological. It must be taken into account that some factors are characteristic of a slope and remain

stable over the time whereas others must be periodically and continuously checked since they are characterized by extreme variability.

Referring to this observation, landslides can be initiated by natural or anthropogenic factors able to change the existing equilibrium conditions. For this reason, it is necessary to distinguish between predisposing factors, those particular boundary conditions that make a slope more or less susceptible, from the triggering factors that are natural or anthropogenic phenomena altering stability conditions. Among the predisposing factors, it is important to include those remaining almost unchanged over time and which are widely discussed in the bibliography (Cruden & Varnes, 1996 and Wieczorek, 1996):

- Geological and structural factors such as the type of rock, weak, sensitive, weathered, sheared or jointed or fissured materials; presence of fractures or faults, surface layering, adversely oriented structural discontinuity, unconformity.
- Morphological factors, such as tectonic or volcanic uplift, glacial rebound, fluvial erosion of slope toe, wave or glacial erosion of slope toe, subterranean erosion (solution, piping), deposition loading slope, vegetation removal by forest fire.
- Physical factors, such as intense or prolonged precipitations, rapid snow melt, earthquakes, volcanic eruptions, freeze-and-thaw weathering.
- Human causes, such as excavation of slope or its toe, loading of slope or its crest, deforestation, irrigation, mining, artificial vibrations.

The shear strength of rocks and soils is usually the sum of friction and cohesion in different ways according to the conditions in which they are located. Also, a slope rarely appears as inhomogeneous and compact because it is crossed by several fractures, stratification or other surfaces weakness along which virtually only the force of friction operates. In materials whose shear strength is also due to cohesion, failure occurs along more or less regular concave surfaces (“spoon shaped”). On the other hand, materials whose shear strength is due only to friction do not have a true failure surface although there is a settling of particles with the tendency to recreate a surface whose inclination coincides with the friction angle.

Water is usually the most important agent for destabilizing slopes. When soils are saturated, the failure mechanism is more complex and mainly concerns conditions in which over-pore pressure

does not exist (drained condition) or does exist (undrained condition) during deformation. However, since saturation is a factor of great importance for most of landslides, a brief outline is necessary. If one considers the influence on cohesion, water has a minimal destabilizing effect on coherent materials (e.g. rocks or soft rocks) limited to the dissolution of the matrix binding the particles when it has soluble nature, in incoherent materials it has different effects according to the initial conditions. When water is at less than saturation levels it does not completely fill the voids between particles, thus it creates a thin but tenacious film that envelops the particles (capillary meniscuses).

If grain size is fairly small (sand, silt or clay) the water film holds together the particles by electrostatic forces. The smaller the grain size is, the bigger the attraction forces. This phenomenon, which accounts for the capillarity, acts as an increase in shear strength by means of an adjunctive form of cohesion existing only in unsaturated conditions. In fact, when water content undergoes complete saturation there is a complete filling of voids between particles and then the cohesion due to the capillary water bonding soil particles vanishes determining a global decrease of the shear strength. This form of cohesion is called apparent cohesion ¹.

The fundamental landslide classifications, among those considered significant for the comprehension of instability phenomena involving ash-fall pyroclastic cover, are described in the following chronological order. The Varnes' classification (1978) will be omitted because it is largely included and updated in that of Cruden & Varnes (1996).

It is necessary in this context to include, among others, a physically relevant and quantitative classification based on the rheological behavior of materials involved in subaerial flow-like movements (Pierson & Costa, 1987). It is based on the rheological response of a poorly sorted water-sediment mixture to an applied shear stress. The Authors single out, in a two-dimensional matrix, three main thresholds where sediment concentration varies from 0 (clear water) to 100 (dry sediment), depending on sediment concentration (Figure 2.4). The latter is the main feature controlling the rheological behavior of a water-sediment mixture and, to a lesser extent, grain size distribution and physical-chemical features of the particles. The authors indicate sediment-water flows referred to as streamflow and hyperconcentrated streamflow.

A normal streamflow is a Newtonian fluid, defined as a fluid whose stress at each point is linearly proportional to the strain rate at that point and whose viscosity is independent of shear rate.

¹ In this research a special effort was carried out on the comprehension of unsaturated conditions and their effects on shear strength (Chapter IV).

2.1. Landslides phenomena and their classification

In most natural streams fine-grained sediment and bubbles are commonly dispersed in the water; as long as the dispersion is relatively diluted, the sediment particles and air do not interact and the fluid maintains the characteristics of a continuous phase (Van Wazer et al., 1963). Normal streamflow is defined in Pierson & Costa (1987) classification as “flowing water with a sufficiently small sediment concentration that its flow behavior is not affected by the presence of sediment in transport”. As the particle concentration suspended in the mixture increases, the point at which the particles start to interact and the fluid starts to be non-Newtonian acquiring a yield strength, is reached. At this point, the concentration of particles is the same at which the threshold is crossed and it is highly dependent on the grain size distribution.

Hyperconcentrated streamflow is a flowing mixture of water and sediment possessing a measurable yield strength but which appears as to flow like a fluid (Figure 2.4).

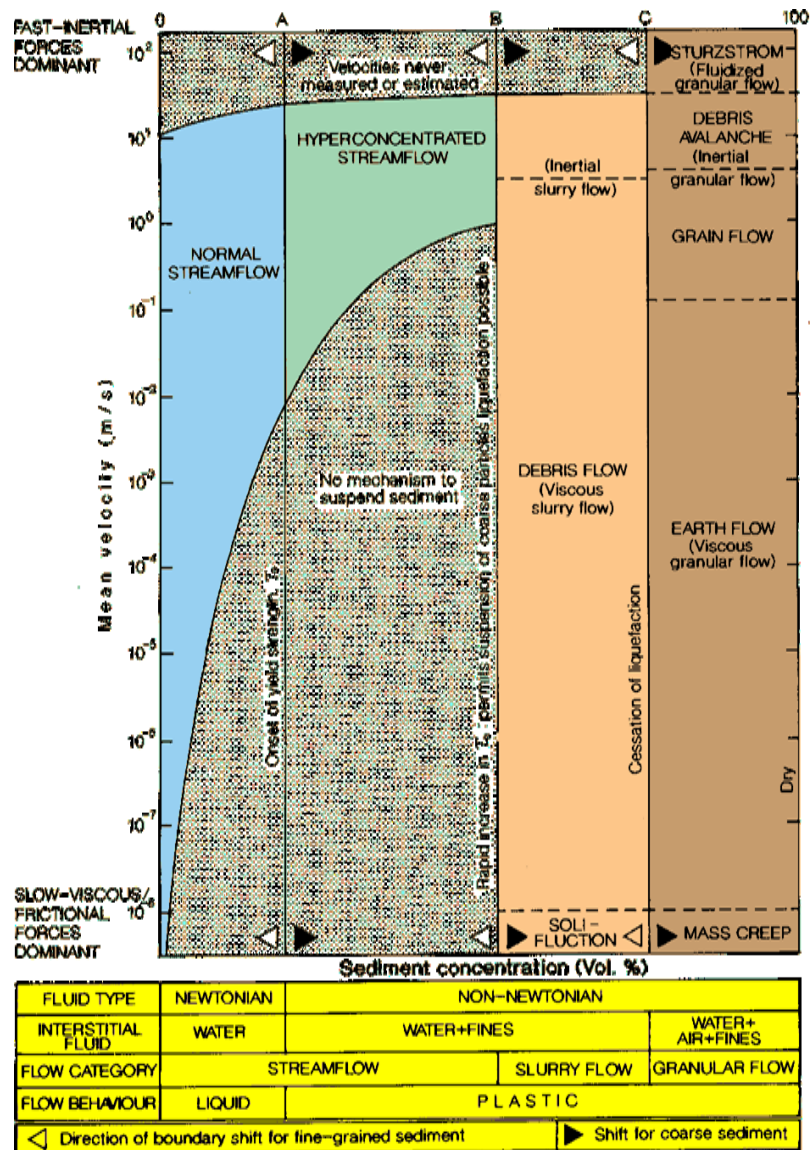


Figure 2.4: rheologic classification of sediment-water flows (modified after Pierson & Costa, 1987).

One of the main classifications of slope movements was carried out by Hutchinson (1988), and mainly regards the morphology of slope movements which are strongly related to specific geological, morphological and hydrogeological frameworks as well as geotechnical features of materials involved in landsliding. This classification is based on the previous work of Hutchinson (1968), Skempton & Hutchinson (1969), and in particular that of Varnes (1978). Among different types of mass-movement recognized by the author it is fundamental to focus on the “flow-like” movements category in which landslides occurring in pyroclastic cover can be classified. The main criteria of classification are based on the type of material involved, the morphology and the type of failure surface. The main types of mass-movements identified by the author are listed below.

- A) Rebound, corresponding to deformation of the ground caused by natural (e.g. erosion) or artificial (e.g. excavation) unloading. In this case, the deformation can be considered as a partial recovery of the original deformation due to the natural loading (e.g. deposition of sediments) that can occur either with elastic (hard soils and rocks) or swelling (clay) mechanisms.
- B) Creep, corresponding to extremely slow movements, which can be recognized only in long periods of observation. It can be differentiated in three types.
 - 1) Superficial creep, corresponding to extremely slow downslope movement of fine-grained regoliths, also known in non-periglacial climates as soil creep and due moisture change of soils to frost. It can occur also in periglacial climates, also involving coarser materials.
 - 2) Deep-seated, mass creep, due to viscous behaviour of materials when subject to a constant stress during time.
 - 3) Pre-failure creep, consisting in accelerating viscous deformations preceding the global failure of slopes.
- C) Sagging of mountain slopes, corresponding to enormous mass-movements involving whole mountain slopes and recognizable by morphological effects more than on actual measurements. This category can be also considered as intermediate between mass-movements due to tectonics and gravity.
- D) Landslides, consisting in relatively rapid down-slope movements of soil and rock, which characteristically take place on one or more discrete bounding slip surfaces which define the moving mass. This category can be differentiated in the following sub-classes.

- 1) Confined failures that may occur on natural or man-made slopes. They do not produce a continuous and outcropping failure surface, because the displacement is not sufficiently developed (Figure 2.5a).
- 2) Rotational slips occurring in thick homogeneous deposits of silt or shale, granular materials or closely jointed rocks where pore-water pressure is high enough to generate a rotation, rather than translational failure. This type of instability occurs with a moderate speed and are discriminated in the following:
 - i) Single rotational slips, with a single and concave upward slip surface. This type form can also occur as a sequence of shallow or moderately deep-seated rotational slips (successive rotational slips), that are typical of freely degrading cliffs or fissured clays.
 - ii) Successive rotational slips, consisting in a succession of shallow rotational slips, arranged approximately head to toe up a slope and usually of retrogressive habit.
 - iii) Multiple rotational slips, that is the retrogression of a single rotational slip that causes the formation of more slipped blocks. They are typical of situations where relatively thick layers of clays or shale are sub-horizontal and are underlain by a more competent stratum (Figure 2.5a).
- 3) Compound slides, that are an intermediate type forms between rotational and translational failures, and are characterized by a non-circular slip surface. They can be released by internal shearing. If the material is of low-medium brittleness, the failure velocity is moderate and the slip surface is lystric or bi-planar (Figure 2.5a).
- 4) Translational failures characterized by planar surface, are discriminated in: sheet slides, that is very shallow translational failures, affecting dry and cohesionless materials (Figure 2.5b). Slab slides in coherent but unlithified materials (Figure 2.5b). Peat slides, in homogeneous cover (Figure 2.5a), rock slides with a planar slip surface, involving rocks with discontinuities, such as joints, cleavage or foliation planes filled by clayey material (Figure 2.5b).

2.1. Landslides phenomena and their classification

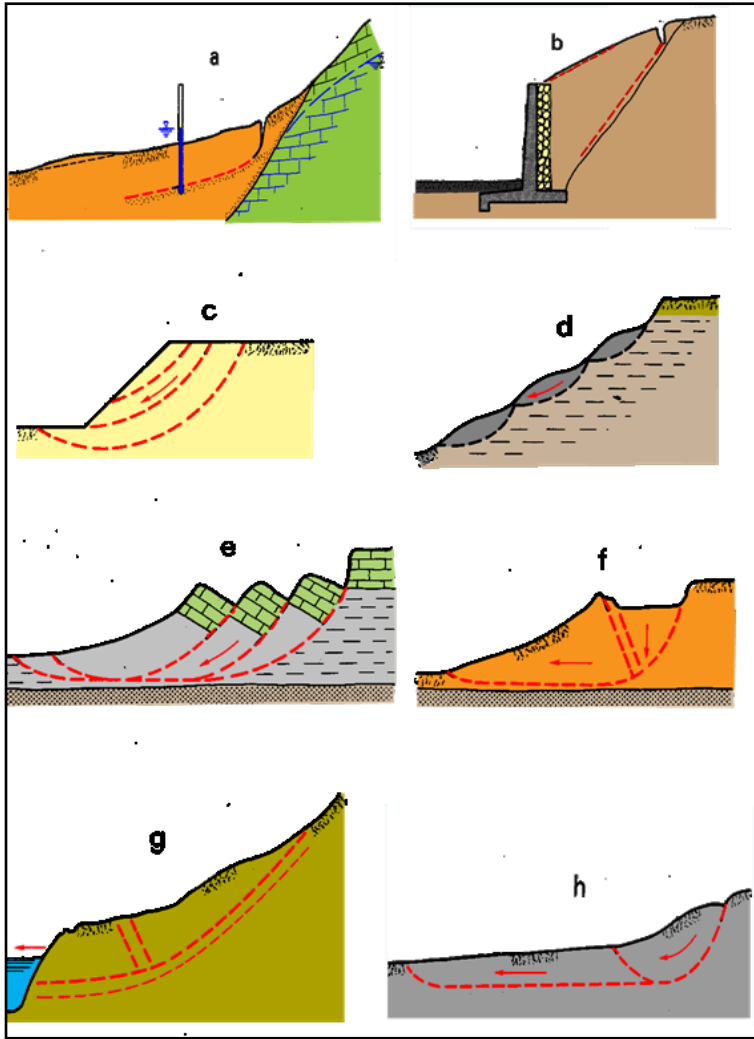


Figure 2.5a: confined failures: (a) in natural slopes, (b) in man-made slopes; rotational slips: (c) single, (d) successive, (e) multiple; compound slides: (g) released by internal shear, (h) progressive slides (Hutchinson, 1988).

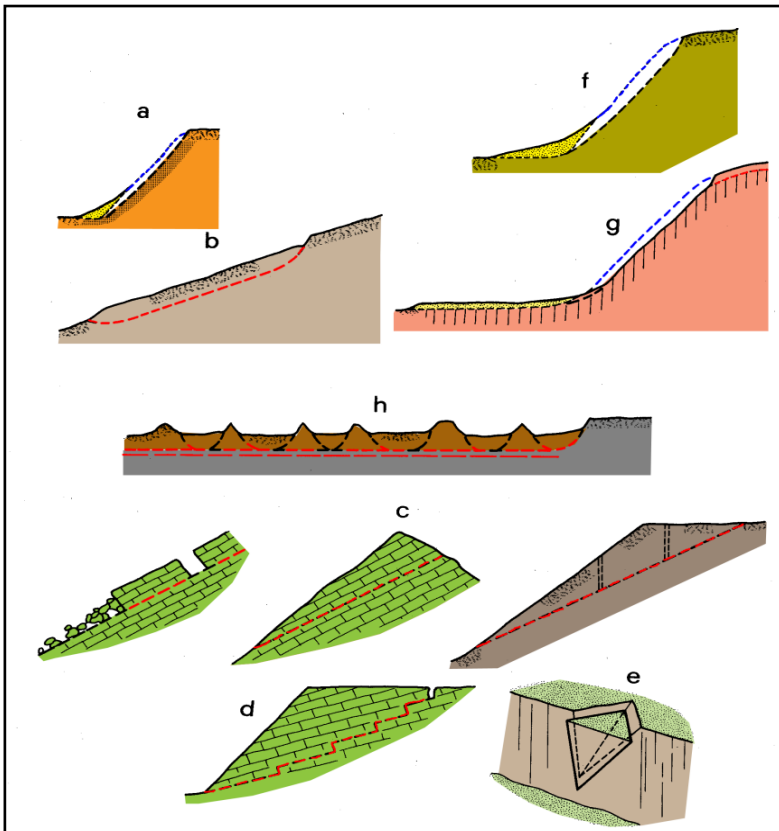


Figure 2.5b: (b) main types of translational failures ©(a) shear slides, (b) slab slides, (f) slab of debris, (g) active layer slide; rock slides (c) planar slides, (d) stopped slides, (e) wedge failures (Hutchinson, 1988).

- 5) Debris movements of flow-like form that differ in the type of movement.
- 6) Mudslide is mostly a slide rather than flow, is slow-moving and involves soft clay (Figure 2.6). Longitudinal profile is generally steeper in the back part of the slope and less inclined in the downstream part where debris accumulates. Mudslides (Figure 2.6) are distinguished in periglacial and non-periglacial: the latter are slow-moving masses of accumulated debris in a softened clayey matrix. Periglacial mudslides arise from periglacial solifluction, previously described by Hutchinson & Bhandari (1971).
- 7) Flow slides have a varying degree of sliding and flowing in loose cohesionless materials, lightly cemented silts, high porosity, weak rocks; they are characterized by a sudden collapse and extensive, very to extremely rapid run-out. Due to some disturbance, the overburden load is partially or fully transferred to the pore fluid where overpressures are generated. The loss of strength gives the falling material a semi-fluid character thus allowing a flow slide to develop (Figure 2.6). An important mechanism in debris flow is the generation of excess of pore pressures both in water or air. The consequent loss of strength gives the falling material a semi-fluid character and allows a flow slide to develop (Figure 2.6). The pore fluid is usually water, but in some circumstances can be also gaseous. In this connection Casagrande (1971) suggested for “Flow slides” the terms “liquefaction slides” and “fluidization slides” (Hutchinson 1988).
- 8) Debris flow also has a slide and flow mechanism and is very to extremely rapid wet debris. It can involve loose, cohesionless materials, fine sand, lightly cemented and high porosity silts and weathered rocks. This kind of slope movement is associated with mountainous areas where a sudden access of water can mobilize debris mantling slopes.
- 9) Sturzstroms are extremely rapid flows of dry debris (Figure 2.6). Some large rockslides and rockfalls transform into high-speed streaming flows of debris called “sturzstroms” by Heim (1932). In fact, these types of flows reach velocities of about 30 m/s. The motion of sturzstroms depends on turbulence of grain flow with upward transfer due to momentum of the collision of grains; this mechanism may explain the sturzstrom-like features on the moon.

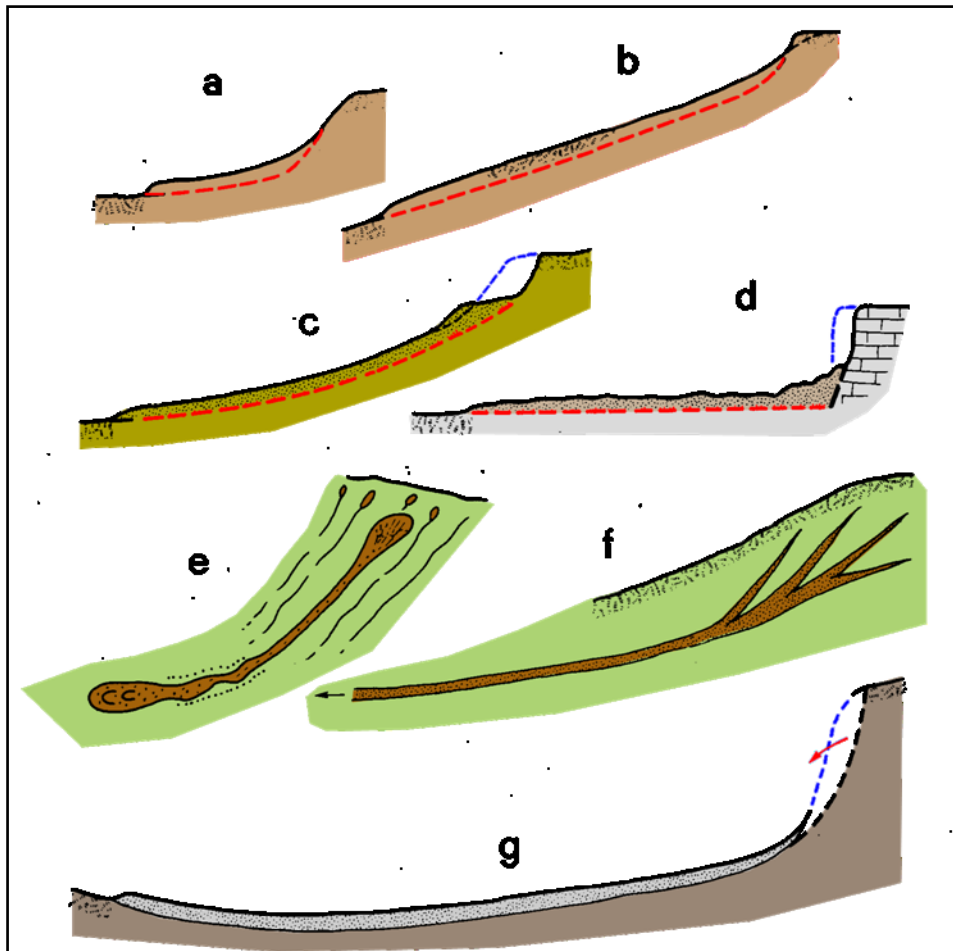


Figure 2.6: main types of debris movement of flow-like form: mudslides (a) and (b); flowslides (c) and (d); debris flow (e) and (f); sturzstrom (g)(Hutchinson, 1988)

- E) Topples occur when the resultant vector of applied forces falls through or outside a pivot point in the base of the affected block. The Author distinguishes between topples bounded by pre-existing discontinuities and topples released by tension failure in previously intact material (Figure 2.7).
- F) Falls comprise the more or less free and extremely rapid descent of masses of soil or rock of any size from steep slopes or cliffs. They were considered as primary when bonds between prone-to-instability blocks and soil or rock mass are broken. Moreover, a secondary category of falls which occur by means of the mobilization of unbounded blocks is considered.
- G) Complex slope movements when two or more of the abovementioned types of slope movement are combined to form a complex movement (Varnes, 1978).

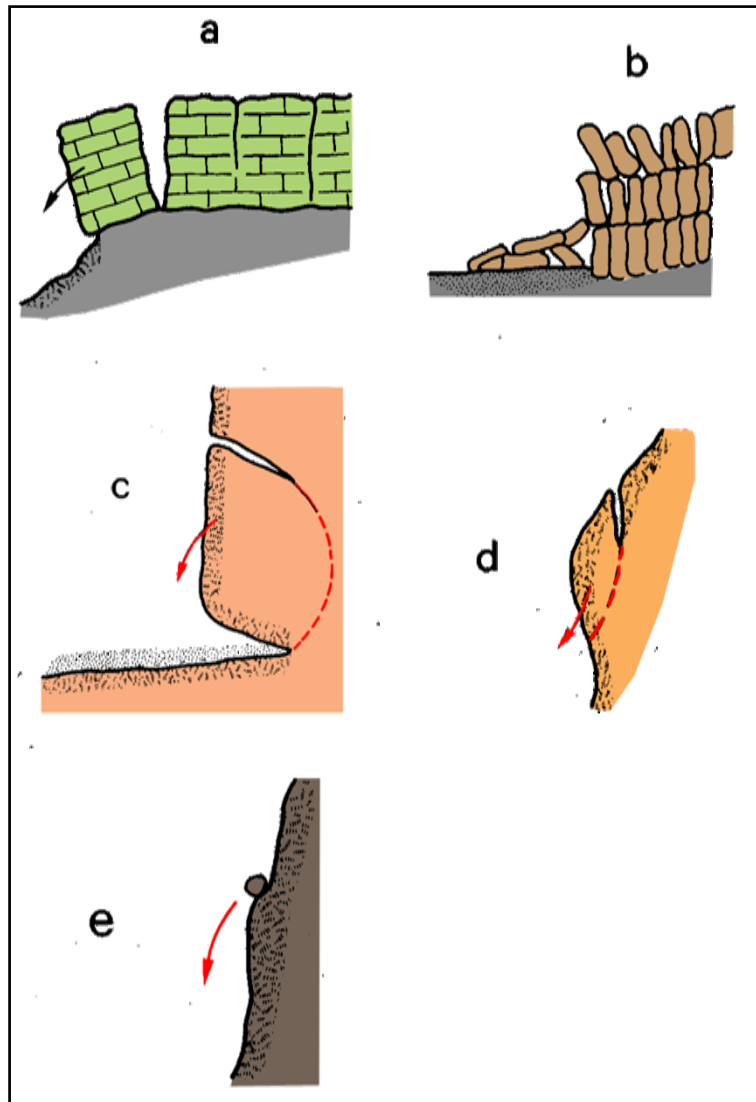


Figure 2.7: main toppling and falls: bounding by pre-existing discontinuities: (a) single, (b) multiple; released by tension failure at rear (wave cut notch at the bottom) (c); falls: (d) primary, rock and soils falls, (e) secondary, stone falls (Hutchinson, 1988).

Another classification that is important to consider in this introductory chapter is the one proposed by Cruden & Varnes (1996). It is important because it considers parameters introduced for the first time, such as water content of unstable mass, and reconsiders velocity classes as proposed in the previous classification of Varnes (1978), thus taking in account movements ranging from extremely slow to extremely rapid (Table 2.1).

The classification proposed by Cruden & Varnes (1996) is based on two main features and basically combines *movement and material type* terms. It enables an appropriately descriptive

2.1. Landslides phenomena and their classification

landslide name to be formulated. Description can be more detailed with the addition of other descriptive features related to activity state, style, distribution of movements, water content and rate of movement if known (e.g. *active, complex, extremely rapid, dry rock fall-debris flow*). Only a small selection of the wide spectrum of landslide types that may develop in nature are shown below (Figure 2.8).

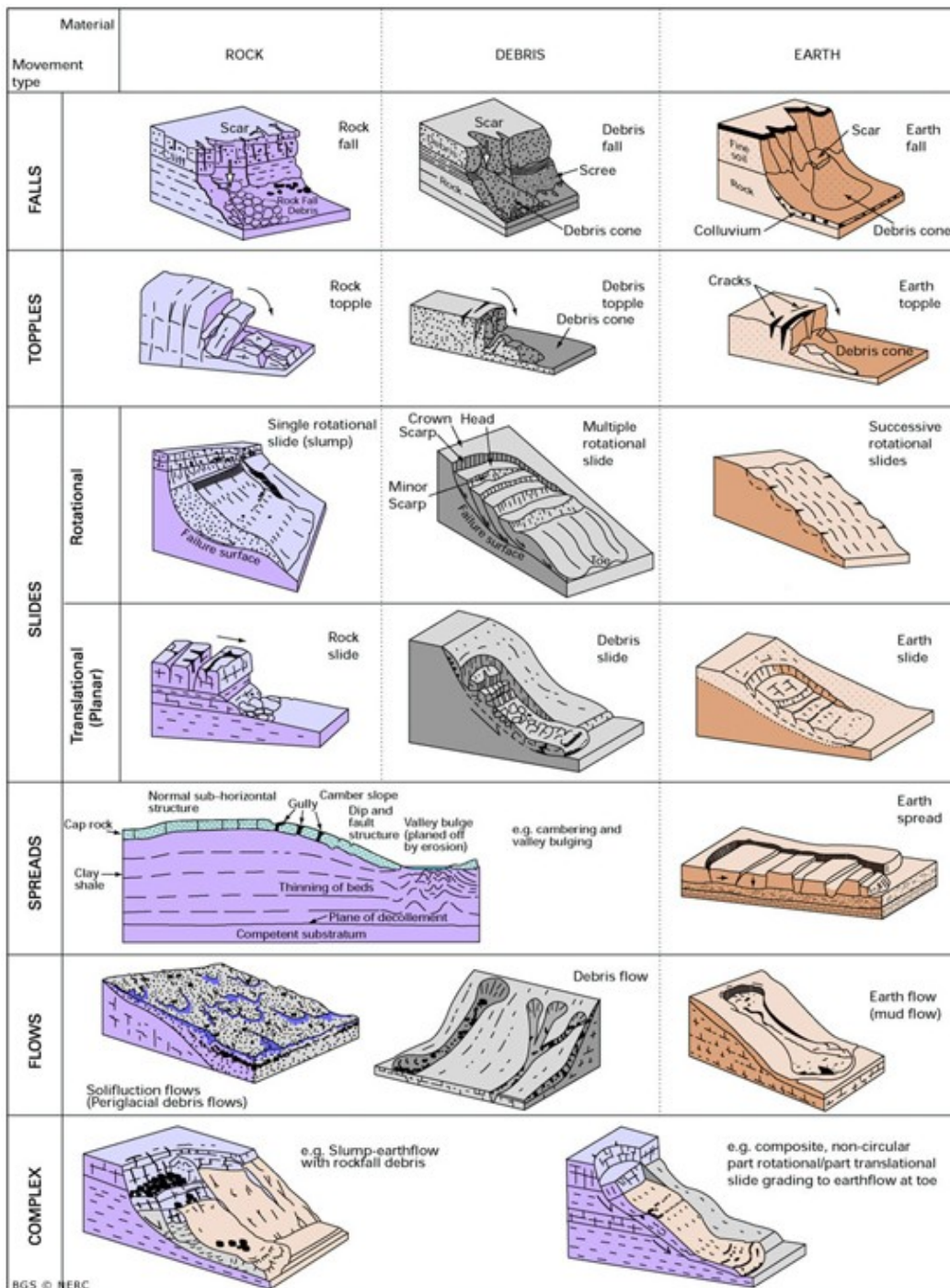


Figure 2.8: scheme terminology is also suggested by the UNESCO Working Party on the 'World Landslide Inventory (WP/WLI 1990, 1993a) (http://www.bgs.ac.uk/science/landUseAndDevelopment/landslides/How_does_BGS_classify_landslides.html).

| VELOCITY CLASS | DESCRIPTION | VELOCITY | Typical velocity |
|----------------|------------------------|----------|------------------|
| 7 | extremely rapid | 5.00E+00 | 5 m/sec |
| 6 | very rapid | 5.00E-03 | 3 m /min |
| 5 | rapid | 5.00E-04 | 1.8 m/hr |
| 4 | moderate | 5.00E-06 | 13 m/month |
| 3 | slow | 5.00E-08 | 1.6 m/year |
| 2 | very slow | 5.00E-10 | 16 mm/year |
| 1 | extremely slow | - | - |

Table 2.1: Landslide velocity after Cruden & Varnes (1996).

In addition, the classification introduces velocity (based on a quantified scale) and moisture content that is used for a second order of subdivision. A distinctive feature of a landslide and certainly much considered by many authors is the type of movement. It is detectable to a high degree of accuracy and with little margin of error by surface observations and analysis of aerial photographs. It refers to relative motion between the landslide body and the material not mobilized. As regards the nature of the involved material, a distinction made for landslides classification regards lithotypes with cohesion due to hardening material with resistance to simple compression > 25 MPa (rocks) and lithotypes with friction behavior and possible presence of cohesion (earths). Soils are further distinguished as regards debris when the fraction of gravel ($\emptyset \geq 2$ mm) is greater than 20% and fine earth (earth) when the gravel fraction is lower than 20%, topples, rotational slides (slumps), translational (planar) slides, spreads, flows and complex slides (Figure 2.8).

In general, the state, distribution and style of a landslide activity is also defined:

- The state of activity describes what is known about chronology of movement. The activity of a landslide is described as: active, reactivated, suspended (landslides that moved within the last annual cycle, but not at the present), inactive (quiescent), inactive (naturally or artificially stabilized), inactive (relict) (WP/WLI, 1990, 1991, 1993).
- The distribution of activity is how the landslide evolves and in which direction, thus allowing classification of landslides in function of their evolution: advancing, retrogressive, widening (surface of rupture extends at one or both margins), enlarging (surface of rupture enlarges, continually adding to the volume of displaced material - Hutchinson, 1988) diminishing (volume of material displaced is decreasing with time)

and confined landslides (movements that have a scarp, but not visible rupture surface at the foot of the displaced mass (Hutchinson, 1988).

- The style of activity indicates that different movements within a landslide may contribute to its total movement. It can be composite (different types of movements occur in different areas simultaneously), multiple (repeated movement of the same type), successive (type of movement is the same, but the displaced mass or rupture surface are not the same), single (single movement of material, often as unbroken block).

Finally, as shown in the figure below the classification of a landslide can be made by rules based on the state of activity, distribution, style, velocity, water content, material and type of movement. This type of succession can be repeated in the case of complex landslides (Figure 2.9).

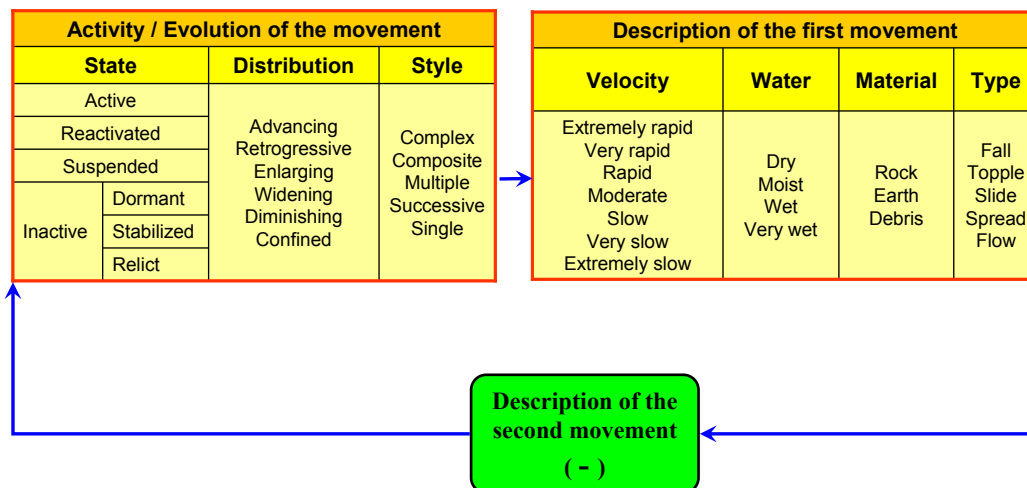


Figure. 2.9: rules to be respected for classification of a single movement type or complex landslide (Cruden & Varnes, 1996). The cycle can be repeated more times in the case of complex landslides characterized by more than two type of movements.

Finally, it is necessary to mention a more recent classification of landslides of the flow-type (Hungr et al., 2001) that relates the involved materials, the water content, special conditions and velocity of the landslide to get the formulation of a unique nomenclature for several landslides (Table 2.2). The authors also deal with correspondence of three different classifications (Table 2.3): Varnes (1978), Hutchinson (1988) and that of Hungr et al, (2001).

2.1. Landslides phenomena and their classification

| Material | Water Content ¹ | Special Condition | Velocity | Name |
|--|--------------------------------------|---|--------------------|--|
| Silt, Sand, Gravel, Debris (talus) | dry, moist or saturated | - no excess pore-pressure, - limited volume | various | Non-liquefied sand (silt, gravel, debris) flow |
| Silt, Sand, Debris, Weak rock ² | saturated at rupture surface content | - liquefiable material ³ , - constant water | Ex. Rapid | Sand (silt, debris, rock) flow slide |
| Sensitive clay | at or above liquid limit | - liquefaction <i>in situ</i> , ³ - constant water content ⁴ | Ex. Rapid | Clay flow slide |
| Peat | saturated | - excess pore-pressure | Slow to very rapid | Peat flow |
| Clay or Earth | near plastic limit | - slow movements, - plug flow (sliding) | < Rapid | Earth flow |
| Debris | saturated | - established channel ⁵ , - increased water content ⁴ | Ex. Rapid | Debris flow |
| Mud | at or above liquid limit | - fine-grained debris flow | > Very rapid | Mud flow |
| Debris | free water present | - flood ⁶ | Ex. Rapid | Debris flood |
| Debris | partly or fully saturated | - no established channel ⁵ , - relatively shallow, steep source | Ex. Rapid | Debris avalanche |
| Fragmented Rock | various, mainly dry | - intact rock at source, - large volume ⁷ | Ex. Rapid | Rock avalanche |

¹ Water content of material in the vicinity of the rupture surface at the time of failure.
² Highly porous, weak rock (examples: weak chalk, weathered tuff, pumice).
³ The presence of full or partial *in situ* liquefaction of the source material of the flow slide may be observed or implied.
⁴ Relative to *in situ* source material.
⁵ Presence or absence of a defined channel over a large part of the path, and an established deposition landform (fan). Debris flow is a recurrent phenomenon within its path, while debris avalanche is not.
⁶ Peak discharge of the same order as that of a major flood or an accidental flood. Significant tractive forces of free flowing water. Presence of floating debris.
⁷ Volume greater than 10,000 m³ approximately. Mass flow, contrasting with fragmental rock fall.

Table 2.2: classification of landslide of flow type (Hungr et al., 2001)

| Varnes (1978) | Hutchinson (1988) | Hungr et al. (2001) |
|----------------------|------------------------|------------------------|
| Wet, sand, silt flow | Flow slide | Sand, silt, flow slide |
| Rapid earth flow | Flow slide (clay) | Clay flow slide |
| Loess flow | Flow slide (loess) | Loess flow slide |
| Dry sand flow | - | Dry sand flow |
| Earth flow | Mudslide | Earth flow |
| - | Mudflow | Mudflow |
| Debris avalanche | Hillslope debris flow | Debris avalanche |
| Debris flow | Debris flow | Debris flow |
| - | Hyperconcentrated flow | Debris flood |
| Rock avalanche | Sturzstrom | Rock avalanche |

Table 2.3: correspondence between different classifications (from Hungr et al., 2001).

2.1.2. Landslides types on peri-vesuvian hillslopes

Due to their catastrophic nature and geological peculiarity, these landslides were of great interest to the scientific community since the '70s (De Riso and Nota D'Elogio, 1973) and especially after the catastrophic events of May 5th and 6th 1998 after which several hundred papers, employing different methodologies were published. These landslide events affected areas of five towns in the Campania region (Bracigliano, Siano, Quindici, Sarno) causing serious damage and great loss of lives. The consequent crisis provoked by the event highlighted the necessity of beginning a series of scientific activities coordinated by the National Group for Defense from Hydrogeological Disasters (GNDCI) and aimed at emergency management,

The main research was aimed at resolving important issues regarding the identification of the extent of the areas potentially affected by further landslides. Additional aims were the establishment of a threshold value of rainfall for the temporary evacuation of the population and the identification of guidelines for control and safety of areas at risk.

It is also important to assess risk due to debris flow in the whole of Campania. Results of studies conducted in the area are in agreement with a preliminary evolution model of the slope at the mountain relief scale. It is based on geological, geomorphological and hydrogeological analyses and on analyses of historical events that in the last century affected the Pizzo D'Alvano area and, in particular, the five towns affected by the May 1998 flowslides.

The historical analysis of previous landslides events was carried out in order to better understand the spatial and temporal distribution of the landslides. It was based on the analysis of thematic maps produced between the 18th century and the present combined with the study of the urban growth of the municipalities involved in the disaster. A very important factor in specific risk assessment ($R_s = P \times V$) in addition to the magnitude of the event is also the occupation of areas not suitable for urban development (UNESCO, 1972, WP/WLI 1993b). This observation becomes important when considering that, starting from the reconstruction of the municipalities after the war and continuing to the present and due to the lack of guidelines for urban growth, there was a gradual urbanization of areas previously used for other purposes and this growth moved progressively closer to the effluent of mountain basins.

Field investigations were also carried out in order to prepare thematic maps on a large scale (1:5000 and 1:2000) such as "incipient instability map", "pyroclastic cover thickness map", "litho-structural map". Topographical surveys, together with the interpretation of aerial photos, were

fundamental to acquiring data over the entire area of study and for the creation of detailed thematic maps used to assess the volumes involved in the initiation phase flowslides May '98.

Based on past scientific achievements, one can define these mass movements more generally known by the term debris flow. They can also be considered as *landslide triggered debris flows* (*sensu* Hungr & Jacob, 2006) and may propagate with high speed downstream and increase their volume with complex mechanisms. To understand better the characteristics and the kinematics of debris flow, they should be defined in the following way:

- An initial stage, where the initial slide, also classifiable as soil slip (Campbell, 1975), involves small volumes of pyroclastic soils with a gravel content greater than 20% (debris) and defined as *debris slide* (Cruden & Varnes, 1996).
- An intermediate stage of *debris avalanche* (Hungr et al., 2001, Fiorillo et al., 2001) in which the mass mobilized by the slide impacts downstream on terrains close to saturation determining its liquefaction due to undrained loading mechanism (Hutchinson & Bhandari, 1971, Sassa, 1985). This flow involves increasing volumes of soil with a mechanism quite similar to an avalanche (Figure 2.10), expanding on an open slope and assuming a typical triangular shape.
- A final stage, which does not always exist, namely *debris flow*, occurring when the flow is channeled into the existing hydrographic network (Hungr et al., 2001).

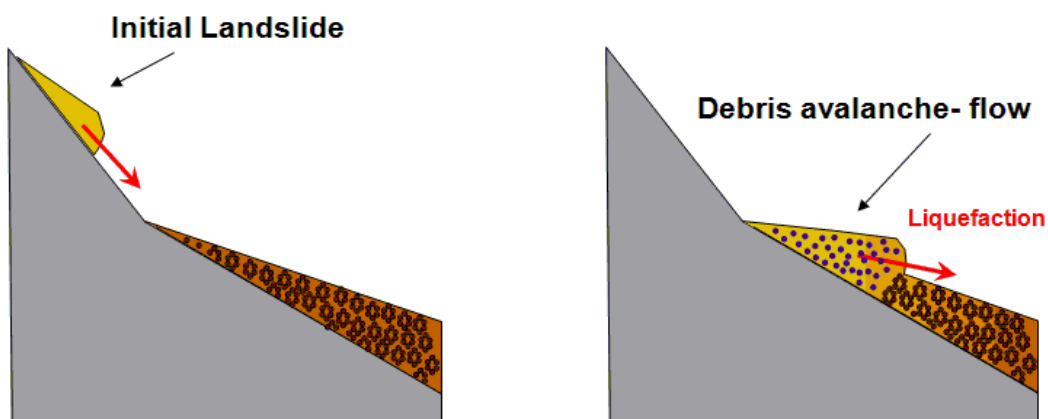


Figure 2.10: Landslides triggered debris flow (after Hutchinson & Bhandari, 1971; Sassa, 1985).

With regard to the stages following the first, according to Cruden & Varnes (1996), the rate of movement varies from rapid to extremely rapid and the propagation takes place far away from source areas. These types of landslides are characterized by high mobility (Corominas, 1996). The sequence of phases can be differentiated according to the morphological conditions of the slope and to the presence of pyroclastic cover. The initial slide may evolve directly into channeled flow (debris flow), or to an avalanche (debris avalanche). The initial stage of sliding is always present and can be regarded as the trigger of the following phases.

The problem of transition from soil slip to debris flow of complex landslides was analyzed in detail by several authors starting from the eighties. Particular attention should be given to the issue regarding the mobilization of debris flows. Many qualitative hypotheses were advanced to explain debris flow mobilization and a quantitative model was formulated by some authors (Iverson, 1997).

Field observations, laboratory experiments, and theoretical analyses indicate that landslides may mobilize to form debris flows by means of three processes: *a*) widespread Coulomb failure within a soil mass; *b*) partial or complete soil liquefaction by high pore-fluid pressures that may cause or accompany Coulomb failure, and *c*) conversion of landslide translational energy to internal vibrational energy (i.e. granular temperature). These processes can operate independently, but in many circumstances they appear to operate simultaneously and synergistically. Early work (e.g. Johnson & Rahn, 1970; Rodine 1974; Takahashi 1978) on debris-flow mobilization described a similar interplay of processes but excluded pore-pressure effects that cause soil liquefaction (Iverson et al., 1997). Besides, most landslides that mobilize to form debris flows are triggered by increased pore-water pressures associated with rainfall, snowmelt, or groundwater inflow from adjacent areas. If soil pore space throughout the landslide mass is saturated or nearly saturated at the time of slope failure, the potential for debris-flow mobilization is increased.

Regarding the terminology used in this thesis, it should be specified that “initial landslide” represents the first stage of evolution of these complex phenomena (soil slip) that is dealt with in some detail in this section. The research concerns the triggering mechanisms of initial landslides constitute the specific topic of this research.

The area historically most involved in debris flow is the Campanian carbonate ridge close to eruptive vents of the Somma-Vesuvius, the Phlegrean Fields and the Ischia Island belonging to the Sarno, Lattari and Salerno Mountain Ranges. These reliefs often have slope angle values ranging from 30° to 35° up to 90 degrees and, during the different volcanic eruptions which occurred during

Pleistocene and Holocene, these slopes were covered by ash-fall pyroclastic deposits that strongly influenced their stability. Indeed, they were often affected by debris flows activated as a result of intense hourly / daily meteorological events, and especially if preceded by rainy periods of days or months.

These kinds of high speed, highly destructive landslides occur without warning signs on steep slopes. In addition, flows may develop on “regular” slopes without incisions where “unchannelled landslides” take place (Figure 2.11). Along slopes etched by one or more watersheds on the other hand, “channeled landslides” may develop in a torrential head for example (Di Crescenzo & Santo 2005).

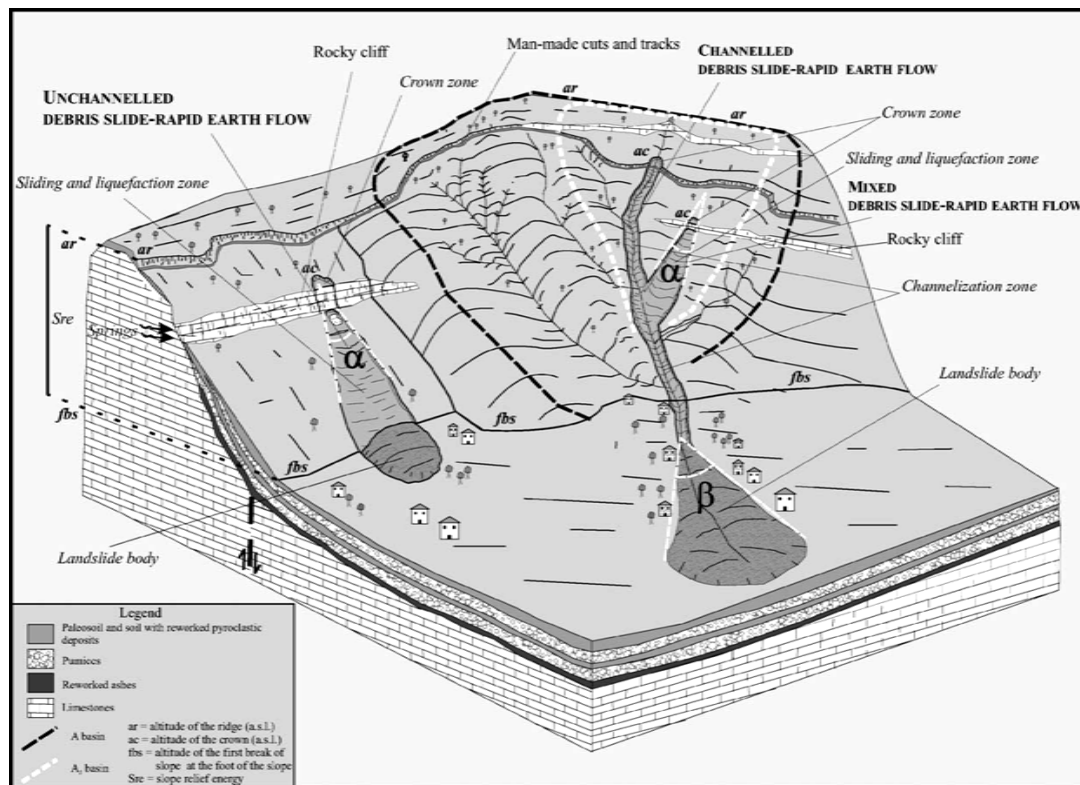


Figure 2.11: scheme of the main morphological and morphometric parameters concerning slips of debris/ rapid earth flow (Di Crescenzo and Santo, 2005).

In order to investigate the role played by pumiceous lapilli in the triggering mechanisms of the initial landslides, detailed surveys were carried out in the source areas of some of the most relevant debris flow which occurred in the main carbonate contexts of Campanian region (Di Crescenzo & Santo, 2005). The authors use the term “detachment area” or “crown”, meaning the highest sector of landslide which includes two distinguished areas (Figure 2.12).

- The area of “first break” is often localized at a road cut or on top of a rocky cliff and is characterized by very high steep slopes (ranging from 35° to 45°). Slide often involves few m³ of material and may be due to fall or sliding that can have a translational or a rotational component (Di Crescenzo & Santo, 2005).
- “Planar sliding zone”: is placed immediately in the downstream area of first break, with steepness values mostly between 25° and 35°. In this case, large volumes of volcanoclastic deposits are involved. In this zone, the landslide mass is subjected to a liquefaction process (Olivares et al., 2002) and intensifies downstream (Di Crescenzo & Santo, 2005).

Stratigraphical differences between the two zones cannot be neglected since derivation of stratigraphy in the detachment area of the landslide in most of the case studies show a limited presence and thickness of pumiceous levels. The failure surface in this area is almost always settled into one of the interposed paleosoils between the several eruptions.

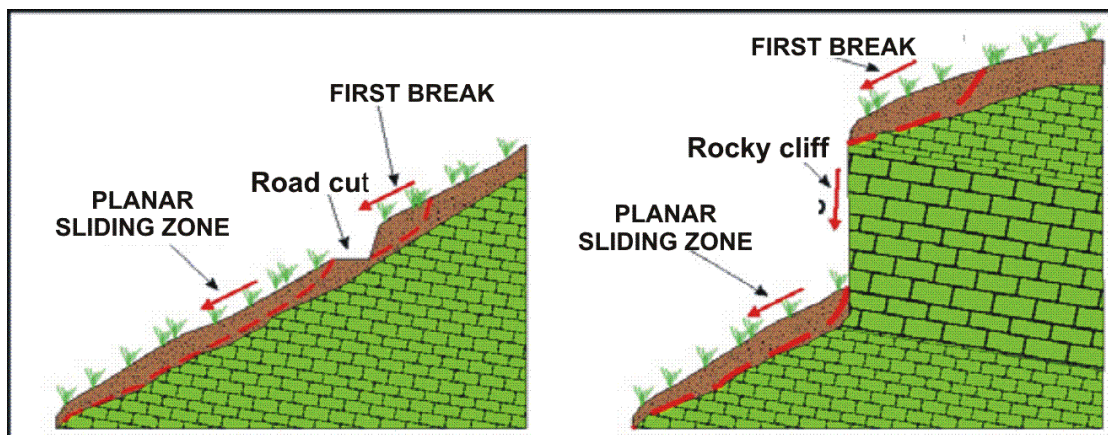


Figure 2.12: detachment area, distinction between “crown zone” and planar sliding (Di Crescenzo and Santo, 2005).

Areas affected by planar sliding zone on the other hand, are located where wide layers of pumice are present. They're attributable, depending on Campanian contexts, either to *79 AD eruption* (Lattari - Sorrento Peninsula), or *Mercato eruption* (Pizzo D'Alvano - Sarno and Bracigliano sides), or *Avellino eruption* (Pizzo Alvano - Quindici-side), or *Agnano-Monte Spina eruption* (Avella Mountain-Cancello) or *Avellino eruption* (Partenio Mountains).

Often, a morphological separation between the detachment area and the planar sliding zone is present due to lithological discontinuities or road cuts (Figure 2.12), but in some cases

morphological continuity exists and it is not always easy to make a clear distinction. Important differences were also found (Di Crescenzo e Santo, 2005) in slope steepness which are generally greater than 35° in the detachment zone and lower ($28^\circ - 35^\circ$) in the planar sliding zone. Initial slides usually involve limited volumes and may have different origins - mostly from collapse or sliding (mainly translational and rarely with a rotational component). They play a key role since they act as a "detonator" for the development of a successive portion, sliding over a broader planar surface, which develops in most cases at the base or within an extensive and continuous pumice level. In the different stages of a debris flow Di Crescenzo & Santo (2005) discriminate a first phase of impact on the underneath slope against a further phase of planar slip and liquefaction and channeling of landslide mass. The pumice horizons play an important role in influencing the planar sliding and, consequently, the phase of "areal enlargement" of the landslides. Indeed, in the sectors of slope where these conditions do not exist or where pumice levels are not widespread the landslide tends to stop near the source.

In conclusion, the study showed that, especially for analyses aimed at defining landslide susceptibility, it is very important to understand the triggering mechanisms of debris flows. It is also essential to define the geomorphological and stratigraphic features of the areas located downstream of the possible initiation zones. Indeed, the pumice levels may greatly facilitate translational slide, liquefaction and amplification phases rather than influence the triggering mechanism. In conclusion, it is possible to state that these landslides are quite complex and characterized by different evolutionary phases which can be summarized as follows:

- First break (soil slide or fall).
- Impact on the underneath slope (in case of fall or rapid overthrust).
- Liquefaction, and propagation on open slopes with avalanche mechanism (depending on slope morphology).
- Channeling of the flow (depending on slope morphology).

Also other studies, e.g. (Cascini, 2004) carried out by means of a geotechnical approach, highlighted that the failure planes are generally located within pumice levels. Moreover, they showed that the phases of liquefaction and spreading of pyroclastic soils involved in the landslide are greatly influenced by the porosity of the medium and therefore by the amount of sandy-pumice levels. In this study, starting from these assumptions and after initial careful bibliographical

analysis, detailed surveys of the pumice horizons nearby the source areas of the landslides were carried out.

Different researchers that studied such a type of landslide used different terminology for their classification ranging from rapid earth flow to debris flow and to flowslides. However, such varied points of view are becoming much less so in recent years being now limited to two basic interpretations: flowslide (Cascini et al., 2003; Olivares et al., 2003; Picarelli et al., 2004; Bilotta et al., 2005), *sensu* Hutchinson (1988) and Hungr et al. (2001), meaning an undifferentiated mechanism of sliding and flow involving very loose and close to saturation pyroclastic soils and debris slide – debris avalanche – debris flows, (Fiorillo et al., 2001; Di Crescenzo & Santo, 2005; Guadagno et al., 2005), *sensu* Cruden & Varnes (1996), Hungr et al. (2001) and Jakob and Hungr (2005). This research followed the second type of classification, thus allowing the differentiation of the evolutionary stages of a landslide and their analysis. The first stage of these complex landslides was named “initial landslide” in this work .

2.2 Morphological factors of slopes controlling susceptibility of initial landslides and propagation along the slopes

Field surveys and observations carried out by some researchers in the initiation areas of the landslides which occurred on 5th and 6th May 1998 in the Sarno Mountains (Celico & Guadagno, 1998; Crosta and Dal Negro, 2003; Guadagno et al., 2005; Di Crescenzo and Santo, 2005) pointed out that there are many morphological factors triggering initial landslides. Among these, natural and artificial morphological factors were recognized. One of the most recurrent factors, among the others is road cuts or abrupt lithological interruptions that, by breaking off the continuity of the pyroclastic cover, might favor unstable conditions (Celico & Guadagno, 1998).

Landslide initiation in uphill areas of the Pizzo D'Alvano slopes show rather complex kinematics; they are classified as debris slide (soil slip). According to the authors, the main morphological conditions ruling the “initial soil slip” or “initial debris slide” are morphological discontinuities that may cause instable conditions due to natural slopes, artificial cuts, road filling (in the downhill sector or in correspondence of bends), and to local stratigraphic and hydrogeological conditions that, even though they influence only a minority of cases, emphasize the important role of water outflow in the triggering mechanisms at the natural scarps, bedrock joints, or karst cavities (Figure 2.13).

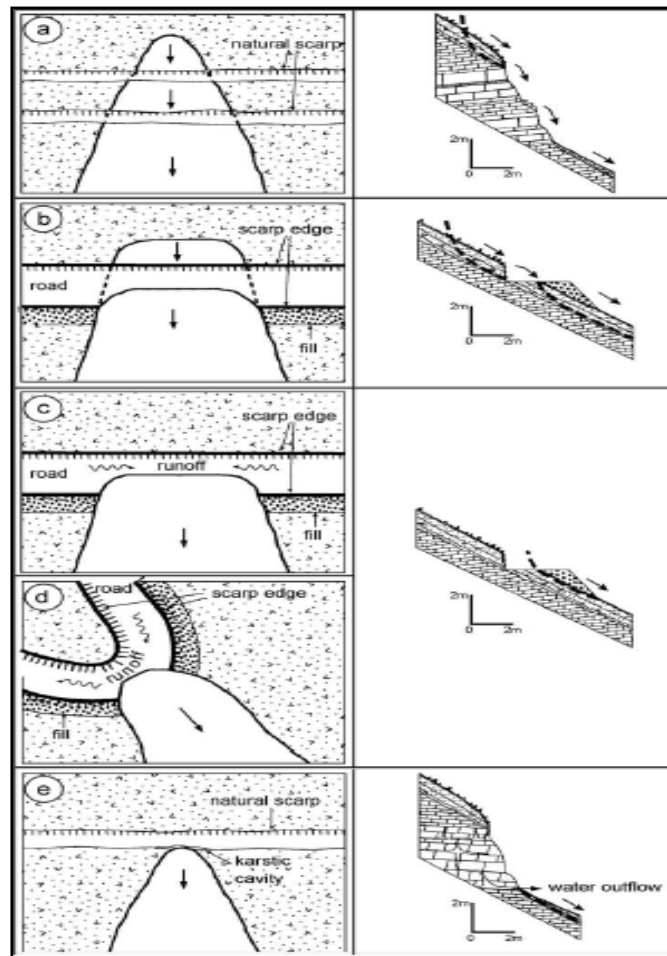


Figure 2.13: geomorphological structures of the main triggering conditions for landslides of Pizzo D'Alvano in May 1998 (Guadagno et al., 2005).

These factors are responsible for the typical triangular shape of the landslides, and their apical angle appears to be the most important morphological parameter because it seems to have an important influence on the volume of material mobilized by landslides (Guadagno et al., 2005). The apical angles of the landslides seem to be related to the impact energy of the initial rupture and to the geometry of the pyroclastic cover. Indeed, the action of the abrupt load caused by the arrival of material from upstream leads to the broadening of the landslides. Accordingly, due to local variations of morphology, the volume of material involved in the debris avalanche may vary significantly.

On the basis of these assumptions, a statistical analysis of morphometric parameters was performed (Guadagno et al., 2005). It is clear that the ratio between the initial volumes and the

volumes of debris avalanche (V_i / V_a) decreases as length of the slope increases, i.e. the volume of debris avalanche increases with increasing path length (Figure 2.14).

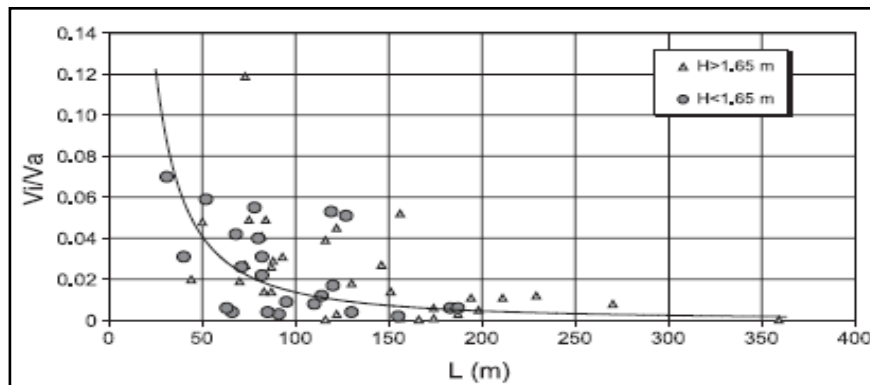


Figure 2.14: relationship between volume of material involved in the initial break and volume involved in the debris avalanche against slope length (Guadagno et al., 2005).

The role of discontinuities in pyroclastic cover was identified by means of a statistical study of landslide initiation zones. It was found that 75% of the landslides occur along the axes of the channels or on its sides or at points of convergence of shallow water flow (Crosta & Dal Negro, 2003). Statistical analyses show that more than half of the initial soil slips or debris slides occurred in correspondence with the upstream areas of morphological discontinuities and that the landslides triggered in limestone cliffs in the southern side of Pizzo D'Alvano massif are the most impressive, while in the northern sector there is a greater presence of landslides triggered by road cuts (Figure 2.15).

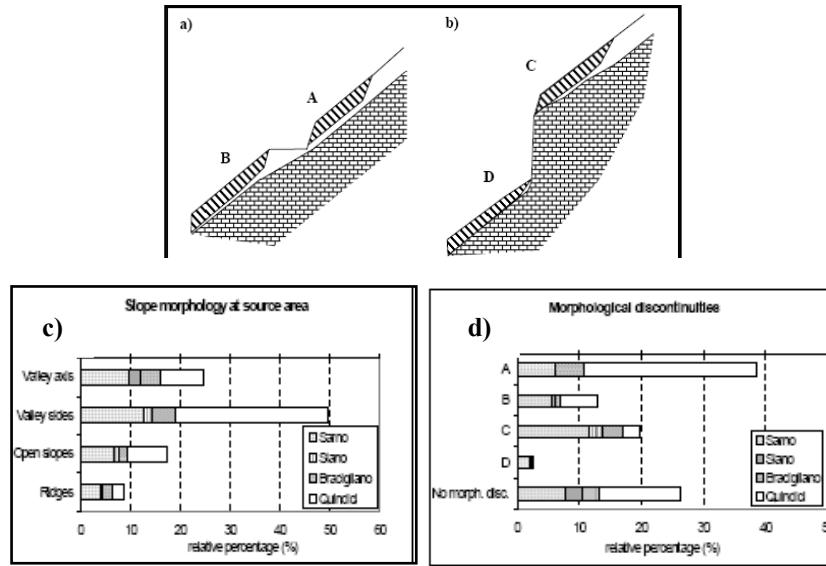


Figure 2.15: a) road cuts with instability in the upstream sector and within the filling material; b) rocky benches causing instability; c) Morphological characteristics of source areas and relative frequency for the towns of Sarno, Siano, Quindici and Bracigliano; (d) percentage of landslides triggered where discontinuity exist, for the four towns Sarno, Siano, Quindici and Bracigliano (Crosta & Dal Negro, 2003).

Among the main geomorphologic factors predisposing initiation of landslides in pyroclastic cover and especially channeled ones, there are road cuts or lithological benches which interrupt the continuity of the pyroclastic cover. Di Crescenzo and Santo (2005) highlighted the role of the presence and distribution of vegetation. Results ensuing from the statistical analysis show that most of the May 1998 landslides were triggered in presence of shrubs. Nevertheless, it should be pointed out that this is not a significant parameter because landslides were triggered both in forested and non-forested areas (Figure 2.16).

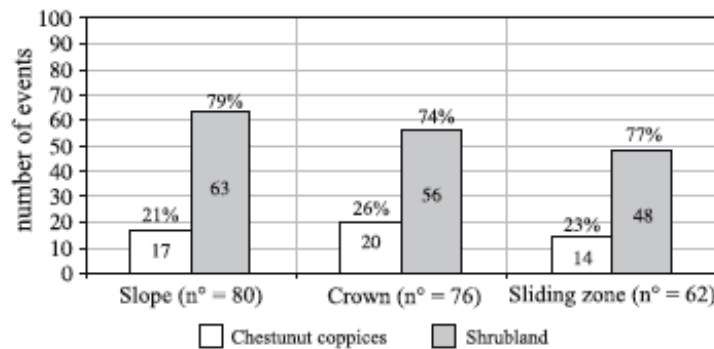


Figure 2.16: distribution of vegetation along slopes, with the crown zones and the sliding areas; the number refers to the considered elements for each case (Di Crescenzo and Santo, 2005).

Four types of slopes (Figure 2.17) can be distinguished where channelled, unchannelled and mixed debris slide-rapid earth flow may occur: planar slopes without drainage basin, slopes with a single and non-hierarchized drainage basin, slopes with lowly hierarchized basins, slopes with highly hierarchized basins. Complex landslides such as “debris slide-rapid earth flows” are characterized by initial rupture and a subsequent phase of slip on slopes and planar channeling in the main impluvium and sometimes in the secondary one.

Geomorphologic analysis to identify different types of slopes and landslides and a detailed morphometric analysis of them based on descriptive parameters were carried out (Figure 2.18a, 2.18b, 2.18c), in order to identify semi-quantitative values of morphometric parameters useful for highlighting areas to be monitored or stabilized (Di Crescenzo and Santo, 2005).

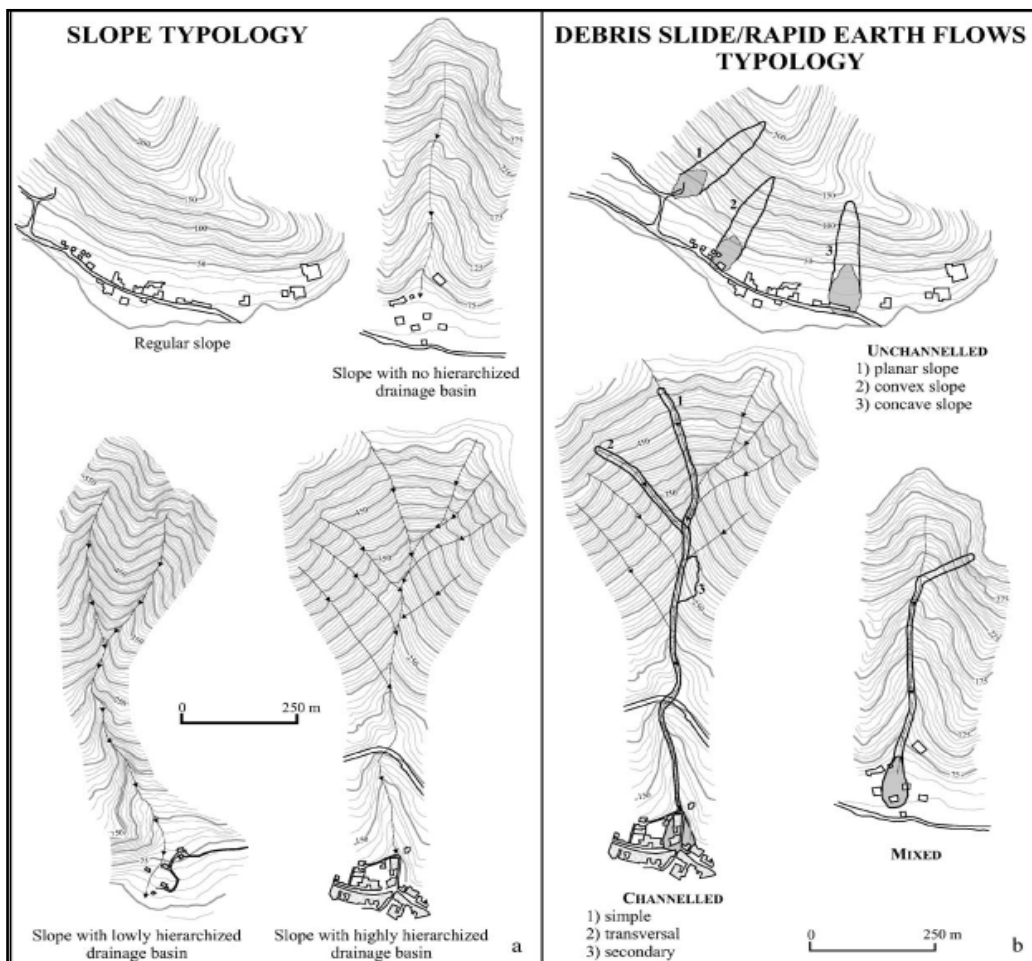


Figure 2.17: topographical diagrams representing the types of slopes and landslides: (a) regular slopes discriminated in concave, convex, planar, without hierarchized drainage basins, with lowly and highly hierarchized drainage basins (b): three main types of landslides, channelled, not channelled, and mixed debris slides / earth flows, representing a kind of midway between soil slips-debris flows rapid earth flow and are characterized by an initial triggering phase and planar sliding on the slopes, followed by the channelization main channels (Di Crescenzo and Santo, 2005).

2.1. Landslides phenomena and their classification

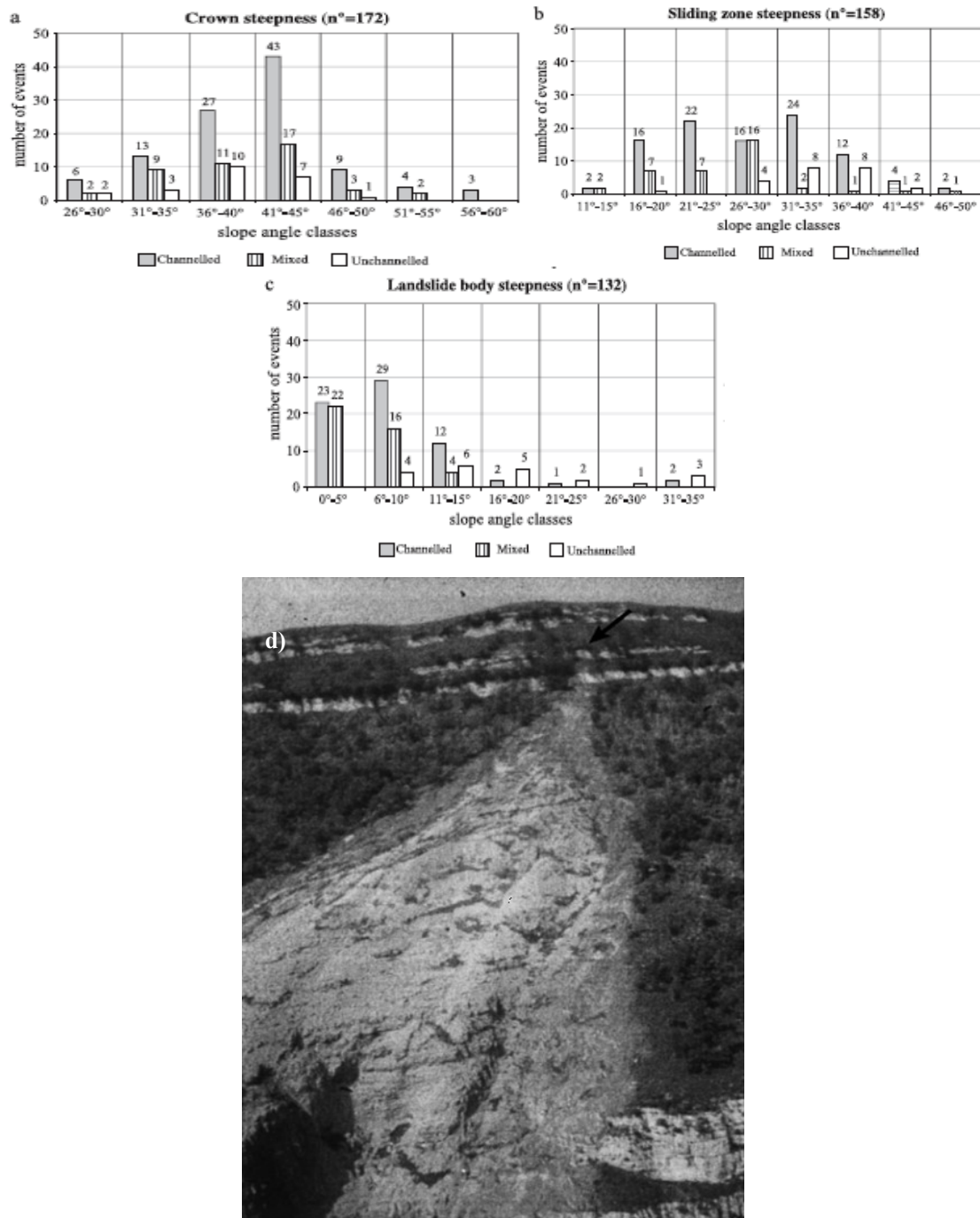


Figure 2.18: morphometric data related to soil slip / rapid earth flow, the classes of slope angle are differentiated between crown zone (a) slip area (b), landslide body (channeled, not channeled, mixed, debris slide / rapid earthflow; (d) triangular shape of landslide on Pizzo D'Alvano relief, where it is possible to observe the small extent of triggering area, if compared to the one affected from debris avalanche (Di Crescenzo and Santo, 2005).

The charts (Figures 2.18a, 2.18b, 2.18c) summarize data regarding morphometric parameters commonly found in literature, that is the slope angle of the crown zone, of the sliding zone and of the landslide body of studied landslides according to each typology of landslides.

The morphology of debris flow / earth flow path in pyroclastic soils is characterized by small crown zones and by size of sliding area 10-20 times greater due to the amplification process (Figure 18d) of the landslide mass (Di Crescenzo and Santo, 2005).

Based on a statistical analysis, the critical values of apical angle (α) were calculated and for most landslides it varies between 15° and 29° . The authors distinguished between channeled and mixed (figure 2.19a) and unchanneled landslides (figure 2.19b).

In such an interpretation the Authors consider as sliding zone the whole area pertaining to the initial debris slide, and they recognize that can it be interpreted as belonging to the avalanche phase,

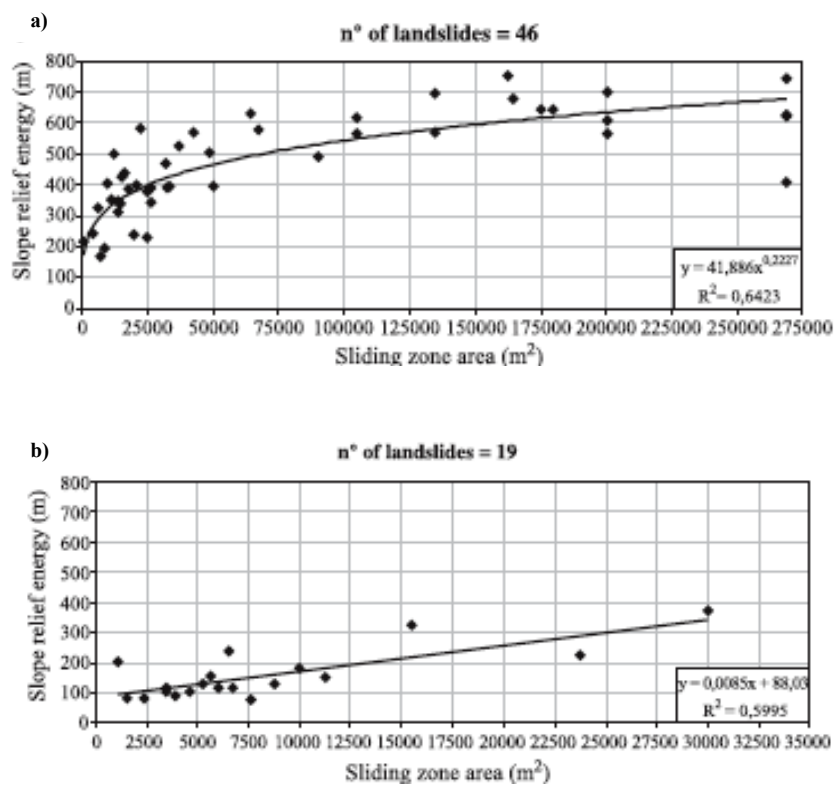


Figure 2.19: relations between slope relief Energy and slip zone : (a) channeled and mixed landslides: the distribution of points is represented by an power law, (b) not channeled landslides: distribution of points is approximated to a linear law (Di Crescenzo & Santo, 2005).

Finally, the authors found some interesting relationships between morphometric parameters, including the relationship between the height of the crown area and of slope relief energy. It is defined as the difference in elevation between the watershed line of the slope affected by a landslide and the first slope break at the foot of the slope that, in most of the landslides, is higher than 80%.

This result may be used to predict the zones of potential triggering “PZT” for slopes not yet affected by landslides.

2.3 Landslide mobility

As previously mentioned, debris flows involving pyroclastic soils can suddenly initiate and move downhill with high mobility covering on most occasions long distances and then stopping hundreds of meters or even some kilometers away from the source. It is, therefore, clear that both the path of landslides and run-out distances must be estimated in order to assess the potential impact on buildings and infrastructures.

The parameters that must be considered in the calculation include the maximum distance reached by the flow, its velocity, thickness and the distribution of deposits and flow behavior where it is forced to bend due to obstructions in the flow path. Based on literature data and morphometric parameters derived from field investigations, a specific empirical analysis for this type of landslide was performed (Budetta and De Riso, 2004), aimed at determining the mobility of landslides on the slopes of Sarno, Siano, Quindici and Bracigliano. Two main types of flows were identified: unchanneled flow (very common on the Lattari Mountains area and the Sorrento Peninsula) and a channeled flow (as those found on the Quindici and Sarno slopes)

Frequently, these phenomena can flow along existing roads at the foot of a slope for much longer distances. Bends in the channel, bifurcations and obstacles in its path can strongly influence the distance of the flow. This is clearly visible on the Sarno slopes where the debris banging against a quarry slope often divides in two segments one of which crosses the watershed interposed between the two incisions and joins the debris flow coming along another channel.

The two types of flows above mentioned are characterized by different mobility determined by the relationship between the height (H), considered as the difference in altitude between the uppermost point of the crown and the tip, and the horizontal distance (L) (Hutchinson, 1988; Corominas, 1996). The debris avalanches show greater mobility because they consist of thick suspensions of pyroclastic/debris sediments consisting primarily of volcanic sands and ash, of clayey soils and pumice with low resistance and also include small blocks arising from erosion of the limestone bedrock that are transported for long distances. Probably, this is due to block lifting

because of the forces acting on fine particles in suspension as a result of friction between the fluid and rock blocks sunk for gravity (Budetta and De Riso, 2004).

The relationship between the tangent of angle of reach (which indicates the mobility of a landslide) and the logarithm of the volumes of material involved seems to show a decreasing linear trend for increasing amounts of material mobilized. Data set in Figure 2.20 refers to all investigated landslides, both channeled and non-channeled (indicated as points from 1 to 6, 8, 9, 11, 14 and 23).

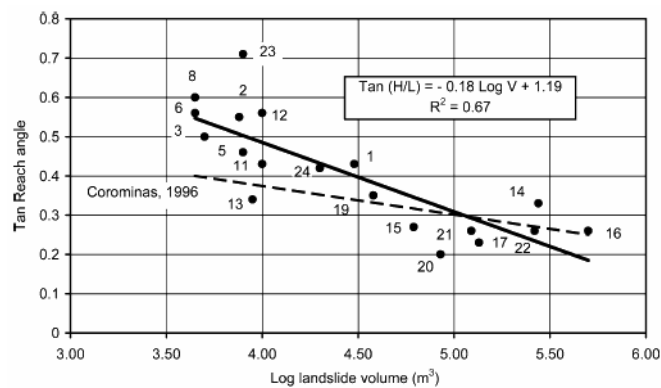


Figure 2.20: Relationship between the tangent of angle of reach and the logarithm of involved volume. The dashed line is the theoretical one (Budetta e De Riso, 2004).

Besides the greater mobility of channeled debris flows with respect to the non-channeled ones (debris avalanche, *sensu* Hungr et al., 2001), due to the concentration of kinetic energy, differences in mobility can probably also be enhanced by differences between lithostratigraphic features characterizing slopes involved in the landslides. Pizzo D'Alvano massif, in fact, is characterized by an abundance of thick pumice layers that, due to the low consolidation and susceptibility degrees to the hydrostatic and hydrodynamic lifting of the suspension of fine particles, turns out to have a great mobility. Therefore, factors that influence the degree of mobility of debris are length and steepness of the path. These landslides can have the characteristics of hyperconcentrated flows in which the water is the main factor that favors long paths.

2.4 The cause-effect relationship between heavy rainfalls and landslide initiation

The instability phenomena involving pyroclastic layers are essentially shallow landslides that are triggered by hydrological conditions, such rainfall and soil moisture conditions, related to the period preceding the failure. The time scale of precipitation influencing landslides is generally proportional to the magnitude of the event. The daily rainfall readings at Montoro Superiore were, therefore, taken into account; it was the only data available at the time.

Many studies aimed at understanding the critical values of precipitation for slope stability were carried out by means of an empirical approach (Cascini & Versace, 1986), thus permitting the graphical interpretation of hydrological parameters recorded in the period immediately before the start of the landslide. Such graphical analysis can identify the minimum values of the hydrological parameters which can trigger a landslide. These conditions describe a lower envelope known as the empirical hydrological threshold, because it is based on a database (archive) of recorded homogeneous landslide events for which hydrological measurements were recorded.

Some hydrological thresholds were issued for landslide initiation in pyroclastic soils covering mountain slopes surrounding the Somma-Vesuvius considering the following as hydrological parameters: a) intensity/duration of precipitation (Caine, 1980); b) the amount of precipitation in the day of the landslide *vs* the cumulated precipitations of the days before the day of the event (Crozier and Eyles, 1980); c) hydraulic conceptual model of the pyroclastic cover corresponding to a “leaky barrel” model (Wilson and Wiezoreck, 1995).

The first hydrological thresholds for the initiation of landslides in pyroclastic soils covering mountain slopes surrounding the Somma-Vesuvius were presented considering Caine’s (Guadagno, 1991) intensity / duration model. Subsequently, after the deadly landslides of 5th and 6th May 1998, other empirical hydrological thresholds were issued based on: Crozier and Eyles’s model (De Vita, 2000; Chirico et al., 2000; De Vita and Piscopo, 2002), Caine’s model (Calcaterra et al., 2000; Crosta and Dal Negro, 2003) and Wilson and Wiezoreck model (Fiorillo and Wilson, 2004).

Following Crozier and Eyles’s model and from analysis of daily precipitation sequences (De Vita, 2000; De Vita and Piscopo, 2002), rainfall parameters were derived for the precipitation of the day of the event (P), the day before the event (P₋₁) that accumulated on the days preceding the event including the day of the landslide event. Also, the hydrological analysis considered the precipitation

recorded during the periods before the event: five days (ΣP_5), ten days (ΣP_{10}), twenty days (ΣP_{20}), forty days (ΣP_{40}), sixty days (ΣP_{60}).

Thus, links between P and the cumulative rainfall of previous periods were created: one day (P_{-1}), four days (ΣP_{5-P}), nine days (ΣP_{10-P}), nineteen days (ΣP_{20-P}), thirty-nine days (ΣP_{40-P}), fifty-nine days (ΣP_{60-P}). For debris flows which occurred in Lattari Mountain-Salerno (Figure 2.21), these relationships show a lower envelope representing a hydrological threshold. In particular, as the previous cumulative period increases, the envelope evolves until it reaches stabilization for the highest previous periods (in the curves for 39 and 59 days). In these cases, the envelope decreases to values of $P = 50$ mm while the previous periods rise highlighting the strong influence of the soil moisture content and evapotranspiration in the previous period (Figures 2.21 and 2.22). The envelope for the highest antecedent periods indicates a strong reduction of the antecedent cumulative rainfall on the threshold values and might be considered as a valid empirical hydrological threshold for Lattari and Salerno Mountain (Figure 2.21).

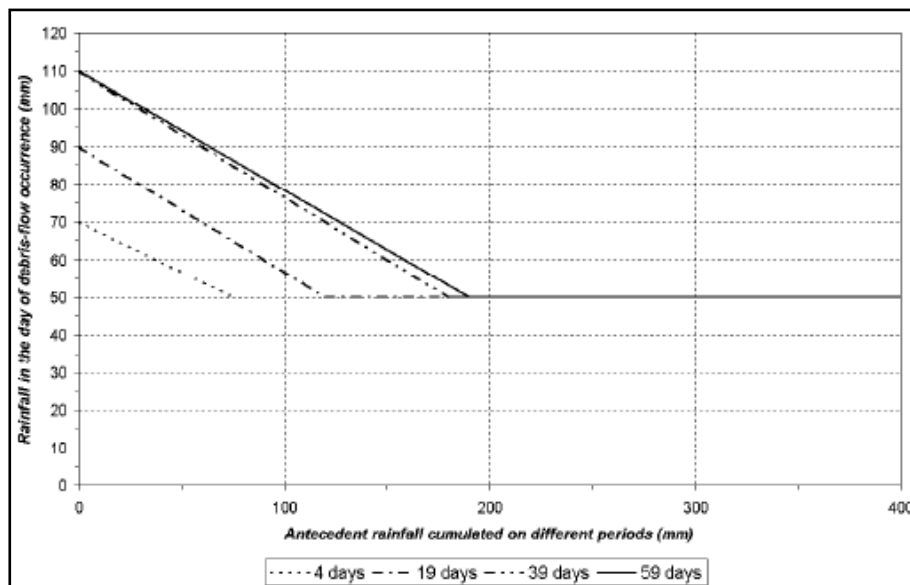


Figure 2.21: lower envelopes (hydrological threshold) for historical data of rainfall events at the day of the event vs the antecedent rain, cumulated for several periods; there is a general migration and stabilization of the envelope to increase as the period before increases (De Vita and Piscopo, 2002).

Rainfall sequences regarding landslides which occurred in Sarno and Lattari Mountains were also analyzed (Figure 2.22) Historical analysis carried out by the authors shows that, in two cases, the sequence takes place during autumn rainfall followed by landslide in the winter which means that during the autumn season soil moisture is still being charged and this gives further evidence suggesting that the sequence of homogeneous rainfall is not enough to trigger a landslide.

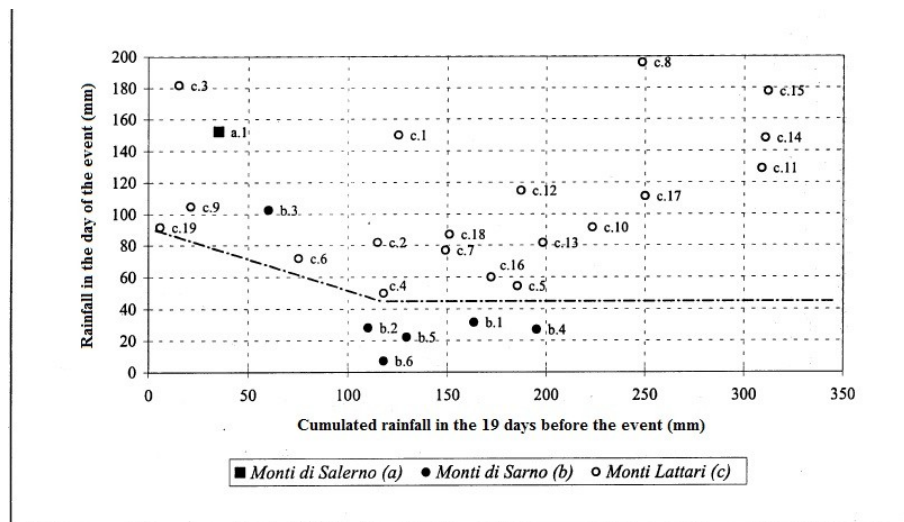


Figure 2.22: example of relation between rainfalls in the day of the event (P) and cumulated rainfalls, in this case related to four days before the event (ΣP_{5-p}). The relations relative to 9, 19, 39, 59 antecedent days show the same trend, but increasingly marked (De Vita & Piscopo, 2002).

Finally, it can be argued that the critical conditions for initiation of debris flows differentiates the Lattari and Salerno areas from the Sarno Mountains. The former are, in fact, characterized by rainfall values greater than 50 mm on the day of the event and by highly significant cumulative rainfall in the period before the event. On the other hand, in the second case, rainfall values are less than 32 mm and cumulated rainfalls are characterized by a homogeneous distribution over a very long time. In order to check the homogeneous distribution of precipitation in the analyzed rainfall sequences, correlation coefficients between the cumulated daily rainfall values and elapsed time were also calculated.

In the cases of the landslides which occurred on the Sarno Mountains, the high value of the correlation coefficient indicates that it is, approximately, a straight line indicating a homogenous distribution of values of cumulated rain in antecedent periods. According to the authors (De Vita, 2000), this might indicate, total amount and duration of rainfall being equal, the presence of a more homogeneous sequence distribution of rainy days and may be regarded as qualitatively indicative of the best conditions for the infiltration of a rainfall sequence for medium-low permeability soils.

Subsequently, different thresholds were proposed, (Crosta and Dal Negro, 2003), based on Caines' intensity - duration model that was synthesized into a single graph (Figure. 2.23).

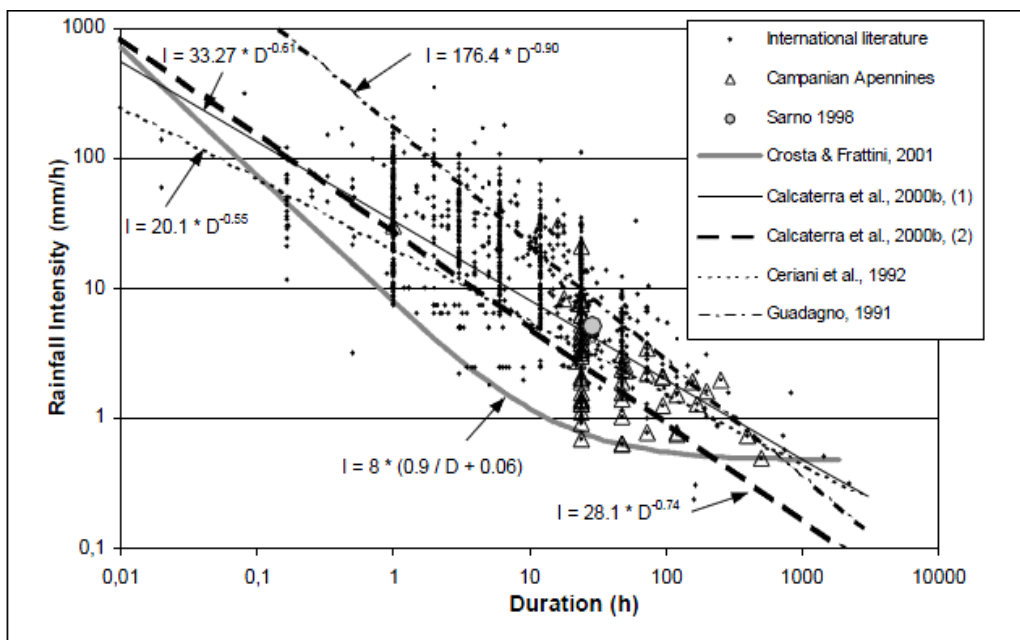


Figure 2.23: empirical hydrological thresholds determined with the Caines' intensity – duration model for debris flows initiation in pyroclastic soils mantling mountain slopes that surround the Somma-Vesuvius (Crosta and Dal Negro, 2003). It is possible to observe hydrological thresholds proposed by Guadagno (1991) and Calcaterra et al. (2000).

In order to analyze historical data related to rainfall and debris flow occurrence in western Campania and to examine the type of relationship, a model based on the combination of physical and empirical approaches was proposed by Fiorillo & Wilson (2004) following the “leaky barrel” approach (Wilson and Wiezoreck, 1995).

Some of the most intense rainfall events analyzed triggered several debris flows and affected large areas with at least one rain gauge in them.

The rain gauges network only recorded the most intense events in part (Tables 2.4 and 2.5).

2.4 The cause-effect relationship between heavy rainfalls and landslide initiation

Main storms recorded at Cervinara (S. Martino V.C.), Sarno, Lauro and Castellammare rain gauges

| Rain gauge, yearly mean | Main storm | Rainfall (mm) | Duration (h) | Max return time (years) for a specific rainfall duration | Antec. rainfall (mm) | Damage ^a | Debris flows (estim. n _s) |
|--------------------------|---------------------|---------------|---------------------|--|----------------------|--|---------------------------------------|
| Cervinara 1386 mm | 16–19 December 1968 | 378.4 | 72 | >100 (24 h–5 days) | 385.2 | Flood in the Caudina Valley | 1 |
| | 16–19 November 1975 | 199.2 | 67 | 17 (2 days) | 334.4 | – | – |
| | 14–15 April 1978 | 138.2 | 39 | 4 (2 days) | 1127.6 | – | – |
| | 13 November 1997 | 141.2 | 6 | >100 (3 h) | 334.4 | Many erosion phenomena and damages in Sarnio area. See also Lauro rain gauge. | – |
| | 14–16 December 1999 | 341.4 | 52 | >100 (12 h–3 days) | 496.8 | Cervinara village was destroyed. Many damages in S. Martino V.C. | >10 |
| Castellammare 1099 mm | 15–16 February 1963 | 100 | 2 days ^b | 2 (2 days) | 883 | Many damages in Gragnano village. | >10 |
| | 1–3 January 1973 | 345 | 3 days ^b | >100 (2–5 days) | 388.9 | Many damages in Naples area due to flooding. | – |
| | 17 November 1985 | 78.6 | 12 | 16 (6 h) | 117.2 | See Sarno rain gauge. | – |
| | 9–10 November 1987 | 182 | 16 | 58 (1 day) | 137.6 | Inundation in Naples area. Rock falls near Castellammare. | – |
| | 26 October 1990 | 75.2 | 8 | 36 (3 h) | 182.2 | Rock falls near Castellammare. | – |
| | 10 January 1997 | 163 | 38 | 50 (24 h) | >753 | Flood of Sarno river. Shallow landslides in Naples area. Many landslides in the Sorrento Peninsula. | >50 |
| | 4–5 May 1998 | 136.2 | 26 | 5 (2 days) | 936.6 | See Sarno rain gauge. | – |
| Sarno 1016 mm | 19–20 December 1964 | 124 | 2 days ^b | 15 (2 days) | 345.6 | See Lauro rain gauge. | – |
| | 1–3 January 1973 | 166.2 | 57 | 51 (2 days) | 387 | Flood of Sarno river. | – |
| | 3–4 November 1976 | 103.8 | 35 | 8 (2 days) | 251.6 | Flood near Nola. Rock fall along Sorrentina State Road. Flood of Sarno river. Landslide in Salerno. | * |
| | 17–19 November 1985 | 226.4 | 48 | >100 (6 h–5 days) | 159.8 | Inundation in Naples area. Flood of Sarno river. Landslides near Ariano Irpino and Cava de' Tirreni. | – |
| | 4–5 October 1992 | 101.2 | 11 | 60 (3 h) | 63.4 | Flood of Fenestrelle torrent. | 1 ^c |
| | 9–10 January 1997 | 121.8 | 40 | 8 (2 days) | 719.4 | Flood of Sarno river and in Celzi di Forino. | >5 |
| | 4–5 May 1998 | 93.6 | 30 | 4 (2 days) | 812.8 | Sarno, Siano, Bracigliano, Quindici and S. Felice a Cancello villages were hit by landslides. | >100 |
| Lauro 1152 mm | 18–21 December 1964 | 109.2 | 57 | 6 (2 days) | 454 | Flood of Sarno and Volturo rivers. Many damages in Puglia (nearby region). Landslide in Positano. | >10 ^d |
| | 1–3 January 1973 | 140.2 | 63 | 7 (2 days) | 389 | See Sarno rain gauge. | – |
| | 17–19 November 1985 | 222.2 | 43 | >100 (6 h–5 days) | 200 | See Sarno rain gauge. | – |
| | 23–24 November 1986 | 139 | 32 | 23 (12 h) | 177.8 | – | – |
| | 11–12 January 1987 | 124.2 | 35 | 10 (24 h) | 400.2 | Damages along the coast. Rock fall near Castellammare. | – |
| | 13 November 1997 | 61.4 | 19 | 2 (6 h) | 256.1 | Flood near Avellino. Snow above 700 m u.s.l. | 1 ^e |
| | 4–5 May 1998 | 154.8 | 31 | 22 (24 h) | 812.8 ^f | Many damages in Sarnio area. See Sarno rain gauge. | – |

The estimated number of debris flows was obtained from the literature data and by aerial photos.

^a Data from news and literature.

^b No hourly data.

^c Debris flow occurred near Bracigliano.

^d Debris flows occurred near Torrette di Mercogliano and Mugnano del Cardinale, about 20 km from Sarno.

^e Few debris flows occurred also near Monteforte Irpino and Gaudi, about 20 km from Lauro.

^f Data from Sarno rain gauge.

Table 2.4: main pluviometric events recorded in Cervinara (S. Martino V. C.), Sarno, Lauro and Castellammare rain gauges (Fiorillo & Wilson, 2004).

Main debris-flow events occurred in Campania since 1954

| Date | Locality | Death (Nr.) | Deb. flows (Nr.) | 2 days cum. rainfall, mm (rain gauge) |
|------------------|--------------------------------|-------------|------------------|---------------------------------------|
| 26 October 1954 | Salerno, Vietri, Maiori. | 318 | >100 | 504 (Salerno) |
| 8 December 1960 | Nocera | – | 2 | 128.3 (Nocera) |
| 17 February 1963 | Gragnano | – | >10 | 238.8 (Gragnano) |
| 24 November 1966 | Vico Equense | 3 | 1 | 182.5 (Gragnano) |
| 9 January 1968 | Sarno | – | 1 | 24.2 (Sarno) |
| 15 March 1969 | Agerola | – | >10 | 178 (Agerola) |
| 2 January 1971 | Gragnano | 6 | 1 | 176 (Gragnano) |
| 6 March 1972 | Nocera | 1 | 1 | 115 (Nocera) |
| 16 February 1973 | Termini | 9 | 1 | 62 (Turro) |
| 22 February 1986 | Palma Camp., Castellamm. | 8 | 4 | 43 (Palma Camp.) |
| 23 February 1987 | Castellammare | – | 1 | 80 (Castellamm.) |
| 3 October 1992 | Bracigliano | – | 1 | 102.6 (Sarno) |
| 10 January 1997 | Castellamm., Nocera, Quindici | 5 | >50 | 163 (Castellamm.) |
| 13 November 1997 | Lauro | 1 | 1 | 61.4 (Lauro) |
| 5 May 1998 | Sarno, Quind., Siano, Bracigl. | 161 | >100 | 157.8 (Lauro) |
| 16 December 1999 | Cervinara, S. Martino V.C. | 5 | >10 | 321.2 (S. Mart. V.C.) |

Table 2.5: main debris flow occurred in Campania region, starting from 1954 (Fiorillo & Wilson, 2004).

The analysis of data from Sarno, Lauro, Castellammare and Cervinara rain gauges was based on records of hourly rainfall. The isohyets map for the May 4th and 5th 1998 event is shown in Figure 2.24. Although less intense than others, it produced several large-scale debris slides exceeded only by the event of October 1954 (Figure 2.24).

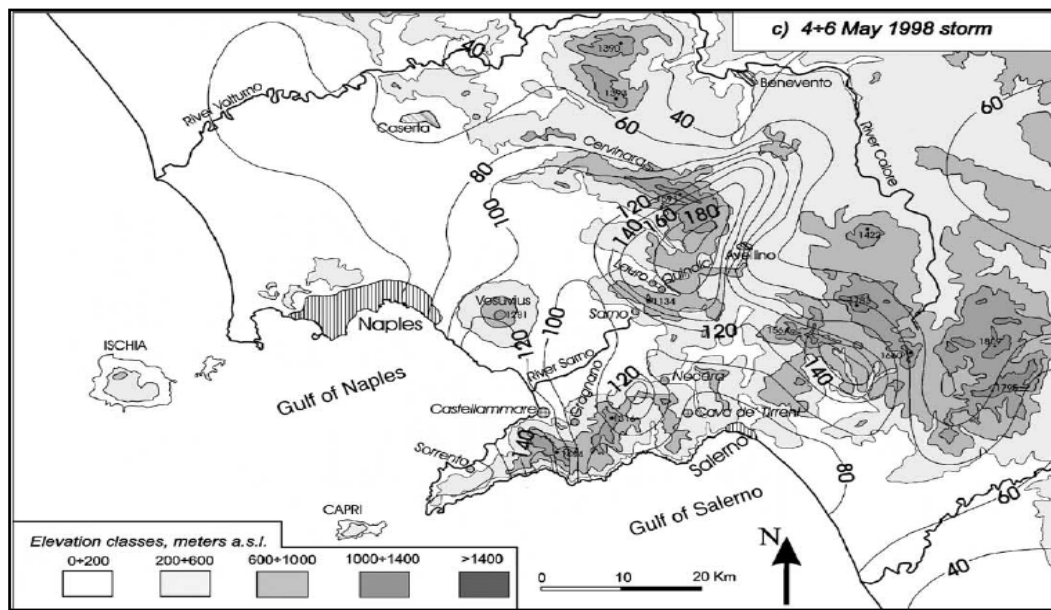


Figure 2.24: isohyets relative to the May 1998 event (Fiorillo e Wilson, 2004).

The authors observe that the amount of rainfall able to trigger debris flows depends on the percentage of water in the soil in the antecedent period. In a way, they identify the hydrological thresholds above which positive pore pressures can be established and hence the initiation of debris flow (Figure 2.25).

The authors established empirical hydrological thresholds (Figure 2.25) that are linked to storms occurring when soil moisture is close to field capacity (h_{max}); rainfall needed to reach field capacity was estimated in the range between 350 and 450 mm from the beginning of the rainy season (Fiorillo & Wilson, 2004). The duration of these events, capable of triggering debris flows is 12-24 hours. Finally, short storm (duration up to 6 h) does not seem to favor initiation of debris flows since the high intensity rainfall does not allow infiltration (Reid, 1994).

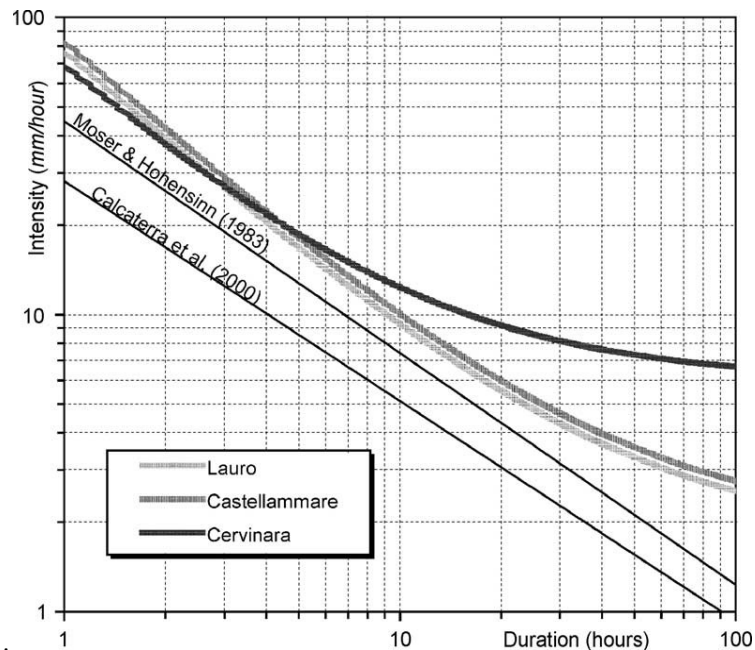


Figure 2.25: empirical hydrological thresholds for debris flow initiation in Campania region, derived from data from only one rain gauge, while theoretical thresholds are derived from more rain-gauge data (Fiorillo and Wilson, 2004).

2.4.1 Hillslope conceptual hydrogeological models

Many researchers investigated the hydrogeological features of the superficial system pyroclastic cover-carbonate bedrock in order to discover the direct cause-effect relationship between heavy rainfall and landslide initiation. Different hydrogeological models were issued based on the hydraulic interpretation of the complex superficial stratigraphy of the slopes surrounding the Mount Somma-Vesuvius. This complex stratigraphical system is the result of the superimposition of incoherent ash-fall pyroclastic deposits produced by volcanic eruptions of Somma-Vesuvius and Phlegrean Field volcanoes on the carbonate rocks which constitute the bedrock. The deposits are characterized by lateral and vertical variations of hydraulic conductivity that, together with the top layer of the bedrock, form a rather complex hydrogeological system. The bedrock is characterized by a hydraulic conductivity varying with the degree of fracturing and filling of joints and can have a high altitude groundwater flow as well as a very large basal one.

With particularly high rainfall, an occasional groundwater flow may develop and give rise to a temporary water table that feeds ephemeral springs. It is important in this context to emphasize the presence of marly interbeddings (marls with *Orbitolinae*) that behave as which are relatively impermeable and which leads to the formation of small underground reservoirs that feed the high

altitude springs. The analysis of the factors that promote water circulation at high altitude is also essential in order to understand the hydrological processes involved in the initiation of debris slide / debris flow.

The presence of large plains and endorheic morphology due to combined tectonic and karstic factors characterize the top of the Campanian peri-Vesuvian massifs and, in particular, the Sarno Mountains. This structure allowed the preservation of the whole sequence of volcanoclastic products of the Somma-Vesuvius and reaches a considerable thickness. Geoelectric surveys carried out on the pyroclastic cover of the Sarno ridge (Figure 2.26) reveal decreasing resistivity with depth. This might be interpreted as a clay-like pyroclastic horizon with low permeability able to create a suspended perennial water table whose flow is directed towards the points where the electrohorizon reaches the minimum values (De Vita et al., 2003).

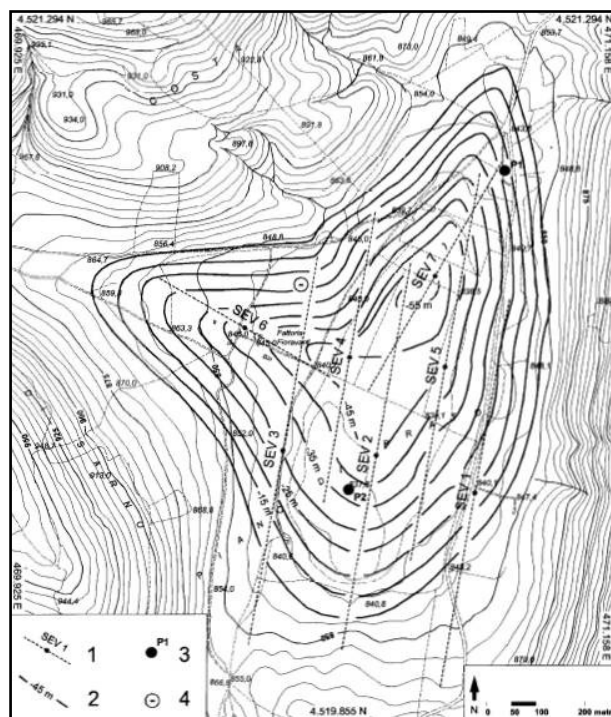


Figure 2.26: (1) location of SEV traces on the endorheic depression of Prato Plan and Torriello locality; (2) isopachs of the top of the bedrock; (3) wells; (4) recent sinking connected to a buried sinkhole. The water table depth is about 20 m (De Vita et al., 2003).

Since 1986 and after 1998, some authors, in order to explain the hydrogeological conditions predisposing the activation of landslides phenomena at Pizzo D’Alvano during heavy rainstorms, invoked different hydrogeological models. These models take into account variability of stratigraphic and morphological structure of coverage as well as the degree of jointing and also the

permeability of the carbonate bedrock. They have assumed the form of an occasional perched water table during heavy rainstorms in different conditions leading to the instability of the pyroclastic cover by means of the reduction of shear strength and the increase of shear stress.

The first model (Celico et al., 1986) suggested that effective infiltration percolates through the upper part of carbonate slopes which lack a part of their coverage due to erosive processes. This allows infiltration phenomena which both feed the basal water table, typical of carbonate mountains, and form a flow almost parallel to the slope that creates perched occasional water tables, especially during heavy rainfall (Celico, 1986).

After 1998, other hydrological models based on the observation of the existence of a low hydraulic conductivity basal paleosol that would isolate the pyroclastic mantle from the bedrock were published. Moreover, during particularly heavy rainfall, the formation of occasional perched water tables within pumice layers may take place (Celico and Guadagno, 1998; Celico et al., 2000; Celico et al. 2002) (Figure 2.27).

The first model includes a pyroclastic mantle several meters thick and a slip surface within the mantle where there are two layers with hydraulic conductivity greater than or equal to 10^{-5} m/s, followed by a layer of less than 10^{-6} m/s.

The second model has a slightly fractured bedrock covered by thinner, coarser and more permeable pyroclastic layers. In this case, an increase of pore pressure in the pyroclastic mantle due to the lower hydraulic conductivity of the carbonate bedrock is possible.

The last model is found in most crown zones and is characterized by a reduced thickness of very permeable pyroclastic cover on a bedrock characterized by a strong variation of permeability along the vertical (for the presence of marl intercalations). Hence, a gradual increase in hydraulic conductivity follows with a depth that achieves a reduction in infiltration capacity in saturated conditions in the deeper layers.

In these models, suspended occasional water tables can form during rainfall whose intensity is not lower than the infiltration capacity at saturation of less permeable layers during the hydrological year in which the demand for water retention was satisfied.

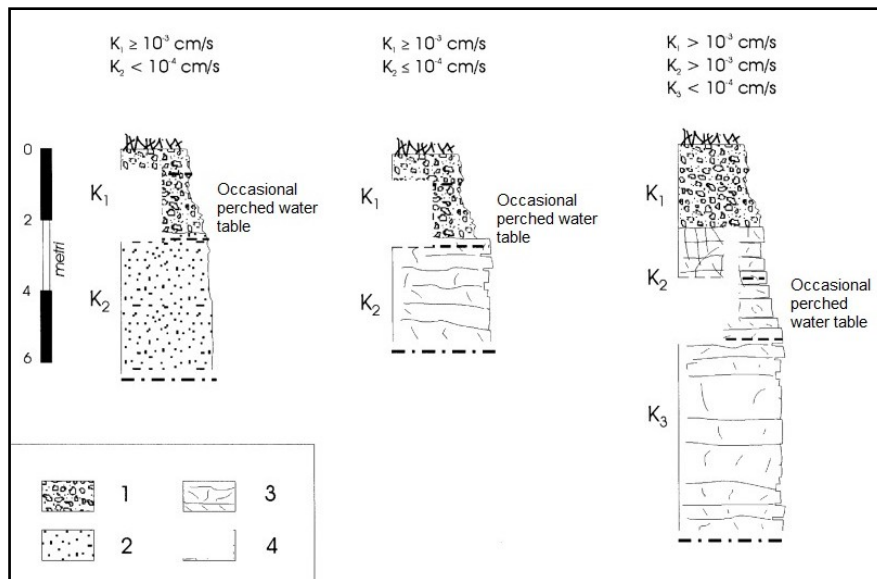


Figure 2.27: possible models of the hydrological system limestone bedrock-pyroclastic cover, assuming the existence of an occasional perched water table. (1) predominantly pumiceous deposits, (2) cineritic deposits, (3) poorly fractured limestone bedrock benches, (4) very fractured limestone layered bedrock.

Finally, the pyroclastic cover in peri-vesuvian mountain slopes is not genetically related to it by the weathering process; it derives rather from an external volcanic source and was transformed by pedogenetic processes. This introduces an important issue since it has strong implications on geotechnical and hydrogeological features which are reflected on the mechanical behavior of soils and of water circulation conditions. The multilayered sequence of pyroclastic soils can be considered as a complex system whose evolution in turn depends on the original morphology of the bedrock underneath and on the slope angle, as well as geotechnical and hydrogeological characteristics. Variations of the original morphological conditions due to erosion or human activities can affect shallow and groundwater circulations and can cause significant changes in original balances within the pyroclastic cover (Guadagno et al. 2005).

Erosion and weathering processes lead to the formation of colluvium after sedimentation of volcanic products generating a pedo-stratigraphical sequence consisting of “andosols” of different ages but with similar physical features. These properties can mainly be attributed to the frequent repetition of pumice layers between shallow and buried soils with variable properties ranging from humic to glassy.

2.5 Special hydraulic and mechanical properties of andosoils

Andosoils are mostly found in regions where active and recently extinct volcanoes are located (Shoji et al., 1993; Terribile et al., 2000; Guadagno & Magaldi, 2000). These authors point out that the pyroclastic layers mantling the Peri-Vesuvian hillslopes consist of allophane soils, also known as andosoils. Such a term was introduced into Soil Taxonomy by the U.S. Department of Agriculture (USDA, 1998). The “andic properties” result mainly from the presence of significant percentages of allophane, imogolite or aluminum-humus complexes. These minerals are commonly formed by the weathering of tephritic rocks or from similar materials with a significant content of volcanic glass. The genesis of andosoils is so strongly influenced by the properties of the parent material that the general term “volcanic ash soils”, denoting the type of parent material, is often used instead of andisoils. The chemical and mineralogical properties, texture, and depositional features of tephtras are especially important (S. Shoji et al., 1993). Terrains with “andic property” must contain less than 25% by weight of organic matter and are also required to have in the fine fraction:

- a content of Al + $\frac{1}{2}$ Fe equal to 2% or more of total;
- a specific weight measured at 33 kPa of water retention of 0.90 g/cm³ or less;
- a retention of phosphate equal to 85% or more.

Or they must have:

- a volcanic glass content of 5% or more in the range of 0.02-2.0 mm particle size;
- a content in the fine fraction of Al + $\frac{1}{2}$ Fe 0.4% or more of the total;
- a phosphate retention of 25% or more.

The presence of allophane minerals determines the unusual mechanical properties of such soils. In particular, Rao (1995) finds unusual values of natural water content, from 50% to 100%, liquid limits with values greater than 80 % and the shear strength angle ϕ' (29° to 41°).

In order to estimate soil water retention curves and hydraulic conductivity function, a study of andosols was carried out (Terribile et al., 2000; Basile et al., 2003). Charts below (Figure 2.28) show a high variability of values ranging from high to very high. Moreover, anisotropy of hydraulic conductivity of soils results in an increasing water storage capacity where discontinuities, such as sudden increase in slope angle at rocky benches or road cuts, are present. On the other hand, a general decrease of water storage capacity was observed where coverage is continuous (Basile et al., 2003).

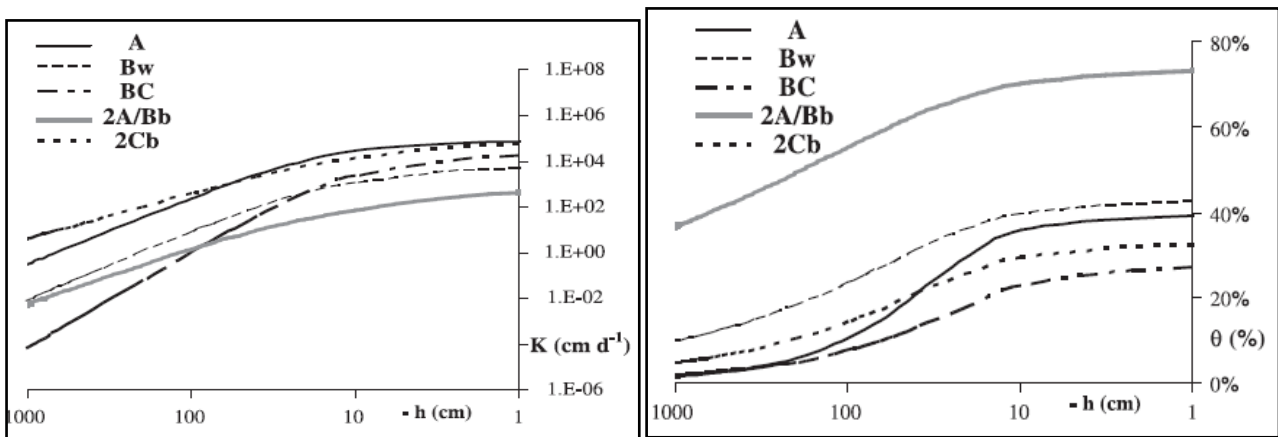


Figure 2.28: Hydraulic conductivity function of andisols (Basile et al., 2003). Andisols depth : A) 0-20 cm; (Bw) 20-38 cm; (BC) 38-71 cm; (C) 71-100 cm; (2A/Bwb) 100-140 cm; (2Bw/Cb) 140-150 cm; (2Cb) 150-200 cm. A Bw and C belong to pedogenetic cycle I; the last two soils belong to pedogenetic cycle II (Basile et al., 2003).

2.6 Geotechnical models

Analyses aimed at characterizing the physical and mechanical properties of pyroclastic cover mantling the Pizzo D'Alvano massif and involved in the May '98 rapid debris flows were carried out by many authors with the purpose of achieving a stability model of the pyroclastic mantle by means of a geotechnical approach. In this section, the most significant results will be discussed.

The analyses regarded soil suction, physical and mechanical characterization of pumiceous and cineritic soils as well as analyses of the shear strength determined in laboratory. Undisturbed samples in both saturated and unsaturated conditions (natural conditions water content) and remodeled samples were tested (Cascini et al., 2003). The results of direct shear tests on

undisturbed and saturated samples indicate values of internal friction angle (ϕ') ranging between 32° and 37° and low values of effective cohesion (Figure 2.29).

| Geotechnical characterization of soil layers | | | | |
|--|----------------|------------------------|---|-----------------------|
| Soil properties | | Upper ashy soil layer | Pumice soil layer | Lower ashy soil layer |
| Dry unit weight | γ_d | 7.30kN/m ³ | 6.20kN/m ³ | 9.10kN/m ³ |
| Saturated unit weight | γ_{sat} | 13.1 kN/m ³ | 13.1kN/m ³ | 15.7kN/m ³ |
| Porosity | n | 0.58 | 0.69 | 0.66 |
| Saturated hydraulic conductivity | k_{sat} | 10 ⁻⁵ m/s | 10 ⁻⁵ ÷ 10 ⁻³ m/s | 10 ⁻⁶ m/s |
| Effective cohesion | c' | 4.7kPa | 0kPa | 4.7kPa |
| Friction angle | ϕ' | 32° | 37° | 32° |

Figure 2.29: geotechnical characterization for ashy and pumice layers of Pizzo D'Alvano pyroclastic cover (Cascini et al., 2003).

Other authors dealt with this topic also in order to have a preliminary characterization of the areas affected by rapid debris flows (Bilotta & Foresta, 2002). With this aim, several samples were collected in Tuoro, S. Lucia and Tuostolo Valley (Figure 2.30), which belong to the Pizzo d'Alvano massif (Sarno Mountains) and laboratory tests were carried out on undisturbed specimens in order to study shear strength and the hydraulic properties of the materials involved in terms of both total and partial saturation.

On the basis of the grain size analysis (Figure 2.31), the authors distinguish two homogeneous classes: "A" belonging to the fine soils group, and the second one "B", to the coarse soils. Particular attention was given to the variation of shear strength (Figure 2.32) with varying particle size distribution (Figure 2.31a), physical properties (Figure 2.31b) and to the degree of saturation. At first, the shear strength was investigated in partial saturation conditions then in natural water content conditions and finally with a suction value of 50 kPa, that is a maximum value approximately equal to that found by in situ measures (Cascini & Sorbino, 2002).



Figure 2.30: location of sampling sites.

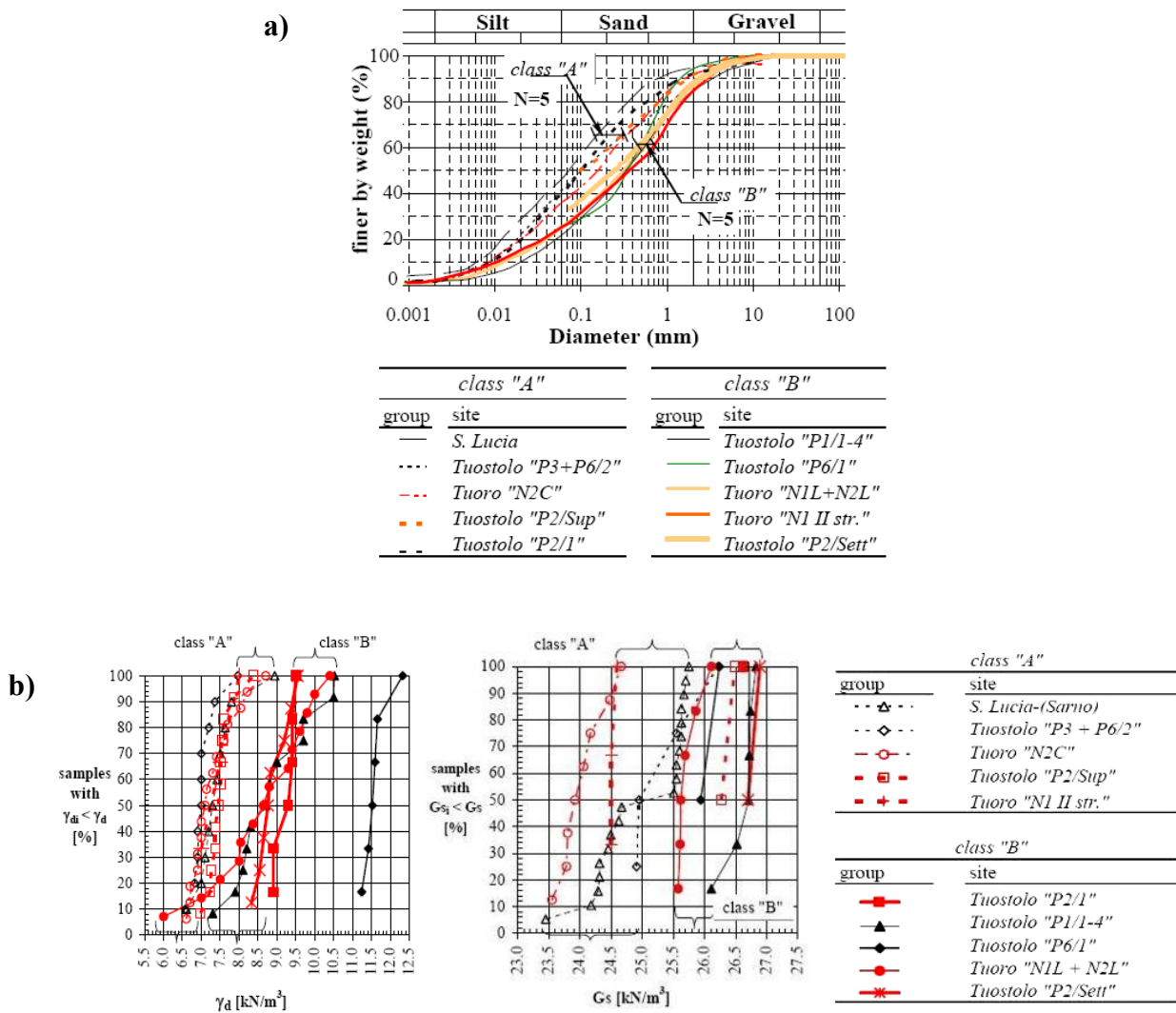


Figure 2.31: (a) average distribution of grain sizes for each sample; (b) physical properties of samples: specific gravity of solid particles (G_s) and dry weight of sample (γ_d). The data are plotted in terms of cumulative frequencies (Bilotta & Foresta, 2002).

As regards the physical properties of soils, these are plotted for each group in terms of cumulative frequencies. The figure 2.31b highlights the fact that cineritic samples, namely those with finer particle size distribution, are more porous and light in terms of the specific weight of the solid particle (G_s) and in terms of dry weight (γ_d).

Results of direct shear tests show (Figure 2.32) that under conditions close to saturation cohesion is absent whereas the effective friction angles have values ranging between 32° and 35° for samples belonging to class “A”. Most of the samples belonging to the group “B” fall into the range between 34° and 37.5° , with minimum values of 32° and a maximum of 40° - 41° (Figure 2.32).

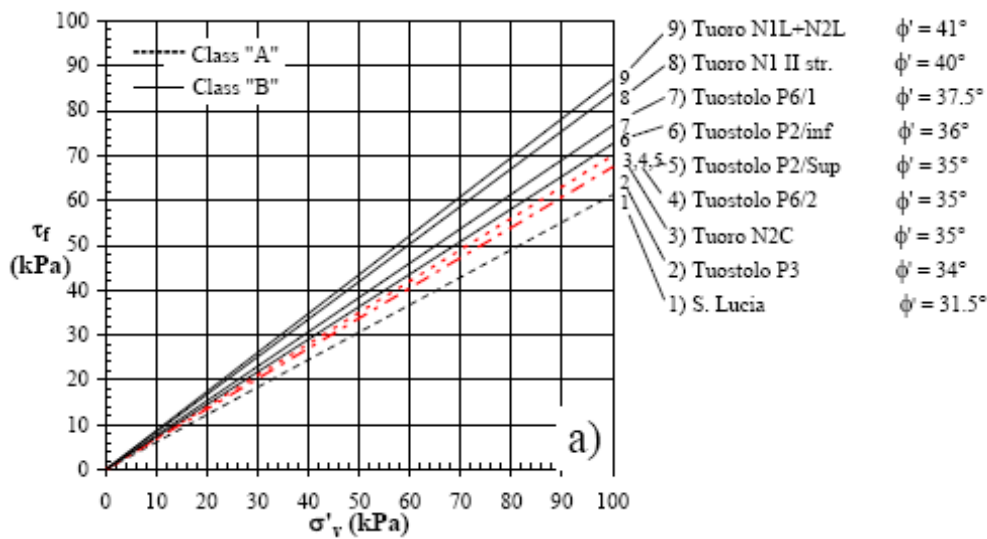


Figure 2.32: measured shear strength for each group of samples (Bilotta and Foresta, 2002)

These results can be linked to the presence of a small clayey fraction (4%) in the first case and to a high fraction (20%) in the second.

In conclusion, the parameters calculated for each group of samples vary with the particle size and physical properties of materials. In particular, finer and porous samples of “A” group appear to have a shear strength lower than those of group “B”. Indeed, when the samples are close to saturated conditions, the effective friction angle increases with particle size, dry unit weight and with decreasing porosity. This evidence suggests that the values of friction angle calculated for both the cineritic and coarse soils vary widely (Bilotta and Foresta, 2002).

2.6.1 Pore pressure regime in pyroclastic mantle and stability analysis

Soil suction is one of the physical properties governing the shear strength of unsaturated soils and accounts for an increase in shear strength that can favor stability in pyroclastic mantle close to a condition of stability. It is responsible not only for the mechanical feedback of the soil but also for the water transfer (through the infiltration, evaporation and transpiration) and energy between the soil and atmosphere (Sorbino, 2005).

On this basis, data on soil suction was acquired (Cascini & Sorbino, 2004) in the source areas of the landslides of May '98 (Sarno, Siano, Quindici and Bracigliano) and those between November 1999 and April 2002 by means of tensiometers installed at depths between 1.5 m and 4.0 m. Data at different altitudes were acquired, either within zero-order basins or outside of these, where the stratigraphic conditions vary from site to site.

As already pointed out by the authors, the extreme variability of conditions in which measures were carried out, (such as variability in altitude where the tensiometers were installed, the different depth of investigation, the variability of rainfall throughout the observation period and the lack of measures during some periods), reflects the extreme dispersion of the plotted data (Figure 2.33).

Nevertheless, in spite of this dispersion as well as variations in the rainfall regime throughout the observation periods (Figure 2.33), all the data confirm the presence (Cascini & Sorbino, 2002) of dry and wet periods during which suction values range from a minimum of 1-2 kPa to a maximum of 65 kPa.

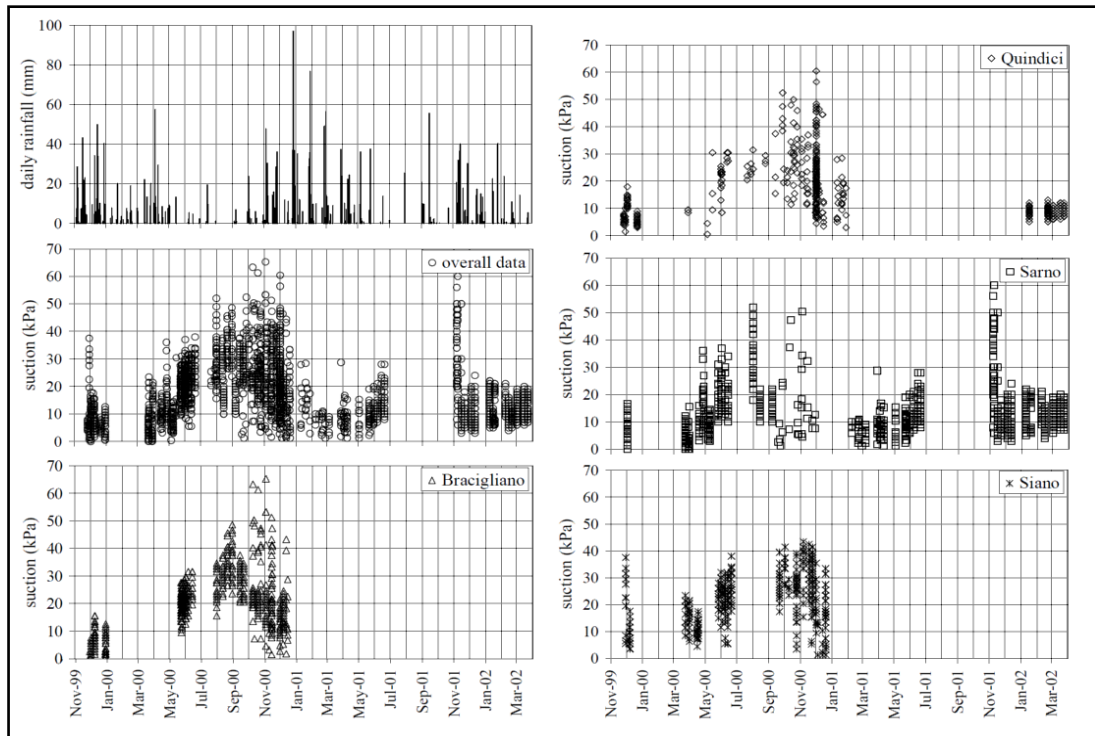


Figure 2.33: suction data for the sites of investigation, related to the rainy day (Cascini & Sorbino, 2004).

To summarize, in Pizzo D’Alvano massif, the trend of monthly suction (Figure 2.34) values seems to be quite regular during the wet season. On an annual scale, the monthly suction values show the same behavior regardless of investigation site as well as a decrease in monthly values of suction during the wet period when the minimum values are observed (10 kPa at depths of less than one meter).

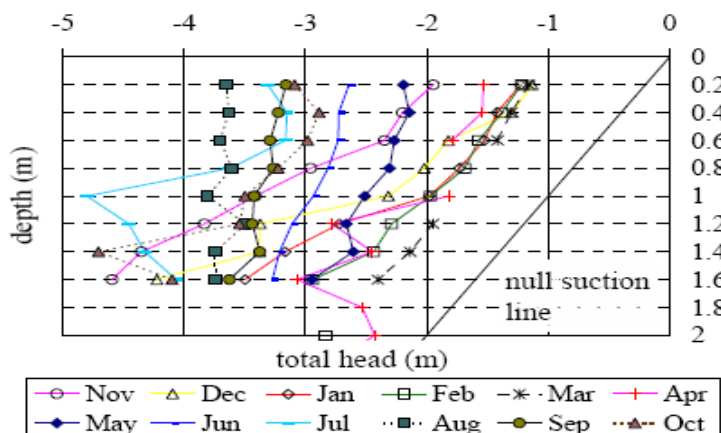


Figure 2.34: total hydraulic as function of depth (Cascini and Sorbino, 2004).

During the period April - August, due to solar radiation and to higher temperatures, the suction increases and, due to evapotranspiration, hydraulic gradients exhibit variations in the flow direction at depths greater than 0.6 m.

In order to find out if there is a relationship between monthly values and initiation of flowslides, the authors performed geotechnical analysis to produce a geomorphological model in order to explain the evolution of the slopes of “Sarno type” (Cascini et al., 2000). The geotechnical model (Figure 2.35) is based on the transient flow regime induced by rainfall and on the water discharge of springs from the bedrock through pyroclastic layer (Cascini, 2003).

In the sample basin of Tuostolo Basin (Figure 2.30), pore pressures distributions were measured. The results of this model showed that the bedrock springs are a key factor enabling the pyroclastic cover to reach failure conditions (Cascini, 2003; Cascini et al., 2010).

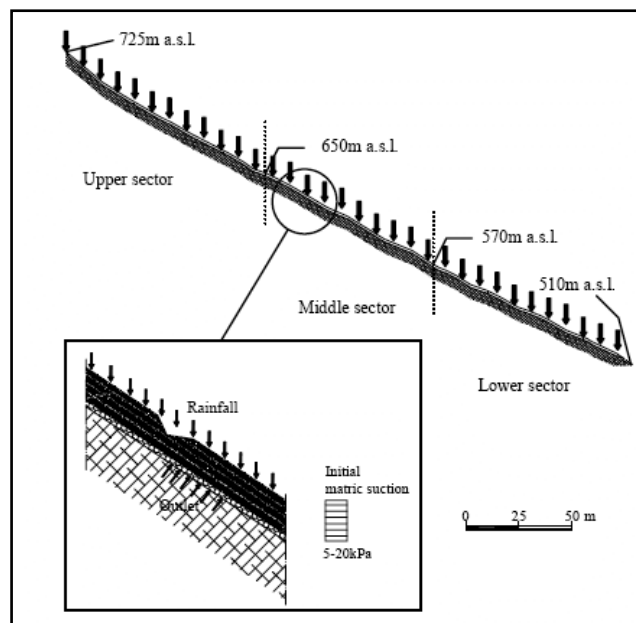


Figure 2.35: initial conditions for the analysis of the transient flow (Cascini, 2003).

Geotechnical analyses carried out by some authors concerned the simulation of infiltration conditions in pyroclastic cover during the period January '98 - May '98. Pore pressure was calculated for some verticals along a section of the slope with different initial conditions and values of saturated hydraulic conductivity of 7.5×10^{-5} m/s for pumice layers on May 3rd. In Figure 2.35, the dashed line represents the potential sliding surface used by the authors in the limit equilibrium

analysis. It is possible to observe how coverage layers situated above this line are under partially saturated conditions and pore pressures values are more or less uniform and not influenced by the initial conditions. These may or may not create the conditions for the formation of a perched water table within the pyroclastic cover.

A possible explanation for this behavior according to Cascini et al. (2003) may be related to the presence of pumice layers and to their hydraulic properties. Although the saturated hydraulic conductivity of pumice levels is the highest among the pyroclastic levels (Figure 2.36), it decreases more rapidly in relation to suction (Cascini et al. 2003; Sorbino, 2005).

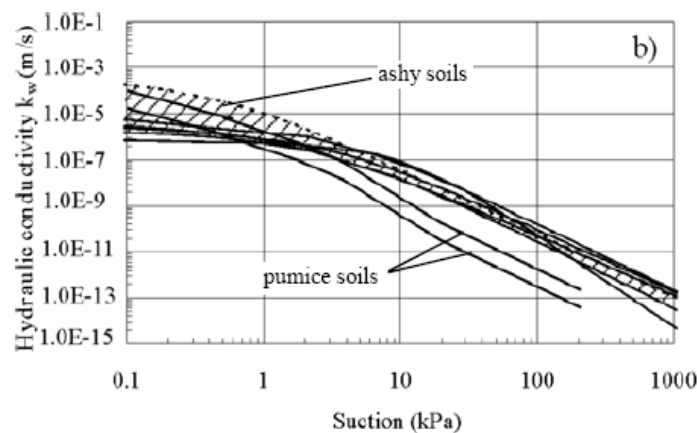


Figure 2.36: suction values concerning the hydraulic properties of pumiceous and cineritic levels (Cascini et al., 2003).

In particular, the hydraulic conductivity of the pumiceous lapilli ranges across two orders of magnitude compared to suction when this varies between the minimum and maximum values (5 and 20 kPa) assigned as the initial conditions. For initial values of suction 5 kPa, pumice levels are able to channel large amounts of water at depth and also due to the movement of water at depth, pore pressure increases if compared to the initial values.

For initial values of suction, pumiceous lapilli behave like low permeability levels; the amount of water infiltrating at depth is lower and the negative pore pressures are almost unchanged (Figure 2.37). To summarize, the analysis of the role of pumice levels is relevant in terms of infiltration and distribution of pore pressures.

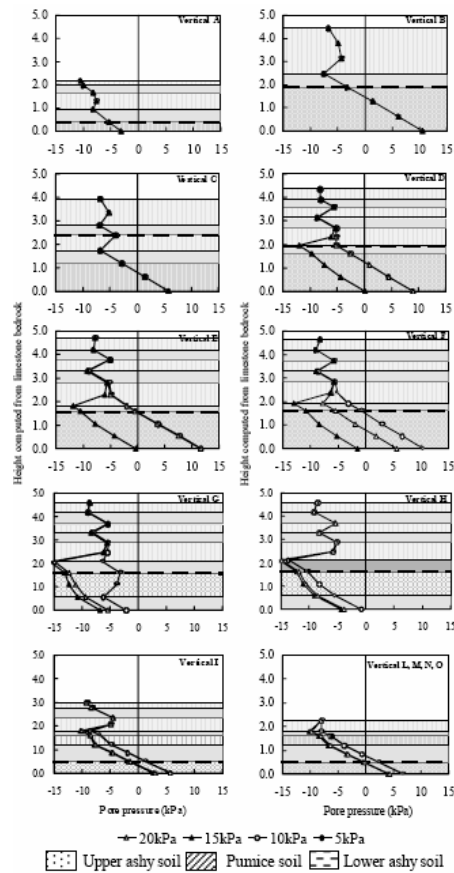


Figure 2.37: calculation of daily pore pressures on May 3th 1998, with different initial conditions on the day 1 January 1998 (from Cascini et al., 2003).

Geotechnical analyses performed (Cascini et al., 2003) show how the areas of initiation of landslides are located mainly in the Zero Order Basins filled with colluvial terrains derived from pyroclastic soils coming from uppermost part of the slope (Guida, 2003; Cascini et al., 2005; Sorbino, 2005; Cascini et al., 2008).

The results achieved from this model overestimate the extent of the initiation areas and locate the temporary sources in the upstream areas i.e. on rocky benches. This model, developed in order to assume the failure conditions, seems to be valid only if one considers the role of temporary sources at the time of rupture (Sorbino, 2005). The importance of sources from the temporary spring results from this study especially as regards the interpretation of the 1998’s debris flow, in this case classified as flowslide (Cascini et al. 2003; Cascini et al., 2005; Cascini & Sorbino, 2004).

Based on the acquisition of geological and geomorphological data it was observed that most of the initiation areas were located within the Zero Order Basins (Figure 2.38) and that the material deposited by the debris flow was located in the alluvial fans at the base of the slopes.

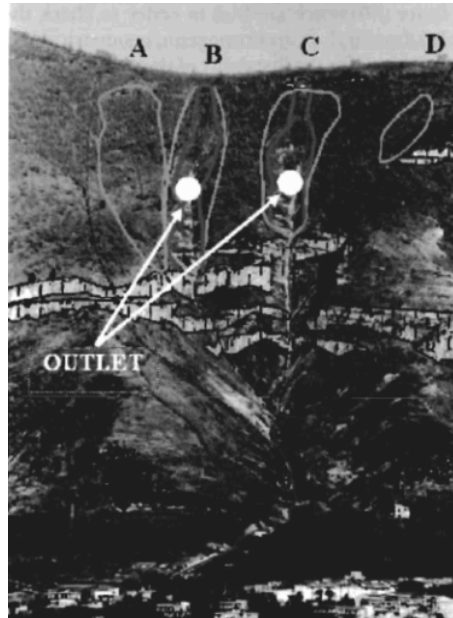


Figure 2.38: location of areas of Zero Order Basin and temporary springs of bedrock (Cascini et al., 2005).

In the upper part of the Tuostolo sample basin, there is a stream below the surface, (sub-surface flow), characterized by the presence of perched water tables whose regime is closely related to the settlement of secondary structural elements acting as relatively impermeable (Guida, 2003).

These structural elements are wedge-shaped and are closely related to seasonal and temporary springs of the bedrock and placed in the uppermost portions of the slopes (Figure 2.39), mainly within the ZOB and at the river heads (Cascini, 2002; Cascini, 2003).

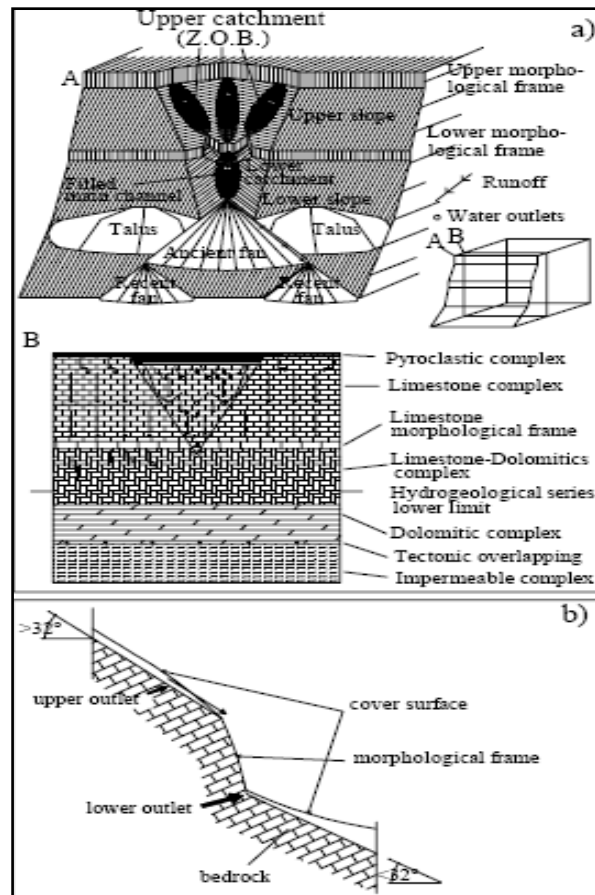


Figure 2.39: hydro-geomorphological model (Cascini, 2002; Cascini et al. 2008).

Regarding the Zero Order Basins, they can be considered as source of material which is subsequently involved in flowslides. The evolution of a zero-order basin is mainly controlled by localized creep on the watershed between the hollows (Hack and Goodlett, 1960) and shallow slip on the sides of slopes.

The transfer of the material along the slopes gradually fills the hollows and causes thickening of debris and soil which is then transferred to the transition channels through laminar erosion, stream erosion and piping. When, due to the filling process, debris is thick enough, shallow slope failures may occur thus evacuating part of the material accumulated in the hollows (Guida, 2003). In the presence of particularly intense or prolonged rainfall on very steep slopes, the shallow failures may evolve into “debris flow” because additional coarse material, previously accumulated in channels of first and second order, can be scraped off from the bedrock (Guida, 2003). After the evacuation phase of debris, the missing volume can be filled with material from the sides of the

Zero Order Basin and a new cycle starts (Figure 2.40). During many cycles, fall out deposits hide the bed of a Zero Order Basin and add extra material to the existing one.

The “self-driven cycle” of filling-evacuation-refilling of the Zero Order Basins was also adopted for other mass wasting-controlled landscapes (Hack and Goodlett, 1960; Tzukamoto and Minematsu, 1987; Crozier et al., 1990). It was used in “Sarno type” slopes for the possibility of additional recharge of Zero Order Basins besides the ash-fall pyroclastic deposition.

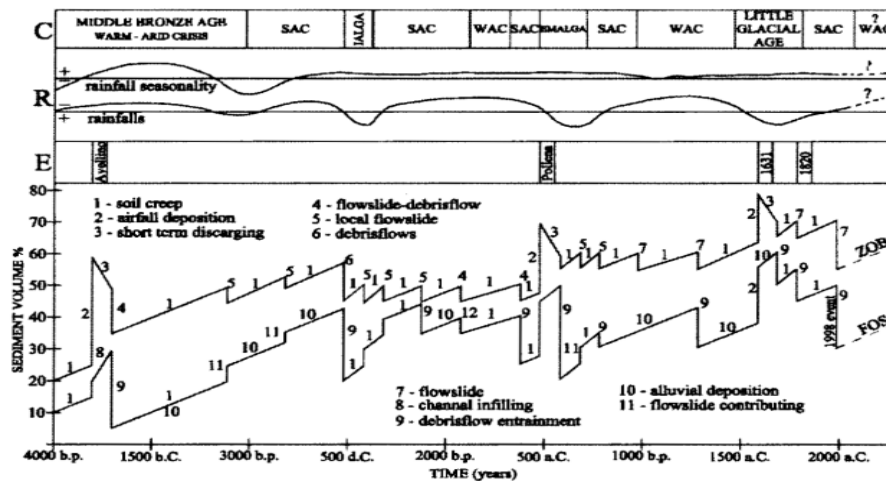


Figure 2.40: temporal sediment series accumulated /evacuated and processes correlated to the ZOB, in the Pizzo D' Alvano massif, starting from 4Ka: fall out deposits from main Plinian phases (modified from Rolandi et al, 1998; C climatic phases; R rain regime (Guida, 2003). SAC: Similar to Actual Climate; WAL: Warm Arid Climate.

2.6.2 Geotechnical modelling of landslide initiation

The initiation of the debris flows which occurred on 5th and 6th May 1998 considering sample areas (Tuostolo headwater) and daily rainfall recorded in the period between January and May '98 was modeled by means of a geotechnical approach (Cascini et al., 2003). The process of evapotranspiration was not considered since it was already considered as negligible effect in the modeling of suction regime during the spring and winter (Sorbino, 2005). The initial conditions of the distribution of suction within the pyroclastic cover were considered uniform with initial values of 5, 10, 15 and 20 kPa respectively. The conditions of stability of the pyroclastic cover were assessed by using the limit equilibrium method, and by considering the heavy rainfall on May 4th and 5th 1998 by using the distribution of pore pressures previously calculated.

For this purpose, the shear strength in both saturated and non-saturated conditions was calculated by means of Mohr-Coulomb envelope considering also the increase due to apparent

cohesion that was accounted for the Fredlund and Rajardo model (1987). The geotechnical analysis allowed the identification of the factors leading to failure conditions such as thickness of pyroclastic cover, the bedrock profile, suction regime and shear strength properties of the cineritic levels.

In particular, the bedrock profile and the distribution of thickness of pyroclastic cover in a section of the slope may generate unfavorable pore pressures in a ZOB area causing local instability conditions mainly located above the cineritic levels.

In other words, in the temporary springs, the authors identify the key factors for the initiation of failure phenomena affecting the whole slope according to a complex sequence of multiple failures. The timeline sequence of failures in terms of mobilized areas was obtained by considering different initial conditions of suction and hydraulic conductivity for pyroclastic horizons. The simulation pointed out that any initial condition has a little influence on mobilized areas, thus demonstrating the necessity of a hydraulic contribution from the carbonate bedrock (buried spring) for a huge mobilization (Figure 2.41).

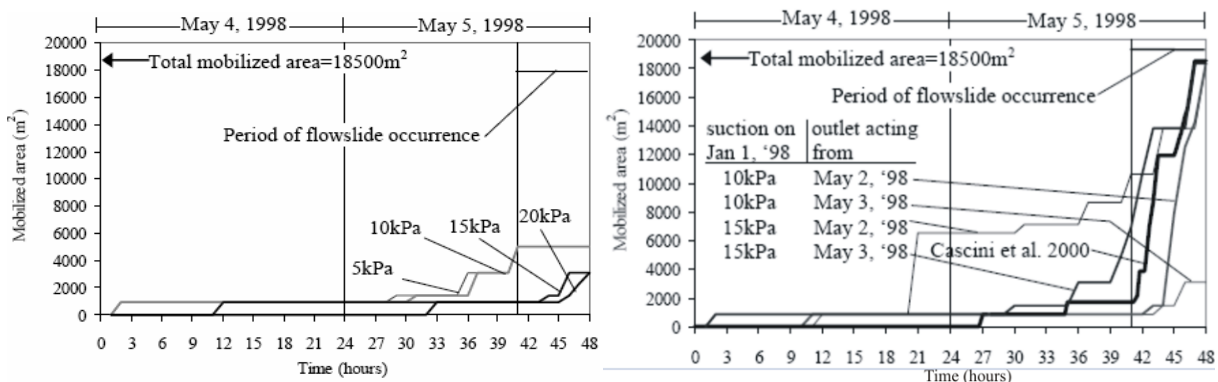


Figure 2.41: temporal simulation of the triggering mechanisms, considering absent the entries from the bedrock; (b) time simulation of the triggering mechanisms considering contributions of the substrate (Cascini et al., 2003).

Aiming at obtaining a better adaptation to the hydro-geomorphological model above described, a second analysis was carried out considering contributions from the bedrock with a flow rate of $1,3 \times 10^{-3} \text{ m}^3/\text{min}$ according to field tests. The best simulations were obtained by taking into account saturated hydraulic conductivity values of $7.5 \times 10^{-5} \text{ m/s}$, initial suction values equal to 10-15 kPa and the beginning activity of the sources from May 2nd and 3rd.

Chapter 3

Objectives and methods of the research

3.1 Objectives and phases of the research

As mentioned in the previous chapter, flow-like landslides in cohesionless granular materials are very complex phenomena and can be considered among the most serious natural hazards above all for their typical high velocity. The May 1998 events occurred in the Sarno Mountains are dramatically unique examples of multiple complex landslides triggered by high intensity and prolonged rainfalls. They affected slopes covered by ash fall pyroclastic deposits, as well as colluvial and detrital deposits derived from volcanic deposits themselves.

The difficulty in the approach to understand landslide triggering mechanisms and post-failure evolution derives from the complexity of the issue due to several aspects, such as: i) stratigraphic setting; ii) variability of morphological conditions; iii) comprehension of the groundwater pathways reaching the landslide areas after the infiltration; iv) triggering mechanisms and the following rheological behaviour of the landslides; v) the antecedent hydrological conditions influencing the rainfall critical values for triggering (threshold); vi) geotechnical properties of the soils involved; vii) human factors determining the instability of pyroclastic overburdens.

This research is necessarily based on the review of scientific contributions known in literature. and it is aimed to the improvement of some crucial aspects. In fact over the past 10 years the Scientific Community provided many contributions for the understanding of triggering mechanisms of these landslides, resulting in many conceptual and numerical models that were issued. Results and interpretations hypothesised although valid in general, did not led to a unique interpretative model about the cause-effect relationship between rainfall and landslide initiation, above all for the methodological approaches broadly diversified.

Following the first hydrogeological model formulated on these phenomena (Celico et al., 1986), the predisposing condition for instability is the formation of a perched groundwater flow within the most superficial and permeable part of the carbonate bedrock. It would provoke a pore pressure increase below pyroclastic mantle, thus determining initial instabilities.

Among morphological elements responsible for instability, the rocky scarps are linked to the abrupt change in slope angle (Figure 3.1), which interrupt the continuity of the pyroclastic cover along the slope. The artificial interruption of the pyroclastic mantle are man-made cuts built along the slope. Under these conditions, the pyroclastic cover lies under free kinematic conditions.

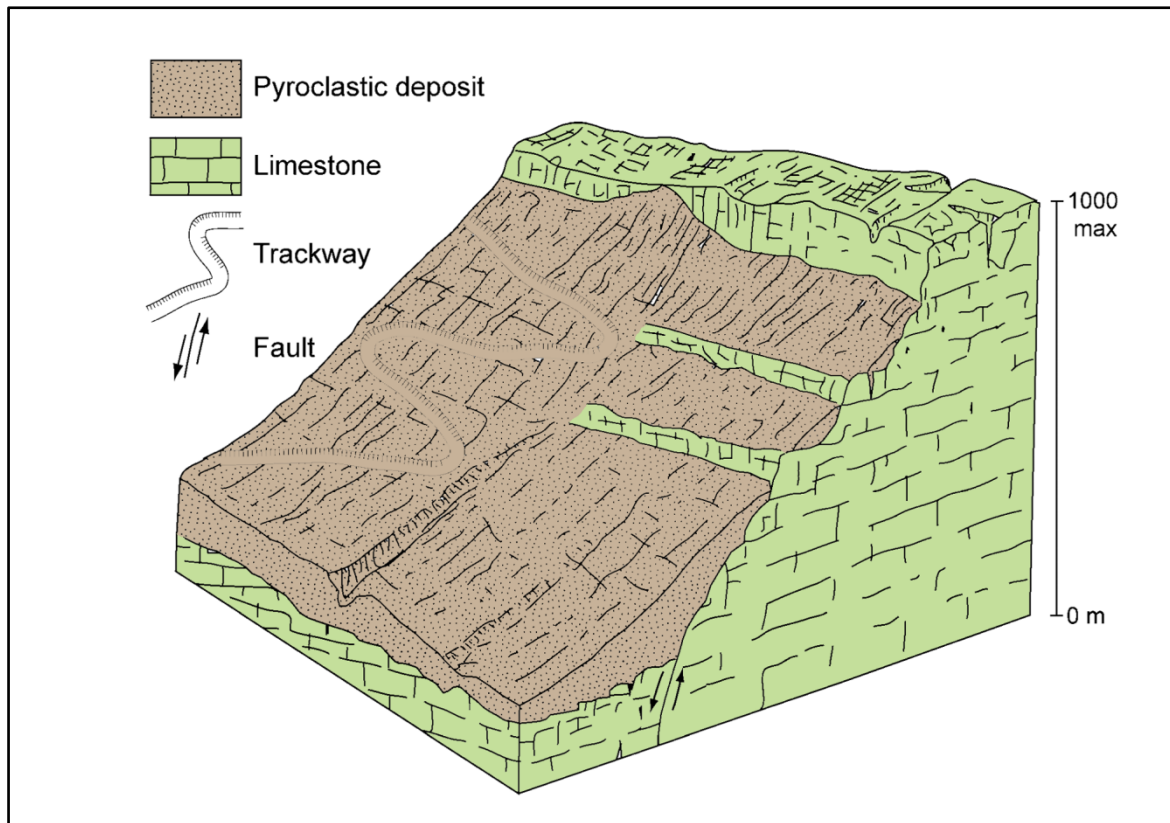


Figure 3.1: Schematic representation of the geomorphological characteristics of the peri-vesuviani hillslopes (Guadagno et al., 2005).

The first conceptual hydrogeological model (Celico et al., 1998) formulated to interpret the triggering of this type of landslides had some limitations, especially when the pyroclastic mantle is considered homogeneous, and it was subsequently amended by the same authors. The new conceptual model recognized the existence, within the pyroclastic mantle, of vertical hydraulic discontinuities. These correspond to interlayer of gravelly pumiceous lapilli horizons, with higher hydraulic conductivity, between finer grain size horizons (Bb horizons or paleosoils).

This more realistic physical model would hypothesize the formation of a perched water table within the horizons with higher hydraulic conductivity which would cause an increase in pore pressures up to saturation, and then the reduction of effective pressure and thus of the shear

strength. Moreover, the increase in water content led to further gain in specific weight, thus increasing the forces acting in favor of instability.

In the scientific literature, other conceptual hydrogeological models on a slope scale were issued also invoking a hydraulic contribution coming from the bedrock. Such models were based on results arisen from the stability analysis of the pyroclastic cover, that assessed rainfalls as insufficient to the instability. This demonstrated the necessity to invoke the hydraulic contribution from the carbonate bedrock (Cascini et al., 2000; Guida, 2003; Cascini et al., 2010), according to the abovementioned hydrogeological model (Celico et al., 1986). Also, these models predict the existence of groundwater flow during rainfall events characterized by high intensity/duration, in the shallowest zone of the carbonate bedrock, more fractured and karstified than the deeper zone. It might generate hydraulic under-pressures below the pyroclastic layers, thus determining the instability.

In the last formulation Cascini et al. (2008) and Cascini et al. (2010) postulated the presence of high altitude springs of seasonal, permanent or temporary character, with different capacity. They are associated with the presence of wedge-shaped hydro-structures caused by the convergence of fractures involving the bedrock, and characterized by a hierarchical order.

In order to identify the typical source areas, six slope models (M1 to M6) were proposed (Cascini et al., 2008). These in turn are associated with morphological features of the slopes, which can be related to the volume of unstable pyroclastic cover and to the increased distances reached from the flow. In general, the latter triggering models hypothesized that localized pore pressures, induced by the bedrock, must be a necessary condition leading to the failure of pyroclastic mantle.

All these models of source areas highlight peculiar properties of pyroclastic cover that certainly were unknown before the May 1998 events. Although they allow to take a step forward in the context of landslides in ash fall pyroclastic deposits, they seem to be quite general. Indeed they are valid on the slope scale and are hardly able to characterize these phenomena on a punctual scale, as the initial debris slides are in the source areas.

The research carried out in this thesis can be considered as belonging to the wide and complex framework regarding the initiation of pyroclastic flows phenomena characterizing the peri-Vesuvian hillslopes. In order to improve the understanding of the initiation mechanisms it was necessary to acquire new data able to enrich the previous knowledge. In particular, improving the understanding about triggering mechanisms it would be possible to plan appropriate works of active defence for the inhibition of landslides initiation. The models known in literature, briefly summarized in this section and widely discussed in the previous chapter, allowed to focus the aims of this thesis to the improvement of triggering models, especially if considering that the whole landslide phenomenon

($10^3 \div 10^5 \text{ m}^3$) can be triggered by a very small initial debris slide ($10^2 \div 10^3 \text{ m}^3$). In such a view, surveys and measurements were carried out on a detailed scale within the initial landslide areas. The specific aim of this doctorate thesis is to experiment a different approach in the study of the triggering mechanisms of these complex phenomena. This was possible by carrying out field and laboratory experimentations regarding some landslides among those occurred on May 5th and 6th 1998 along the Sarno Mountains, and by modelling hydrological and mechanical conditions leading to initial instabilities. Indeed, the definition of hydrological thresholds for triggering of initial landslides through a deterministic approach (Godt and McKenna, 2008) was based on the reconstruction of detailed engineering geological models and hydrological and stability modelling.

To achieve this purposes it was planned to perform some fundamental steps of the research, based on the application of different methods, that will be carefully explained in this chapter applied both in field and laboratory:

- A. Research and analysis of the broad bibliography concerning landslides phenomena involving ash-fall pyroclastic deposits covering Campanian hillslopes.
- B. Definition of engineering geological models of initial debris slides triggering debris flows, based on detailed surveys and measurements of stratigraphic and geometric features of pyroclastic mantle.
- C. Mechanical and physical characterization of pyroclastic soils, for each of the stratigraphic horizons that are relevant in landslides initiation.
- D. Saturated and unsaturated hydraulic characterization of pyroclastic soils, with determination of Soil Water Retention Curves (SWRC), for each of the stratigraphic horizons that are significant for landslides initiation.
- E. Hydrological and mechanical modeling of stability of initial landslides by means of finite differences numerical models.
- F. Definition of deterministic hydrological thresholds for landslide initiation.

The issue of the instability of pyroclastic cover is known to the scientific community since the 70s, but after the May 1998 events that caused the loss of 156 human lives, it was studied with different approaches: mechanisms of initiation and evolution of the landslide (Celico & Guadagno, 1998; Del Prete et al., 1998; De Riso et al., 1999); mineralogical aspects of soils of pyroclastic origin (De Gennaro et al., 2000) and geotechnical properties (Cascini, 2004, Esposito & Guadagno, 1998; Guadagno & Magaldi, 2000); hydrological triggering conditions (Chirico et al., 2000, De

Vita, 2000, Fiorillo et al., 2001; Guadagno, 1991); characteristics of the soils of pyroclastic origin (Terrible et al., 2000); morphological factors predisposing instability (De Vita et al. 2006a, 2006b; Brancaccio et al., 2000; Cascini et al., 2000; Celico & Guadagno, 1998; Di Crescenzo & Santo, 1999); superficial hydrological models (De Vita & Piscopo, 2002), stability model of pyroclastic cover (Cascini, 2004; Crosta & Dal Negro, 2003, Guadagno et al. 2000); role of unsaturated conditions on the stability (Scotto Di Santolo, 2000), analysis of the debris flow path (Budetta & De Riso, 2004; Revellino et al., 2004). Results of the bibliographic analysis, limited to the most relevant papers consistent with the specific purpose of this research, have been discussed in the previous chapter.

Engineering geological models of the initial debris slides were reconstructed by means of specific field and laboratory experimentations. Analyses were conducted on a detailed scale being proportionate to the small size of initial landslides often smaller than 10 m both in width and length.

Specifically, starting from field evidences that initial landslides have frequently small volume ($10^1 \div 10^2 \text{ m}^3$), the object of this research was focused on the analysis of the results of detailed surveys, carried out in some representative source areas.

Owing to the detailed characterizations and geometric reconstructions, we consider our attempt a real possibility to improve results already obtained from stability analysis of pyroclastic soil for a single landslide initiation (Crosta and Dal Negro, 2003; Guadagno et al., 2003) and from definition of hydrological thresholds (Calcaterra et al., 2000; Chirico et al., 2000; Crosta and Dal Negro, 2003; De Vita, 2000; Fiorillo and Wilson, 2004; Guadagno, 1991).

The definition of physical and mechanical properties of the pyroclastic mantle of the sample areas were planned as follows: determination of hydraulic conductivity at saturation; characterization of physical properties and engineering-geological classification of pyroclastic soils; determination of the shear strength parameters.

Hydrological and mechanical modelling was performed by means of implementation of finite difference models of hillslope hydrological processes, by means of VS2DTI. On the basis of the results of hydrological modeling with different intensity / duration rainfalls, a slope stability analysis was performed allowing the definition of deterministic hydrological thresholds.

3.2 Identification of representative sample sites

The study area is included in the steep slopes of the Sarno Mountains that culminates with the Pizzo D'Alvano relief (1.133 m a.s.l), that is a carbonate massif. It is located in the SE area of the Campanian Plain, delimited in the W sector by the Nolan Plain, in the S by the Sarno Plain, to the N by the Lauro valley (Figure 3.2).

In the study area, some sample sectors corresponding to sources of landslides occurred in May 1998 were identified in order to carry out a survey on a detailed scale.

On the basis of preliminary surveys, three representative initial landslides easily accessible in the source area, were identified (Figures 3.2 and 3.3), and named Landslide 1, Landslide 2 and Landslide 3.

This choice arises from literature data based on statistical analysis of all the landslides occurred at Pizzo D'Alvano in the 1998 event, showing that there are at least three main types of landslides triggered in different morphological conditions (Guadagno et al., 2005) depending on morphology of the source areas (Figure 3.5).

A broad statistical analysis (Figure 3.4) concerned the morphological characteristics of the source areas of landslides (Crosta & Dal Negro, 2003). It showed that about 75% of the landslides took place at sites with morphologic and stratigraphic interruptions of pyroclastic covers, generally at located the edges of scarps, corresponding to outcropping limestone scarps. Figure 3.5 shows the same type of instability at short distance from a man made cut. In both cases, the volcaniclastic material can be considered to be in kinematic freedom conditions.

As emphasized by Guadagno & Perriello Zampelli (2000) and demonstrated, for this specific setting of the Campanian Apennines by Guadagno et al. (2003) through numerical modeling, the presence of cuts or scarps along slope breaks the continuity of the infinite slope condition. It also induces significant changes in both surface water and groundwater circulation patterns. Field observations demonstrate that a large part of the initial failure surfaces are generally located in the pyroclastic multilayer mantle.

3.2 Identification of representative sample sites

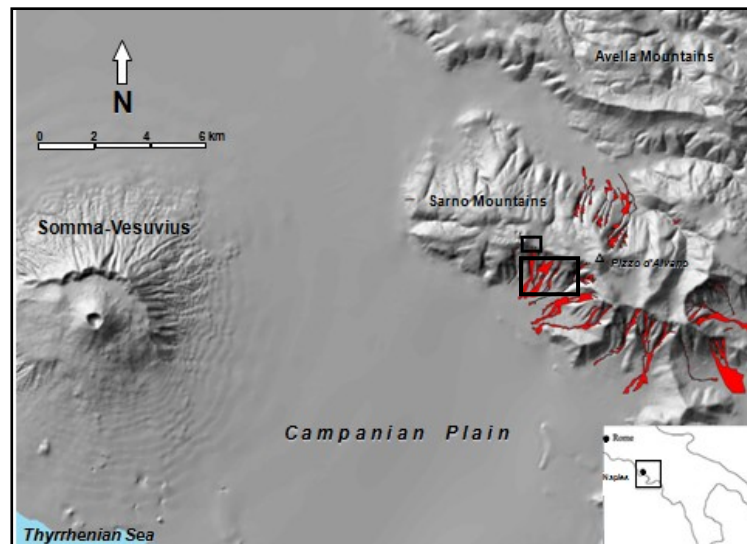


Figure 3.2: Location of the area surrounding Somma-Vesuvius complex. Black rectangle is zoomed in the next Figure 3.3.

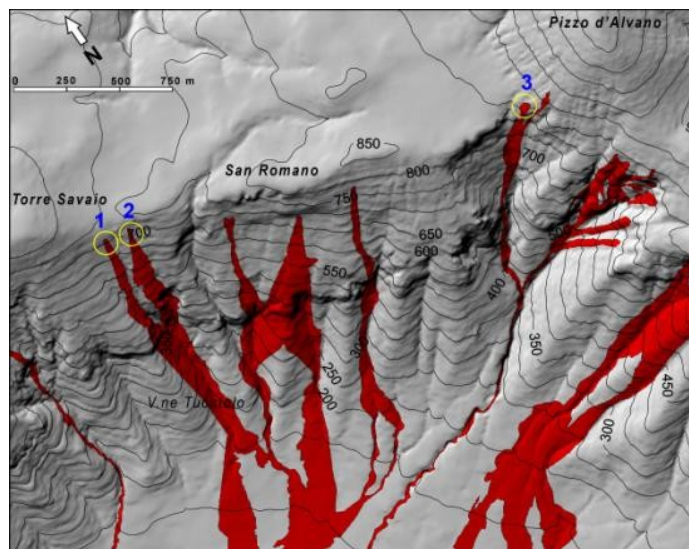


Figure 3.3: location of the sample area and landslides object of study.

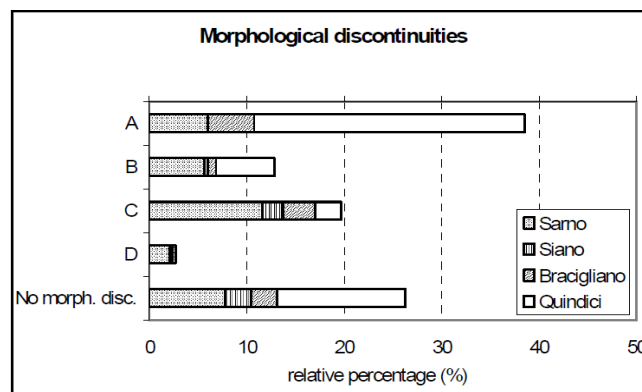


Figure 3.4: Morphological characteristics of source areas and relative frequency: (A) road cut with instabilities in the upslope sector and within the (B) downslope earth fill; (C) above rocky cliff inducing a natural interruption of volcaniclastic cover; (D) below a rocky cliff; (E) percentage of landslides without morphological discontinuities (Crosta & Dal Negro, 2003).

Definitively three representative cases were identified (Figure. 3.5):

1. Landslide 1: in correspondence of a knickpoint, namely a sector of slope with a progressive increase of slope angle that accounts for a progressive thinning of the pyroclastic cover that remains continuous.
2. Landslide 2: above a road-cut (type b in Figure 3.5).
3. Landslide 3: above a rocky cliff accounting for an sudden interruption of the pyroclastic cover (type a in Figure 3.5).

Other cases were not considered because of difficult logistic conditions that avoided specific surveys and transportation of the equipment.

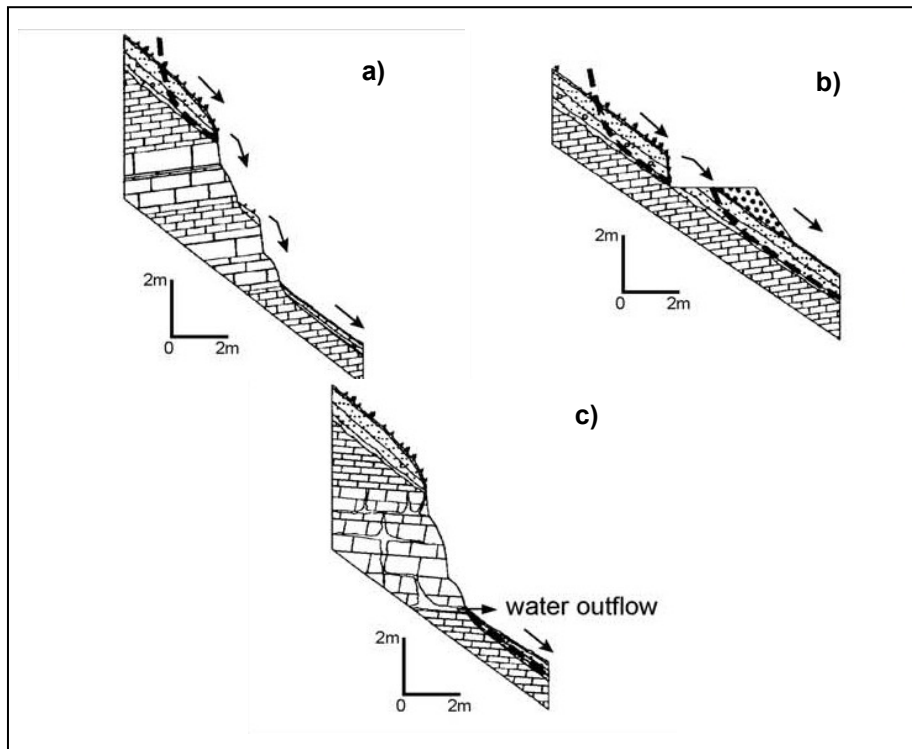


Figure 3.5: geomorphological setting of the three main source area types for the 1998 landslides, among those identified by the authors; typical example showing an initial slide that occurred on natural scarps, artificial cuts, road filling material, local stratigraphic and hydrogeological conditions (Guadagno et al., 2005).

3.3 Engineering geological characterization of pyroclastic cover mantling Pizzo d'Alvano massif: field methodologies

As aforementioned, the gently dipping monocline structure of the Sarno Mountains consists of a sequence of dolomitic limestones alternating with Lower Cretaceous detrital limestones and Upper Cretaceous grey limestones, whose transition is marked by a marly-conglomeratic level which is displaced at different altitudes by direct fault systems. Ridges have often slope angles average from $30^\circ \div 35^\circ$ up to verticality. These slopes are discontinuously mantled by ash-fall pyroclastic soils derived from the volcanic activity of Somma-Vesuvius volcano. Pyroclastic ash-fall deposits basically derived from six main eruptions (from 17 k-years to 1631 AD) form a composite volcanoclastic sequence in which past and present pedogenetic processes are very relevant. The pyroclastic cover shows an inhomogeneous and discontinuous distribution along the slopes, controlled by the slope angle. In the next paragraphs laboratory and field methods are described. The resulting engineering geological models of these complex landslides, are focused on the initial stage of sliding evolving to debris flow, the so called "initial landslides".

3.3.1 Topographical surveys

Based on preliminary surveys, three easily accessible landslides were identified as the most representative within the population of "initial" landslides (Figure 3.3). A topographical field survey was carried out in order to reconstruct axial and longitudinal topographic profiles, in Torre Savaio locality (for Landslides 1 and 2) and Pizzo D'Alvano (for Landslide 3).

Stratigraphic and geometric characterization were addressed to the reconstruction of the pyroclastic mantle – carbonate bedrock system of Pizzo D'Alvano by means of a theodolite and a laser inclinometer "Leica Disto A8".

A theodolite is essentially an opto-mechanical instrument for measuring angles, that is able to measure distances, geographic and magnetic azimuth and zenith. It consists of a base, fixed to the ground by a tripod (Figure 3.6). Angle measurements are carried out on graduated circles; the circle for the equatorial angle is normal to the primary axis (is horizontal when the instrument is in the station), and the circle for zenith angles is normal to the secondary axis, and lies in a vertical plane if the primary axis is vertical. Estimation of distances are indirectly obtained through measurements of azimuth angles with respect to a reference point, and zenithal angles with respect to readings on

known length on a vertical graduated rod. Such graduated rod, also called stadia, consists of rectangular sections (2×10 cm), 2 to 4 m long, whose front face shows the decimeters. It is moved on the ground in front of the teodolite by an operator.

The Leica Disto A8 is an optical instrument for measuring distances. The operating principle is based on the reflection of a laser beam emitted by the tool against an obstacle such as a board, a wall or other reflective surfaces. Being known the propagation speed of the beam and the time it takes from emission to reception of the signal after being reflected, the instrument gives: the distance of the reflection point, and angle between the direction of the measuring point and the horizontal plane by means of an inclinometer. Moreover the Disto A8 can measure the zenithal angle above the horizontal. To carry out the measurement, the Disto A8 was fixed to a tripod with a three-rotating-axes head, thus ensuring the rotating movement in the vertical plane, describing in this way a topographic section in polar coordinates (Figure 3.6).

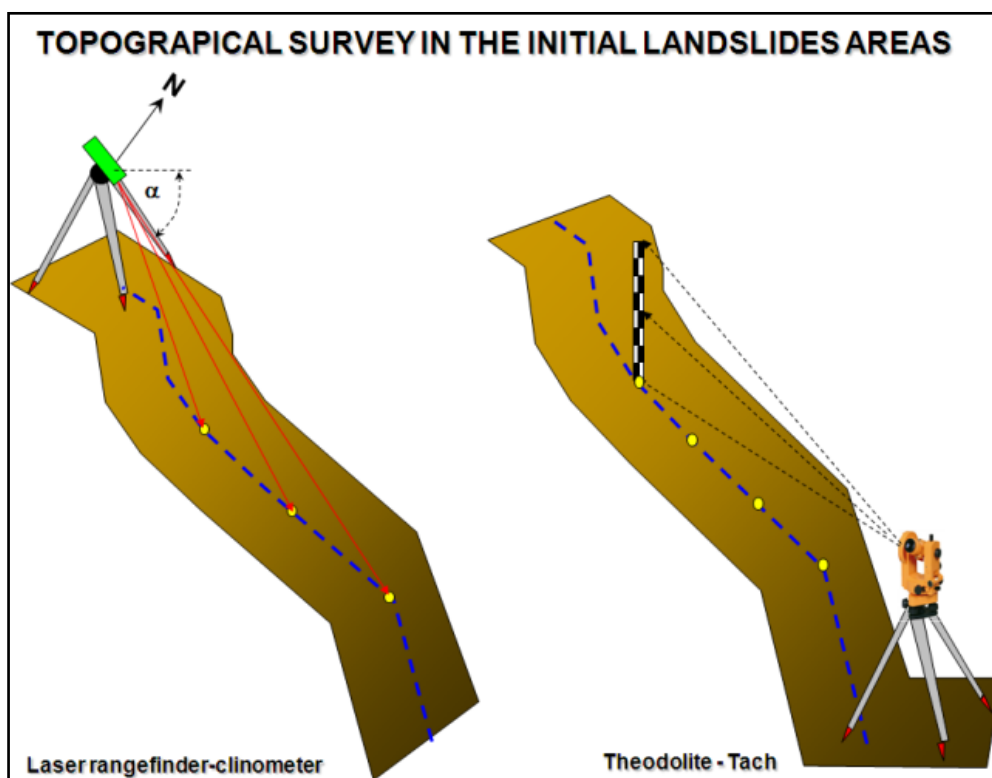


Figure 3.6: instrumentation used for field topographical survey in areas of initial landslides.

3.3.2 Stratigraphical characterization

Stratigraphical data were also acquired through exploratory pits, trenches, and drillings and were carried out by means of Hedelman's hand auger. Indirect measurements were carried out by means of dynamic penetration tests (DPL and DPM) in alignment with the topographic profiles. Exploratory pits and trenches were carried out by hand digging in the main scarp of the source zones, at the sides of the landslides and anywhere it was possible reach the bedrock. This operation allowed to clarify the stratigraphical sequence characteristic of the initiation zone. This permitted to understand: the thickness of the different pyroclastic levels; the type of deposition (primary or secondary); the characteristics of the eruptive events to which they belong; the pedogenetic processes they underwent over the time. The stratigraphic analysis was performed by using Hedelman's hand auger, that is a very appropriate equipment for the investigation of the first few meters under ground level. The equipment consists of metal rods of standard length that allow to reach the depth of interest and an ergonomic "T" shaped handle, which gives the torsion to enter the auger. The drilling equipment can reach depth ranging from 8 to 10 meters, depending on several factors such as the depth of the bedrock from ground level and the characteristics of the material.

Dynamic penetrometric tests are useful and often appropriate tools for geological prospecting in pyroclastic soil mantling hillslopes, because they can clearly identify both the carbonate bedrock depth and the variation of dynamic resistance within the pyroclastic mantle. This would allow to identify the horizons of gravelly pumiceous lapilli, which are characterized by the highest dynamic resistance among the others pyroclastic horizons. This methodology allowed to achieve the in situ shear strength parameters of soils, by means of a continuous penetration of a conical tip at the bottom of a series of steel rods.

Two dynamic penetrometers were used. An on-purpose designed light penetrometer (DPL), very portable on steep slopes, was extensively used (Figure 3.7a). It was characterized by energy provided by a falling mass of 6 kg, dropped from a constant height of 0.5 m on a 3.2 kg steel anvil that was connected to a 0.016 m diameter steel rod series (1.58 kg/m) (m') at whose bottom was located a standard tip (CEN/TC341) with a $6 \times 10^{-4} \text{ m}^2$ sectional area (A) (Specific Energy = 49.05 kJ/m^2). For deeper penetration tests a medium dynamic penetrometer (DPM) was used (Figure 3.7b), characterized by a mass of 30 kg falling from 0.2 m height. According to geotechnical standards, the resistance to penetration was defined by the number of blows required to penetrate the tapered tip for a defined depth interval (0.10 m). This test is particularly recommended for a first evaluation of the stratigraphy of the sites in comparison with stratigraphical data obtained by trenches and pits. It may be used for a qualitative evaluation the shear strength of pyroclastic

soils. In this research empirical correlations were not used, owing to peculiarity of pyroclastic soils but it was used the generalized Dutch formula (Sanglerat, 1972) which allows the estimation of the dynamical resistance:

$$R[\text{MPa}] = \frac{m \times H \times g}{A \times \frac{z}{N_z}} \times \frac{m}{m + m'}$$

where:

m is the beating mass; H is the falling height; m' is the steel anvil and rod mass; A is the sectional area; N_z is the number of blows for every 0.10 m of penetration (z); g is acceleration of gravity.

The use of such a formula allowed to compare the results obtained with two different dynamic penetrometers, converting the N_{10} values in dynamic resistance (R).

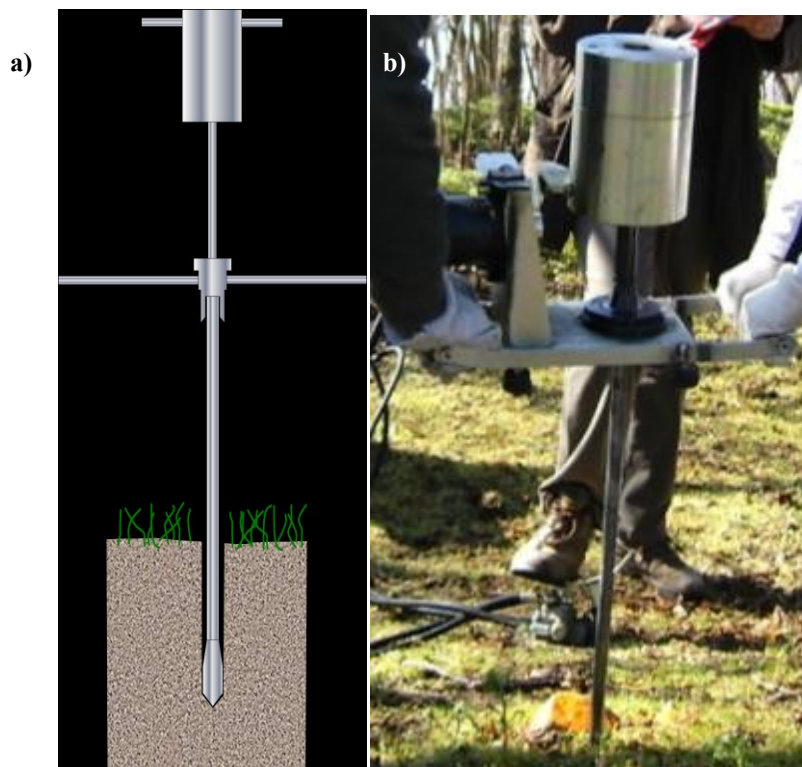


Figure 3.7: a) DPL; b) DPM.

On the basis of a careful bibliographical analysis (Celico et al., 2000; Crosta & Dal Negro, 2003; De Vita et al., 2006a; De Vita et al., 2006b; Terribile et al., 2000), it was possible to perform a preliminary characterization of pyroclastic soil horizons in some areas where initial landslides are

located. The following criteria were taken into account, for the identification of pyroclastic mantle - bedrock system of Pizzo D'Alvano massif:

- 1) lithological, lithostratigraphic and engineering-geological criterion (based on characterization through laboratory tests and USCS international classification)
- 2) pedological criterion (Terribile et al, 2000; Soil Survey Staff, 1998), based on the recognition of the main soil horizons.

The pedological approach, is fairly recent since the classical literature on landslides focus primarily on the geology and geomorphology, considered as absolutely important but not exhaustive about characterization and interpretation of shallow landslides. Pedological processes transform volcanic deposits in a special type of soils named andosols. Such a group of soil is present in a wide area of the Campania region (Di Gennaro et al., 1998).

Their properties play a key role in the triggering mechanisms of landslides. Their inventory is based on Soil Taxonomy (Soil Survey Staff, 1998): allophane soils in fact, show particular geotechnical features, i.e. the low specific gravity, high porosity, high values of saturated water content at high liquidity limit and low plasticity. The soils of the study areas have tixotropic property, that is the capacity of a soil to change its viscosity when subjected to shear stress or pressure due to the presence of a low degree of crystallinity of the clay. This feature might have an important role in the propagation and amplification of the initial slide.

The principal soil horizons are described by the following letters, representing the basis for the designation of pedological profile (Figure 3.8):

- O** is the horizon dominated by decomposed organic matter, or undergoing to decomposition, or being deposited on the surface.
- A** indicates mineral horizon at the surface or below the O horizon. It has totally lost the original structure of rock and commonly shows an accumulation of humified organic matter, linked to the mineral fraction of soil and / or property resulting from disturbance, as for example grazing. It has a typical dark color, caused by the presence of organic matter and granular structure and / or polyhedral sub-angular.
- B** indicates the horizon formed below the horizon A or O, where the original rock structure is completely or partially lost. It may appear as a horizon enriched in clay (for alteration processes), oxide of iron and aluminum (for residual accumulation) and other elements.

Usually, its color is lighter than the A horizon and its structure is usually prismatic or angular (but also columnar in some cases). On its top, a transitional horizon may be present, that is designated as AB if there are predominant features of the above horizon, or BA if there are prevailing characters of B.

-**C** indicates the horizon of incoherent pedogenic substratum and is usually not hard. Above this horizon may be a transition that is designated BC or CB depending on the prevailing character of the horizon, respectively B or C.

-**W** indicates the presence of water within the soil.

-**R** indicates the bedrock, hardened or strongly cemented, that is not possible to reach by means of regular digging.

Several secondary characterizations can be attributed to each principal soil horizons (Soil Survey Staff, 1998) with the addition of a lowercase second letter. Among the various secondary characterizations, the feature buried (**b**) is useful for stratigraphical description of pyroclastic soil horizons (e.g. Bb horizon means buried B horizon, namely it indicates a paleosoil).

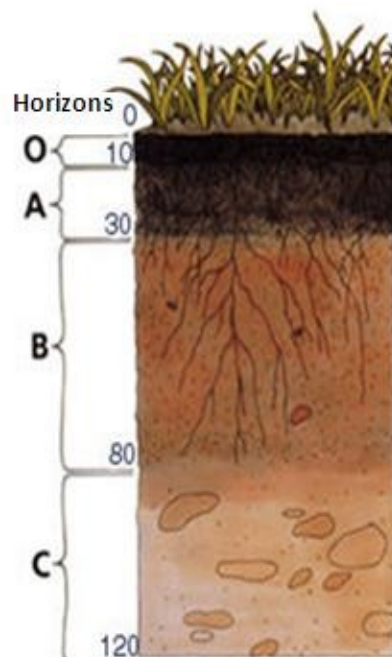


Figure 3.8: Schematic representation of principal soil horizons.

3.3.3 Undisturbed sampling for characterization of physical and mechanical properties of pyroclastic horizons

Owing to their high porosity and loose structure of pyroclastic soils, physical parameters, such as unit weight (γ) and dry unit weight (γ_d) were determined by means of field procedure based on the insertion of a Shelby cylindrical sampler into the soil (Turner and Shuster, 1996), and by estimating gross weight and volume respectively by means a portable spring balance, and measuring the inner volume occupied by the soil specimens (Figure 3.9a). Subsequently, after an oven-drying procedure carried out in laboratory, the dry unit weight (γ_d) was measured. Such a procedure was applied on 30 soil samples homogeneously distributed among various soil horizons.

Sampling was carried out using a cylindrical stainless steel tube (Figure 3.9b), with a length 40.5 cm, diameter 5.7 cm and an empty weight of 810 grams. The tube was driven in pyroclastic levels, through shots given by means of a hammer of 8 kg, on the top of a metal rod connected to the upper part of the sampling tube.



Figure 3.9: a) spring balance weighing the sampling tube; b) sampling tube.

After sampling, the natural unit weight (γ) and the dry unit weight (γ_d) were calculated from the known dimensions of the sampling tube, through which was calculated the sampled volume by using a dynamometer (Figure 3.7a) it was possible to know their weight, by means of the equation:

$$\gamma_n = \frac{P_l - P_t}{3,1416 \cdot \left(\frac{D}{2}\right)^2 \cdot (L_f - L_v)}$$

where:

P_l = gross weight (g) (sampling tube + sample); P_t = tare weight (g) (sampling tube); D = sampling tube diameter (cm); L_f = sampling tube length (cm); L_v = length of the filled part of the sampling tube (cm).

In order to collect soil samples to use for the characterization of mechanical properties, an undisturbed sampling was carried out in the crown areas of the three representative landslides, plus other adjacent landslides located at Pizzo D'Alvano. It was carried out in different periods, that is at the end of Winter and the beginning of Summer, and through the use of steel cubic boxes open on one side, 12 × 12 × 12 cm sized, and characterized at the base by a cutting edge to minimize resistance during the driving, and at the opposite side by a flat surface where to drive blows with a hammer of 8 to 10 kg (Figure 3.10). Sampling was carried out, for a good representativeness, upslope of sources in the crown zones (Table 3.1), and did not involve the pumice horizons (since these horizons are very loose).



Figure 3.10: sampler for shear tests and physical characterization of pyroclastic soils covering Pizzo D'Alvano massif.

| Horizon ID | Sampling depth (m) |
|---|--------------------|
| B* | 0.40 |
| Bb* | 1.10 ÷ 1.40 |
| Bb _{basal} ** | 2 |
| *In the uphill area of the crown zone **in the area downstream of the crown zone | |

Table 3.1: undisturbed sampling depth of soils for direct shear test.

Another type of sampler used to carry out laboratory hydraulic conductivity tests was designed and developed by Prof. P. De Vita and Prof. N. Roberti (Department of Earth Sciences of University of Naples “Federico II”). This equipment (Figure 3.11) is characterized by a stainless steel tube with a cutting base, to minimize resistance during the driving into the ground and on the other side, from a flat surface. It consists of three parts which are assembled by thread, created within a lodging for the sampler s.s., thus trapping undisturbed material. The interior part of the sampler consists of a plexiglass cylinder of length 14.9 cm and diameter equal to 7.4 cm, that was conceived for observing through the transparent plexiglass the state of the sampler just after collection and then to decide whether or not it is representative of the sampled material.



Figure 3.11: sampler for collection of undisturbed samples, for laboratory hydraulic conductivity tests.

As regards samples that were tested for hydraulic assessment through “Tempe cells”, sampling was carried out by means of the brass ring that makes up the assembly of equipment, which is described in the section 3.5.2. This methodology arises from the necessity to cause

minimal disturbance to the samples subject to hydraulic characterization, to make as representative as possible the soil-water characteristic curves of each soil object of study. Depth of sampling for specimens tested with the six Tempe cells constituting the whole apparatus, are shown in Table 3.2.

| Sample ID | Sampling depth (m) | Landslide n° | N of tests (tempe cell n°) |
|-----------|--------------------|--------------|----------------------------|
| B | 0,40 | 2 | 6 (1-6) |
| C | 1,50 | 2 | 6 (1-6) |
| Bb | 2,40 | 2 | 2 (1-2) |
| | | 5 | 2 (3-4) |
| Bbbasal | 2,20 | 5 | 2 (5-6) |

Table 3.2: depth and location of sampling.

3.3.4 Field tests for hydraulic conductivity measurement

The knowledge of the hydraulic parameters of the unsaturated zone has a considerable importance in problems of different nature such as: land use and irrigation, slopes erosion or landslides, contamination of groundwater recharge of aquifers. Numerous equipment and different methods were developed in order to evaluate the hydrological parameters of the unsaturated zone of a soil. As regards the *in situ* tests, hydraulic devices used to estimate the hydraulic conductivity allow to carry out adsorption tests either from soil surface or within a hole. In both cases, field tests are based on infiltration capacity evaluation. The term infiltration involves physical processes allowing water entry within the soil pores from the surface. The computed hydraulic conductivity is defined field hydraulic conductivity ($K_{sat \text{ field}}$), and it is lower than $K_{sat \text{ s.s}}$, since the saturation process takes place from the top. It causes the air bubble trap within the soil particles, thus reducing hydraulic conductivity:

$$K_{sat \text{ field}} \approx 0.75 \div 0.5 K_{sat}$$

(Bower, 1966; Reynolds & Erik, 1986).

Infiltration model used for infiltration capacity (f) assessment is Philip (1957), that is an evolution of (Horton, 1940):

$$f = \frac{1}{2} S \cdot t^{-0.5} + A$$

where S is sorptivity [$\text{m/s}^{0.5}$]

And since:

$$\lim_{t \rightarrow \infty} f(t) = K_{sat}$$

The first equation can be written in a simpler form:

$$f = \frac{1}{2} S \cdot t^{-0.5} + K_{sat}$$

Among several instrumentations used, the single ring infiltrometer (Figure 3.13) consists of a cylinder of diameter larger than height (up to 60 cm), which is driven in the soil for a few centimeters. In this type of hydraulic instrument, the diameter's width allows to estimate hydraulic conductivity (K_{sat}) on a greater volume of soil, thus becoming more representative of the real K_{sat} .

In this case the infiltration flux is not laterally confined; it is influenced both by capillarity phenomena and it is controlled by the gravity. The flux first reaches a transitory phase, during which it asymptotically decreases down to a constant value, corresponding to the saturated hydraulic conductivity (K_{sat}), thus reaching the steady state (Figure 3.12). Then, when infiltration capacity gets the saturated hydraulic conductivity value (K_{sat}), the capillarity flux has a negligible effect on the infiltration process occurring through the infiltrometer ring.

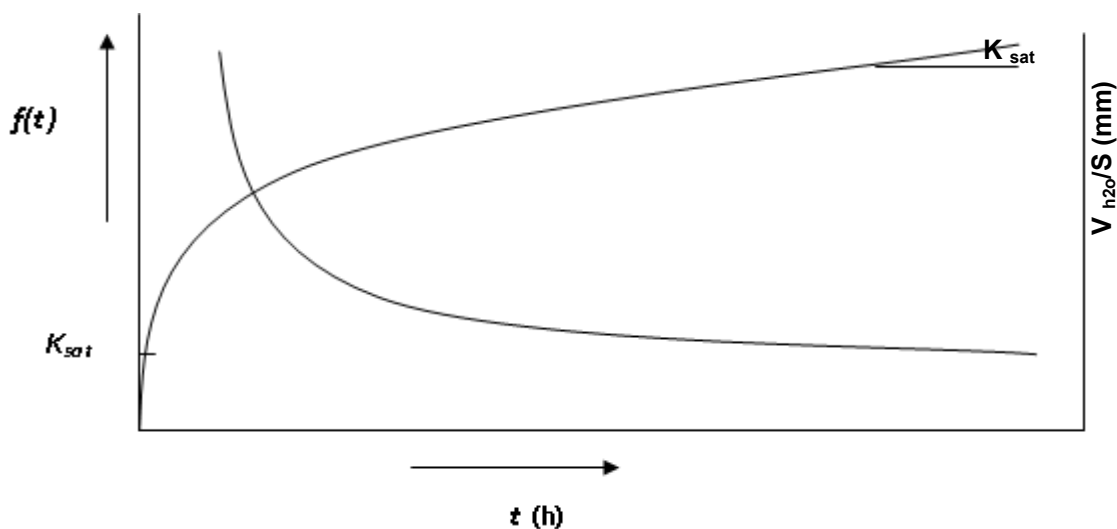


Figure 3.12: infiltration capacity according to the Horton and Philip models.



Figure 3.13: single ring test method combined with a Mariotte bottle that allows to keep constant the water level within the infiltrometr ring.

Another field instrument for hydraulic conductivity assessment is the “Constant Compact Head Permeameter” (Figure 3.14a). It is a device that allows to keep constant the hydraulic head (H) and the water supply required by infiltration in the soil, within a borehole (below the ground level) by means of a graduated reservoir.

This hydraulic device is based on the principle of Mariotte bottle which is closed to the atmosphere by a top cap and filled with water. Through the cap a thin plexiglass tube open on both sides is inserted, in which the lower one is submerged below the water level and the upper one is open to the atmosphere. Laterally, and at the base of the bottle, a hole is drilled. The bottle is filled with water in order to partially immerse the glass tube; by the side hole, driven by hydrostatic pressure, water overflows.

The saturated hydraulic conductivity (K_{sat}) can be estimated with Constant Compact Head Permeameter, by means of the Glover formula (Zangar, 1952) :

$$K_{sat} = \frac{CQ}{2\pi H^2}$$

where:

$$C = \sin h^{-1} \left(\frac{H}{r} \right) - \left[\left(\frac{r}{H} \right)^2 + 1 \right]^{1/2} + \frac{r}{H}$$

H is the height of the water level in the borehole (m); r is borehole radius (m); Q is the infiltrated flow in the hole (m^3/s).

The method allows the estimation of field saturated hydraulic conductivity ($K_{sat \text{ field}}$) at different depths and values of the desired hydraulic head: the depth at which the water level can be kept constant depends on the number of constant head tubes mounted on the instrument. However it is limited to about 6 ÷ 7 m depending on the physical properties of the water that boils at the usual temperature range under a negative pressure of 0.6 ÷ 0.7 atm.

The connection of a series of constant head tubes allow to increase the reference level of water in the hole, thus allowing to reach greater depths (Figure 3.14).

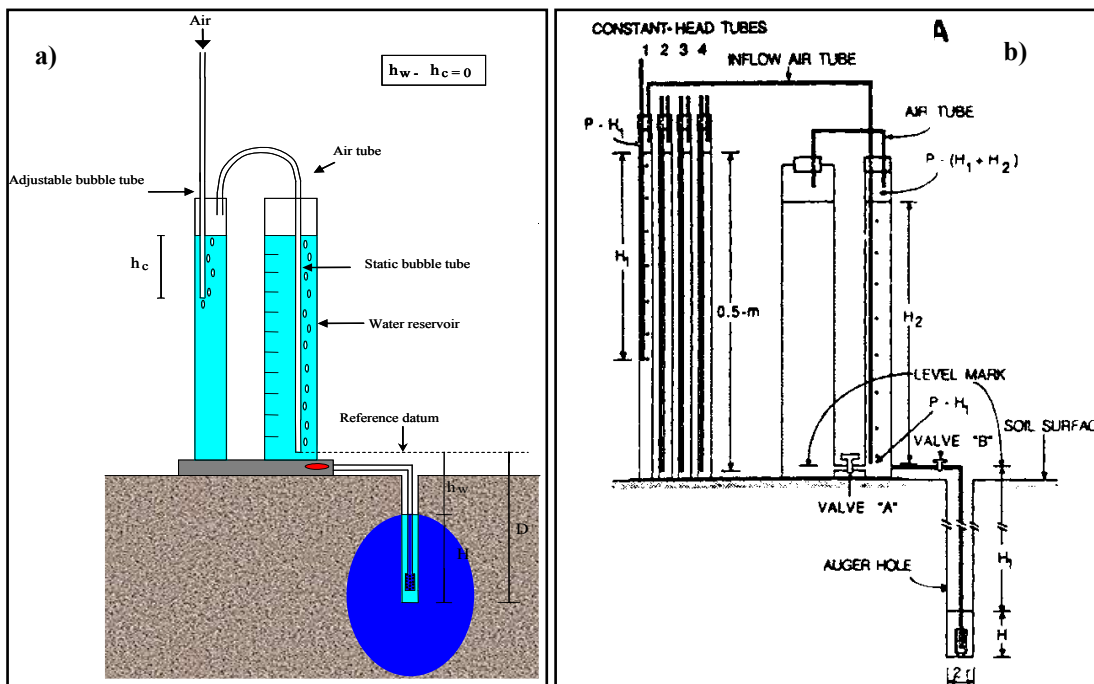


Figure 3.14: (a) Borehole Constant Compact Head Permeameter (Amoozegar, 1989). (b) CCHP with tubes connected in series.

3.4 Laboratory methodologies for the characterization of pyroclastic soils

In this section, the laboratory methods used to determine the main physical index and mechanical properties of pyroclastic soils of Pizzo D'Alvano slopes are described. Laboratory tests allowed to discriminate the geotechnical characteristics of pyroclastic horizons sampled during field survey, and to classify them according to current engineering geological classifications.

3.4.1 Physical characterization of pyroclastic soils

The water content (w) (ASTM D2216-80) of a soil is defined by the ratio between the weight of the water contained in the interstitial voids and the weight of the mineral phase.

The unit weight of a soil is the ratio between the weight of the sample (P) and the volume of the same sample (V), expressed with gr/cm^3 or kN/m^3 units. In natural conditions, the natural unit weight (γ_{nat}) is considered taking into account the solid skeleton and the fluid contained in the pores. The weight of volume varies according to the water content, but it is comprised between two extreme values: the dry unit weight (γ_{dry}) and the saturated unit weight (γ_{sat}). Starting from these physical and volumetric parameters it is possible to obtain porosity (n).

The porosity (n) of a soil is defined by the ratio between the volume of voids and the total volume (V_v/V_t) in natural water content conditions, and by the relation V_w/V_t under saturated conditions. This is a-dimensional parameter and it is expressed in percentage. It is indirectly estimated, starting from the existing relationship between weights and volumes of the different phases. The void ratio (e) characterizes the densification degree of a soil.

For the determination of the specific weight of solid particles (G_s) carried out for particle diameters lower than 4.75 mm (*ASTM D 854-83; BS 1377-75 Test 6B; CNR-UNI 10010, 10013*), the pycnometer method is used, where 3 to 5 gr of soil passing through the sieve N°200 ASTM (75μ) are poured and mixed with distilled water. The gas phase of the obtained mixture (distilled water + soil) is removed by means of a vacuum pump, thus allowing to obtain the value of P_t (pycnometer weight + water weight + dried sample weight). The G_s indicates the weight of volume of the solid skeleton and is equal to (P_s/V_s).

In a cohesive and fine-grained soil, the change in volume and its rheological behavior are closely related to its water content. Any variation of moisture content may cause changes of physical state of a soil, passing from solid, to semisolid, to the plastic and finally to the liquid rheological state. Atterberg (1911), stated that the transition from a rheological state to another in a cohesive soil takes place when a certain moisture content (w) is exceeded. During laboratory experience, Atterberg limits were calculated, and in this context standard methodologies for these tests are briefly described as follows.

- The liquid limit (w_L) (ASTM D4318; BS 1377: Part 2: 1990), that is the water content of cohesive soil, represents the transition from plastic to liquid state. The determination of this limit was made through the use of the penetrometric cone apparatus (Sherwood and Ryley, 1970). This instrument consists of a steel rod sustained on a support at whose bottom is placed a steel cone (length 35 mm, apical angle 30°, and 80 g in weight). The rod is free to move with minimal friction along the vertical, measuring such movements by means of a micrometer. The cone is connected to the rod, placed in contact with the sample surface and after being released from an electromagnet (timed at five seconds) it sinks in the specimen. It is defined as liquid limit the water content at which the rod and the conical tip sink in the specimen for 20 mm. Another standard method is applicable by means of the Casagrande's cup apparatus (ASTM D 4318-84; BS 1377: Part 2: 1990) but it was used only the first described.
- The plastic limit (w_P) is the water content at which a soil changes from semisolid to plastic state. The standard method (ASTM D 4318-84; BS 1377: Part 2: 1990; CNR-UNI 10014) is based on the assessment of the plastic limit by measuring the water content corresponding to the incoming of superficial cracks during hand molding of cylindrical rods of samples (3-mm in diameter). The apparent subjectivity of the procedure justified the use of the experimental method proposed by Esposito and Di Clemente (2003), derived from the Wroth & Wood method (1978). It provides the use of penetrometer cone, whose tip is 80 g in weight, and is based on the dependence of w_L on the undrained resistance C_u . The sinking of the cone tip is a function of soil resistance, so this unit is able to directly provide the value of the undrained strength, and this concept is expressed by the formula:

$$C_u = \frac{K_a \cdot m \cdot g}{d^2}$$

This formula derives from Kumar, and M. Wood, (1999)

d = sinking of cone (mm); m = cone mass (80g); g = gravity (9,81 m/s²); Ka = form factor depending apical angle of the cone, and corresponding value 0,85.

The grain-size distribution analysis of a soil is a index property of fundamental importance. For its evaluation a standard laboratory procedure is adopted. It consists in the analysis of the frequency of solid particles of assigned dimensions. Such a frequency is given by the relationship between the weight of the grain–size distribution classes and the initial weight of the sample. The distribution is represented by means of the grading curve. As regards the grain-size distribution classes with diameters greater than 75 μ , the grading curve is constructed by means of the sifting analysis (ASTM D 421-85; D 2217-85; UNI 2334, 8520-PART 5; CNR Year V N.23-1971). The mesh dimension of sieves depends on the Tyler’s numerical series, where the sample previously dried passes through. If the percentage passing through sieve N° 200 ASTM (75 μ) is more than 10%, the particle size analysis (ASTM D422) is performed by means of sedimentation, thus highlighting the not negligible presence of fine particles (silt and/or clay).

This test is based on the Stokes law (1850) which describes the sedimentation rate of clasts immersed in a fluid of known viscosity. The sedimentation rate influences the density of soil-water mixture, which varies over time in function of the gradual settling of the particles. In a given moment, the density of the mixture depends on the amount of suspended particles. The average diameter of these is expressed by Stokes law, valid for spherical particles:

$$D = \sqrt{\frac{1800 \cdot \mu \cdot v}{G_s - \gamma_L}}$$

where:

G_s is specific gravity of solid particles (g/cm³), γ_L is the specific weight of the liquid (g/cm³), μ is the viscosity, v is the velocity of a particle to go from free surface of water and the center of mass of the densimeter (cm/s).

The test consists of measuring the rate of sedimentation of particles, that is the time the particles need to travel a distance between the water level and the bulb centre, by reading on the densimeter the value of density of soil-water mixture.

The grain-size curve is used to read off the grain size at which 10% of the sample passed (D_{10}), 30% of the sample passed (d_{30}) and 60% of the sample passed (D_{60}). These numbers are used to calculate the following coefficients: Hazen's effective size (D_{10}) which is used to estimate hydraulic conductivity (K); Uniformity Coefficient ($U = D_{60}/D_{10}$) which is used to estimate gradation.

3.4.2 USCS classification for investigated soils

Soil classification is a dynamic subject that is related to the final application, from the structure of the system itself, to the definitions of classes. Soil classification can be approached from the perspective of soil as a material, or as a resource. One of the most common engineering classification system for soils is the Unified Soil Classification System (USCS).

The USCS is a soil classification system used in engineering to group soils with homogeneous engineering properties by means of grain size and/or consistency limits analysis. The classification system can be applied to unconsolidated geological materials (soils), and is represented by a two-letter symbol described in Table 3.3. This classification system is suitable for the pyroclastic soils object of study. The USCS has three major soil classes: 1) coarse-grained soils (sands and gravels) if the passing to the ASTM No 200 sieve is lower than 50%, further subdivisions depend on grain size analysis; 2) fine-grained soils (silts and clays) if the passing to the ASTM No 200 sieve is greater than 50%, further subdivisions depend by consistency limits analysis through the Casagrande's plasticity chart; 3) highly organic soils (referred to as "peat") further subdivided into the three major soil sub-classes (Figure 3.15).

| Symbol | Definition | Letter | Definition |
|----------------------------|------------|---------------|--|
| G | gravel | P, W | poorly graded (uniform particle sizes) |
| S | sand | | well graded (diversified particle sizes) |
| M | silt | H, L | high plasticity |
| C | clay | | low plasticity |
| O | organic | - | - |
| First and/or second letter | | Second letter | |

Table 3.3: symbols used in USCS classification.

If the soil has 5÷12% by weight of fines passing a N° 200 sieve ($5\% < P_{n^{\circ} 200} < 12\%$), both grain size distribution and consistency limits have a significant effect on its engineering properties, and dual notation may be used for the group symbol. For example, GW-GM corresponds to "well graded gravel with silt". If the soil has more than 15% by weight retained on a N° 4 sieve ($R_{n^{\circ} 4} > 15\%$), there is a significant amount of gravel, and the suffix "with gravel" may be added to the group name, but the group symbol does not change. For example, SP-SM may refer to "poorly

graded sand with silt and gravel”. The USCS criteria for well-graded gravels (GW) and sands (SW) are:

1. Less than 5% finer than N° 200 sieve;
2. Uniformity coefficient greater than 4;
3. Coefficient of curvature between 1 and 3.

UNIFIED SOIL CLASSIFICATION SYSTEM

| MAJOR DIVISIONS | | GROUP SYMBOLS | DESCRIPTIONS |
|--|---|---|---|
| COARSE GRAINED SOILS More Than Half Retained on 200 Sieve | GRAVELS More Than Half Coarse Fraction Retained on No. 4 Sieve | Clean Gravels (Little or no Fines) | GW Well Graded Gravels, Gravel - Sand Mixtures, Little or no Fines |
| | | | GP Poorly Graded Gravels, Gravel - Sand Mixtures, Little or no Fines |
| | | Gravels With Fines (Appreciable Fines) | GM Silty Gravels, Gravel-Sand-Silt Mixtures |
| | | | GC Clayey Gravels, Gravel-Sand-Clay Mixtures |
| | SANDS More Than Half Coarse Fraction Passes a No. 4 Sieve | Clean Sands (Little or no Fines) | SW Well Graded Sands, Gravelly Sands, Little or no Fines |
| | | | SP Poorly Graded Sands, Gravelly Sands, Little or no Fines |
| | | Sands With Fines (Appreciable Fines) | SM Silty Sands, Sand - Silt Mixtures |
| | | | SC Clayey Sands, Sand - Clay Mixtures |
| FINE GRAINED SOILS More Than Half Passes 200 Sieve | SILTS and CLAYS Liquid Limit Less Than 50 | ML | Inorganic Silts & Very Fine Sands, Silty or Clayey Fine Sands, Clayey Silts |
| | | CL | Inorganic Clays of Low to Medium Plasticity, Lean Clays |
| | | OL | Organic Silts & Organic Silty Clays of Low Plasticity |
| | SILTS and CLAYS Liquid Limit Greater Than 50 | MH | Inorganic Silts, Fine Sand or Silty Soils, Elastic Silts |
| | | CH | Inorganic Clays of High Plasticity, Fat Clays |
| | | OH | Organic Clays of Medium to High Plasticity, Organic Silts |
| Highly Organic Soils | | PT | Peat and Other Highly Organic Soils |

Figure 3.15: Unified Soil Classification System, used for pyroclastic soils object of study (modified after Casagrande, 1948).

The proposed system is known as Unified System USCS (Unified Soil Classification System) and was adopted by Corps of Engineers and by Bureau of Reclamation of United States since 1952, on a proposal of Casagrande.

USDA Soil Taxonomy, developed by United States Department of Agriculture and the National Cooperative Soil Survey, provides a classification of soil types according to their properties and in several levels: Order, Suborder, Great Group, Subgroup, Family, and Series (Figure 3.16).

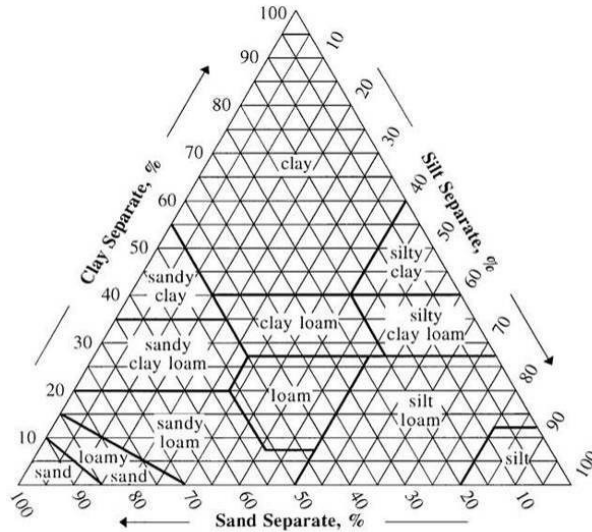


Figure 3.16: soil texture diagram showing the USDA classification system based on grain size (Soil Survey Staff, 1993)

3.4.3 Characterization of mechanical properties

Mechanical properties of pyroclastic soils were determined by means of standard direct shear tests (ASTM D3080-72), which allow to determine mechanical parameters in drained conditions, i.e. in terms of effective stress: effective cohesion (c') and effective friction angle (ϕ'). These two parameters are expressed in the Mohr - Coulomb law:

$$\tau = c' + \sigma' \cdot tg\phi'$$

where:

τ = shear strength; σ' = stress normal to the shear surface.

The effective internal friction angle (ϕ') of a soil is a function of size, degree of selection and degree of roundness of grains, and it is strictly depending on the texture of the material (relative density and degree of consistency). More precisely, it is higher in soils with coarse grains and if the grains are angular.

Effective cohesion (c') is a very important parameter which corresponds to the intercept with the y-axis. This parameter depends on several factors that, although not always coexisting in the same soil, are able to hold the grains together and provide some resistance to the solid skeleton as follows:

- Cementation degree of the soil.
- Roots, which represent a very important contribution, especially when present in non cohesive soils with a low internal friction angle. Indeed they tend to create a network in the soil, able to hold the grains, thus increasing shear strength of the soil and acting like a sort of apparent cohesion.
- Apparent cohesion in unsaturated soil due to pore water. It does not exist under saturated conditions, since the water that completely fills the pores reduces noticeably the cohesion between the grains. Under unsaturated conditions, soil suction influences shear strength, especially in fine grained soil: increase of suction modifies the stress state of the soil capillary water films between grains, thus increasing effective stress acted by capillary meniscuses, and increasing shear strength for the Mohr Coulomb (M-C) law. The extended M-C criterion (Fredlund et al., 1978) describes the shear strength behavior of unsaturated soils. The failure envelope is a planar surface in the space of the stress state variables ($\sigma - u_a$ and $u_a - u_w$), representing the matric suction at failure, and (τ). Taking into account the extended M-C law incorporating Bishop's effective stress and suction stress, shear strength due to apparent cohesion may be expressed as (Lu & Likos, 2002):

$$\tau_f = c' + c'' + (\sigma - u_a)_f \tan \varphi'$$

Where c' and c'' represent shear strength due to the so called apparent cohesion in unsaturated soils:

τ_f is the shear stress on the failure plane, at failure; c' is the cohesion at zero matric suction and zero normal stress; c'' is shearing resistance arising from capillarity effects;

$(\sigma - u_a)_f$ is the net normal stress on the failure plane at failure; φ' is the angle of internal friction associated with the net normal stress; u_a is the apparent cohesion; σ is the normal stress.

The first two terms of the equation represent shear strength due to apparent cohesion in unsaturated soils. The third term represents frictional shearing resistance provided by the effective normal force at the grain contacts. The apparent cohesion captured by the firsts two terms includes the classical cohesion c' arising from inter-particle physicochemical forces such as van der Waals attraction. The second term c'' describes shear resistance arising from

capillarity effects and is defined as “capillary cohesion”, describing physically the mobilization of suction stress in terms of shearing resistance (Lu & Likos, 2002).

It was considered suitable to execute geo-mechanical characterization of shallow soil and paleosols, excluding the intercalated pumice horizons which are difficult to sample in an undisturbed way. As mentioned in section 3.3.3, in order to make the samples representative of the triggering conditions, samples were collected upstream of source areas, that is where the slide occurred. In all cases samples were collected with a low degree of disturbance through a specially designed sampling procedure (see paragraph 3.3.3). Samples were transported to the laboratory and tested with direct shear tests and particle size analysis. Direct shear tests were performed by means of the Casagrande (1930) instrument, consisting of two frames free to move relative to one another so as to impose to the sample a shear stress.

During the test, a normal stress is applied to the box both to consolidate the sample and to simulate the geostatic load insisting on the soil in situ. The normal stress remains constant while the shear displacement increases as the box advances, until it reaches a maximum value (τ_{\max}) that is the shear strength of soil.

All the tests were performed under saturated conditions, and set an advancing rate allowing the dissipation of pore water (drained conditions).

The whole device has three micrometers for measuring horizontal displacement of the box, of any failure or possible swelling and shear stress. This gives the distribution of points for the envelope used to calculate the value of cohesion (c'), corresponding to intercept of the trend line with the y-axis, and the internal friction angle (ϕ'), derived from the slope of the interpolating straight line. This step is crucial for determining the parameters of the Mohr Coulomb's law.

Many tests were performed on the soil specimens sampled during field phase, and involved: shallow soil (B), paleosol (Bb) and basal paleosol (Bb_{basal}), except for the loose gravelly pumice horizon, since their disturbance would be too high to get reliable results. The applied normal stress during the repeated tests are related to the sampling depth of each soil horizon, or the values ranging around those naturally acting at the depth of sliding surface up to double, with the purpose of simulating the load to which they are actually subjected (Table 3.4).

| B | | Bb | | Bb _{basal} | |
|---------------------------------|-------|---------------------------------|-------|---------------------------------|-------|
| σ' (kg/cm ²) | Z (m) | σ' (kg/cm ²) | Z (m) | σ' (kg/cm ²) | Z (m) |
| 0,01255 | 0.1 | 0.1232 | 1.1 | 0.2948 | 2.1 |
| 0.0255 | 0.2 | 0.1360 | 1.2 | 0.323 | 2.3 |
| 0.0318 | 0.3 | 0.1456 | 1.3 | 0.3370 | 2.4 |
| 0.0510 | 0.4 | 0.168 | 1.5 | 0.3514 | 2.5 |
| 0.0765 | 0.6 | 0.1900 | 1.6 | 0.3791 | 2.7 |
| 0.1020 | 0.8 | 0.1904 | 1.7 | 0.3089 | 2.2 |
| 1.1275 | 1 | 0.2140 | 1.8 | | |
| 0.1530 | 1.2 | 0.2380 | 2 | | |

Table 3.4: normal stresses applied during shear tests, and equivalent depth for each investigated pyroclastic soil horizon.

3.5 Characterization of unsaturated pyroclastic soils hydraulic properties

In this section is explained the hydraulic characterization of pyroclastic soil horizons, that is the estimation of the main hydraulic features of the different soil horizons recognized during the phases of engineering geological survey of the pyroclastic cover. Nowadays, it is still difficult to know exactly the processes by which water infiltration influences the stability of the pyroclastic mantle owing to the complex multilayered hydrogeological system and a possible hydraulic contribution occasionally coming from the carbonate bedrock.

It is necessary, in this context, to explain some aspects regarding moisture content of soils (w or θ) and the related soil water potential. In fact, in terms of soil-water management, soil water availability to plants growths is expressed through the water potential Ψ_m , which is expressed in terms of pressure that is negative respect to the atmospheric one (unsaturated condition) also known as matric potential or soil suction or matric suction. Instead, relatively to the atmospheric pressure, positive values mean saturation condition.

At the saturation condition, soil is at its Maximum Retentive Capacity (Figure 3.17). In this circumstances, all soil pores are filled with water. Saturation usually occurs for short periods of time, either during heavy rainfall events or when the soil is being irrigated. At saturation the Ψ_m is close to zero and is nearly the same as pure water; soil porosity corresponds to the volumetric moisture content (θ). Soil remains at saturation as long as water is infiltrating, otherwise in large pores water will freely drain under the gravity forces and after that the soil is considered to be at Field Capacity. It approximates the amount of water that is held in soil after it was fully wetted and

all gravitational water was drained away. At Field Capacity, the soil holds the maximum amount of capillary water that can be stored and extracted by plant roots. The Permanent Wilting Point (Figure 3.17) is defined as the minimum soil moisture at which a plant wilts, and can no longer recover its turgidity. In the field, soil at Permanent Wilting Point will appear dusty and dry. The amount of water held between F.C. and P.W.P. is termed “Available Water Content”, and it is a measure of the amount of water in the soil that is “potentially” available to plants.

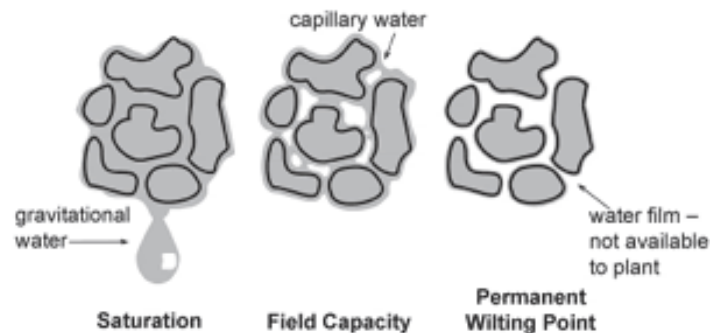


Figure 3.17: moisture conditions of soils and water potential (http://attra.ncat.org/attra-pub/soil_moisture.html).

Measurement of water content retained by soils, namely water molecules tied to solid particles by electrostatic or capillary forces, is possible by means of hydraulic devices capable to extract water in both saturated and unsaturated conditions. This kind of measurements allow to understand unsaturated soil hydraulic behavior, by means of determination of the Soil Water Characteristic Curve, also known as the Soil Water Retention Curve (SWRC): it is an experimental relationship that relates suction (matric, total, or both) to water content or saturation. It is also essential for characterizing the mechanical behavior of unsaturated soils. Experimental practices for direct measurement of the SWRC provide discrete data points, including the relationship between water content and soil suction. Further applications of these measurements for predicting flow, stress and deformations phenomena require that measured SWRC are described in mathematical form.

The parameters used in mathematical models for the SWRC include fixed points pertaining to water content or suction at specific conditions (for example saturation, residual saturation, and air entry pressure) and fitting constants selected to capture the shape of the curve. In a given soil, the relationship between water content and matric suction varies, depending on whether the soil is getting wet (sorption processes) or dry (desorption processes). This discrepancy is referred to as hysteresis phenomenon (Figure 3.18).

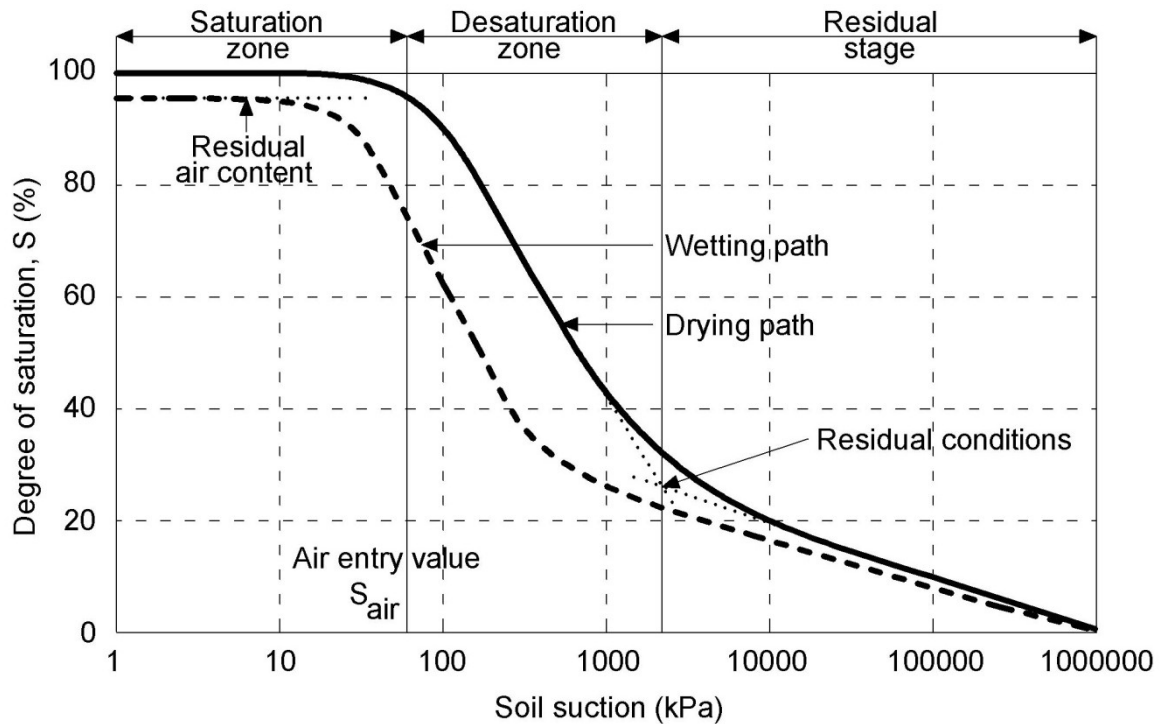


Figure 3.18: hysteresis process referred to as soil-water characteristic curve
[\[http://www3.imperial.ac.uk/pls/portallive/docs/1/33435697.JPG\]](http://www3.imperial.ac.uk/pls/portallive/docs/1/33435697.JPG)

Figure 3.18 illustrates the saturated water content describing the condition where all the available pores in the soil matrix are filled with water (Saturation zone), usually corresponding to the desorption branch of the soil-water characteristic curve (Figure 3.17).

The air-entry, or bubbling pressure (ψ_b), describes the suction value on the desorption branch where air first starts to enter the largest pores and de-saturation begins. The residual condition water content (θ_r) describes the condition where the pore water resides as isolated meniscuses, and large change in suction is required to remove extra water from the system. The water content at a given pressure (ψ) is usually different for a wetting soil than when that soil is drying. This is mainly due to air entrapped in larger pore segments between constrictions (residual air content), the so called “ink-bottle effect”.

3.5.1 Soil water characteristic curve models

Numerous approaches were proposed for mathematical fitting or prediction of the SWRC. In this paragraph models commonly used for geotechnical and engineering applications are described, with specific regard to the one used in this study.

One of the earliest approaches for modeling the soil-water characteristic curves is an equation proposed by Brooks and Corey (1964), based on a big set of measurements concerning suction and water content. The Brooks and Corey model is more appropriate for relatively coarse grained soils, in which drainage occurs over a low and narrow range of suction. In addition, this model loses applicability at high suction values (i.e. approaching the residual water content). The lack of an inflection in the shape of the curve representing the model, often results in a poor representation of SWRC over a wide range of suction values. It is expressed in the form:

$$\theta = S_e = \begin{cases} 1 & \psi < \psi_b \\ \left(\frac{\psi_b}{\psi}\right)^\lambda & \psi \geq \psi_b \end{cases}$$

Where λ is a parameter that is related to the shape of the SWRC. Also, the non-smoothness occurring at the air-entry pressure leads to a sharp discontinuity in the specific moisture capacity and hydraulic diffusivity functions (from the derivative of θ (ψ), leading often to numerical instability.

Van Genuchten (1980) proposed the following three parameter model for the soil – water characteristic curve, that is the model adopted in this research to compute soil matric suction and water content values.

$$\theta_e = \frac{\theta(h) - \theta_r}{\theta_s - \theta_r} = \left[1 + |\alpha \cdot h|^n\right]^{-m},$$

$$\theta(h) = \frac{\theta_s - \theta_r}{\left[1 + |\alpha \cdot h|^n\right]^m} + \theta_r$$

Where: θ_e = effective water saturation; θ_s = saturated volumetric water content; θ_r = residual volumetric water content; h = soil matric suction. In addition α , m , n are fitting parameters for the

curve shape: α is related to the air-entry condition and approximates the inverse of the air-entry pressure; m is related to the general symmetry of characteristic curve and is frequently constrained by relation to the n parameter:

$$m = \frac{1}{n}$$

n is related to the pore size distribution of the soil object of study.

These parameters reduce the flexibility of the model, but allow a considerably simplification of it, thus giving a greater stability to the numerical optimization (unlike the model previously mentioned).

This mathematical form accounts for an inflection point and allows a greater flexibility with respect to Brooks and Corey's model over a wide range of suction, and allows a better capture of the typical shape of the curves; the air-entry pressures transitions and the residual conditions are better captured as well.

The suction term (ψ) can be expressed either in units of pressure (kPa) or pressure head (m or cm). Such a model is completed by the Hydraulic Conductivity Functions (HCF) model, which depends by the same parameters of the SWRC plus the saturated hydraulic conductivity (K_{sat}) and expresses the variation of the hydraulic conductivity with the volumetric water content (θ). The hydraulic conductivity reaches the highest value at saturation (K_{sat}).

$$K(\theta) = K_{sat} \cdot \theta e^{0.5} \cdot \left[1 - \left(1 - \theta e^{\frac{1}{m}} \right)^n \right]^2$$

Furthermore, the Fredlund and Xing's model (1994), is based on pore size distribution, and is expressed in the form:

$$\theta = C(\psi)\theta_s \left[\frac{1}{\ln[e + (\psi/a)^n]} \right]^m$$

where $C(\psi)$ is a correction factor and e is the natural logarithmic constant. Comparison with experimental data indicates that the Fredlund and Xing model is capable to well describe the soil-

water characteristic curve in a wide range of suction values, varying from 0 to 10^6 kPa (Lu & Likos, 2006).

3.5.2 Instrumentations for testing

Experimental techniques for measuring soil suction and the corresponding SWRCs widely vary in terms of cost, complexity and measurement range. As previously mentioned, laboratory and field methods differentiate in terms of the component of suction (matric or total) that is measured. In particular, laboratory methods need undisturbed samples to account for the sensitivity of suction to soil fabric.

Disturbance effects are less important at higher suction values. In this section, the methods used for measuring matric suction (including pressure plate extractor and Tempe cells) are described. Particular regard is given to the description of the instrumentation used for the case study, to calculate matric suction in pyroclastic soils. Indeed the method used to measure the SWRC depends on the texture of the soil (coarse versus fine) and on the magnitude of suction.

Tempe cells are commonly used for applications where low suctions (<100 kPa or 10 m of water) have to be applied. For higher matric suctions pressure plate extractors are used; they have robust pressure cells, which can withstand higher air pressures (typically 1500 kPa). Fredlund and Rahardjo (1993) provided a review of the types of extractors in use today, their ranges of applicability, and their advantages and disadvantages.

The Figure 3.19 shows a schematic section of a typical apparatus for water extraction testing, called “pressure plate extractor”. The primary components of the apparatus are the steel pressure vessels and a saturated HAE ceramic plate.

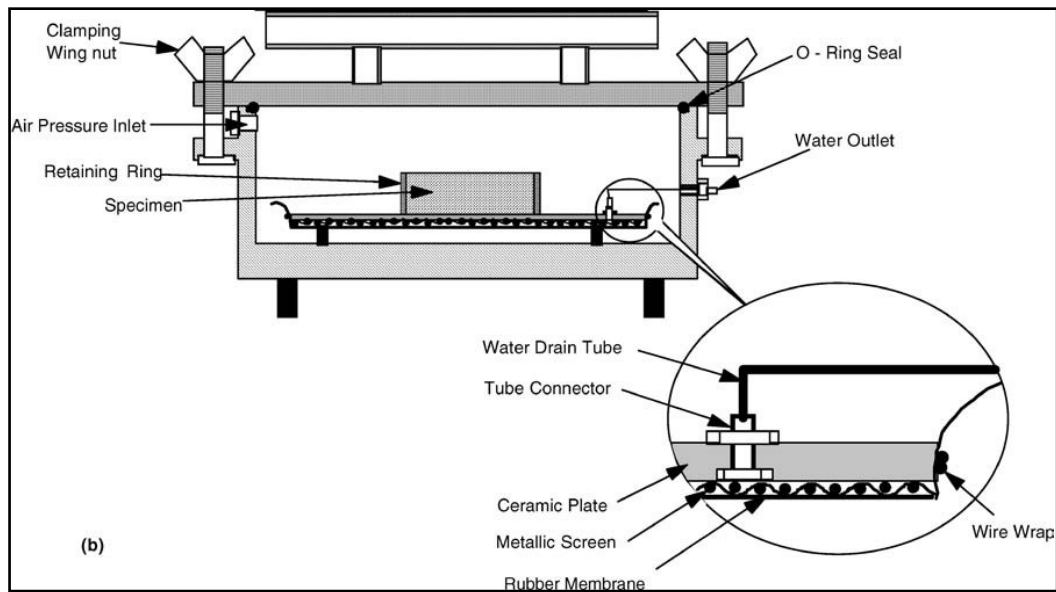


Figure 3.19: schematic section of pressure plate extractor (from Wang & Benson, 2004).

A small water reservoir is formed beneath the plate using an internal metallic screen. This reservoir is vented to the atmosphere through an outflow tube (tube connector and water drain tube) located at the top of the plate. It allows the air pressure in the vessel and the water pressure in the reservoir to be separated across the air- water interfaces, bridging the saturated pores of the HAE material. Several specimens are placed on the top of the ceramic plate so that the pore water is in equilibrium with the water reservoir at the atmospheric pressure. The same specimens must be prepared, in order to test sensitivity of pore water retention to soil fabric, with the same dry density and water content. The specimens must be initially saturated and then, by applying a partial vacuum to the air chamber, the samples are allowed to drain the retained water through ceramic plate. Air pressure in the chamber is then increased to the desired value, while pore water is allowed to drain water until equilibrium is reached. The water outflow is monitored until it stops, thus indicating the reaching of the equilibrium between the air pressure inside the chamber and the capillary water. After obtaining the equilibrium, the chamber is opened and specimens are weighted. Then, the specimens are newly inserted in the chamber and after its closure a higher pressure step is given. At the end the water content of the specimens is calculated for each pressure step after oven drying, thus gathering data requested for the SWRC reconstruction.

In Figure 3.20, a cross section of the “Tempe cell” apparatus is shown. It has a very similar functioning to the pressure plate extractor. It consists of a cylindrical soil container, closed in a

special assembly, in which a known air pressure is applied from the top. In this way the outflow of capillary water from the soil sample is provoked (through a basal porous ceramic disk on which the soil specimen is located).

During each step, air pressure pushes out capillary water up to reach the equilibrium with forces of capillary menisci (soil matric suction), thus accounting for the water outflow annulment. Several data points comprising the soil-water characteristic curve may be obtained by applying increments in air pressure. Equilibrium of water content for each cell, is reached for each air pressure step by observing the annulment of the outflow, and by weighting the entire apparatus. After reaching the maximum level of matric suction the cell is disassembled and the soil specimen is oven dried.

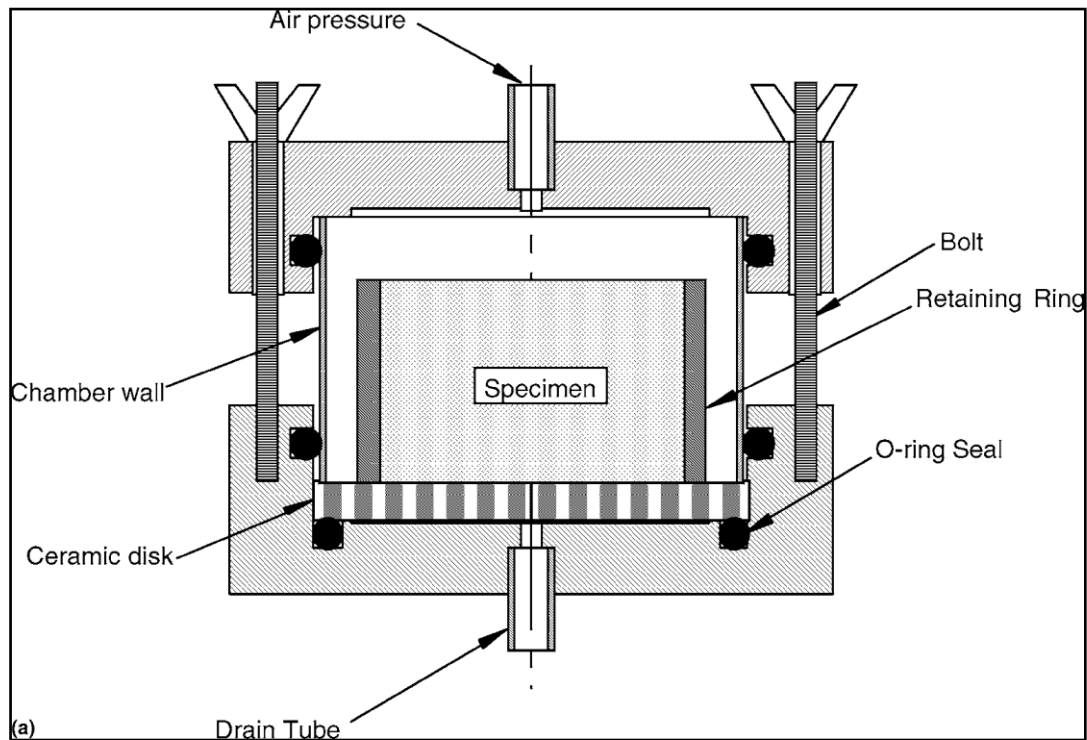


Figure 3.20: schematic cross section of “Tempe cell” (from Wang & Benson, 2004).

These laboratory tests have long execution time (on the order of months) because the time for water extraction increases as pressure steps increases, soil water content decreases and hydraulic conductivity in turn decreases. Several tests were performed contemporary on six Tempe cells connected to the same air compressor and manifold. In order to test soil specimens with the same hydraulic behavior and to have a sufficient number of data, six specimens of the same soil horizon

were tested. After assembling the Tempe cells, increasing pressure steps were applied, and the relative volumetric water content for each of them was calculated.

In order to test very low level of soil matric suction, below the resolution of the manifold (20 cm H₂O), an on-purpose designed air compressor apparatus was designed and utilized. It is constituted of two connected plexiglass cylinders, the first open to the atmospheric pressure and the second connected to the Tempe cells apparatus (Figure 3.21). Both tubes were partially filled creating a difference in hydraulic head, thus a corresponding air pressure in the second tube. In such a way, soil matric suction starting from $h = 5$ cm, corresponding to saturated water content (θ_s), was tested. After flow stabilization of each step, and weighted the water outflow at established time intervals, pressure was increased up to $h = 100$ cm of H₂O. For higher values we used standard air compressor and manifolds with a resolution of 20 cm H₂O. Such a procedure allowed to obtain a higher resolution results than those obtained with the standard manifolds in the lower range of soil suction, thus allowing to better characterize coarser soils like the C horizons with larger inter-particle voids.

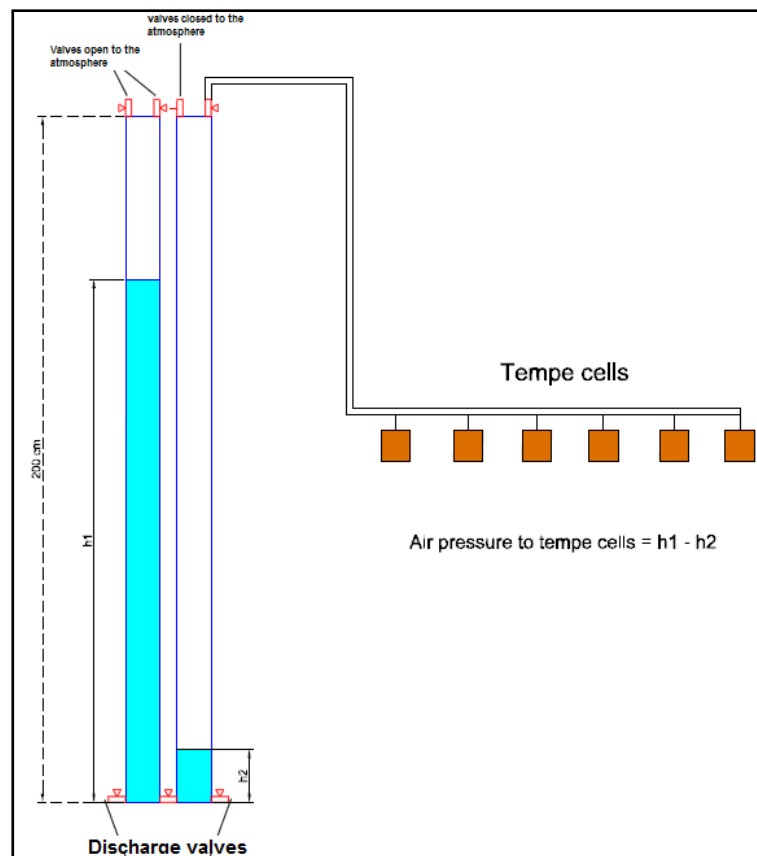


Figure 3.21: schematic sketch of air pressure apparatus for very low levels of matric suction .

For this experiment it was planned to apply increasing pressure steps, according to the scheme shown in Table 3.5.

| Soil horizon | B | C | Bb | Bb _{basal} |
|---|-------|-------|-------|---------------------|
| Pressure steps (cm H ₂ O) | 0.1 | 0.1 | 0.1 | 0.1 |
| | 20.4 | 5.1 | 5.1 | 5.1 |
| | 61.2 | 10.2 | 10.2 | 10.2 |
| | 245 | 20.4 | 20.4 | 20.4 |
| | 387.9 | 40.8 | 40.8 | 40.8 |
| | 510.4 | 81.7 | 81.7 | 81.7 |
| | 796.2 | 163 | 163 | 163 |
| | 939 | 326.6 | 326.6 | 326.6 |
| | | 653.3 | 653.3 | 653.3 |
| | | 979.9 | 979.9 | 979.9 |

Table 3.5: pressure steps applied during “tempe cells” tests

3.6 Characterization of the soils hydraulic behaviour in the saturated domain

The saturated domain is the condition of water content of porous media in which the saturation degree is equal or very close to 100%; this condition means that all the interconnected voids are occupied by water except for rare trapped air bubbles. The study of the hydraulic behavior under these conditions is essentially aimed to define the water filtration through the soil. Under the hydraulic head conditions found in nature, filtration does not take place through all the pore spaces in the soil but only through a percentage of them (the so called effective porosity). It allows the water drainage under the gravity action. The rest of the voids can be occupied by water not subject to gravity and therefore be relatively static. The parameter characterizing the filtration is the saturated hydraulic conductivity, introduced by Darcy. The saturated hydraulic conductivity is influenced by many factors; it varies with grain size and is very sensitive to the amount, type and distribution of the fine particles fraction. It is indirectly a function of density: the greater the unit soil weight, the smaller the hydraulic conductivity owing to the corresponding decrease in void ratio (e) and porosity (n). Hydraulic conductivity is influenced by the arrangement of the grains in the sense that the particles may have a predominant orientation; fine fraction may be dispersed into soil or be concentrated in a not uniform way.

Natural deposits are more or less stratified and irregular in structure. For example, soils that are deposited in presence of water quite often consist of a series of horizontal layers that vary in grain size and permeability: these deposits are generally more permeable in horizontal direction than in the vertical one. Aeolian deposits of sand and silt, in contrast, are often more permeable on the vertical axis than horizontal, because of vertical tubular voids left by plants and grasses. For example, in sandy-gravel deposits, thin layers of clean gravel can radically alter the permeability representative of the deposit. Thus, the saturated hydraulic conductivity (K_{sat}) changes depending on the mode of formation of deposits are quite frequent.

The saturated hydraulic conductivity (K_{sat}) is defined as the product of intrinsic permeability (K_i) for the ratio between gravity and kinematic viscosity of the fluid

It depends on the square of the effective diameter of the grains and has the dimension of a velocity and is usually measured in m/s or cm/s. By the given definition, it follows that the hydraulic conductivity depends not only on the characteristics of the soil, but also on those of the fluid. The hydraulic conductivity of the same soil will be different depending on viscosity of the fluid considered.

It is:

$$k_{sat} = k_i \cdot \frac{g}{\nu}$$

where:

K_i = intrinsic permeability (m^2); g = acceleration of gravity (m/s^2); ν = kinematic viscosity (m^2/s).

Determination of hydraulic conductivity, both in situ and in laboratory, is carried out by referring to the Darcy law, if the condition of validity of Darcy law (laminar flux) is satisfied:

$$Q = K \cdot S \cdot i$$

This equation gives:

$$K = \frac{Q}{S \cdot i} = \frac{Q \cdot L}{S \cdot (L+H)}$$

where:

Q = flow (m^3/s); S = infiltration section (m^2); L = length column of soil affected by flow (m); H = constant hydraulic head (m).

By applying the last equation, it is possible to obtain the value of K , by measuring flow and hydraulic head at time intervals. In general, as regards the assessment of K_{sat} , the main problem in

the study of saturated medium is the difficulty to get saturation, especially when it consists of fine particles. It may happen that trapped air bubbles (Figure 3.22) between soil particles, may reduce the draining section and lead to the consequent underestimation of hydraulic conductivity; this is especially true when the saturation front propagates from the top.

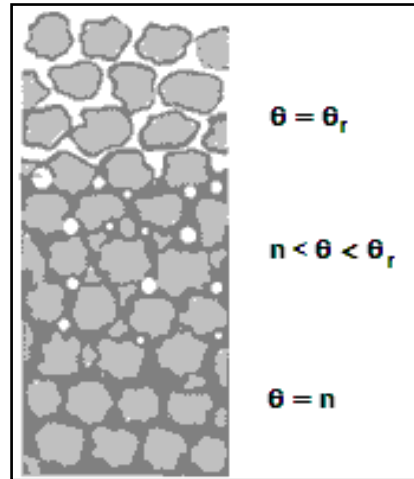


Figure 3.22: influence of volumetric water content on hydraulic conductivity (modified after Zilberbrand, 2003).

During laboratory measurements, it is possible to avoid the abovementioned problem, by getting the saturation of the soil from the bottom and allowing the air to escape upward. Besides, it is also possible to extend the test over a longer time, sufficient to achieve the complete saturation. During in situ tests (paragraph 3.3.1), however, times are limited and saturation must be reached from the upper zone. In these cases, the saturated hydraulic conductivity (K_{sat}) is underestimated depending on the percentage of pores occupied by air bubble. For such a reason it is named as field saturated hydraulic conductivity ($K_{sat \text{ field}}$).

3.6.1 Constant head permeameter

Given the wide range of variation of permeability in the soils, spread in over 10 magnitude orders, there is not a unique laboratory method for all cases study. The types of tests generally include: a) constant head permeameter for medium to coarse soils (sandy and silty soils) with an approximately lower limit of application of about 10^{-7} m/s; b) variable head permeameter for medium and fine soils (silty and clayey soils) with hydraulic conductivity lower than 10^{-7} m/s.

A constant head permeameter was designed and used with undisturbed soil samples collected by means of an on purpose designed sampler. It is constituted of a stainless steel cylinder with a cutting edge containing a coaxial plexiglass cylindrical liner whose diameter is 7.4 cm and length is 15.0 cm. This apparatus was pushed into soil horizons allowing to collect specimens inside plexiglass liners. Samples were closed with screwed caps with valves. Through valves a constant water flow was imposed with a constant head permeameter. The fluid used for the test is water at 23°C. The plexiglass tube is superimposed on a metallic shelter and is connected by a plastic tube to the constant head water collector. The sample is formerly saturated from the bottom, to avoid air bubble formation and thus underestimation of hydraulic conductivity (Figure 3.23). The experiment is carried out on different tests with variable hydraulic head (ΔH). The volume of water collected and the testing time provide the velocity, which is plotted together with the hydraulic gradients on a diagram.

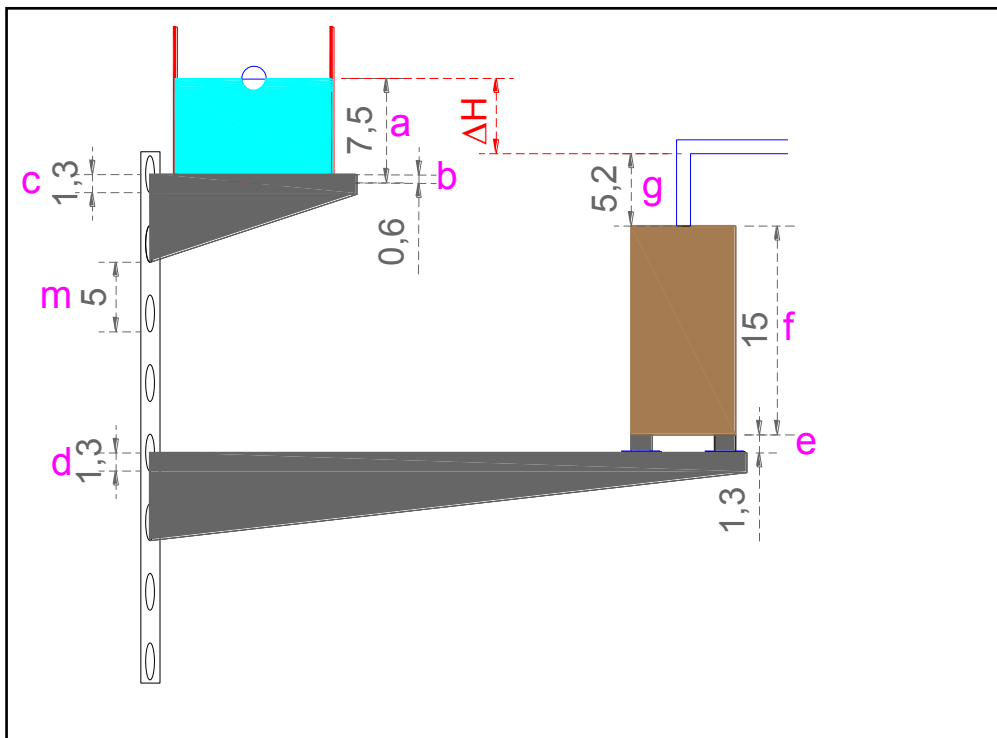


Figure 3.23: constant head permeameter used for laboratory tests, in order to evaluate saturated hydraulic conductivity of piroclastic soils.

The hydraulic device measures hydraulic head, by means of the equation:

$$\Delta H = (m \cdot N) + a - b + c - (d + e + f + g)$$

where (Figure 3.23):

N = number of positions of the shelter;

m = constant distance between successive positions;

f = sample length

a, b, c, d, e, and g = constants.

From this relation follows:

$$\Delta H = m \cdot N - 14,6$$

The hydraulic gradients are given by the relation:

$$i = \Delta H / f$$

The saturated hydraulic conductivity (K_{sat}) can be calculated by means of the Darcy law:

$$K_{sat} = \frac{Volume}{t \cdot S \cdot i}$$

where:

V = water volume;

t = time;

S = sectional area of the cylinder;

i = hydraulic gradient.

3.7 VS2DTI: finite difference hydrological model for variably saturated porous media

On the basis of experimental data regarding hydraulic properties of pyroclastic soils, a further step concerned the hydrological numerical modeling of the slope when subjected to rainfalls, from ordinary to extreme (namely hydrological events with different return time). The modeling was performed by means of a specific computer program, **VS2DI** (Hsieh et al., 2000; Lappala et al., 1987)¹.

It is a graphical software package for simulating fluid flow and solute or energy transport in variably saturated porous media. This software is free and available on the USGS website: (<http://water.usgs.gov/software/lists/groundwater>).

It is suitable for the unsaturated / saturated domains. From this type of modeling it was possible to understand the pore pressure distribution in the initial landslides areas; successively a stability model of pyroclastic cover, being known the shear strength of pyroclastic soils, was carried out.

VS2DI is a software for simulating two-dimensional movement of water, or any other solute flow and transport through variably saturated systems. The understanding of the occurrence and movement of water in variably saturated porous media is also important to develop predictive tools for managing quantity and quality of ground water as well as to predict the pollutant destination within soil that requires estimation of the rate of moisture movement. The package integrates a graphical interface (Hsieh et al., 2000), where the user can draw the simulated domain and enter or modify model parameters with existing models of flow and solute transport (**VS2DTI** for simulation of water and solute transport **VS2DHI** for simulation of water and energy transport), and a standalone postprocessor (**VS2POST**, for displaying results saved from previous simulation runs). **VS2DTI** solves problems of water and solute movement in variably saturated porous media. The finite difference method is used to approximate the flow equation, which is developed by combining the law of conservation of fluid mass with a nonlinear form of Darcy's equation. The resulting mathematical model or flow equation is written in terms of total hydraulic potential, considered as the dependent variable, thus allowing to deal with both saturated and unsaturated conditions. The model can analyze problems in one or two dimensions with planar or cylindrical geometries. There are several options for using boundary conditions that are specific to flow under

¹ http://wwwbrr.cr.usgs.gov/projects/GW_Unsat/vs2di1.2/manapp.html).

unsaturated conditions: infiltration with ponding, evaporation, plant transpiration, and seepage faces. The program is written in standard Fortran 77 and uses a two-dimensional groundwater flow equation: in unconfined aquifers, it is not possible to use the solution found for the 3D form of the equation, since it is complicated by the presence of a “free surface water table” boundary condition. An alternative formulation of the groundwater flow equation may be obtained by invoking the Dupuit assumption (or Dupuit-Forcheimer assumption), in which it is assumed that: 1) groundwater moves horizontally in an unconfined aquifer, 2) the hydraulic gradient is equal to the slope of the free surface of the water, whose head does not vary vertically, and that, 3) the groundwater discharge is proportional to the saturated aquifer thickness. A horizontal water balance is applied to a long vertical column with area extending from the aquifer base to the unsaturated surface. This distance is referred to as the saturated thickness, b . In a confined aquifer, the saturated thickness is determined by the height of the aquifer, H , and the pressure head is non-zero everywhere. In an unconfined aquifer, the saturated thickness is defined as the vertical distance between the water table surface and the aquifer base. If the aquifer base is assumed at null elevation, then the unconfined saturated thickness is equal to the head, i.e., $b=h$.

The hydraulic conductivity and the horizontal components of flow are assumed to be uniform along the entire saturated thickness of the aquifer. As above mentioned, the equation describing the movement of water under equal or constant salinity and temperature is developed by combining the conservation of mass for water, and the equation for fluid flux and storage (described by Darcy’s law extended to variably saturated conditions):

$$\int_v \frac{\partial(\rho s \phi)}{\partial t} dv + \int_{\bar{s}} \rho \vec{u}_n d\bar{s} - \int_v \rho q dv = 0$$

where:

ρ = liquid density [ML⁻³]; s = liquid saturation [adimensional]; ϕ = porosity [adimensional]; t = time [T]; \vec{u}_n = liquid flux per unit area in the direction n , that is normal to \bar{s} that is the surface [LT⁻¹]; q = volumetric source-sink term accounting for liquid added (+ q) or taken away from (- q) the volume v , per unit volume and unit time.

This equation states that the rate of mass change in a volume v must be balanced by the sum of liquid flux across the surface boundary of v , and of liquid added (by source) or removed (at sink). Besides, it is assumed that volume v is small enough that, ρ , s , ϕ , can be considered constant:

$$\int_f \frac{\partial(\rho s \phi)}{\partial t} dv = v \frac{(\rho s \phi)}{\partial t}$$

And:

$$\int_f \rho q dv = \rho q v$$

Hence the equation can be simplified as:

$$v \frac{(\rho s \phi)}{\partial t} + \int_{\bar{s}} \rho \vec{u}_n d\bar{s} - \rho q v$$

As regarding the flux normal to the surface \bar{s} that bounds v , it is described by Darcy's law extended to variably saturated conditions:

$$\vec{u}_n = \frac{K K_r(h) \rho g}{\mu} \cdot \frac{DH}{\partial n}$$

where:

K = intrinsic permeability of the medium [L^2]; $K_r(h)$ = relative hydraulic conductivity to liquid as function of pressure head [L^0]; h = pressure head [L]; g = gravitational acceleration [LT^{-2}]; [$ML^{-1}T^{-1}$]; μ = dynamic viscosity of the liquid, expressed as height of the liquid column [L].

Total hydraulic potential H was chosen as the principal independent variable, thus allowing a simple treatment both in saturated and unsaturated conditions. Pressure head below water table is measured.

The solution of the non-linear flow equation requires that the initial values of H be specified everywhere in the solution domain. The initial conditions usually represent some type of steady state or equilibrium. If initial conditions do not represent steady state, any simulation result will include transient effects from specified initial conditions and the equilibrium conditions. Since flow equation is not linear, it is not possible to subtract out the effects of transient initial conditions (as in fully saturated systems, whose properties are not a function of total porosity). Solutions to flow

equation require boundary conditions that specify either flux of water or fluid across the boundary, and the total potential along the boundary.

Through variably saturated porous media four types of flow which may be excluded, can occur: infiltration, evaporation, plant root extraction, and discharge through seepage faces. At the start of each simulation boundary conditions are read after the initial conditions are set, so they override initial conditions for the boundary cells.

3.7.1 Numerical solutions

An important application of the numerical analysis is the finite differences method, that consists in replacing the derivatives appearing in the differential equation by finite differences that approximate them. In our case the approximations result in a set of simultaneous non-linear equations that must be first linearized and then solved. For the flow equation, spatial derivatives are approximated by a block-centered regular finite difference scheme, that is central differences written about grid-block boundaries, while time derivatives are approximated by a fully implicit backward scheme; the grid can be rectangular (Figure 3.24) or cylindrical.

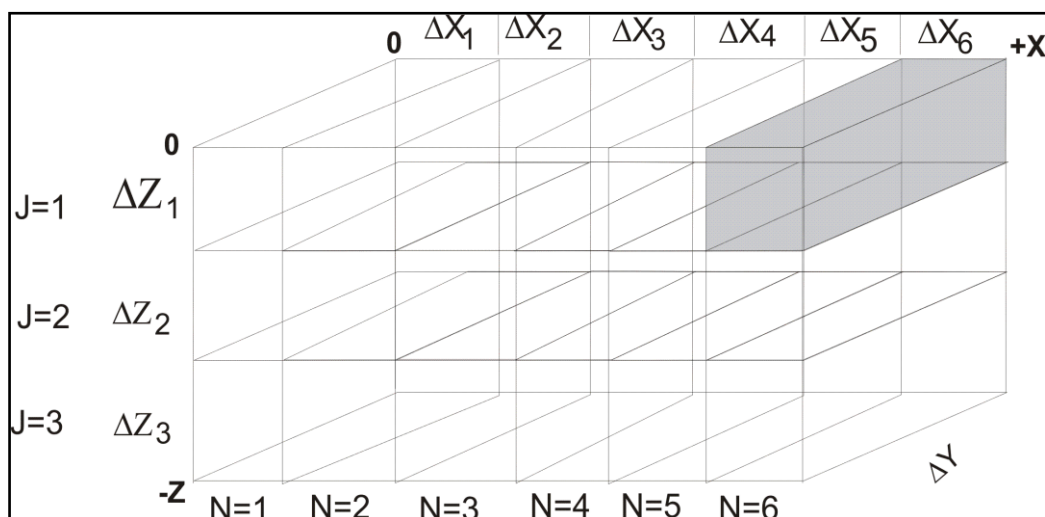


Figure 3.24: rectangular coordinates and grid-block system.

Spatial discretization is based on a nodes grid within the domain: the nodes in each volume subdivision or grid block are located at the center of each block.

Saturated hydraulic conductivities are evaluated at cell boundaries by using distance-weighted harmonic means. Nonlinear conductance and storage terms can be represented by algebraic equations or by tabular data. For the advection-dispersion equation, either central or backward differences may be selected for the spatial and time derivatives. Equilibrium adsorption can be described by either Freundlich or Langmuir isotherms. The matrix equations produced for both the flow and transport equations are solved using the strongly implicit procedure.

Initial conditions required for the solution of the flow equation can be specified by reading initial volumetric moisture content (θ) or the initial head (h). The program computes the pressure head, or the volumetric moisture content, using the appropriate moisture content/pressure head function, or its inverse. Numerical approximation for the boundary conditions required to solve the fluid flow equation are described by the Neumann boundary condition (specified ∇H), that is specified flux boundary condition. The specified potential, or Dirichlet boundary conditions (specified H) is given by an equation that specifies only the total potential. The Neumann boundary conditions can be properly specified, but the Dirichlet conditions cannot; with a face-centered grid, the Dirichlet condition specification is straight-forward, because the nodes are located on the boundaries; flux boundary conditions require special formulation of the equations for each face across which the flux takes place. The specified flux boundary condition is implemented in the code by an equation in which each term represents the flux across a cell face.

3.8 Finite slope stability analysis

On the basis of engineering geological models of the initial landslides and the hydrological modeling of extreme rainfall conditions, a limit-equilibrium finite slope stability analysis was carried out. This allowed to evaluate the critical hydrological conditions leading to the initial failures. Such conditions can be conceived as deterministic hydrological thresholds (Godt and McKenna, 2008) which can be considered an innovative approach respect to the classic empirical approach.

In all methods of limit-equilibrium, finite slope stability analysis, a number of assumptions are necessary to solve the equations of equilibrium. These methods subdivide the landslide (actual or potential) into a number of slices. The equations of equilibrium are statically indeterminate. Therefore, the distribution of interslice forces is assumed by introducing stress-strain relationships to make the problem statically determinate. All the methods known in scientific literature assume a

two-dimensional geometry, and analyze the stability of a cross section parallel to the direction of movement. In general, according to the limit equilibrium principle, that assumes a brittle-plastic rheologic behavior, if the forces available to resist the movement are greater than the forces driving the movement, the slope is considered stable.

The “method of the slices” is generally used for analyzing the stability of a slope in two dimensions, in which the sliding mass above the failure surface is divided into a number of slices. The forces acting on each slice are obtained by considering the mechanical equilibrium of the slices. A Factor of Safety (FOS) is calculated by dividing the forces resisting to the movement by the forces driving to the movement. There are different methods known in the scientific literature that are summarized in the following: the ordinary slices, or Fellenius’ method (1927), Bishop’s simplified method (1955) and the Janbu’s method (1973).

The method of ordinary slices, or Fellenius method (1927), is based on the discretization of the mass displaced in slices, whose number can be identified on the basis of the morphology of the land surface, of the sliding surface, and the homogeneity of the soil involved by the slide. As for all the methods using discretization in slices, the balance must be considered at first for each slice and then for the whole mass. In drained conditions, the forces acting on the individual segments are (Figure 3.25):

$$F = \frac{\sum_{i=1}^n [c' l_i + (W_i \cos \alpha_i - u_i l_i \cos^2 \alpha) \operatorname{tg} \varphi']}{\sum_{i=1}^n W_i \operatorname{sen} \alpha_i}$$

where:

c' is the effective cohesion; φ' is the effective internal friction angle; l_i is the length of the i th slice; u_i is the pore pressure relative to the i th slice; α is the slope of the slice; W_i is the weight of the slice

while in undrained conditions, we have:

$$F = \frac{\sum_{i=1}^n [c_l l_i + W_i \cos \alpha_i \operatorname{tg} \varphi]}{\sum_{i=1}^n W_i \operatorname{sen} \alpha_i}$$

$$F = \frac{\sum_{i=1}^n [c_u l_i]}{\sum_{i=1}^n W_i \operatorname{sen} \alpha_i}$$

where:

c is the total cohesion; φ is the total internal friction angle; c_u is the undrained cohesion.

This method considers null the forces acting on the sides of the slices. Therefore, it takes into account only the components of the force weight (W_i), both normal (N_i) and parallel (S_i) to the respective bases (angle α and length l) of each slice.

The Modified (or Simplified) Bishop's Method (1955) is an extension of the ordinary method of slices. By making some simplifying assumptions, the problem becomes statically determinate and suitable for hand calculations, as the forces on the sides of each slice are horizontal.

The method was shown to compute factor of safety values, even if all limit-equilibrium methods have difficulty with certain deep failure surfaces (Whitman and Bailey, 1967). It satisfies the moment equilibrium for unrestrained slopes, by assuming the failure surface is circular in cross section. It does not satisfy force equilibrium. However, the computation of the normal force on the failure surface is more accurate than in the method of Fellenius, the factor of safety computed by this method is relatively accurate for circular failures:

$$F = \frac{\sum \left[\frac{c' b_i + (W_i - u_i b_i) \tan \phi'}{\psi} \right] \frac{1}{m_a}}{\sum [W_i \sin \alpha_i]}$$

where:

$$m_a = \cos \alpha \left(1 + \frac{\tan \alpha \tan \phi'}{F} \right)$$

and: c' is the effective cohesion; ϕ' is the effective internal friction angle; b is the width of each slice, assuming that all slices have the same width; W is the weight of each slice, u is the water pressure at the base of each slice. This equation must be solved in an iterative way.

Aiming at analyzing a non-circular failure surface it is difficult to find a single point through which many of the force components act. So, the moment equilibrium method used for circular surfaces is no longer appropriate. Janbu (1973) chose to use the force equilibrium method in the analysis:

$$F = \frac{f_0 \sum \left[\frac{c' b_i + (W_i - u_i b_i) \tan \phi'}{\psi} \right] \frac{1}{n_a}}{\sum [W_i \sin \alpha_i]}$$

where:

$$n_a = \cos^2 \alpha \left(1 + \frac{\tan \alpha \tan \phi'}{F} \right)$$

and f_0 is a corrective factor that must be multiplied for the safety factor.

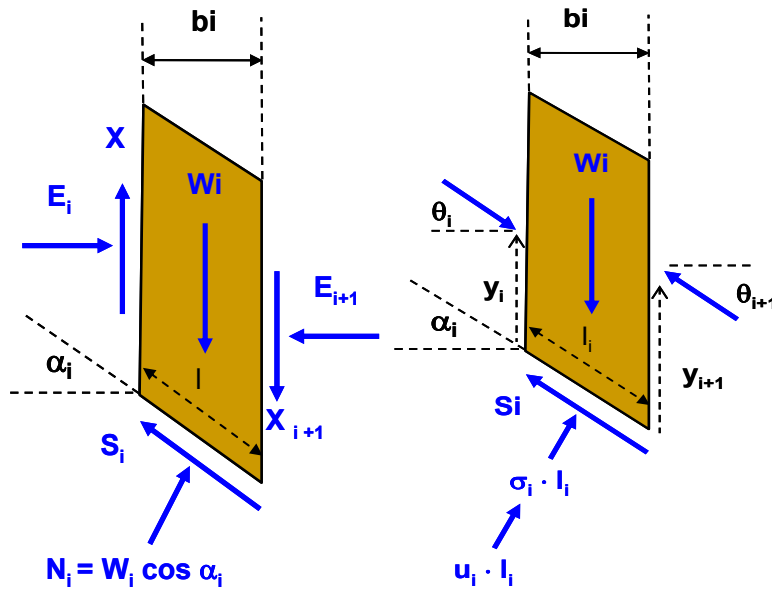


Figure 3.25: schematic representation of a single slice with relative forces acting on it. W = Weight of slice; E = horizontal force, acting perpendicular to the sides of the slice; X = vertical forces, acting parallel to the sides of the slice; N = Forces acting perpendicular to the base of the slice; S = Shear stress acting at the base of slices.

The horizontal forces (E) and vertical forces (X) result from the breakdown of the forces acting on some points of the sides of the slices (y_i), at an angle θ to the horizontal.

According to the approximately circular shape of sliding surfaces, for the case studies the Modified (or Simplified) Bishop's Method (1955) was applied.

Chapter 4

Engineering–geological characterization of pyroclastic cover: results

4.1 Results from stratigraphical analysis

The results and the interpretation of data sets collected during field and laboratory tests are described in this chapter.

As reported in the previous chapter, a preliminary survey and recognition of almost all the initial landslides triggered during 5-6 May 1998 in the Sarno Mountain Range was carried out which allowed the identification of three representative cases occurring in typical morphological conditions:

- i) corresponding to a knickpoint;
- ii) above a rocky scarp;
- iii) above a road cut.

In order to achieve a comprehensive understanding of these type of landslides it was considered as fundamental to investigate such triggering areas on a detailed scale. On the basis of field surveys, initial debris slides were recognised as being approximately of decametric dimensions. Therefore, only detailed engineering geological investigations were considered suitable for defining physical models of initial landslides, useful in order to understand the triggering mechanisms and for the quantitative evaluation of the hydrological and mechanical processes that led to initial instabilities. This detailed-scale and quantitative approach appeared as a unique way for achieving a complete comprehension of the conditions leading to initial instabilities.

Stratigraphical data were gathered by means of exploratory pits and trenches as well as Hedelman's hand-auger drillings. These permitted the stratigraphic reconstructions also in areas characterised by a higher thickness of pyroclastic soils and flat morphology in which direct digging was not applicable.

Detailed identification and geometrical reconstruction of different pyroclastic soil horizons were also assessed by means of dynamic penetration tests (DPL and DPM). The collected data set permitted characterization of the geometrical features of the pyroclastic soil horizons and the

outlining of an engineering-geological model of the pyroclastic cover mantling Pizzo D’Alvano Massif. Stratigraphical correlations were performed combining and interpreting direct and indirect (derived from dynamical penetration tests DPL and DPM) stratigraphical data along longitudinal and transversal section crossing the initial landslide. 2D geometry of soil horizons and distribution of the pyroclastic cover along the slope were reconstructed accounting for variable thickness and stratigraphic setting. Moreover, results coming from penetration tests, permitted the determination of dynamical resistance (R); a parameter that indicatively expresses soil shear strength. Charts or logs of dynamical penetration tests are shown in Figure 4.1. The graphic satisfactorily distinguishes the contrast between the horizons with different resistance, forming the cover of Pizzo D’Alvano where peaks are related to more resistant layers, represented by gravelly pumiceous lapilli interposed between paleosols. At the bottom the highest resistance level and impervious to dynamical penetration is the calcareous bedrock (Figure 4.1). Rocky bedrock was recognized by the absence of any advancing of the tips and by the characteristic elastic rebound of the falling mass on the anvil.

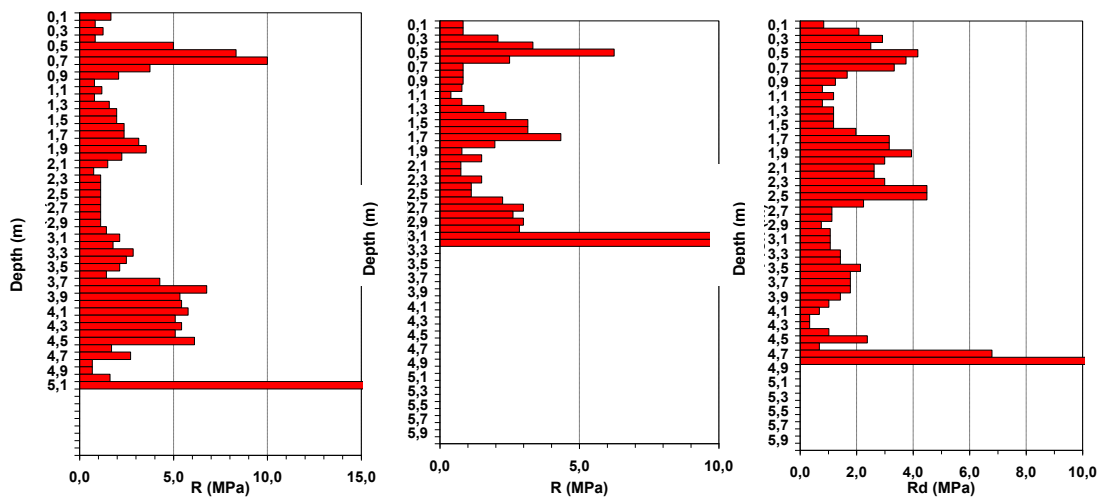


Figure 4.1: some example of dynamic penetration tests; the graphic restitution distinguishes the contrast of dynamic resistance among pyroclastic soil horizons forming Pizzo D’Alvano pyroclastic mantle.

The stratigraphical analysis of ash fall pyroclastic deposits was developed using a Hedelman’s hand auger, which is suitable for the investigation of the first few meters of depth in loose or cohesive soils. Furthermore, by means of digging trenches, which led to further identification and distinction of the different pyroclastic horizons forming the coverage of the slope, it was possible to correlate data deriving from different field methodologies. Results are respectively in good agreement.

Surveys aimed to the acquisition of detailed stratigraphic data, were carried out in order to define geometric relationships between pyroclastic soil horizons constituting the mantle. For the stratigraphical characterization, a lithological and lithostratigraphic as well as engineering-geological criterions were applied. The latter was based on the characterization of index properties by means of laboratory tests that allowed the classification of pyroclastic soil horizons with USCS, and pedological criterion (USDA, 1998, Terrible et al, 2000).

A complete volcanoclastic series was observed in the upper part of the engineering geological cross sections of Landslides 1 and 2, just a few decameters upward of the landslide crowns. The positions of stratigraphic investigation were located outside of the depletion zone, namely upward of the landslide crown and along the landslide flanks. From the top to the bottom, the following soil horizons were identified and classified by means of USCS (Figure 4.2):

- 1) A horizon classified as organic earth (Pt), due to the prevailing presence of humus;
- 2) B horizon, characterized by predominantly pumiceous lapilli, classified as sand with silt (SM);
- 3) C horizon (Pollena eruption, 472 AD [Rolandi et al., 2004]), consisting of greenish pyroclastic pumice, angular and barely altered, with the greatest size of pyroclasts up to 30 mm, classified as clean gravel and sand, well graded (GW or GP);
- 4) Bb horizon, corresponding to a buried B horizon by subsequent depositional event, and therefore considered as paleosol classified as sand with silt (SM);
- 5) Cb horizon, (Avellino eruption of 3.8 k-year [Rolandi et al., 1993]), representing a buried C horizon, consisting of gray pumice pyroclastic variable size from lapilli to coarse ash, with the greatest size of pyroclasts up to 40 mm, classified as the C horizon (GW or GP);
- 6) Bb horizon, corresponding to a B horizon buried by the subsequent depositional event of paleosol, also defined and classified as sand with silt (SM);
- 7) Cb horizon (Ottaviano eruption of the 8.0 k-year [Rolandi et al., 1993]), representing a buried C horizon, consisting of yellowish pumiceous pyroclasts varying in size from lapilli to coarse ash, with the greatest size of pyroclasts up to 20 mm, classified as the C horizon (GW or GP);

- 8) Bb_{basal} horizon corresponding to a residual pyroclastic deposit, strongly affected by pedogenetic processes, representative of the products of the previous eruptions, otherwise defined as basal paleosol and classified as sand with silt (SM);
- 9) R horizon, corresponding to the carbonate bedrock.

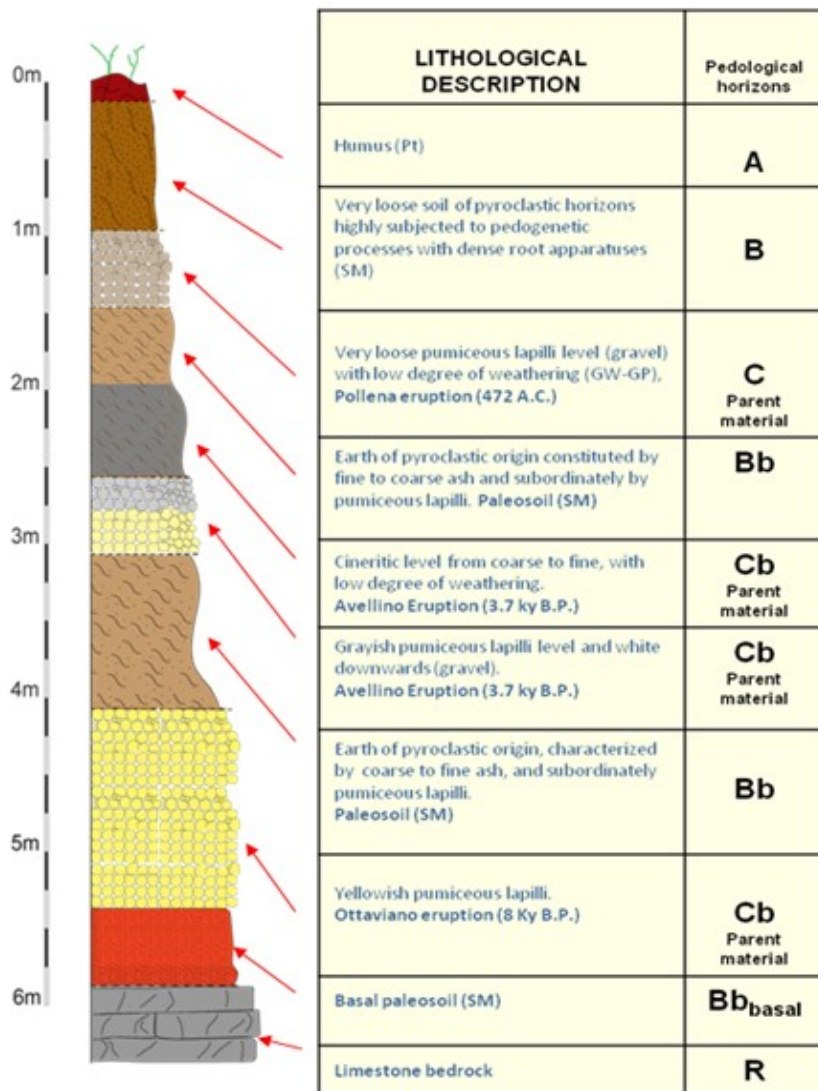


Figure 4.2 stratigraphical and engineering geological column of pyroclastic cover mantling the Pizzo D’Alvano massif achieved from Hedelman’s hand auger drilling and laboratory tests. It is representative of the zone about 30 m upward of the crowns of Landslides 1 and 2, where slope angle gently decreases down to 13°.

In this stratigraphical sequence (Figure 4.2), the Bb horizons can be considered as the product of ancient pedogenetic cycles acting on pyroclastic deposits lying in original position on the slope. The basal Cb horizon correspond to ash fall deposits of the Ottaviano eruption (8 k-year B.P), and characterized by overlapping of two pumice levels: the basal one is made of yellowish pumice of

variable size with lava inclusions (Rolandi et al., 2004), the upper one is made of white pumice and black scoriae. Upward in the sequence, another Cb horizon is related to ash fall deposits of the Avellino eruption (3.7 k-year B.P) that is constituted of two white angular and coarse pumice levels, with dark and tiny scoriae and crystals (the basal level) and grey pumice with coarse and angular elements (the upper level) (Rolandi et al., 1993b). Again upward another C horizon is related to Pollena eruption (472 d.C.) and consists of greenish pumice (diameter of order of millimetres), strongly porphyric and with leucite and biotite crystals, and lithic fragments (lava and carbonate) whose diameter increases upward (Rolandi et al., 2004).

In the upward sector of initial landslide crowns, considered as conservative areas of the slope due to gentle slope angle values that prevented denudational processes, stratigraphical data were conceived as representative of the original volcanoclastic series. Topographical survey was also conducted by means of a rangefinder / laser clinometer “LEICA DISTO A8” and a teodolite. In a such way it is possible to consider results of survey as representative of “undisturbed” sector of the slope. Instead, stratigraphical data collected along the landslide flanks, owing to the high slope angle value, were considered as affected by denudational processes that reduced the pyroclastic soil thickness and condensed the volcanoclastic series, thus according to a distribution model of ash fall pyroclastic deposit along slopes (Paragraph 1.5) by which the total thickness is inversely related to the slope angle (De Vita et al., 2006a).

4.2 Laboratory characterization of the physical index and mechanical properties of pyroclastic mantle

The characterization of physical properties of soils of pyroclastic origin, discussed in Chapter III and the classification of soil horizons by means of index properties, which were discussed in section 4.1, were carried out according to pedological criterion (Terribile et al, 2000). Determinations of the specific weight of solid particles (**G_s**) and organic matter (%) are shown in Table 2.

Determination of the grain size curves relative to B, C-Cb, Bb and Bb_{basal} horizons is shown in Figures 4.3 and 4.4, and the grain size envelopes determined for each soil horizon are shown in Figure 4.5.

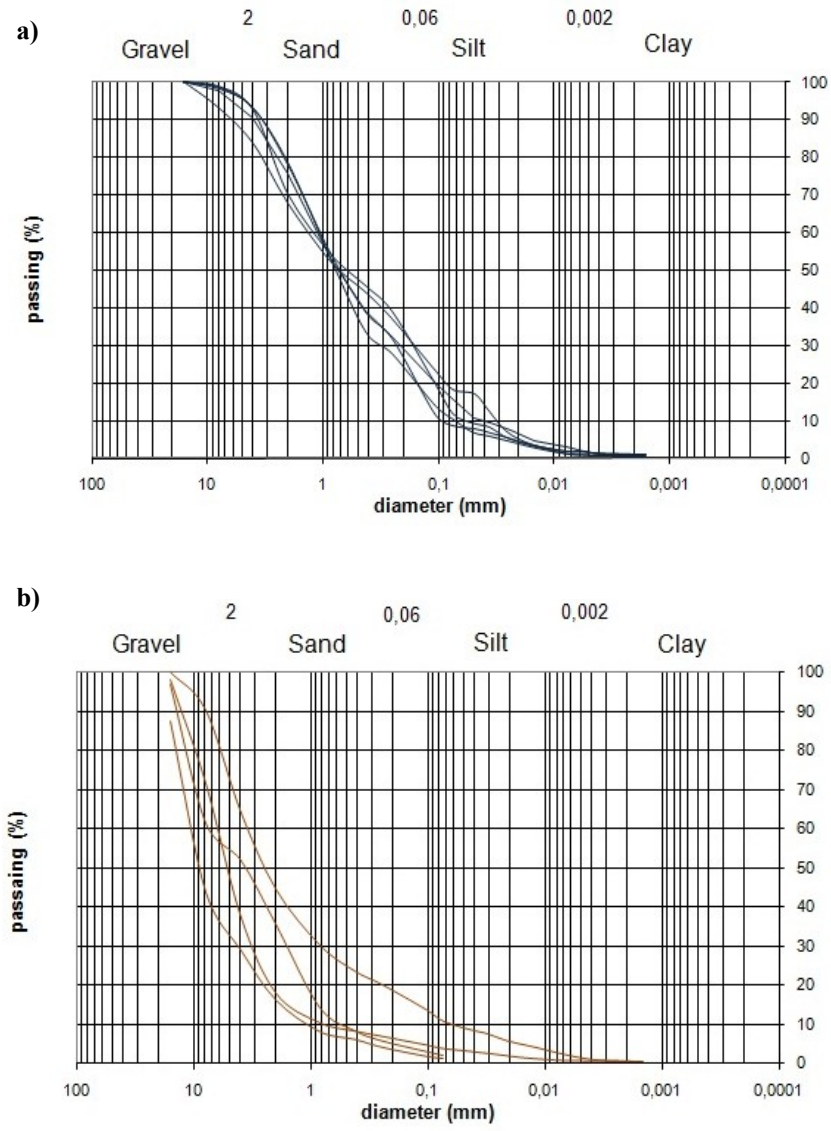


Figure 4.3: grain size curves for: a) B horizon; b) C horizon.

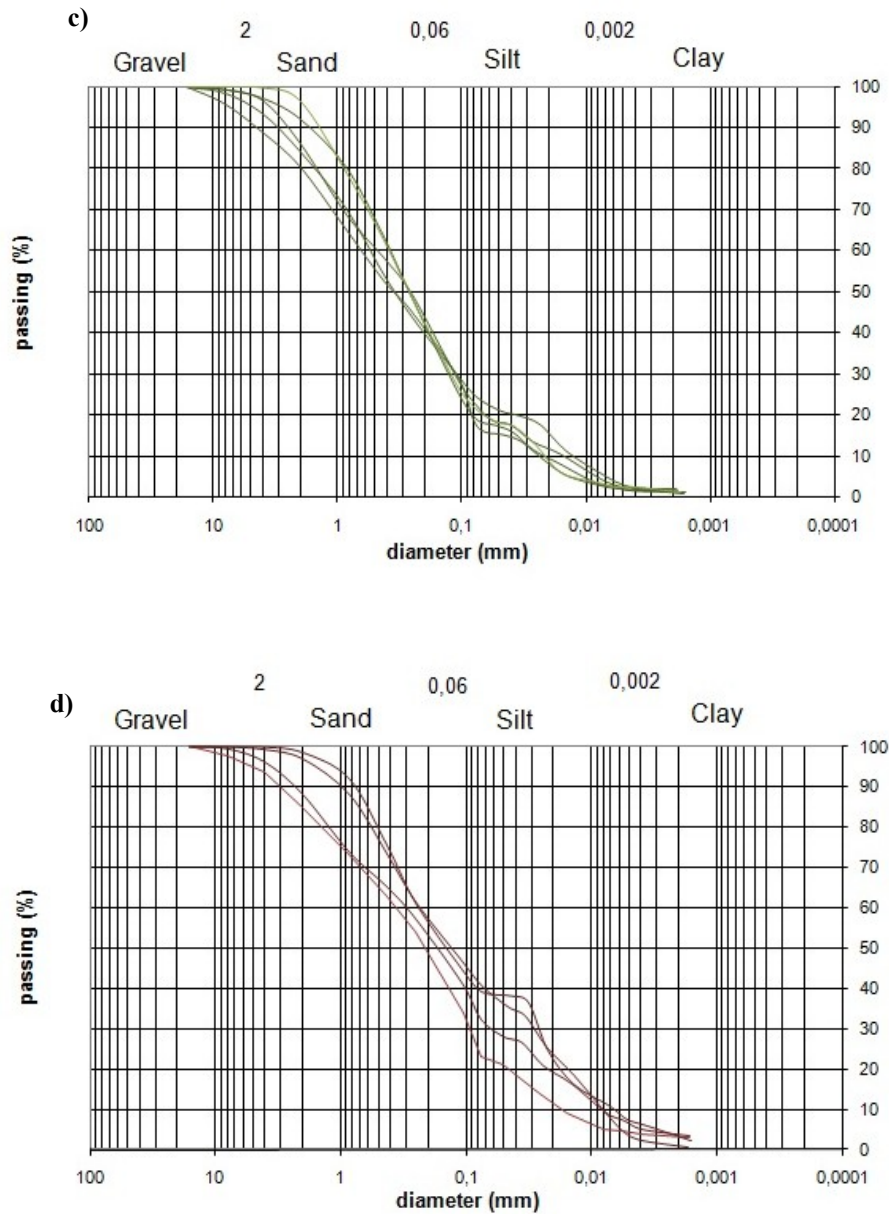


Figure 4.4: grain size curves for: c) Bb horizon and d) Bb_{basal} horizon.

Results of physical and index properties characterization of B, C-Cb, Bb and basal Bb horizons carried out in laboratory permitted the determination of D_{10} , D_{60} , uniformity coefficient U , and consistency limits w_L , w_P thus allowing the USCS classification. Soil physical properties such, unit weights (γ_{nat} , γ_{dry} , γ_{sat}), porosity (n), void ratio (e) were also estimated for each soil horizon (Table 3.3).

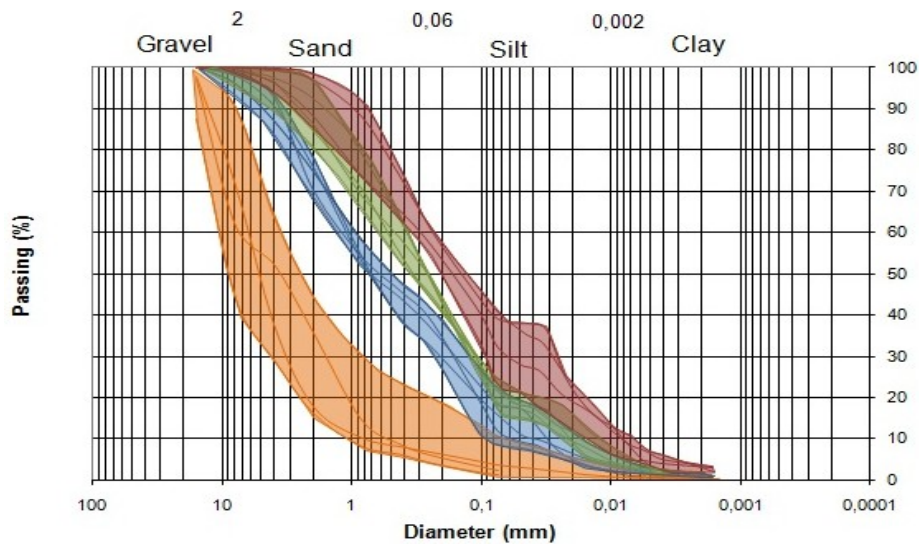


Figure 4.5: grain size envelopes for each soil horizon of pyroclastic mantle: blue) B horizon; orange) C horizon; green) Bb horizon; red) Bb_{basal} horizon.

Laboratory tests regarding the physical characteristics of soils being studied yielded a huge amount of data that were aggregated and statistically analyzed by means of box plot graphs (Figure 4.6).

As generally is recognized, with the decrease of particle size an increase in porosity and in the void ratio was observed. The high values of these parameters reflect the peculiar nature of the volcanoclastic deposits which are typically characterized by a vesicular structure that allows the existence of partially interconnected intraparticle voids. With the determination of the consistency limits, it was also possible to determine the different plasticity of the investigated horizons pointing out how, at increasing depth, horizons tend to decrease in grain size and correspondingly increase in the plasticity index ($IP = w_L - w_P$). A greater percentage of water is therefore required to make the transition from plastic to liquid for the horizons located at greater depths.

Hence, it follows the different behavior of these soils and, in particular, the different role they can play in the initiation of a phenomenon like debris slides - debris flows. Levels with a low plasticity index are more susceptible to the transition to a fluid state, as occurs in the intermediate stage of development of this type of landslide (debris avalanche) and in the final (debris flow), due to a rapid undrained loading (Hutchinson & Bhandari, 1971).

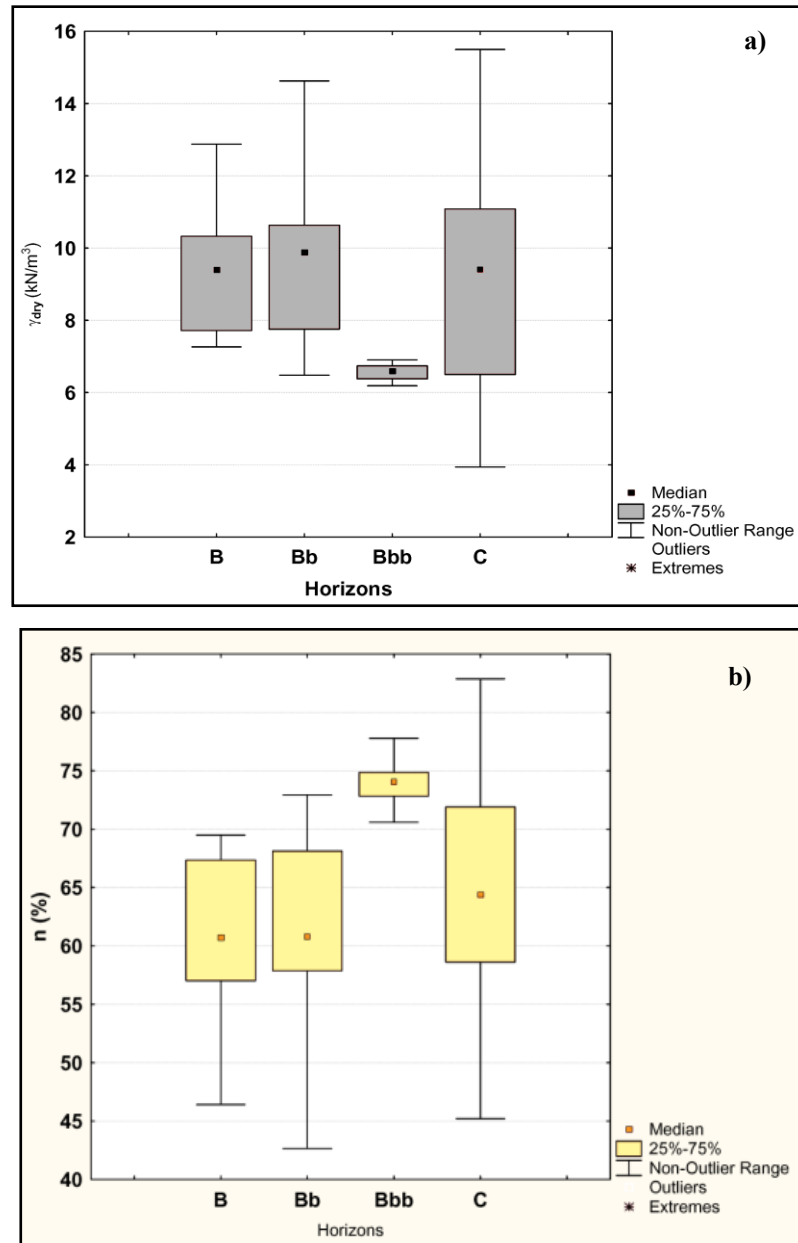


Figure 4.6: box plots of: a) dry unit weight (γ_{dry}); b) total porosity (n).

As regards the mechanical properties, shear strength parameters of pyroclastic layers were determined by standard direct shear tests. On the basis of examination of the stratigraphic relationships between the sliding surface of the initial landslides, it was considered appropriate to subject soil B, and paleosols, Bb and Bb_{basal}, to mechanical characterization but excluding the intercalated pumice level since these deposits are inconsistent and therefore difficult to sample.

In order to make the sampling more representative of soil conditions in the triggering area, it was decided to sample in both in the upslope areas of the Landslides 1 and 2 crowns and along the sliding surfaces to compare the soils involved in the landslides with those not involved.

Direct shear tests provided envelopes representing shear strength of soils. Pyroclastic horizons were subjected to direct shear tests with applied normal stress values closely ranging around those existing at all depths between the top and bottom of each horizon. Results of each test consisted of data pairs (σ' and τ) which allowed the reconstruction of the Mohr-Coulomb envelopes and the estimation of mechanical parameters c' and ϕ' .

Obtained mechanical parameters (c' and ϕ') were statistically analyzed and represented by means of a box plot chart (Figure 4.7). The obtained results can be considered a further advance if compared with other geotechnical studies that have broadly analysed this topic (Cascini et al., 2000; 2003; 2005; 2008; Bilotta et al., 2005; Fiorillo et al., 2001; Crosta and Dal Negro, 2003; Picarelli and Olivares, 2001; Picarelli et al., 2004).

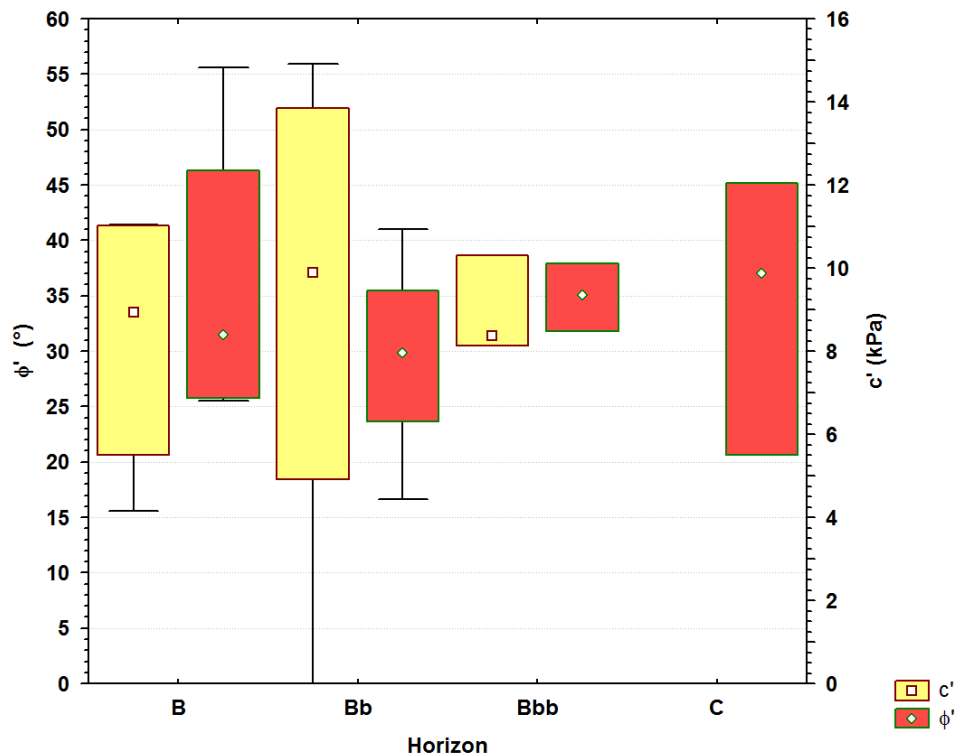


Figure 4.7: box plots of shear strength parameters (c' and ϕ').

Elaboration and interpretation of data clearly show a lack of homogeneity in the properties of shear strength of the pyroclastic soil horizons and the presence of a horizon. Considering the

median value of internal friction angle and the decrease of apparent cohesion of the B horizon due to root apparatuses, not fully evaluated by the direct shear tests, it's possible to hypotesise a local decrease of shear strength, which forms a sort of mechanical discontinuity corresponding to a depth approximately equivalent to that of the sliding surface (ranging from 1.10 m and 2.20 m) where the initial rupture occurred. This is well observed from the chart where shear strength is plotted against the depth (z) (Figure 4.8). In this case, the shear strength is considered ad as a function of the depth $\tau(z)$:

$$\tau(z) = \sigma' \cdot \text{tg } \phi' = z \cdot \gamma \cdot \text{tg } \phi'$$

where γ = soil unit weight.

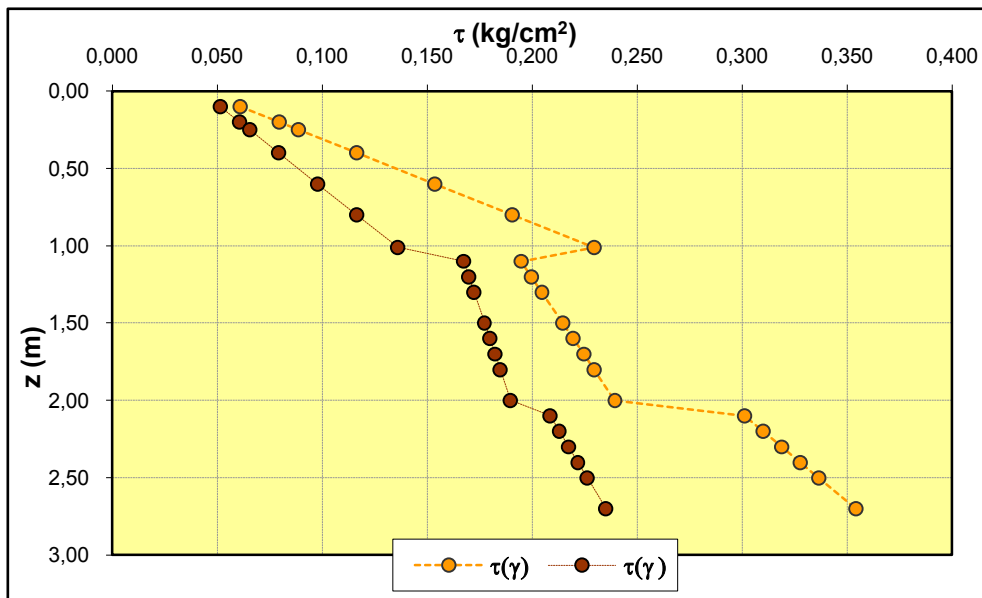


Figure 4.8: log of shear strength as a function of the depth calculated by means of median value of the friction angle (ϕ'). This log clearly shows a discontinuity in shear strength at a depth approximately correspondent to the sliding surface.

4.3 Hydraulic characterization of pyroclastic soil horizons

The pyroclastic mantle is very heterogeneous because it is constituted by alternating soil horizons characterized by different particle grain sizes (from gravel to silt) and thus by different and contrasting saturated hydraulic conductivity (K_{sat}), sometimes up to high levels. The multilayered hydrogeological setting and the unsaturated conditions justify the complexity of water circulation within the pyroclastic cover-carbonate bedrock system. Field and laboratory analyses were carried out for hydraulic characterization of the different soil horizons constituting the pyroclastic mantle. This section describes results of the saturated hydraulic conductivity tests carried out with field and laboratory methods both regarding samples collected nearby the source area.

4.3.1 Results from field and laboratory tests for saturated hydraulic conductivity measurement

The determination of the hydraulic conductivity of a saturated or quasi-saturated soil is an important prerequisite for the interpretation and simulation by means of mathematical models of hydrological phenomena occurring at slope scale as well as any other water flow modeling within soils. For the areas of interest, the determination of representative values of saturated hydraulic conductivity generally involves significant experimental efforts due to its marked spatial and temporal variability.

The dependence of hydraulic conductivity on grain size and structural characteristics of the soil induces a high variability in space and time, up to several magnitude orders. The measurement of K_{sat} can be considered as punctual, related to a volume of some hundreds to thousands of cm^3 .

Repeated field tests were carried out to determine K_{sat} by means of the Amoozegar permeameter also known as Compact Constant Head Permeameter (CCHP) and the “single ring permeameter” for horizons B, C, Bb, whose values are shown in Table 4.1.

4.3 Hydraulic characterization of pyroclastic soil horizons

| Pyroclastic soil horizon | USCS classification | Depth (cm) | Number of measurements | K_{sat} range values (m/s) |
|--------------------------|---------------------|------------|------------------------|---|
| B | SM | 30 - 115 | 24 | $1.00 \times 10^{-4} > K_{sat} > 9.00 \times 10^{-6}$ |
| C | GW-GP | 130 | 13 | $2 \times 10^{-2} > K_{sat} > 2.69 \times 10^{-2}$ |
| Bb | SM | 160 - 230 | 7 | $1.90 \times 10^{-5} > K_{sat} > 1.52 \times 10^{-7}$ |
| Bb _{basal} | SM | > 250 | 6 | $1.86 \times 10^{-7} > K_{sat} > 4.68 \times 10^{-6}$ |

Table 4.1: K_{sat} values from field tests.

In Table 4.1, obtained results of saturated hydraulic conductivity (K_{sat}) are shown. A high range of variability can be appreciated, respectively between 1.00×10^{-4} and 9.00×10^{-6} m/s for the B horizon. Values of about 2.0×10^{-2} m/s for the pumiceous C horizon. Finally to values ranging between 1.90×10^{-5} and 1.52×10^{-7} m/s in the Bb horizon and between 1.86×10^{-7} and 4.68×10^{-6} m/s (Figure 4.9). The paleosol horizons and the basal paleosol have close hydraulic conductivities, while C horizon shows the highest values.

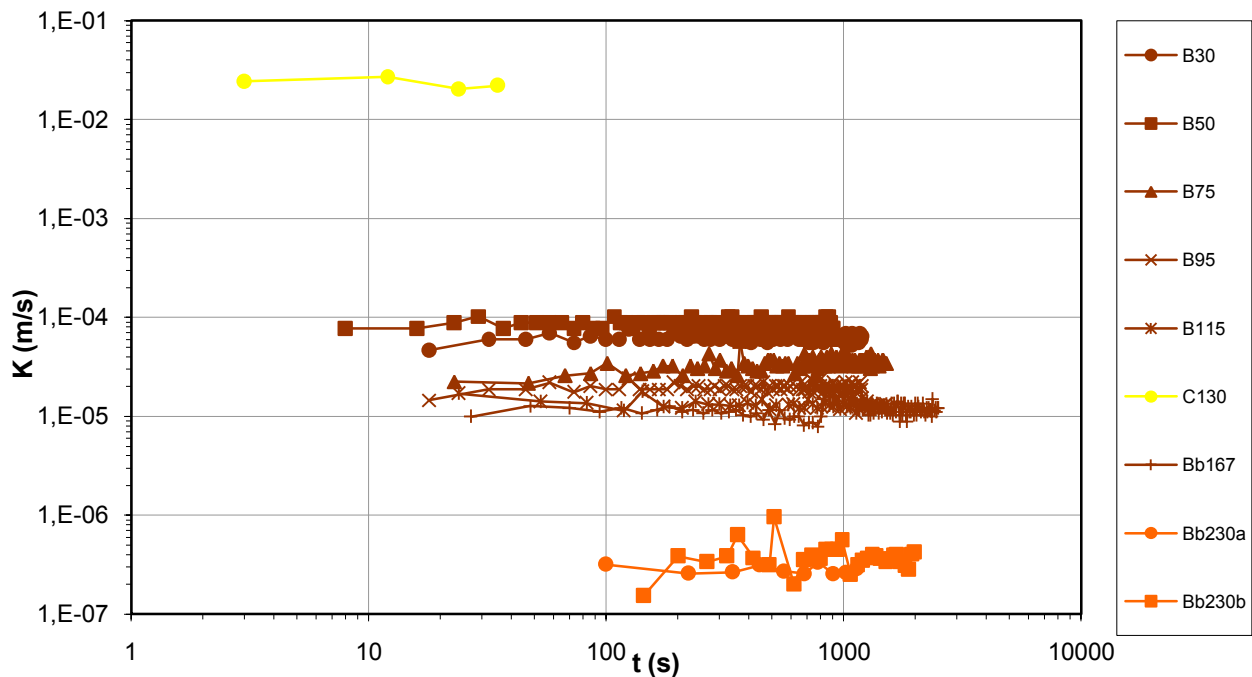


Figure 4.9: field test results, obtained from several experiments carried out through Single Ring Infiltrimeter and Constant Compact Head Permeameter (CCHP). It's possible to highlight the reaching of the steady flow condition, thus the saturated condition.

In combination with field measurements of saturated hydraulic conductivity by means of single ring infiltrometer and Amoozegar permeameter, laboratory measurements were carried out. The adopted methodology was carefully explained in the previous chapter. The repeated laboratory experiments regarding soil (B), paleosol (Bb), and basal paleosol (Bb_{basal}) were executed in a number of samples to perform a statistical analysis of the resulting dataset.

Results, plotted in the charts, show the relationship between time (s) and cumulated volume of water flow through soil specimens under a constant hydraulic head. Several tests (Figures 4.10, 4.11, 4.12) were carried out on the same sample by applying different values of hydraulic gradient, which is the ratio between hydraulic head (ΔH) and length of the water flow path, namely the height of the sample contained in the plexiglass cylinder (Figure 3.23).

This ratio grows up as the ΔH applied at each step increases. Moreover the plots for each investigated horizon shows a good agreement, with an increasing linear trend. For the highest values of the hydraulic gradient, in some samples a non linear behavior of the water outflow was observed. This was attributed to piping phenomena, thus to the alteration of the soil structure. Obviously such results were not considered as valid.

The saturated hydraulic conductivity (K_{sat}) was calculated by means of the Darcy law:

$$K_{\text{sat}} = \frac{\text{Volume}}{t \cdot S \cdot i}$$

where:

V = water volume;

t = time;

S = sectional area of the cylinder;

i = hydraulic gradient.

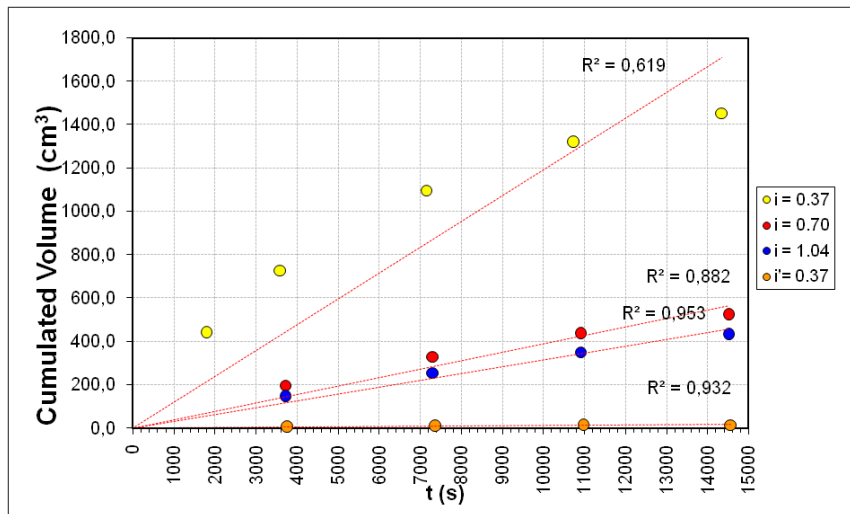


Figure 4.10: example of cumulated water volume in the time for the horizon B under different values of hydraulic gradient.

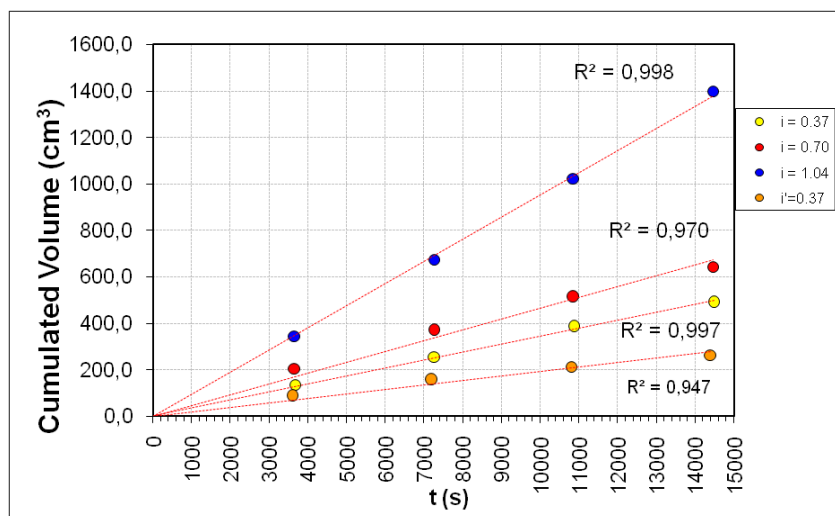


Figure 4.11: example of cumulated water volume in the time for the horizon Bb under different values of hydraulic gradient.

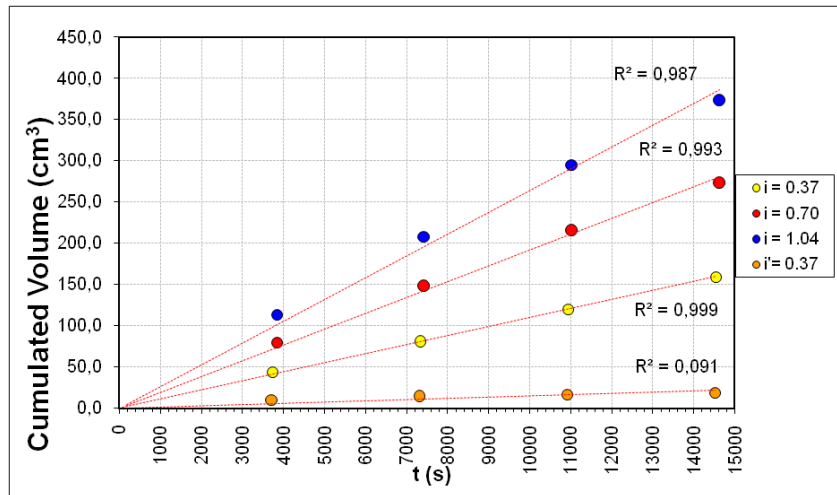


Figure 4.12: example of cumulated water volume in the time for the horizon Bb_{basal} under different values of hydraulic gradient.

The data derived from constant head permeameter were statistically analyzed and plotted in a bar diagram (Figure 4.13). In the diagram, the 10% percentile (the lowest point), the percentile 90% (the highest point) and the median value, are shown. The diagram highlights that, according to laboratory tests, K_{sat} ranges from 1.92×10^{-4} to 2.71×10^{-5} m/s for B horizon, from 1.86×10^{-5} to 6.06×10^{-7} m/s for Bb, and for from 2.08×10^{-5} to 2.99×10^{-6} m/s for Bb_{basal}.

Laboratory data are in good agreement with those determined by means of field tests, except for the samples of the Bb_{basal} horizon that show values corresponding to upper percentiles (>75%) of the field tests data.

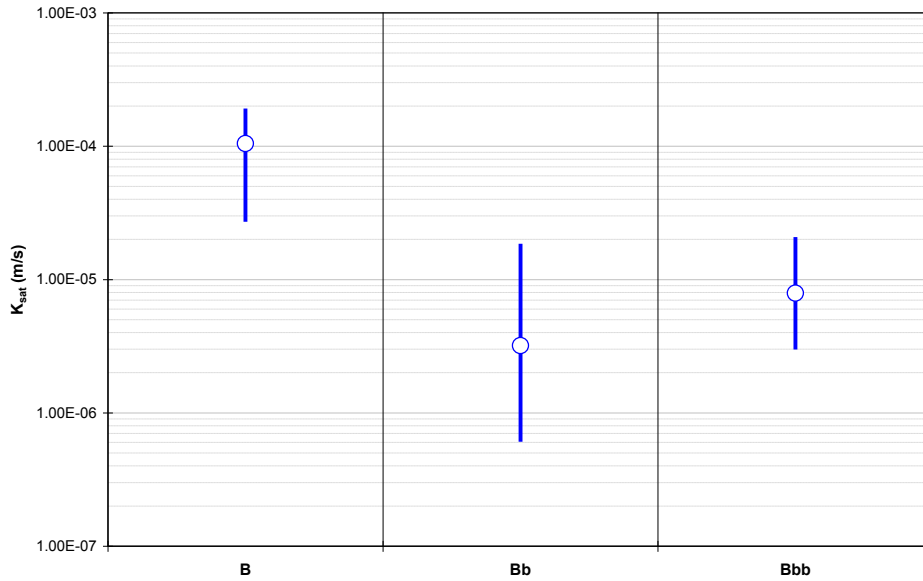


Figure 4.13: K_{sat} measured for specimens belonging to B, Bb (paleosol) and Bb_{basal} (paleosol) horizons. The lowest point represents the 10% percentiles, the highest point represent the 90% percentiles and the circle the median value.

According to the congruence between field and laboratory datasets, all data were grouped for each pyroclastic soil horizon and statistically analyzed (Figure 4.14) by means of box plot with the purpose of using these results for finite element modeling of unsaturated/saturated flow as described in the following Chapter V.

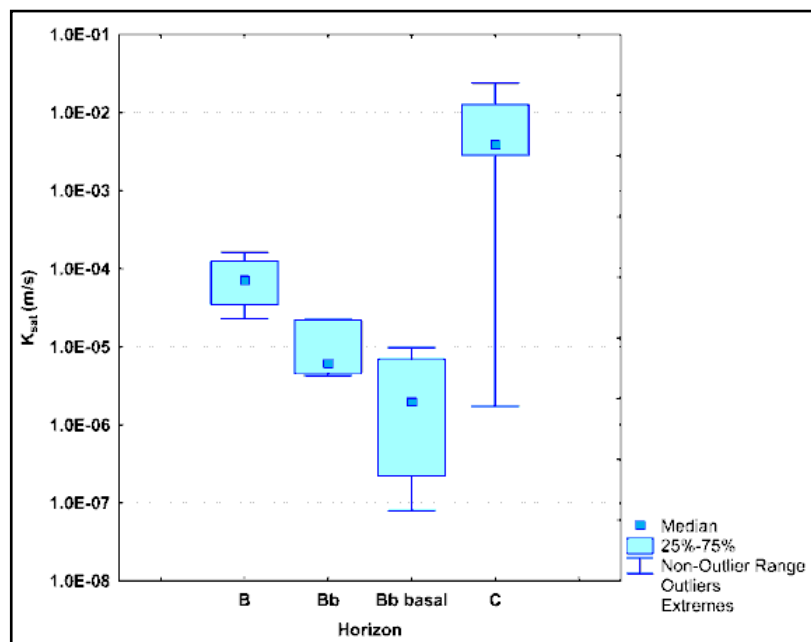


Figure 4.14: box plot of hydraulic conductivity estimated for each pyroclastic soil horizon with single ring infiltrometer tests and Amoozegar permeameter tests.

4.3.2 Unsaturated hydraulic characterization from “Tempe cells”

Soil Water Retention Curves (SWRCs) were determined, by means of “Tempe Cell” apparatus (produced by Soil Moisture Corporation) for each of the pyroclastic soil horizon considered relevant in landslides initiation (namely B, C, Bb and Bb_{basal}). As explained in the previous chapter, the SWRCs, correlate experimental determinations of matric suction to the correspondent water contents. They are essential for the characterization of hydraulic and mechanical behavior of unsaturated soils.

Soil Water Retention Curves were determined by means of Tempe Cell apparatus testing simultaneously No. 6 specimens collected for the same pyroclastic soil horizon (Figures 4.15, 4.16, 4.17). Owing to failure in air leaks of some Tempe Cells apparatuses, SWRCs were obtained only on a subset of samples: 4 for the B horizon, 5 for the C horizon, 2 for the Bb horizon, and 4 for the Bb_{basal} horizon. Those SWRCs affected by such experimental errors were excluded and the most representative SWRCs were selected. From the validated curves, the average of SWRCs were calculated (Figure 4.19) for each soil horizon, aiming at achieving representative data to be imputed in finite element modeling of the saturated / unsaturated flow.

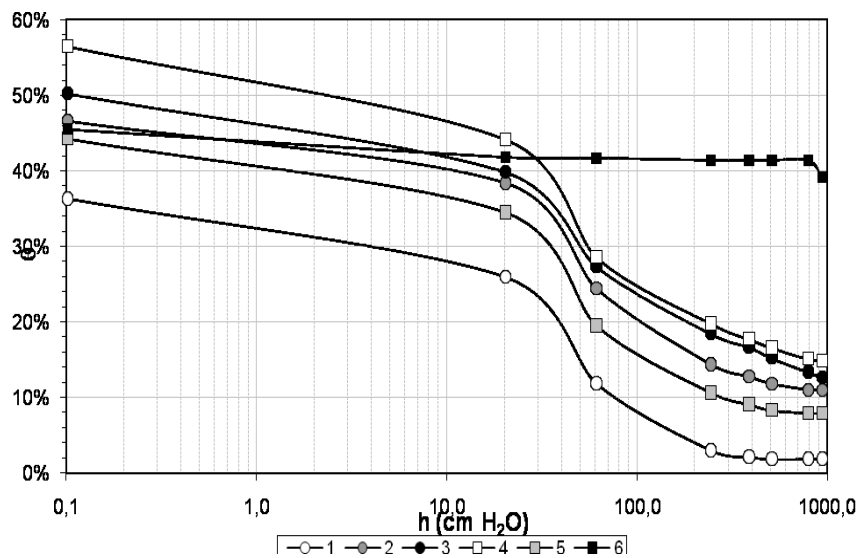


Figure 4.15: SWRCs for horizon B horizon.

In particular, test related to “Tempe Cell” No. 1 for B horizon (Figure 4.15) was excluded, because θ_{sat} value was lower than values observed for the other specimens, probably because it was

not reached the saturation during the preliminary phase of samples preparation during which the Tempe Cell is completely soaked in rain water.

Test related to “Tempe Cell” No. 6 accounting for B horizon (Figure 4.15), failed and then was excluded, since there were air leaks from the O’rings. In fact the experimental curve doesn’t show the typical hydraulic behavior observed for the other specimens.

Test related to “Tempe Cell” No. 1, accounting for C horizon (Figure 4.16) was excluded since it didn’t reach the end of the test, due to air leaks from the O’rings. Test related to “Tempe cell” No. 2 was excluded as well, because θ_{sat} value of this specimen was lower than the others, probably because it was not under saturated conditions.

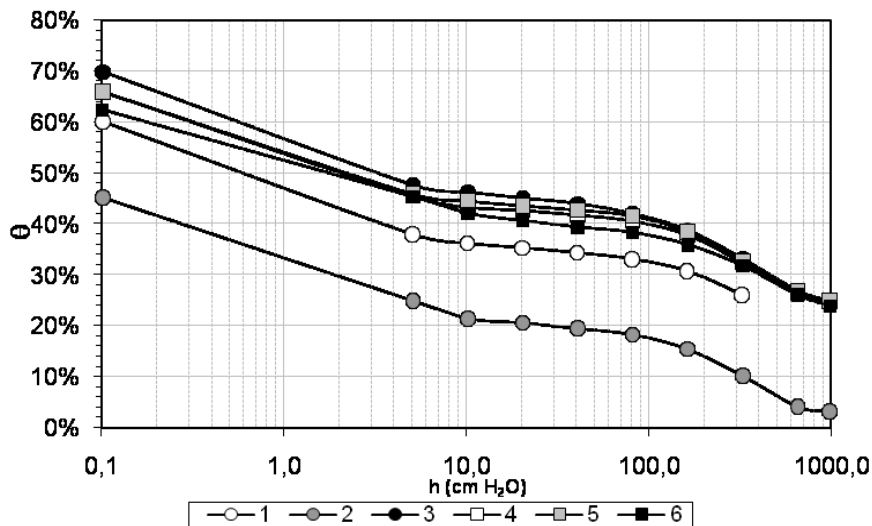


Figure 4.16: SWRCs for C horizon.

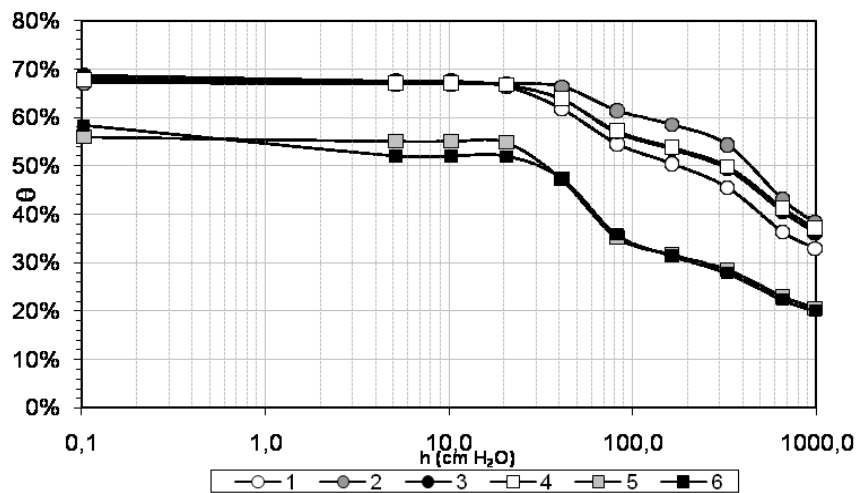


Figure 4.17: SWRCs for Bb horizon (1, 2, 3 and 4) and Bb_{basal} horizon (5 and 6).

After the “Tempe Cells” tests, a final control was carried out on the grain size analysis of soil samples (Figure 4.18), in order to verify similarities with the typical grain size characteristics of the soil horizon. Results demonstrated that soil samples tested with “Tempe Cells” are representative of the correspondent soil horizon.

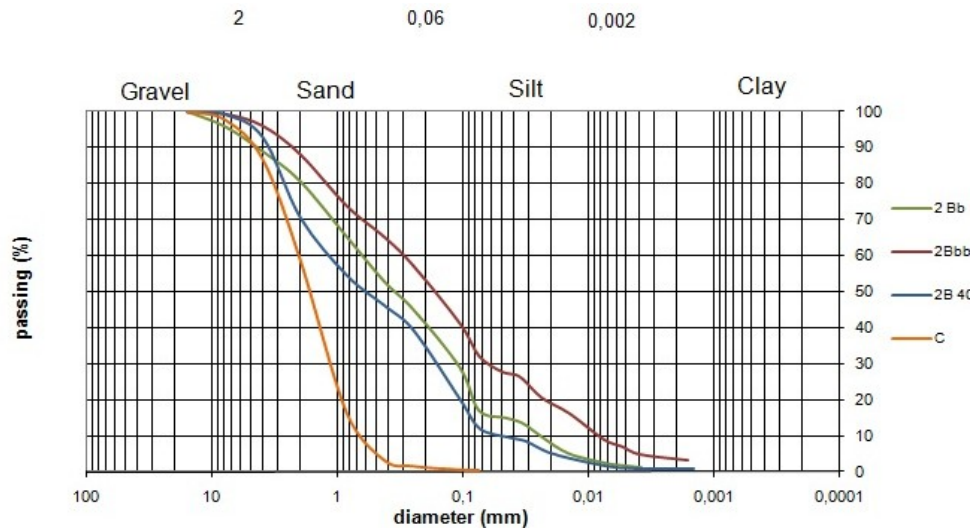


Figure 4.18: grain size analysis for each sample set tested with “Tempe Cells” apparatus. Symbols: blue) B horizon; orange) C horizon; green) Bb horizon; red) Bb_{basal} horizon.

After excluding curves affected by experimental errors, SWRCs were plotted in the same graph (Figure 4.19) allowing to observe that curves can be grouped for similarity in groups exactly corresponding to pyroclastic soil horizons. This observation demonstrates that pyroclastic soil horizons have peculiar unsaturated hydraulic properties as well as distinguishable saturated hydraulic conductivity. Otherwise the comparison between SWRCs highlights a different hydraulic behavior of the soil horizons that, starting from different initial moisture contents and due to different grain size distributions, shows a different residual water content (the bigger θ_s , the bigger θ_r).

However for the B horizon and the Bb and Bb_{basal} horizons it is possible to observe a similar behavior as regards the Air Entry Value, marking the branch of the curve where air first starts to enter the largest pores and the desaturation begins. As regards pumiceous lapilli (yellow curve) a different shape is shown, reflecting the different structure of the soil particles.

Pumiceous lapilli show a very special behavior for a gravelly soil, demonstrating a unusual high water retention capacity due to high specific surface and interconnected intra-particle voids. Curves show a quick drainage ($\Delta\theta = 20\%$) of large inter-particle voids in the pressure range $0 \div 0.10$ m, and

a water retention capacity greater than that observed for Bb horizon in the pressure range above 0.8 m, due to the interconnected intra-particle voids.

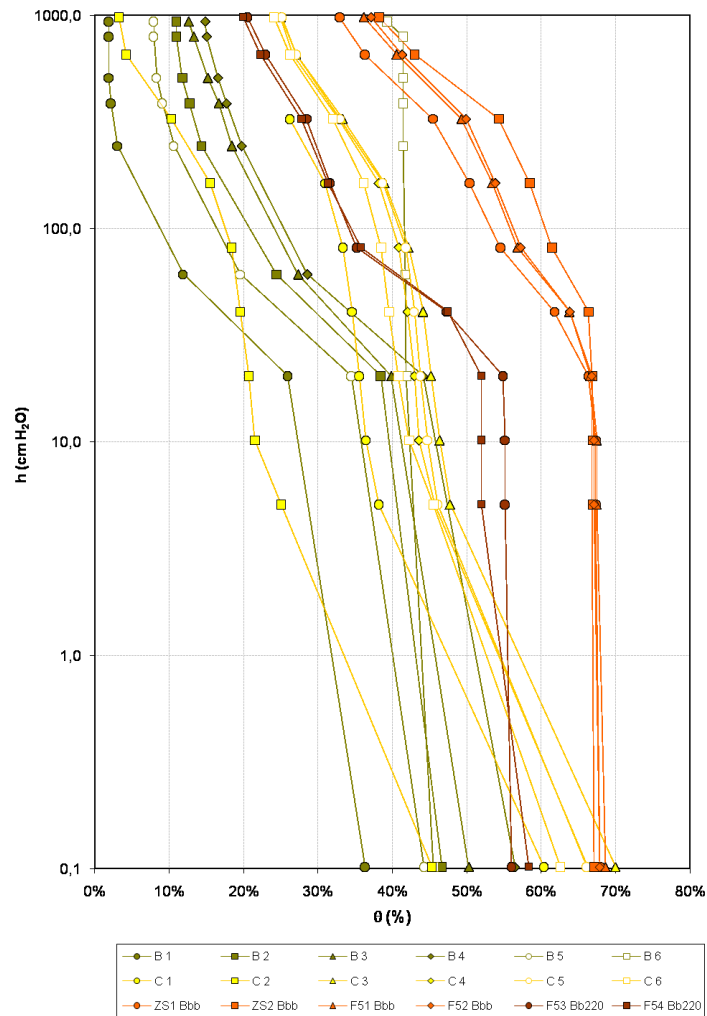


Figure 4.19: synthesis of SWRCs. Average values are represented by the continuous thick curve. Symbols: green) B horizon; yellow) C horizon; orange) Bb horizon; brown) Bbbasal horizon.

Results are in good accordance with other experimental curves proposed for pyroclastic soils equivalent to B and Bb horizons (Terribile et al., 2000; Sorbino and Foresta, 2002; Basile et al., 2003; Frattini et al. 2004; Nicotera and Papa, 2008).

4.4. Engineering geological models of initial landslides

Field surveys were applied to the reconstruction of axial and longitudinal topographical profiles of three main cases of triggering mechanisms. The combined topographic and stratigraphical data allowed the reconstruction of the engineering-geological models on a very detailed scale. In particular, topographical profiles within the source areas were extrapolated from longitudinal and transversal cross sections as well as the volume of the material involved in the initial debris slide - generally in the order of about tens or hundreds of m³.

Landslides 1 and 2 (Figures 4.20 and 4.21) were triggered upslope of natural morphological discontinuities, for example a knickpoint and an outcropping rocky scarp. In particular, in the cross section of Landslide 1 (Figure 4.20) it is possible to observe the progressive reduction of the real thickness of the pyroclastic mantle (measured with an angle at a 90 degree angle to the slope), from about 6 m in the upslope zone to about 2.5 m in the crown area and in the depletion zone where slope angle increases. This can be related to the slope angle increase from about 13° in the upslope area to about 45° in the landslide zone.

The source shows an approximately circular steep slip surface, tangential to the basal paleosol (Bb_{basal}) that outcrops in the terminal part of the landslide scars and that cuts the upper paleosols and the pumiceous lapilli horizons. This pinches out in correspondence of the landslide scar and the upper part of the depletion zone. The morphological reconstruction of Landslide 1 enabled the estimation of the initial slide volume that is approximately 180 m³.

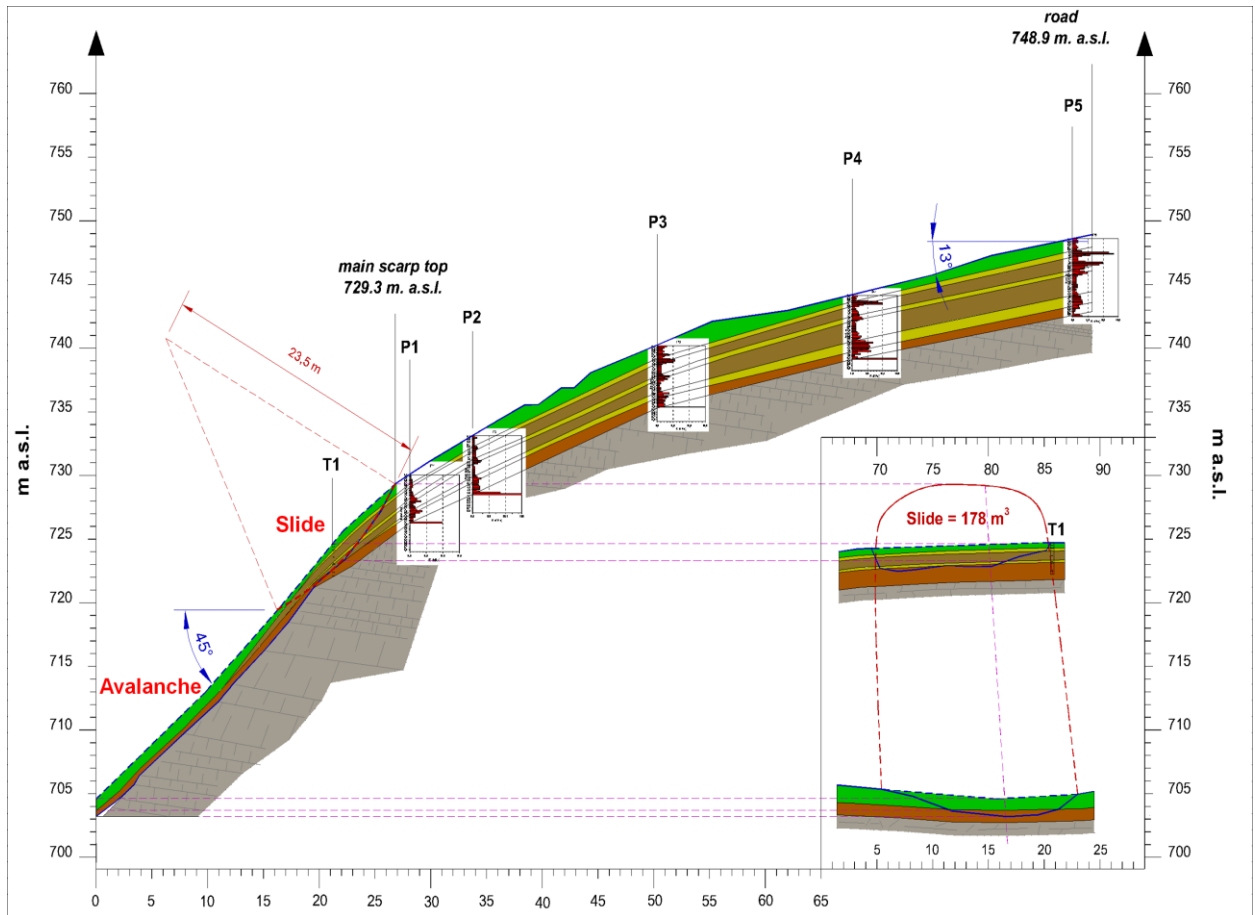


Figure 4.20: longitudinal engineering geological cross section of Landslide 1. Symbols: T) pits dug for stratigraphical characterisation; P) dynamic penetration tests and correspondent logs; green) B horizon; yellow) pumiceous lapilli C horizons; light brown) Bb horizons (paleosols); orange) Bb_{basal} horizon (basal paleosol).

In the engineering geological cross section of Landslide 2 (Figure 4.21), it is possible to recognize a similar reduction of thickness of the pyroclastic coverage, as the slope angle increases, from 13° in the uphill sector of the source area to 37°, measured in proximity of the source area. Moreover it is observed an abrupt termination of the pyroclastic mantle above the rocky scarp. Also this distribution of pyroclastic soils is in accordance with the abovementioned distribution model of pyroclastic soils along slopes that accounts for the annulment of total thickness for slope angle values greater than 50°.

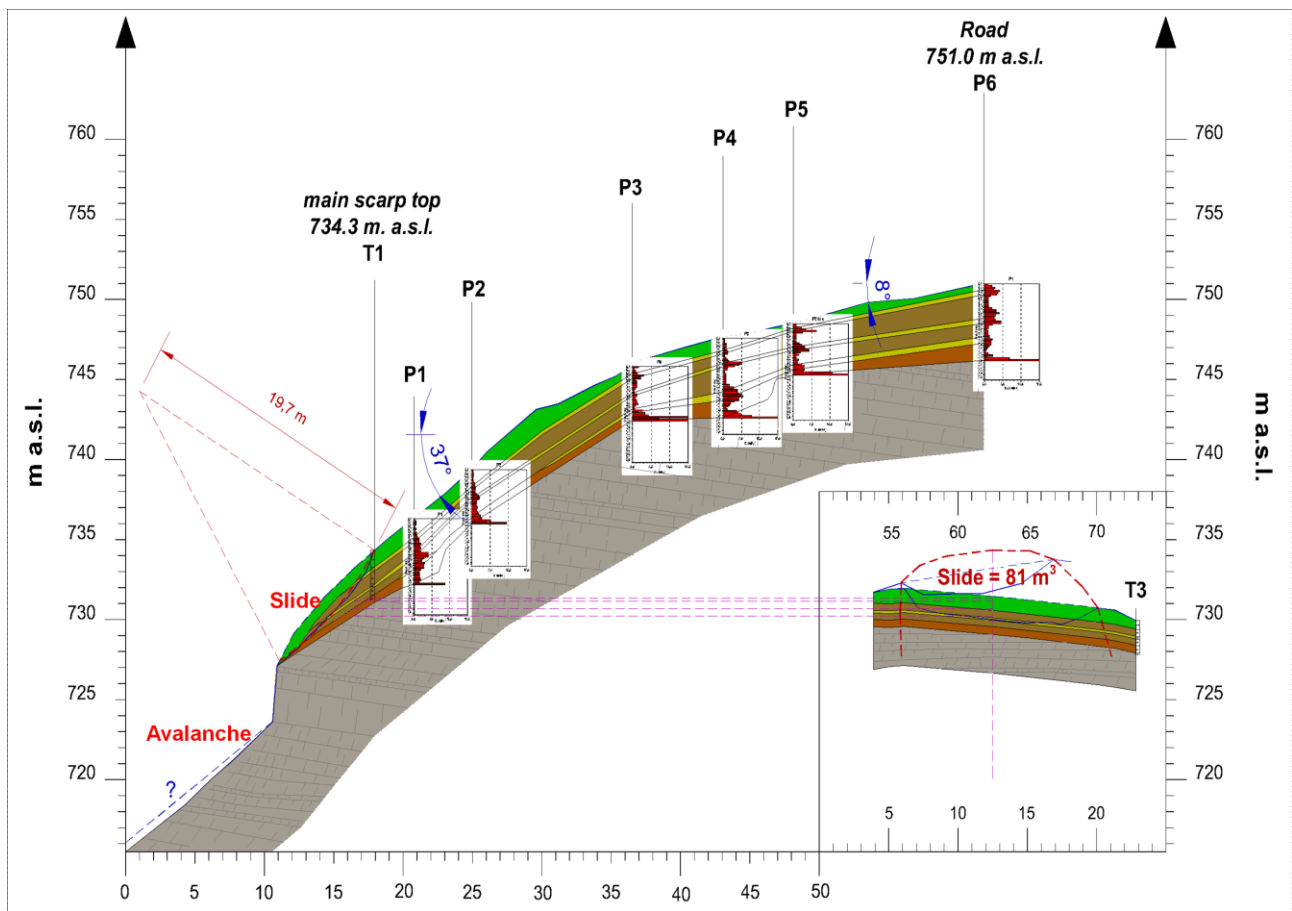


Figure 4.21: longitudinal engineering-geological cross section of Landslide 2. Symbols: T) pits dug for stratigraphical characterization; P) dynamic penetration tests and correspondent logs; green) B horizon; yellow) pumiceous lapilli C horizons; light brown) Bb horizons (paleosols); orange) Bb_{basal} horizon (basal paleosol).



Figure 4.22: typical example of potentially unstable small volume of pyroclastic soils above a rocky scarp kept stable by tree roots.

Total thickness of pyroclastic mantle decreases as slope angle increases determining a strong thinning of pyroclastic cover in the case of Landslide 1 and a sudden interruption in the case of Landslide 2. Real thickness of pyroclastic mantle varies from 5 ÷ 6 m in the upper slope, down to 2 ÷ 3 m in the landslide crown. Besides measurements of the total thickness, a more complete volcanoclastic series does exist in the upper slope of the crown zone respect to those observed in the landslide main scarps. Below the B horizon, a complete series consists of the alternation up to three C horizons constituted by pumiceous lapilli and interposed Bb horizons (paleosoils). The deepest horizon is the basal paleosoil Bb_{basal}, which always covers the carbonate bedrock. On the basis of lithological features, C horizons were correlated to deposits of 8 ky B.P. “Ottaviano”, 3.5 ky B.P. “Avellino”, 472 AD “Pollena” eruptions. In landslide main scarps, pyroclastic series reduces and the lack of the deepest C horizon (8 k-years “Ottaviano” eruption) was observed. The reconstruction of geometrical settings of pyroclastic soil horizons along longitudinal cross-sections clearly shows a draping deposition, typical of ash-fall deposits, which accounts for a stratigraphical setting generally parallel to external morphology (Fisher, 1985). Stratigraphical correlations between the upper part of slope and landslide scarp, show the progressive thinning of each horizon and demonstrate the pinch-out of the deepest C horizon (De Vita et al., 2006b).

Sliding surfaces for Landslides 1 and 2 appear with circular shapes that is possible to inscribe in circles with a radius respectively of 23.5 m and 19.7 m. Rupture surfaces cross soil horizons, becoming tangent to the basal paleosoil (Bb_{basal}) that outcrop in the terminal part of landslide scars. Measured transversal widths are respectively of 18 m and 15 m. Estimated volumes of initial slides are respectively of 178 m³ and 81 m³.

At last, the Landslide 3 is the case of the interruption of the volcanoclastic mantle due to man-made road-cut. Unlike previous landslides, in this case the basal rupture surface shows a rectilinear profile and is characterized by an average slope angle of about 33° (Figure 4.23). Stratigraphical reconstruction allowed to estimate an approximately constant real thickness of about 3 m, and a volcanoclastic series characterised by two C horizons that is possible to correlate respectively to deposits of 472 AD “Pollena” and 3.5 k-years “Avellino” eruptions. The sliding surface has a composite shape, with an approximately vertical upper sector cutting pyroclastic horizons, and a following rectilinear sector, parallel with external topography and tangent with the Bb_{basal} horizon. Measured transversal width is about 28 m; the estimated volumes of initial slide is about of 600 m³. The relevant differences in width and volume with respect to Landslides 1 and 2 are justified by the effect of a linear road cut along a topographic contour.

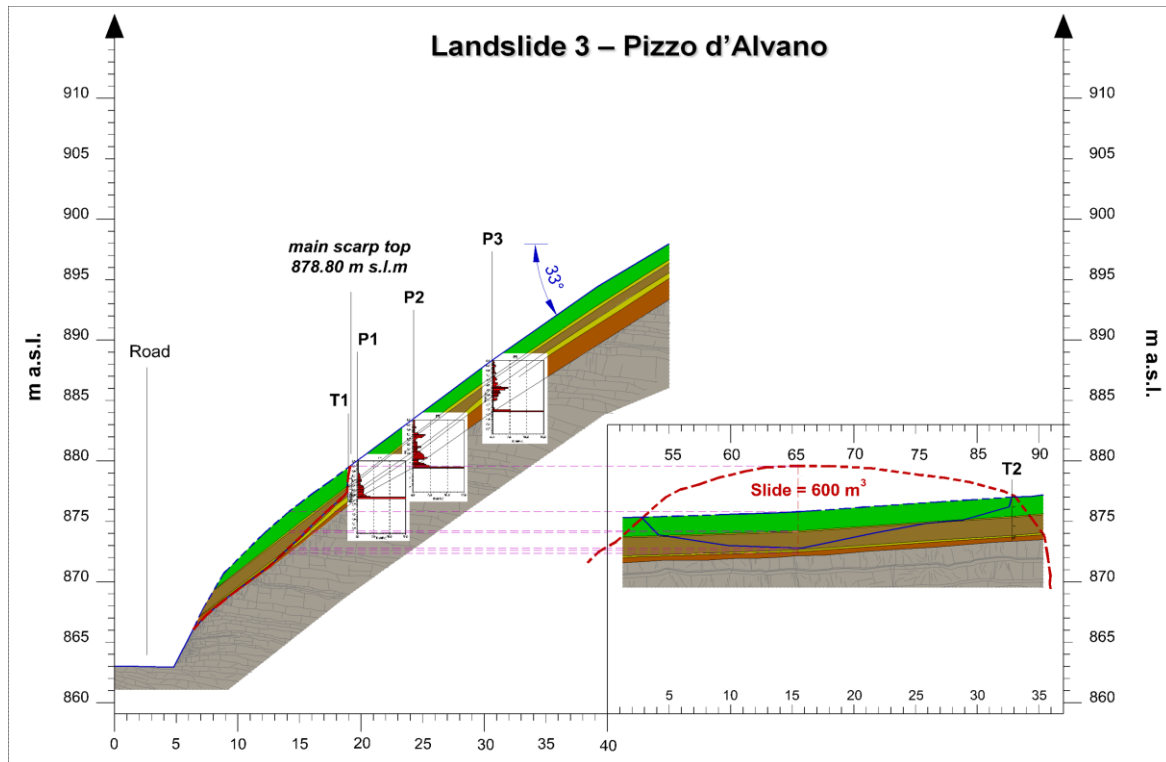


Figure 4.23: longitudinal engineering geological cross section of Landslide 3. Symbols: T) pits dug for stratigraphical characterization; P) dynamic penetration tests and correspondent logs; green) B horizon; yellow) pumiceous lapilli C horizons; light brown) Bb horizons (paleosols); orange) Bb_{basal} horizon (basal paleosol).

Field observations show that the sliding surfaces of the initial landslides developed above the basal paleosol with low hydraulic conductivity (Figures 4.20, 4.21, 4.23 and 4.24). This evidence implies a different interpretation of the triggering mechanisms of the initial landslides, with respect to the previous models known in the scientific literature, highlighting the existence of the hydrogeological conditions sufficient to originate a sub-surface flow within the pyroclastic mantle. The onset of the initial landslides always takes place upslope of morphological discontinuities, and involves small volumes with tens-hundreds m^3 of magnitude.

Areas with higher susceptibility for the initial landslides match those where natural discontinuities of bedrock morphology are located. These correspond to the sudden increase of slope angle that implies a reduction of the thickness of the pyroclastic layer downslope. Hence, the existence of particular hydrological conditions involving the increase of localized pore pressures during rainstorms of high intensity and short duration, was observed. The geometry of pyroclastic horizons is highly dependent on the slope angle. It may lead to the pinch-out of the pumiceous

lapilli (gravel), that tend to reduce more than cineritic intercalations (sandy-loam), thus allowing the welding of horizons lying to the top and bottom of the disappeared one.

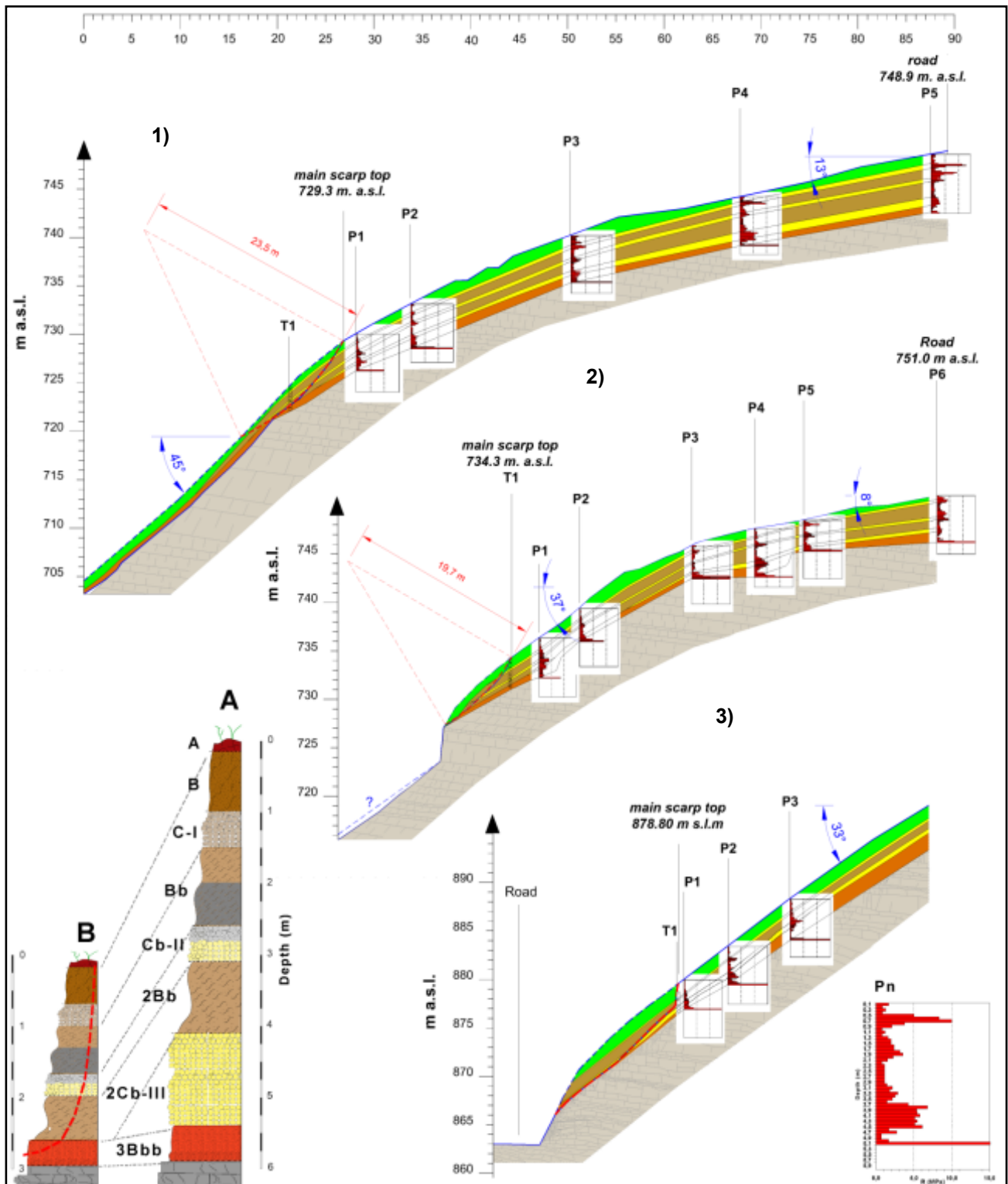


Figure 4.24: synthesis of engineering geological models of the initial debris slides (Landslide 1, 2 and 3 from the top) and stratigraphic columns representative, for Landslide 1 and 2, of the lower slope angle zone in the upper slope (A) and of the landslide main scarps in lower slope zone (B). Red dashed curve represents sliding surfaces and in bottom right is a zoomed dynamic penetrometric log (Pn).

4.5 Distribution of ash-fall pyroclastic soils on slopes in the study areas

In order to verify the existence of a relationship between ash-fall pyroclastic soil thickness and slope angle, real thickness data collected during field surveys by means of pits, hand auger drillings and dynamic penetrometric tests were plotted vs the slope angle (Figure 4.25). Such elaboration confirmed a strong relationship between total thickness and slope angle as previously demonstrated (Figure 1.13).. In fact, the total thickness of pyroclastic mantle corresponds approximately to the maximum theoretical fallen in the area only for slope angles less than 30°, while for higher values the thickness decreases, until values equal to zero for slope angle equal to 50° (De Vita et al., 2006a; 2006b).

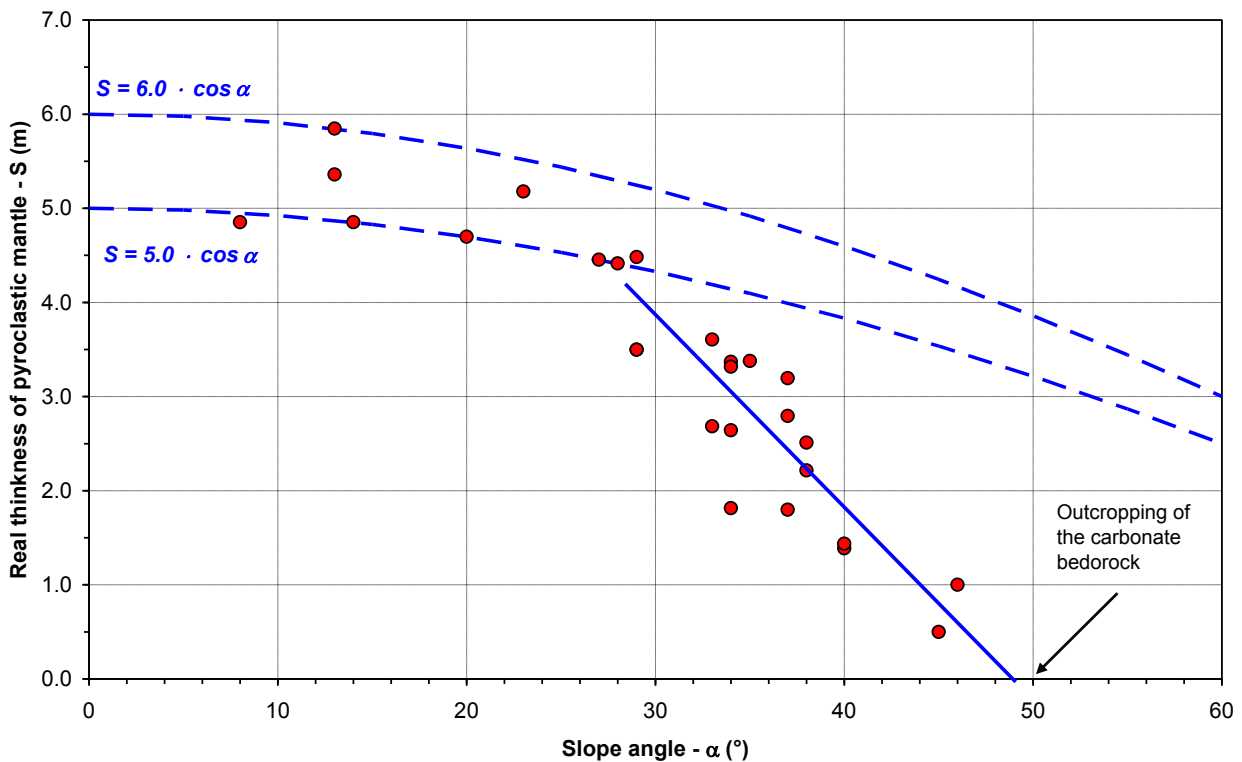


Figure 4.25: distribution of real thickness of pyroclastic mantle vs slope angle. Dashed blue curves represent theoretical distribution of ash-fall pyroclastic soils for a theoretical total thickness ranging from 5.0 to 6.0 m and red dots represent field data.

The correlation of the measured real thickness of pyroclastic mantle with the slope angle (Figure 4.25) shows a good agreement with the general distribution model of ash-fall pyroclastic deposits along slopes.

The analysis of the real thickness of the pyroclastic layers shows a distribution in agreement with the theoretical distribution, reconstructed by means of the algebraic sum of isopach maps of the main Somma-Vesuvius eruptions (Figure 1.12), that predicts a theoretical maximum total thickness of the pyroclastic mantle ranging from 5 m to 6 m (Figure 4.26).

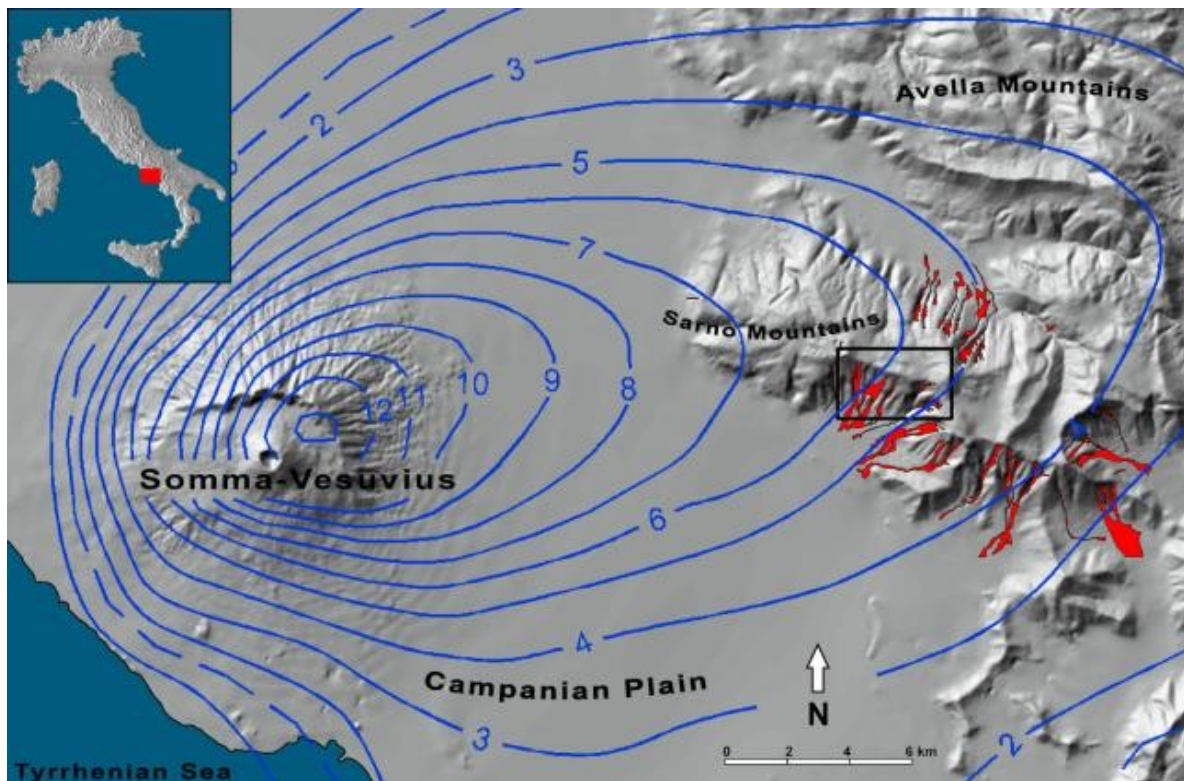


Figure 4.26: total ash-fall isopach map of area surrounding Somma- Vesuvius (De Vita et al., 2006a). The black rectangle represents the study area (De Vita et al., 2006)

4.5 Distribution of ash-fall pyroclastic soils on slopes in the study areas

| Table 4.2: sampling depth, organic matter, specific weight of soil horizons object of study | | | | | |
|---|-----------|------|--------|-----------------------|----------------|
| Horizon ID | Eruption | top | bottom | Gs | Organic matter |
| | | (cm) | (cm) | (gr/cm ³) | (%) |
| B | | 10 | 45 | - | - |
| B | | 10 | 45 | - | - |
| B | | 10 | 110 | 2.45 | 4.75 |
| B | | 10 | 110 | - | - |
| B | | 10 | 110 | - | - |
| B | | 10 | 110 | - | - |
| B | | 10 | 110 | - | - |
| B | | 10 | 110 | - | - |
| B | | 10 | 110 | - | - |
| B | | 10 | 110 | - | - |
| C | 472 A.C. | 130 | 150 | 2.73 | 1.10 |
| C | 472 A.C. | 100 | 160 | - | - |
| C | 472 A.C. | 130 | 150 | - | - |
| C | 472 A.C. | 130 | 150 | - | - |
| C | 472 A.C. | 130 | 150 | - | - |
| C | 472 A.C. | 130 | 150 | - | - |
| C | 472 A.C. | 130 | 150 | - | - |
| C | 472 A.C. | 130 | 150 | - | - |
| Bb | | 130 | 210 | 2.60 | 2.74 |
| Bb | | 130 | 210 | - | - |
| Bb | | 130 | 210 | - | - |
| Bb | | 130 | 210 | - | - |
| Bb | | 130 | 210 | - | - |
| Bb | | 130 | 210 | - | - |
| Bb | | 130 | 210 | - | - |
| Bb | | 70 | 140 | - | - |
| Bb | | 70 | 140 | - | - |
| Bb | | 70 | 140 | - | - |
| Cb | | 140 | 160 | - | - |
| Cb | Avellino | 210 | 290 | 2.36 | 2.88 |
| Cb | Avellino | 210 | 290 | - | - |
| Cb | Avellino | 210 | 290 | - | - |
| Cb | Avellino | 210 | 290 | - | - |
| Cb | Avellino | 210 | 290 | - | - |
| Cb | Avellino | 210 | 290 | - | - |
| Bb | | 70 | 140 | - | - |
| Bbbasal | | 185 | 220 | 2.39 | 8.05 |
| Bbbasal | | 185 | 220 | - | - |
| Bbbasal | | 185 | 220 | - | - |
| Bbbasal | | 185 | 220 | - | - |
| Bbbasal | | 185 | 220 | - | - |
| Bbbasal | | 185 | 220 | - | - |
| Bbbasal | | 185 | 220 | - | - |
| Cbbasal | Ottaviano | - | - | - | - |
| B | | 10 | 90 | 2.43 | 3.84 |
| B | | 10 | 90 | 2.43 | 4.25 |
| Bb | | 110 | 190 | 2.55 | 7.54 |
| Bb | | 110 | 190 | 2.55 | 7.17 |
| Bbbasal | | 210 | 290 | 2.38 | 6.40 |
| Bbbasal | | 210 | 290 | 2.38 | - |
| B | | 10 | 90 | 2.43 | - |
| Bb | | 110 | 190 | 2.55 | - |

4.5 Distribution of ash-fall pyroclastic soils on slopes in the study areas

| Table 4.3: Laboratory characterization of soil horizons | | | | | | | | | | | | |
|---|----------------------|----------------------|--------|--------------------|--------------------|--------|-------|--|--|--|---------|-------|
| Horizon ID | d ₁₀ (mm) | d ₆₀ (mm) | U | w _L (%) | w _p (%) | IP (%) | USCS | γ _{dry} (gr/cm ³) | γ _{nat} (gr/cm ³) | γ _{sat} (gr/cm ³) | e (ad.) | n (%) |
| B | 0.004 | 0.11 | 27.5 | 33.35 | 33.08 | 0.27 | SM | 1.123 | 1.347 | 1.664 | 1.179 | 54.2 |
| B | 0.006 | 0.092 | 15.33 | 34.19 | 33.35 | 0.84 | SM | 1.313 | 1.684 | 1.766 | 0.870 | 46.4 |
| B | 0.009 | 0.11 | 12.22 | 50.24 | 46.67 | 7.57 | SW-SM | - | - | - | - | - |
| B | - | - | - | - | - | - | - | 0.967 | 1.128 | 1.572 | 1.53 | 60.53 |
| B | - | - | - | - | - | - | - | 1.053 | 1.247 | 1.623 | 1.33 | 57.02 |
| B | - | - | - | - | - | - | - | 1.081 | 1.273 | 1.64 | 1.27 | 55.88 |
| B | - | - | - | - | - | - | - | 1.055 | 1.257 | 1.624 | 1.32 | 56.94 |
| B | - | - | - | - | - | - | - | 1.031 | 1.219 | 1.61 | 1.38 | 57.92 |
| B | - | - | - | - | - | - | - | 0.982 | 1.201 | 1.581 | 1.49 | 59.92 |
| B | 0.083 | 0.61 | 7.35 | 39.19 | 36.26 | 2.93 | GW | - | - | - | - | - |
| C | 0.006 | 0.33 | 55 | 29.23 | 29.00 | 0.22 | SW-SM | 1.213 | 1.489 | 1.769 | 1.250 | 55.56 |
| C | - | - | - | - | - | - | - | 1.050 | 1.100 | 1.666 | 1.600 | 61.52 |
| C | - | - | - | - | - | - | - | 0.998 | 1.050 | 1.632 | 1.740 | 63.44 |
| C | - | - | - | - | - | - | - | 1.130 | 1.200 | 1.718 | 1.410 | 58.48 |
| C | - | - | - | - | - | - | - | 0.947 | 0.810 | 1.6 | 1.880 | 65.31 |
| C | - | - | - | - | - | - | - | 1.580 | 1.656 | 2 | 0.730 | 45.20 |
| C | - | - | - | - | - | - | - | 1.130 | 1.200 | 1.714 | 1.420 | 58.75 |
| C | 0.0017 | 0.072 | 42.35 | 35.38 | 34.96 | 0.42 | SM | - | - | - | - | - |
| Bb | - | - | - | - | - | - | - | 1.019 | 1.121 | 1.627 | 1.550 | 60.80 |
| Bb | - | - | - | - | - | - | - | 1.074 | 1.187 | 1.661 | 1.42 | 58.70 |
| Bb | - | - | - | - | - | - | - | 1.053 | 1.153 | 1.648 | 1.47 | 59.50 |
| Bb | - | - | - | - | - | - | - | 1.003 | 1.093 | 1.617 | 1.59 | 61.43 |
| Bb | - | - | - | - | - | - | - | 1.137 | 1.250 | 1.70 | 1.29 | 56.27 |
| Bb | - | - | - | - | - | - | - | 1.084 | 1.187 | 1.667 | 1.40 | 58.30 |
| Bb | 0.002 | 0.065 | 32.5 | - | - | - | SM | 1.099 | 1.532 | 1.676 | 1.37 | 57.73 |
| Bb | 0.0011 | 0.0052 | 4.73 | 29.95 | 30.37 | -0.042 | SP-SM | 1.491 | 1.915 | 1.917 | 0.74 | 42.65 |
| Bb | 0.0018 | 0.11 | 61.11 | 26.34 | 27.16 | -0.82 | SM | 1.474 | 1.903 | 1.909 | 0.76 | 43.31 |
| Bb | 0.0074 | 0.22 | 29.73 | 53.5 | 46.16 | 7.34 | SW-SM | 0.971 | 1.375 | 1.560 | 1.43 | 58.86 |
| Cb | 0.02 | 0.21 | 11.67 | 47.97 | 42.41 | 5.56 | SW-SM | - | - | - | - | - |
| Cb | - | - | - | - | - | - | - | 0.546 | 0.706 | 1.315 | 3.32 | 76.86 |
| Cb | - | - | - | - | - | - | - | 0.644 | 0.816 | 1.371 | 2.66 | 72.70 |
| Cb | - | - | - | - | - | - | - | 0.575 | 0.768 | 1.331 | 3.1 | 75.64 |
| Cb | - | - | - | - | - | - | - | 0.493 | 0.643 | 1.284 | 3.79 | 79.11 |
| Cb | - | - | - | - | - | - | - | 0.626 | 0.82 | 1.361 | 2.77 | 73.47 |
| Cb | - | - | - | - | - | - | - | 0.682 | 0.883 | 1.393 | 2.46 | 71.10 |
| Cb | 0.00075 | 0.034 | 45.33 | 50.37 | 45.46 | 4.91 | SM | 1.007 | 1.584 | 1.586 | 1.37 | 57.9 |
| Bb | 0.00081 | 0.022 | 27.16 | 67.66 | 52.72 | 14.94 | SM | - | - | - | - | - |
| Bbbasal | - | - | - | - | - | - | - | 0.681 | 0.995 | 1.418 | 2.8 | 73.71 |
| Bbbasal | - | - | - | - | - | - | - | 0.653 | 0.949 | 1.401 | 2.97 | 74.79 |
| Bbbasal | - | - | - | - | - | - | - | 0.651 | 0.937 | 1.4 | 2.98 | 74.86 |
| Bbbasal | - | - | - | - | - | - | - | 0.631 | 0.907 | 1.387 | 3.1 | 75.64 |
| Bbbasal | - | - | - | - | - | - | - | 0.704 | 1.022 | 1.432 | 2.68 | 72.82 |
| Bbbasal | - | - | - | - | - | - | - | 0.672 | 0.887 | 1.413 | 2.85 | 74.05 |
| Bbbasal | 0.0013 | 0.14 | 107.69 | 55.04 | 50.01 | 5.03 | SM | 1.152 | 1.376 | 1.664 | 1.05 | 51.2 |
| Cbbasal | 0.0075 | 0.12 | 16 | 47.61 | 42.37 | 5.24 | SW | 1 | 1.123 | 1.588 | 1.427 | 58.8 |
| B | 0.003 | 0.09 | 29.33 | 59.27 | 48.28 | 10.99 | SM-SC | 0.812 | 0.991 | 1.493 | 2.137 | 68.1 |
| B | - | - | - | - | - | - | - | 0.691 | 0.904 | 1.420 | 2.688 | 72.9 |
| Bb | 0.0014 | 0.034 | 24.29 | 69.23 | 55.65 | 13.58 | SM | 0.699 | 0.836 | 1.405 | 2.400 | 70.6 |
| Bb | - | - | - | - | - | - | - | 0.687 | 1.106 | 1.398 | 2.464 | 71.1 |
| Bbbasal | 0.0053 | 0.11 | 20.755 | - | - | - | SM | - | - | - | - | - |
| Bbbasal | 0.002 | 0.06 | 25.306 | - | - | - | SC | - | - | - | - | - |
| B | 0.0008 | 0.03 | 37.5 | - | - | - | SM-SC | - | - | - | - | - |

Chapter 5

Hydrological modeling and slope stability analysis: results

The distribution of ash-fall pyroclastic soils along mountain slopes surrounding Somma-Vesuvius and the detailed reconstruction of engineering geological models of initial landslides in three representative areas constituted the basis for hydrological and stability modelling of slopes. This singular approach to the issue of shallow landslide susceptibility in ash-fall pyroclastic deposits distinguishes this research from those known in literature. Further analysis and insights were obtained through the finite elements modeling of unsaturated / saturated flow and the consequent slope stability modeling in such representative models.

Starting from the engineering geological model and the experimental results of laboratory tests, concerning both physical, hydraulic and mechanical properties of pyroclastic soils, it was possible to develop a further step of the doctorate's research at the "Landslide Hazard Program" of the USGS in Golden (Colorado, USA) in collaboration with Dr. Rex Baum and Dr. Jonathan Godt. This step concerned data processing and their implementation in a numerical model of unsaturated/saturated seepage flow within the pyroclastic cover, coupled with a stability model. The hydrological-mechanical stability coupling allowed to find out estimations about both threshold values/patterns of rainfall events.

5.1 Hydrological modelling of the initial landslides through VS2DTI

The hydrological modeling of physical models of initial landslides was applied to a well known case of a layered medium characterized by alternating fine-grained with coarse grained horizons (from silt to gravel) and with different hydraulic conductivity along the vertical.

Infiltration into a non horizontal layered medium is a complicated process. If a thin surface layer of fine grained materials overlies a coarser grained layer, the infiltrated water will initially be retained above the interface between the layers. This process occurs because the water at the wetting front is subject to a pressure head which is too low to enter the large openings constituting the pore spaces of the coarse layers, resulting in both head and saturation buildup above the interface. Following, the potential gradient may become too small to maintain infiltration at the

applied rate, and ponding may occur. Once flow starts within the coarser layer, the pressure head above the interface declines, and the infiltration rate increases (Lappala et al., 1987). Thus the ponding process is still governed by either specified flux or a specified pressure potential, but it is possible for the specified pressure-potential boundary condition to revert to one of specified flux.

In order to understand the above mentioned phenomena, typically occurring in a multilayered system, such that existing in the pyroclastic mantle covering peri-vesuvian hillslopes, a two-dimensional modeling of unsaturated/saturated flow was performed. Starting from the known geometry and the stratigraphy of pyroclastic cover-carbonate bedrock system, it was possible to clarify the sub-surface flow processes taking place within the multilayered sequence of Pizzo D'Alvano massif. It was taken into account three main cases study, whose results are at the base of the following slope stability analysis that are discussed in section 5.2. From this type of modeling it was possible to comprehend pore pressure distribution in the initiation areas and consequently to model the stability of pyroclastic mantle, being known shear strength of pyroclastic soils. It was performed a two-dimensional modeling of unsaturated/saturated flow, taking into account the three cases study.

On the basis of the reconstruction of the engineering-geological models for three case study, the domain was defined by means of AutoCad profiles regarding each landslide, and stratigraphical relationships between horizons forming pyroclastic cover and carbonate bedrock as well were defined.

The geometries of the considered cases were set up in VS2DTI (Figures 5.3 - 5.5). Afterwards it was set as input data the hydraulic properties accounting for each pyroclastic horizon whose values were chosen among available experimental data, achieved from elaboration of field and laboratory tests. These were run by means of RETC (van Genuchten et al., 1991), a specific software for the optimization and fitting of theoretical models with experimental results by a trial and error procedure.

Specifically, RETC (van Genuchten et al., 1991) is a computer program able to analyze soil water retention and hydraulic conductivity functions of unsaturated soils. These hydraulic properties are key parameters in any quantitative description of water flow into and through the unsaturated zone of soils. The program allows to select one of the following parametric models:

1. Brooks-Corey (1964);
2. van Genuchten (1980).

The model chosen in the analysis was the VG model (van Genuchten, 1980).

After testing the sensitivity of the computer program VS2DTI, by running experimental data in RETC (Table 5.1), the results were fitted by trial and error with VG theoretical curves, and hydraulic conductivity functions for each horizon were determined (Figure 5.1).

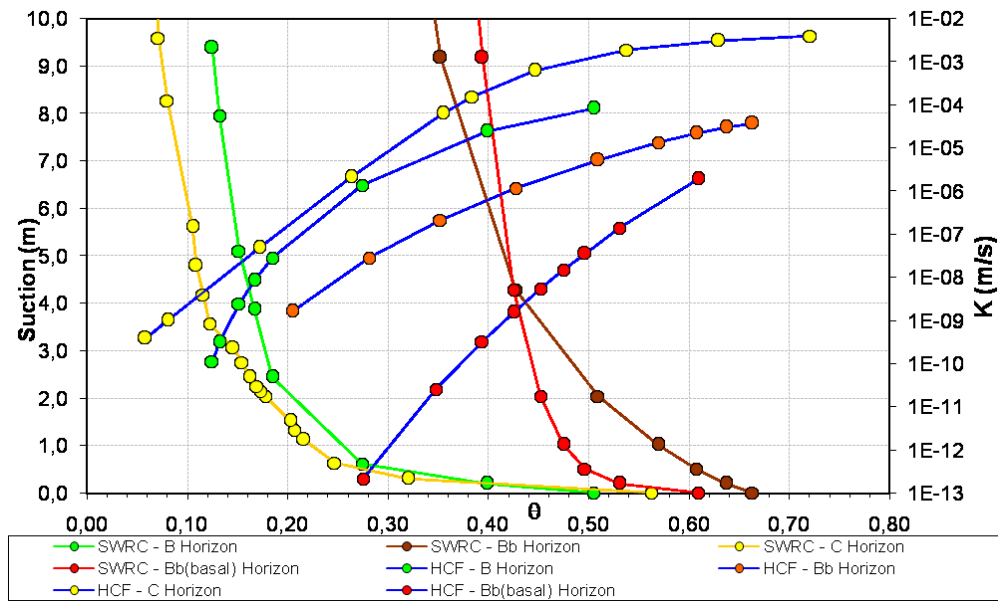


Figure 5.1 soil water retention curves and hydraulic conductivity functions determined for each horizon.

The hydraulic parameters tested with RETC, set as input data in VS2DTI are shown in the following Table:

| Horizons ID | B | C | Bb | Bb _{basal} | Fractured Bedrock n = 2% filled by Bb _{basal} |
|----------------------------------|----------|----------|----------|---------------------|--|
| K _{zz} /K _{hh} | 1 | 1 | 1 | 1 | 10 |
| K _{sat} (m/s) | 1.26E-04 | 1.08E-02 | 2.64E-05 | 6.84E-06 | 1.37E-07 |
| S _s | 0.05 | 0.10 | 0.06 | 0.07 | 0.14 |
| θ _s (ad.) | 0.500 | 0.560 | 0.590 | 0.630 | 0.030 |
| θ _r (ad.) | 0.080 | 0.001 | 0.200 | 0.001 | 0.020 |
| α _{RETC} | 5.600 | 4.200 | 0.730 | 7.200 | 4.310 |
| n _{RETC} | 1.570 | 1.430 | 1.320 | 1.110 | 3.100 |

Table 5.1: tested hydraulic parameters for each horizon.

Given the reconstructed geometries of pyroclastic soil horizons, topographic surface was set as a boundary condition of entering vertical flow, corresponding to infiltration with constant intensity values that were chosen for each landslide respectively to 5 mm/h, 10 mm/h and 20 mm/h. Taking into account porosity of the carbonate rock mass due to prevailing vertical fracturing as approximately correspondent to 2%, and the constant filling of discontinuity sets with soil belonging to Bb_{basal} horizon, carbonate bedrock was considered as characterized by a porosity and a vertical hydraulic conductivity (K_z) set to 2% of the basal paleosol (Table 5.1). Horizontal hydraulic conductivity (K_h) was considered ten times lower. The bedrock was modeled with the abovementioned hydraulic characteristics, considering it with a thickness of about 5 m and setting it with a free seepage lower boundary condition for simulating open fractures and free percolation to the basal groundwater body. A seepage boundary condition was also set at downstream face. Initial hydrological conditions were set not considering the existence of a groundwater table but a distribution of unsaturated pore pressure within pyroclastic soil horizons derived from the modeling, by means of the software SEEP (Geoslope Corp.) of a steady state infiltration rate of 0.1 mm/h. The obtained results showed a distribution of pore pressure values ranging from -5 to -15 kPa that is in good agreement with typical hydrological conditions of pyroclastic mantle during late Winter and early Spring (Bilotta et al., 2005; Sorbino, 2005).

On the basis of experimental data, initial conditions were included by setting isobars within each horizon constituting the pyroclastic mantle, and boundary conditions for each case study, testing different conditions of pyroclastic cover when subjected to rainfalls, from ordinary to extreme (namely, hydrological events with different return time). This choice arises from the need of identifying elements represented by experimental points that might indicate hydrological threshold suitable for the Pizzo D'Alvano area, congruent with those existing in scientific literature, on the basis of patterns of rainfall events and the inherent probability of initial landslide triggering.

For each landslide four types of rainfall events from low to extreme were assumed, considering intensity/duration conditions derived from the empirical hydrological threshold proposed by Guadagno (1991) for the initiation of debris flows in pyroclastic soils. From this empirical threshold, constant rain rates were chosen: 5 mm/h, 10 mm/h, 20 mm/h, 40 mm/h; with duration of 192 hours, 96 hours, 48 hours, and 48 hours respectively (Figures 5.2, 5.3, 5.4). Physical models were discretized in VS2DTI with a very fine mesh, constituted of square cells with side of 0.1 m. At the end it was set a series of observation points in correspondence of sliding surfaces of each landslide, previously identified by means of topographic surveys, in order to have accurate monitoring of pore pressure distribution.

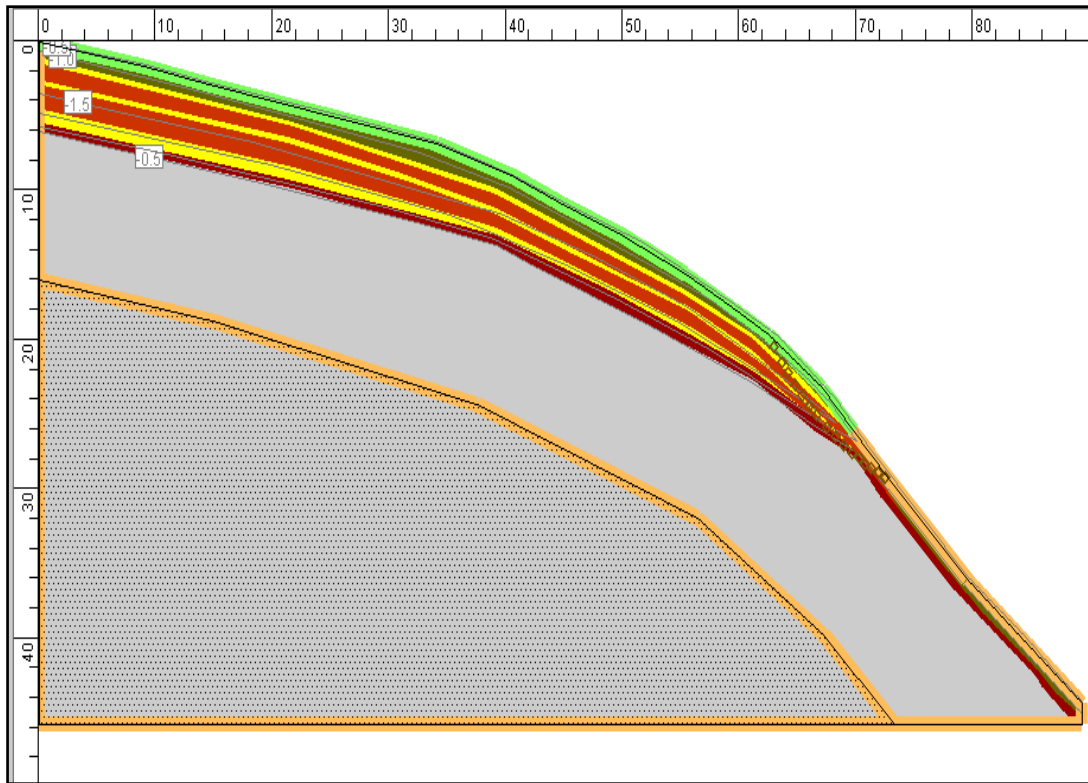


Figure 5.2: Landslide 1: domain, geometry of the pyroclastic soil- carbonate bedrock system. Initial pressure head (whose values are indicated in the white boxes); boundary conditions: green represents infiltration that is equal to rain rate, orange is possible seepage faces. Brown circles represent the location of the observation points on sliding surface.

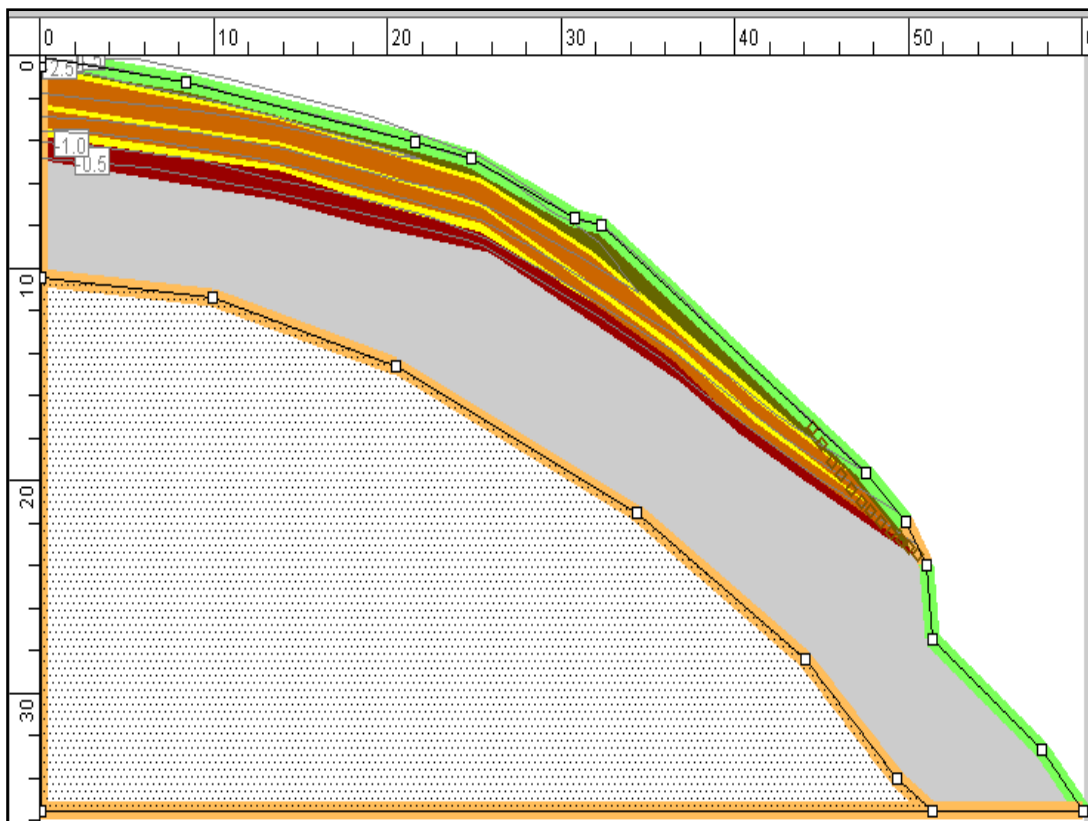


Figure 5.3: Landslide 2: domain, geometry of the pyroclastic soil-carbonate bedrock system. Initial pressure head (whose values are indicated in the white boxes); boundary conditions: green represents infiltration that is equal to rain rate, orange is possible seepage faces. Brown circles represent the location of the observation points on sliding surface.

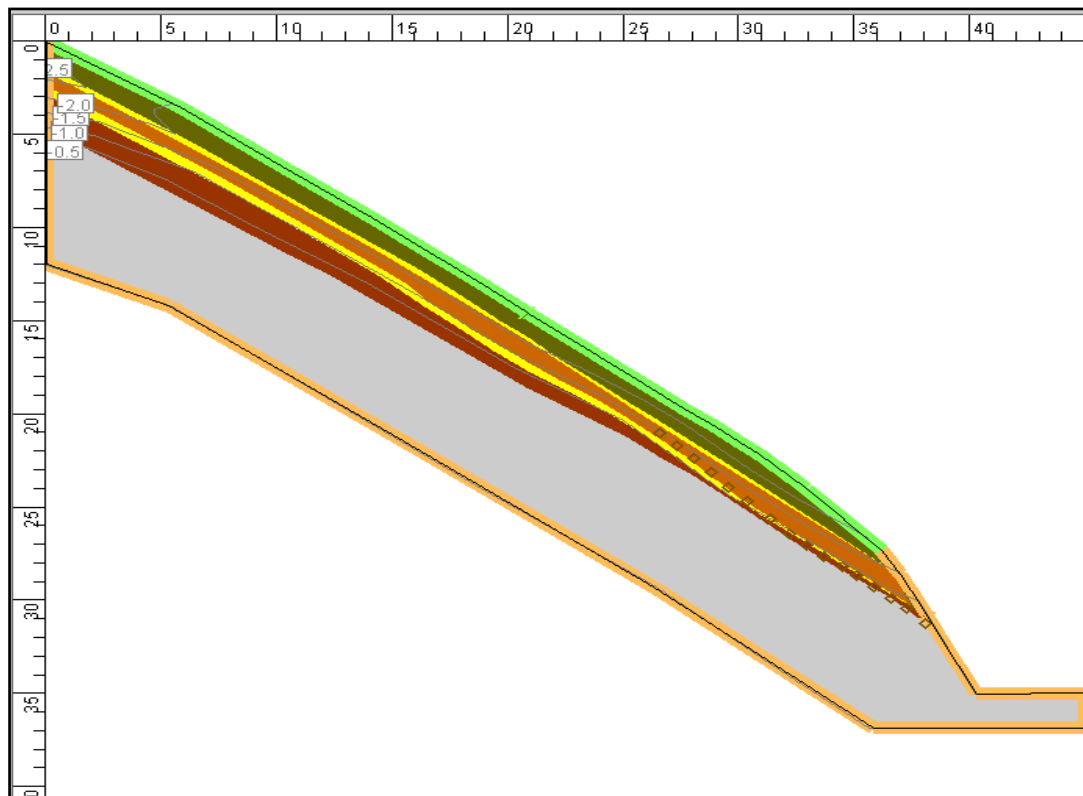


Figure 5.4: Landslide 3: domain, geometry of the pyroclastic soil- carbonate bedrock system. Initial pressure head (whose values are indicated in the white boxes); boundary conditions: green represents infiltration that is equal to rain rate, orange is possible seepage faces. Brown circles represent the location of the observation points on sliding surface.

5.1.2 Results of hydrological modeling

After running VS2DTI, data from output files were obtained by means of the postprocessor VS2DTPOST. One of the advantages of this software consists in the ability to manage the huge quantity of output data, such as by means of an Excel[®]. This allowed to make these data available for the final step of the research, that is the stability analysis. Results were elaborated and they involved pore pressure distribution and water content for each of the applied rain rates. Results clearly indicated concentration of water in correspondence of failure surfaces for each case study.

The results of the modeling may be explained stating that the unsaturated flow that first establishes within the higher hydraulic conductivity layers, becomes saturated and concentrates in where the pumice levels pinch out. This would cause an increase in pore pressure and might be responsible of landslide initiation.

In fact, the highest pore pressures were observed in correspondence and above the sliding surfaces, within the horizons involved in the detachment zone. These , according to the engineering-

geological model, are positioned within the basal buried paleosol above the limestone bedrock. An example for each landslide is shown below (Figures 5.5 - 5.7), when saturation is reached and failure occurs for an applied rain rate of 5 mm/h.

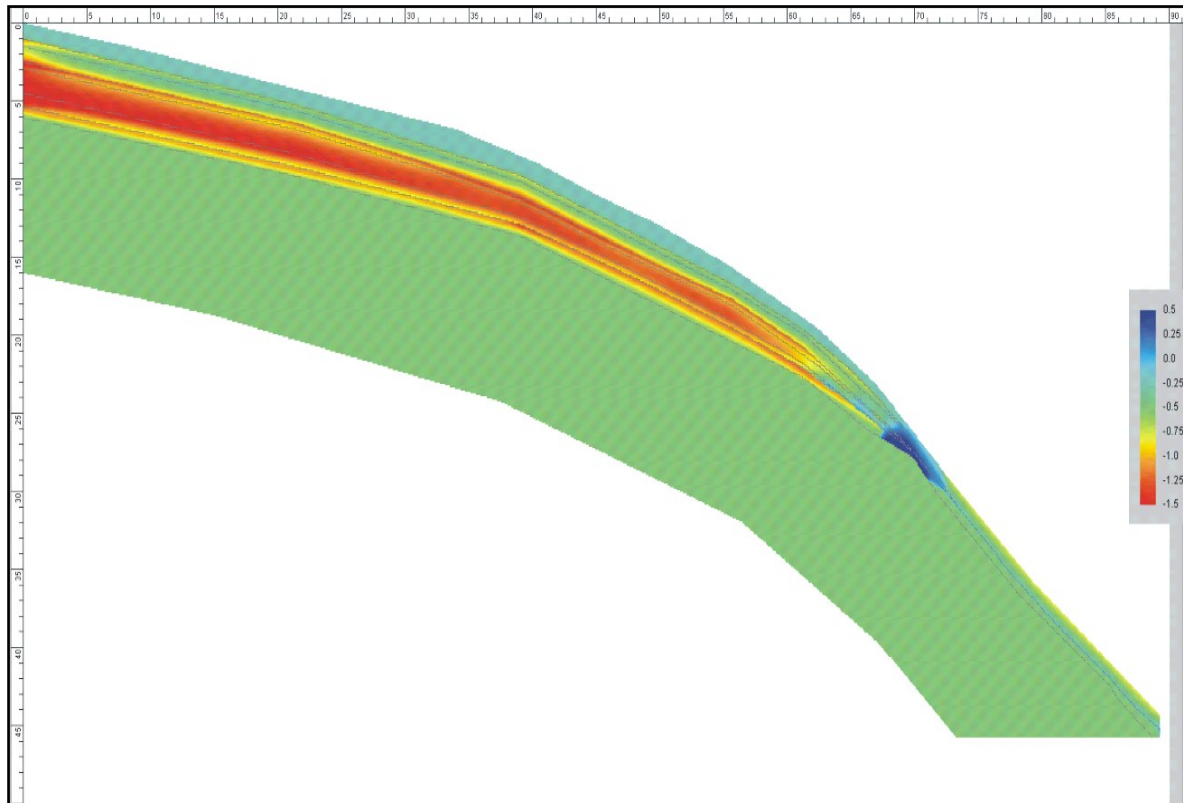


Figure 5.5: pressure head values (P) at failure time in the case of applied rain rate of 5 mm/h for landslide 1

It is important to highlight that the effect of concentration of the unsaturated flow is more clearly observed with the intensity of 5 mm/h but it is also present, although less visible, even with other rainfall intensity (10 mm/h, 20 mm/h, 40 mm/h). In particular, for higher rainfall intensities, a greater increase in pore pressures in the superficial horizons than in deeper layers can be observed.

As is shown in figure 5.5, it is possible to observe that, for landslide 1, the unsaturated flow moves from shallowest to deepest horizons and concentrates up to pore pressure values greater than 0, where gravelly pumiceous lapilli (C horizons) pinches out, that is in this case, in correspondence of abrupt natural increase of slope angle.

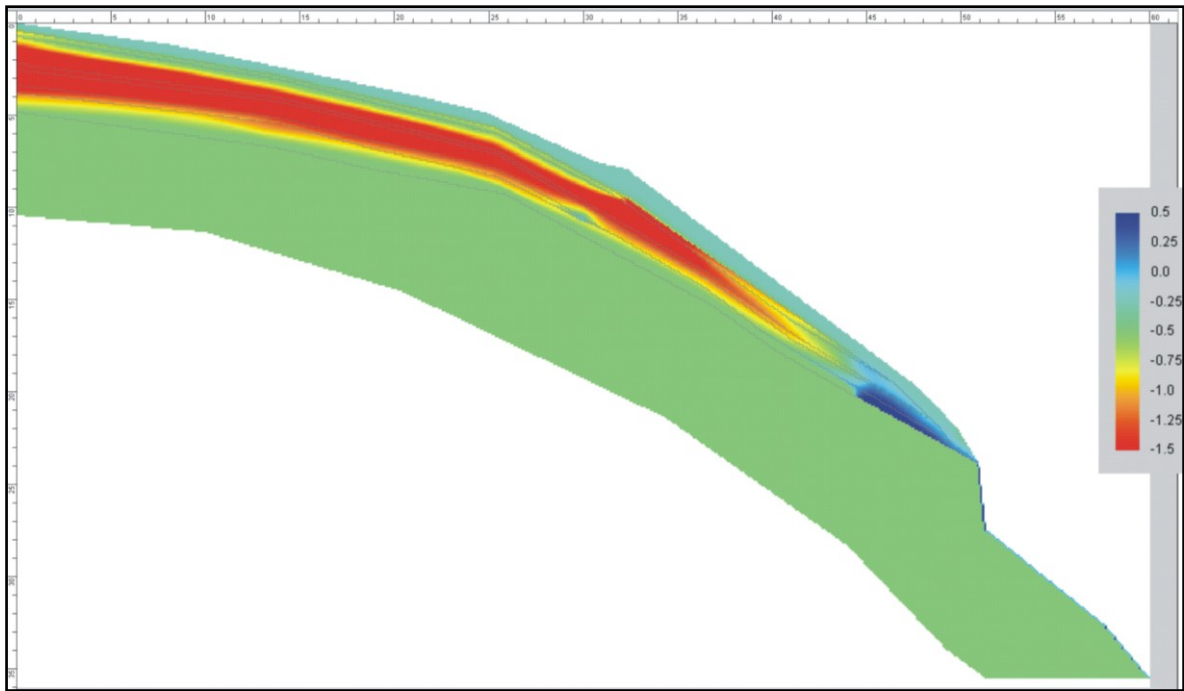


Figure 5.6: pressure head values (P) at failure time in the case of applied rain rate of 5 mm/h for landslide 2.

In the case of Landslide 2 (Figure 5.6) it is possible to state that, after reaching saturation at failure time step, the saturated flow concentrates in correspondence of the thinning and consequent pinch out of the pumice layer, in correspondence of morphological discontinuity.

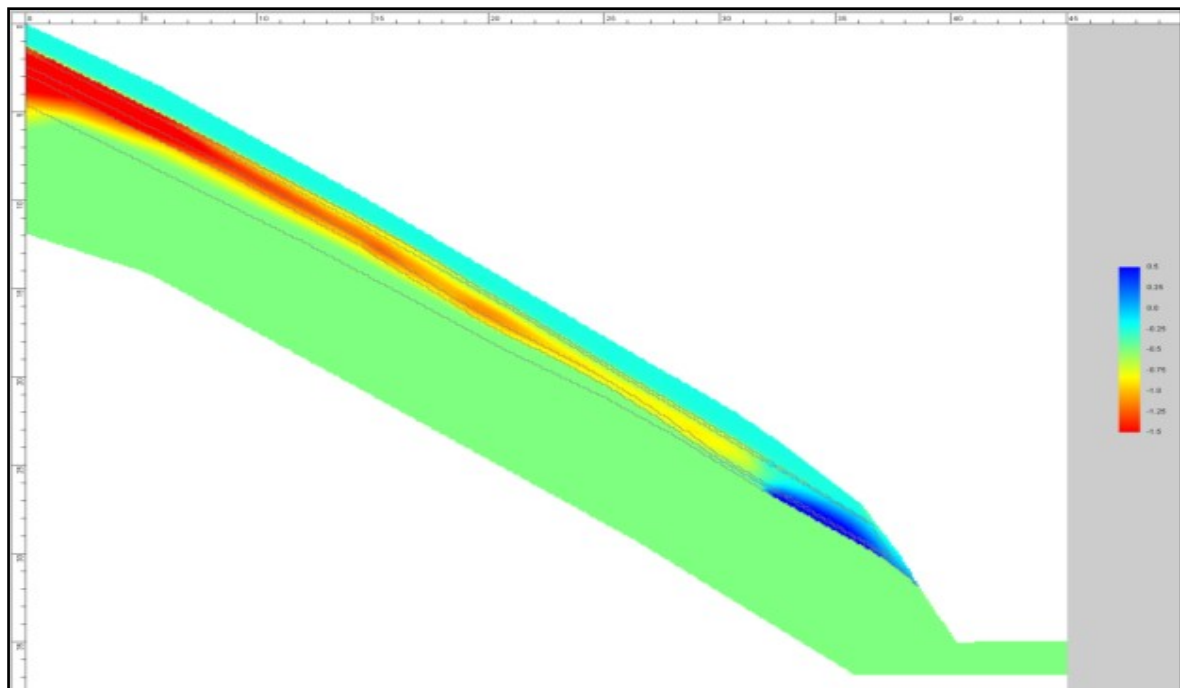


Figure 5.7: pressure head (P) values at failure time in the case of applied rain rate of 5 mm/h for landslide 3.

A similar phenomenon takes place also for landslide 3 (Figure 5.7), where at failure time step, after reaching saturation there is a saturated water flow whose front reaches the lower buried paleosol, where detachment occurs. Also in this case, the flow is concentrated behind the free-to-air face, that is the man-made cut, which constitutes a capillary barrier (Basile et al., 2003).

5.2 Stability modeling of initial landslides

On the basis of the hydrological modeling results, the stability modeling of initial landslides was performed. It was based on physical and mechanical properties of the pyroclastic soil horizons and on the geometrical reconstruction of the initial sliding surface. Particularly, VS2DTI allowed the creation of detailed numerical output files of pressure head (P), water content (θ) and degree of saturation (S), for each rainfall intensity condition assumed, and for each time step and observation point. These data were employed in the stability analysis, which are discussed in detail in this section.

The detailed reconstruction of the sliding surfaces of the initial landslides allowed to recognize their discrete geometry. In particular, a shape for Landslides 1 and 2, and a complex shape, for Landslide 3 were assumed. On the basis of a such observation, stability analyses were carried out by means of finite slope methods.

5.3. Setting of the hydro-mechanical model

Results from hydrological modelling, coupled with the mechanical parameters analysis of the pyroclastic mantle covering Pizzo D'Alvano massif, were used to formulate a hydro-mechanical model, whose main steps are summarized in the flux chart shown in figure 5.14 (at the end of this chapter).

The first step was to divide the body of each landslide into a series of slices identified on the basis of the soil homogeneity, crossed by the sliding surfaces and discretized by approximating the circular arc to a number of linear segments (Figure 5.8a, 5.8b, 5.8c): 12 for Landslide 2; 16 for both Landslide 1 and Landslide 3. Such a discretization allowed to perform calculations with the Modified (or Simplified) Bishop's Method (1955).

An observation point was set at the base of each slice in VS2DTI. After running the program, three numerical output files, concerning the three hydrological variables (water content (θ), pressure head (P) and degree of saturation (S)) monitored for each observation point during the simulations, were obtained.

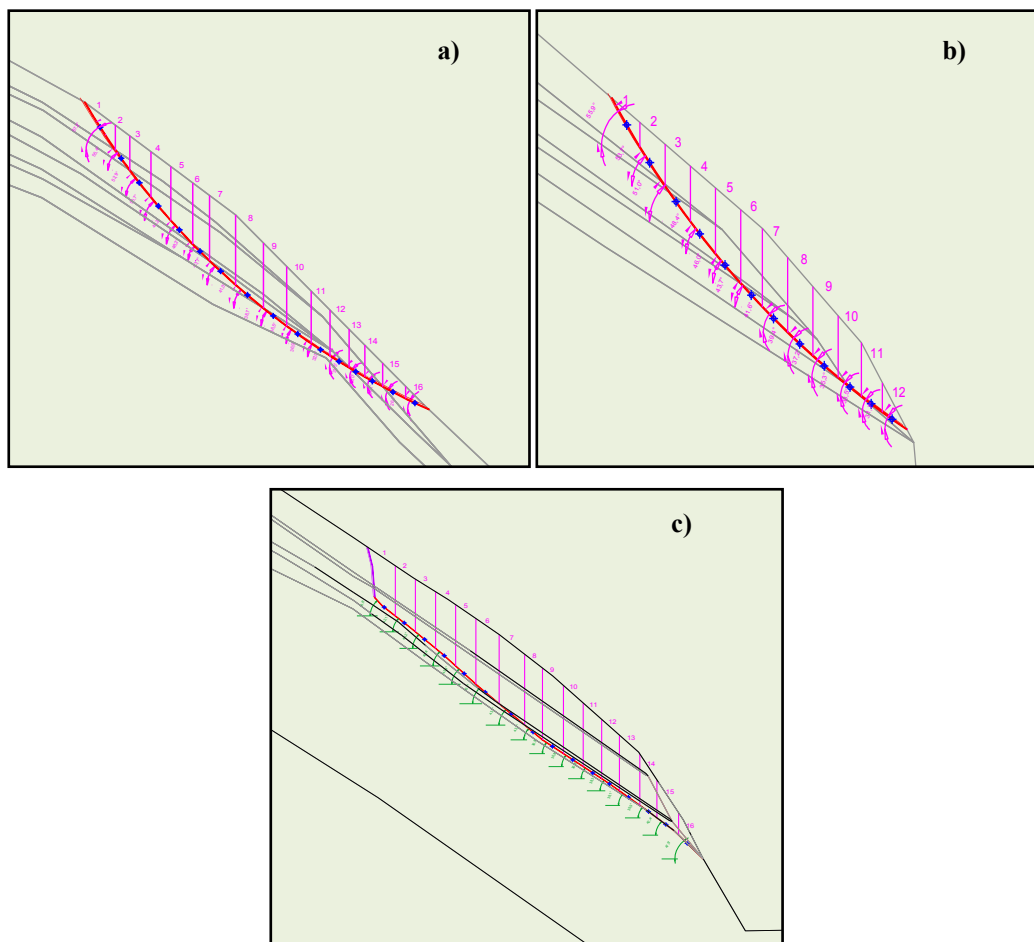


Figure 5.8: generalized method of slice applied to the three landslides case study: landslide 1 (a); landslide 2(b); landslide 3 (c).

For each slice, the sectional area, the length of the sliding surface, and the value of the angle that the slice forms with horizontal (α) were measured by means of AutoCAD. In such operation, the type of soil horizon crossed by the sliding surface was recorded.

According to the wide range of variability of physical and mechanical properties as well as of the hydraulic parameters, which characterize pyroclastic soil horizons, a sensitivity approach was adopted. As regards the hydraulic conductivity, values of K_{sat} corresponding to 25% and 75% percentiles were assumed (Table 5.2). Considering the high variability of effective friction angle (ϕ') due to the dilatancy effect and crashing of coarse pyroclasts, we considered the 50% percentile. Instead percentiles of 5% and 10% were considered for effective cohesion (c') in order to avoid the effect of intercept cohesion due to the crashing of pumiceous pyroclasts (Table 5.3). In both cases we obtained values similar to those used in other stability analyses (Cascini et al., 2005; Bilotta et al., 2005).

| Horizon ID | B | Bb | C | Bb _{basal} |
|----------------------------|-------------------------|-------------------------|-------------------------|-------------------------|
| K _{sat} 25% (m/s) | 4.82 × 10 ⁻⁵ | 6.00 × 10 ⁻⁶ | 2.82 × 10 ⁻³ | 2.48 × 10 ⁻⁷ |
| K _{sat} 75% (m/s) | 1.26 × 10 ⁻⁴ | 2.64 × 10 ⁻⁵ | 1.26 × 10 ⁻² | 6.84 × 10 ⁻⁶ |

Table 5.2: K_{sat} values utilised for VS2DI modelling.

| Horizon ID | B | Bb | C | Bb _{basal} |
|------------------------|-----|-----|-----|---------------------|
| φ _{50%} (°) | 32 | 34 | 37 | 35 |
| c _{25%} (kPa) | 4.5 | 1.8 | 0.0 | 8.1 |
| c _{75%} (kPa) | 5.0 | 3.4 | 0.0 | 8.2 |

Table 5.3: values of mechanical parameters utilised for stability modelling.

Driving forces were computed with a variable unit weight (γ) of pyroclastic soil horizons depending on water content (θ). The following formula was applied to VS2DTI numerical output.

$$\gamma = \left[\gamma_{\text{dry}} \left(1 + \frac{\theta}{\gamma_{\text{dry}}} \right) \right]$$

The contribution to the increase in shear strength due to unsaturated conditions (τ_u) was estimated by adopting the unified effective stress criterion for saturated and unsaturated conditions (Lu and Likos, 2006; Godt et al., 2009). It considers the effect of changes in soil suction and water content during infiltration (Lu and Likos, 2004). The unified effective stress criterion for variably saturated soils is:

$$\sigma' = \sigma - \sigma^s$$

$$\sigma^s = \frac{\theta - \theta_r}{\theta_s - \theta_r} (u_a - u_w) = -\theta_e \cdot (u_a - u_w) = \theta_e \cdot P$$

where u_w is the pore water pressure; u_a is the pore air pressure; θ is the volumetric water content (%); θ_s is the saturated water content; θ_r is the residual volumetric water content; and P the pressure head.

It follows that the increase of shear strength for unsaturated conditions is derived as the extension of the Mohr-Coulomb criterion:

$$\tau_u = P \cdot \theta_e \cdot \tan \varphi'$$

Hydrological modelling by means of VS2DTI allowed to assess, for each time step, the pressure head distribution across 2D models of the three representative landslides. Results from the initial to the failure conditions (Figure 5.9) permitted to appreciate the existence of a prevailing vertical water flow due to infiltration process up to distances greater than 5 m ÷ 10 m from morphological discontinuities (knickpoint, rocky scarp and road cut).

Instead, a concentration of water flow with horizontal component (throughflow *sensu* Kirby, 1978) can be identified at the uphill sector of discontinuities. Here, the total thickness of pyroclastic mantle reduces and C horizons pinch out, or pyroclastic series is abruptly interrupted by a road cut. In such a distance range and in limited zones close to the discontinuities, pumiceous lapilli horizons mainly contribute to water flow, increasing pressure head and water content up to saturation. The sliding surfaces, which are extended upslope beyond saturated zones, cross the sectors with different pressure head values from unsaturated to saturated conditions.

As regards the artificial interruptions of pyroclastic mantle, the open to air road cut behaves as a capillary barrier that causes a localised reduction of hydraulic conductivity and the increase of water content (Kirkby, 1978; Basile et al., 2003).

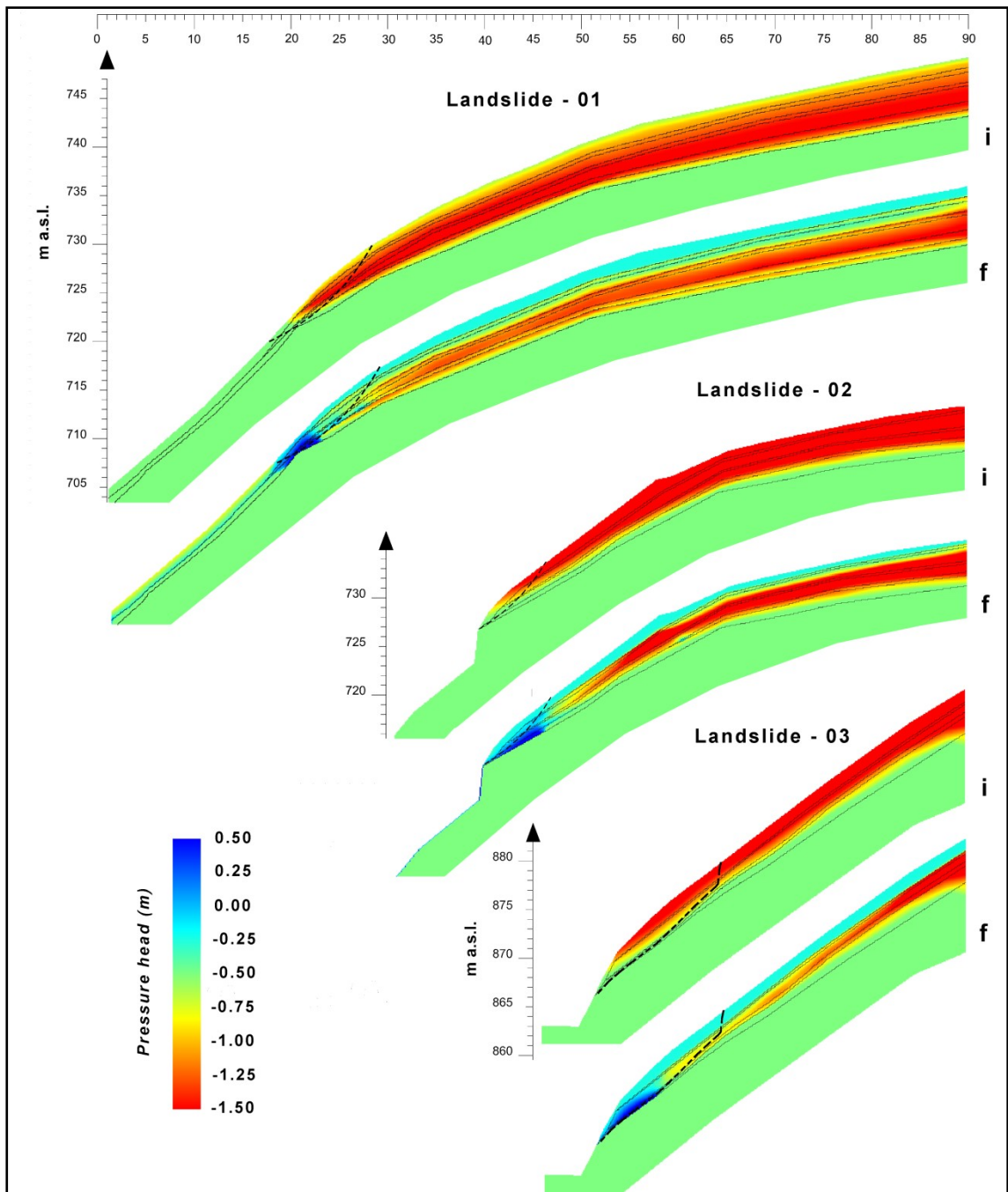


Figure 5.9: distribution of pressure head (P) at initial (i) and failure (f) conditions for landslide 1, 2 and 3. Dashed black lines represent the sliding surfaces.

With the purpose of analysing conditions leading to failure and their changes during the infiltration process, the average pressure head values along sliding surfaces ($P_{average}$) weighted by the area of each slice, were calculated and plotted as function of the Factor of Safety (FOS) versus time. In order to carry out a sensitivity analysis, for each rainfall intensity three different conditions were considered (Figures 5.10, 5.11, 5.12):

- 1) $K_{\text{sat}} = 25\%$ percentile, $c' = 5\%$ percentile and $\phi' = 50\%$ percentile;
- 2) $K_{\text{sat}} = 75\%$ percentile, $c' = 5\%$ percentile and $\phi' = 50\%$ percentile;
- 3) $K_{\text{sat}} = 75\%$ percentile, $c' = 10\%$ percentile and $\phi' = 50\%$ percentile.

Time series of average pressure head along sliding surface and FOS show a nonlinear behaviour with abrupt increases and decreases due to the incoming throughflow, mainly conditioned by the C horizons. Such a hydraulic phenomenon appears stronger and in shorter times from the beginning as much as higher the intensity values of rainfall. Sensitivity analysis highlights that variability of mechanical properties have a stronger influence on time to failure, than variability of hydraulic conductivity.

When observing times to failure (Figure 5.10, 5.11, 5.12) for the lowest condition of hydraulic conductivity and mechanical characteristics ($K_{\text{sat}}=25\%$ percentile, $c'=5\%$ percentile, $\phi'=50\%$ percentile), it is possible to highlight that triggering conditions for the three representative landslides occur with a constant rainfall intensity of 20 mm/h with duration from 18 to 27 hours and a P_{average} from -3.0 to -1.0 kPa. With a constant rainfall intensity of 10 mm/h, failure conditions occur with a duration from 36 to 48 hours and a P_{average} from -1.0 kPa to 0.0 kPa. Finally, with a constant intensity rate of 5 mm/h, failure conditions occur for a duration from 74 to 85 hours and a P_{average} from -1.0 to 0.0 kPa. These results indicate an approximately constant total amount of rainfall of about 400 mm and increase of P_{average} for lower intensity and longer precipitations.

In particular, for Landslide 1 (Figure 5.10), critical conditions for failure occur at a constant rainfall intensity of 20 mm/h, for a duration of 24 hours, and a P_{average} of -0,6 kPa; at a constant rain rate of 10 mm/h for a duration of 41 hours and a P_{average} of -0,4 kPa; at a constant rainfall intensity of 5 mm/h for a duration of 85 hours and a P_{average} of -0,1 kPa.

For Landslide 2 (Figure 5.11) the critical conditions for failure occur at a constant rainfall intensity of 20 mm/h, for a duration of 18 hours, and a P_{average} of 0,1 kPa; at a constant rain rate of 10 mm/h for a duration of 36,6 hours and a P_{average} of 0,1 kPa; at a constant rainfall intensity of 5 mm/h for a duration of 74,5 hours and a P_{average} of 0,2 kPa.

For Landslide 3 (Figure 5.12) the critical conditions for failure occur at a constant rainfall intensity of 20 mm/h, for a duration of 27,5 hours, and a P_{average} of -0,3 kPa; at a constant rain rate of 10 mm/h for a duration of 47,6 hours and a P_{average} of -0,6 kPa; at a constant rainfall intensity of 5 mm/h for a duration of 80,6 hours and a P_{average} of -1,0 kPa.

5.3. Setting of the hydro-mechanical model

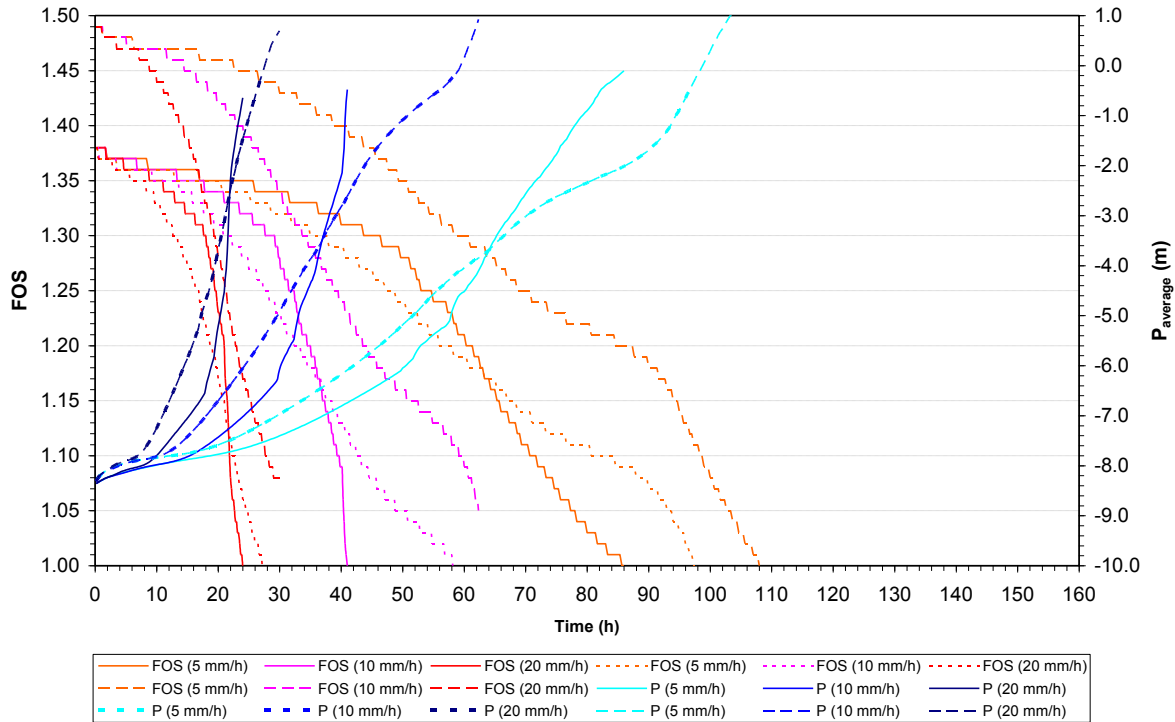


Figure 5.10: factor of safety (FOS) and average pore pressure (P_{average}) along sliding surface versus time for landslide 1. FOS: continuous lines are for condition 1, dotted lines are for condition 2, dashed lines are for condition 3. P_{average} : continuous lines are for $K_{\text{sat}} = 25\%$ percentile, dashed lines are for $K_{\text{sat}} = 75\%$ percentile.

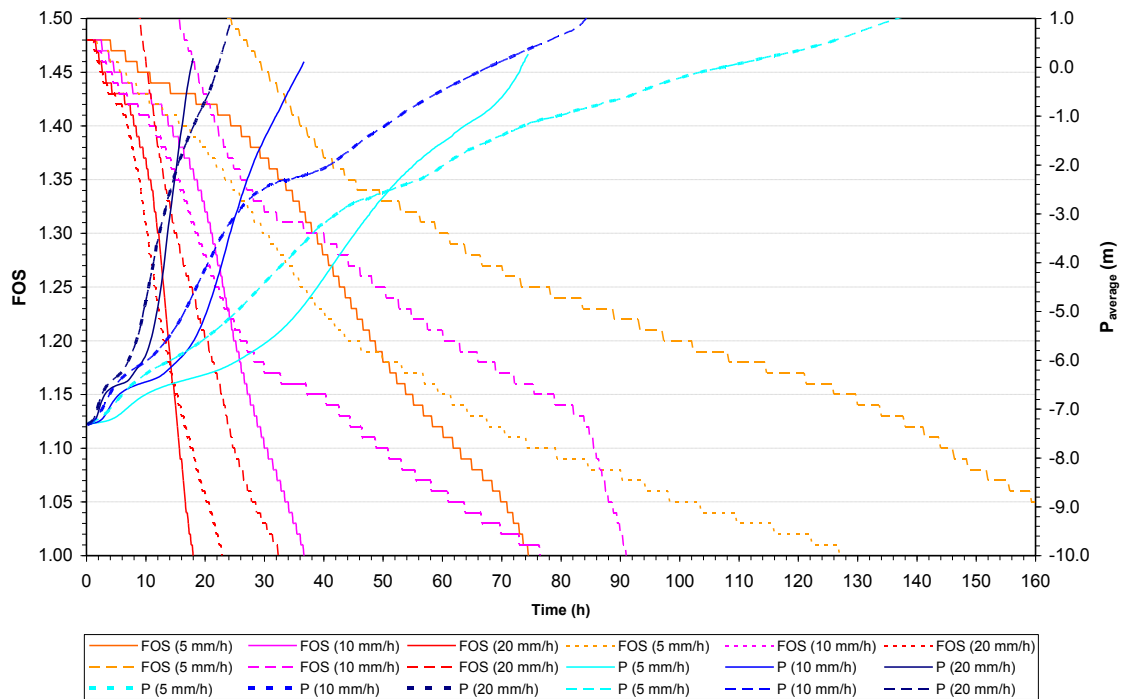


Figure 5.11: factor of safety (FOS) and average pore pressure (P_{average}) along sliding surface versus time for landslide 2. FOS: continuous lines are for condition 1, dotted lines are for condition 2, dashed lines are for condition 3. P_{average} : continuous lines are for $K_{\text{sat}} = 25\%$ percentile, dashed lines are for $K_{\text{sat}} = 75\%$ percentile.

5.3. Setting of the hydro-mechanical model

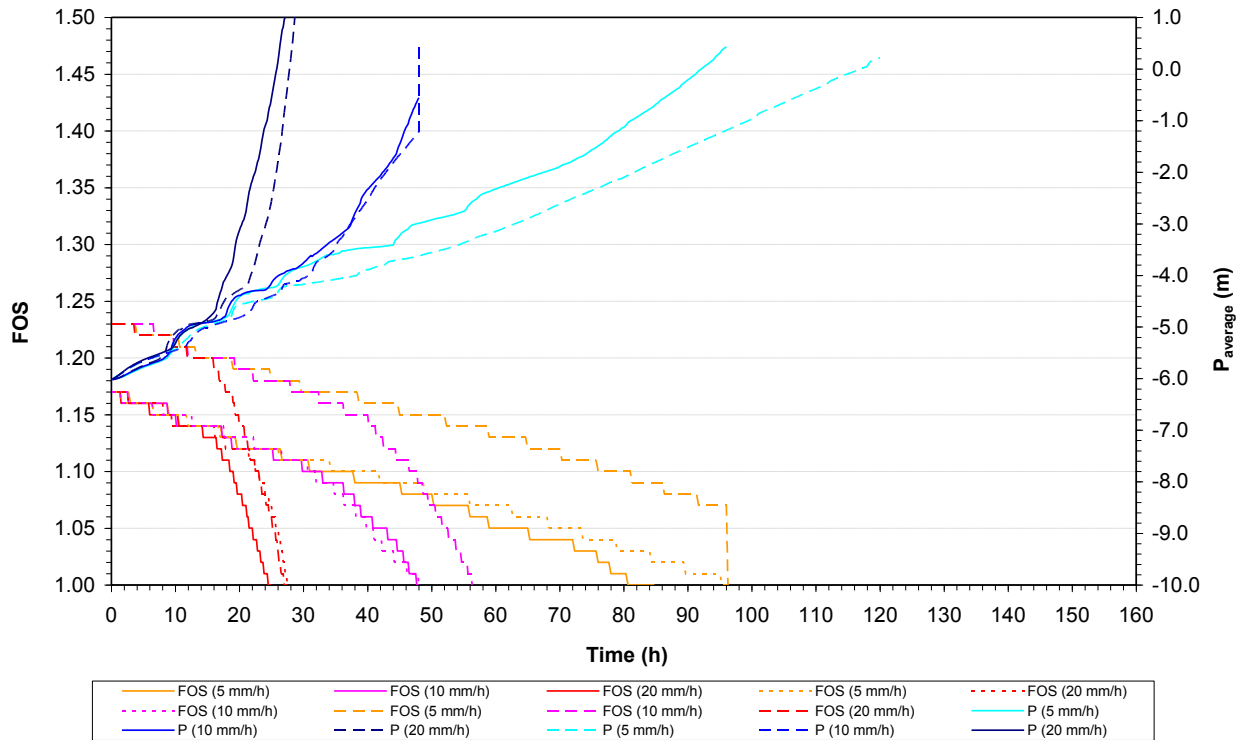


Figure 5.12: factor of safety (FOS) and average pore pressure (P_{average}) along sliding surface versus time for landslide 3. FOS: continuous lines are for condition 1, dotted lines are for condition 2, dashed lines are for condition 3. P_{average}: continuous lines are for $K_{\text{sat}} = 25\%$ percentile, dashed lines are for $K_{\text{sat}} = 75\%$ percentile.

5.4 Deterministic hydrological thresholds

Combining intensity values with durations of rainfalls to failure, related to different hydraulic and mechanical parameters derived from the sensitivity analysis, deterministic thresholds were reconstructed (Figure 5.13).

Rainfall intensities applied during numerical modelling were chosen from low to high: 2,5 mm/h, 5 mm/h, 10 mm/h, 20 mm/h and 40 mm/h.

Notwithstanding the wide variability range in which the sensitivity analysis was carried out, the deterministic intensity / duration hydrological thresholds leading to the initial slope failure show a lower envelope much greater of any other empirical threshold established worldwide. Differences between deterministic hydrological thresholds established for each of the three representative initial landslides are very similar, showing difference in duration of the rainfall to failure of some hours, if considering a constant rain rate. This observation could justify the almost continuous occurrence of many landslides during the night between the 5th and the 6th of May 1998, even if the supposition of a constant rain intensity is a strong simplification.

It should be highlighted that such hydrological thresholds take into account cohesion of pyroclastic layers and that thresholds are too high also taking into account the lowest mechanical parameters. However a necessary and sufficient condition is to consider non-zero values of cohesion, but attributing low values. In fact, if cohesion was neglected, this would make the slope unstable itself, thus invalidating any subsequent calculation for slope stability. This problem was already found in other works of literature, where effective friction angle values have a rather broad range of variation and cohesion is considered null (Bilotta & Foresta, 2002; Cascini et al., 2003) or varying from zero values to about 5 kPa (Cascini et al., 2003).

Furthermore, the comparison of the results with other intensity / duration empirical thresholds (Caine, 1980), established for shallow landslides in Campanian pyroclastic covers (Calcaterra et al., 2000; Guadagno, 1991) and worldwide (Baum and Godt, 2010), shows more severe hydrological conditions (Figure 5.13) for studied landslides. This would confirm the peculiarity of hydraulic and geotechnical characteristics of pyroclastic soils that account for medium to high permeability, low unit weight and medium to high shear strength. However, it is straightforwardly to observe that the empirical hydrological threshold established for ash-fall pyroclastic deposits mantling hillslopes

surrounding the Somma-Vesuvius (Guadagno, 1991) is the more similar to those reconstructed by means of a deterministic approach.

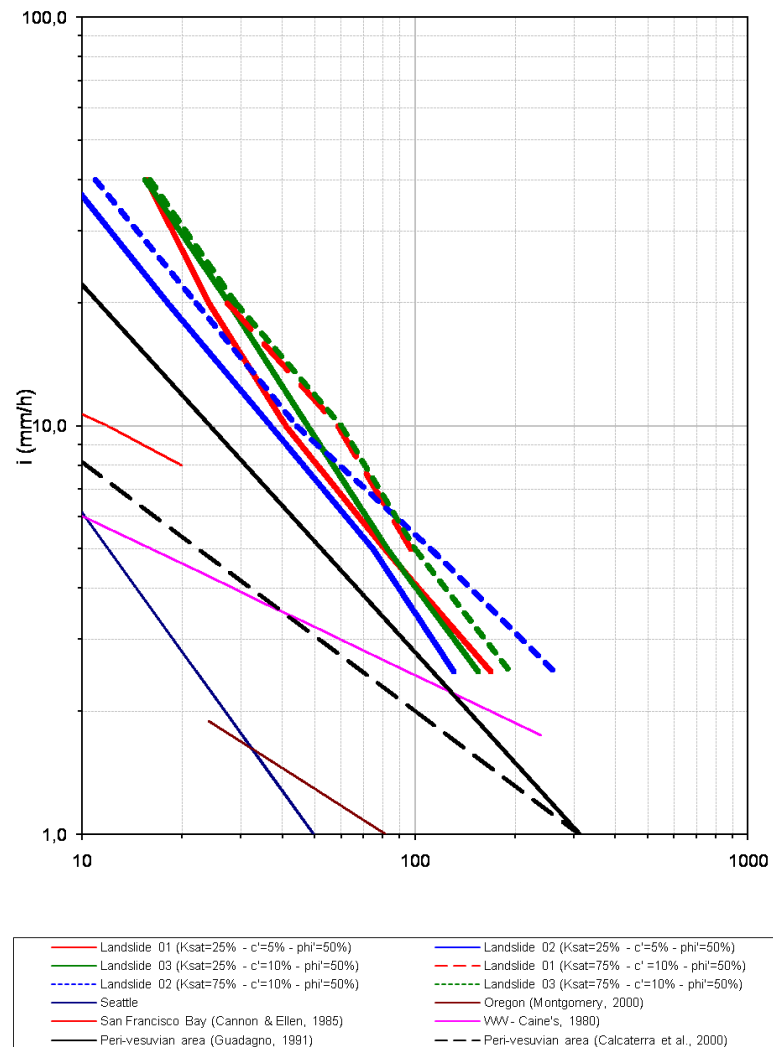


Figure 5.13: deterministic hydrological thresholds for triggering initial debris flows in comparison with other worldwide empirical hydrological thresholds. Extremes derived from the sensitivity analysis are shown for each landslide ($K_{sat}=25\%$ - $c'=5\%$ - $\phi'=50\%$ \rightarrow $K_{sat}=75\%$ - $c'=10\%$ - $\phi'=50\%$).

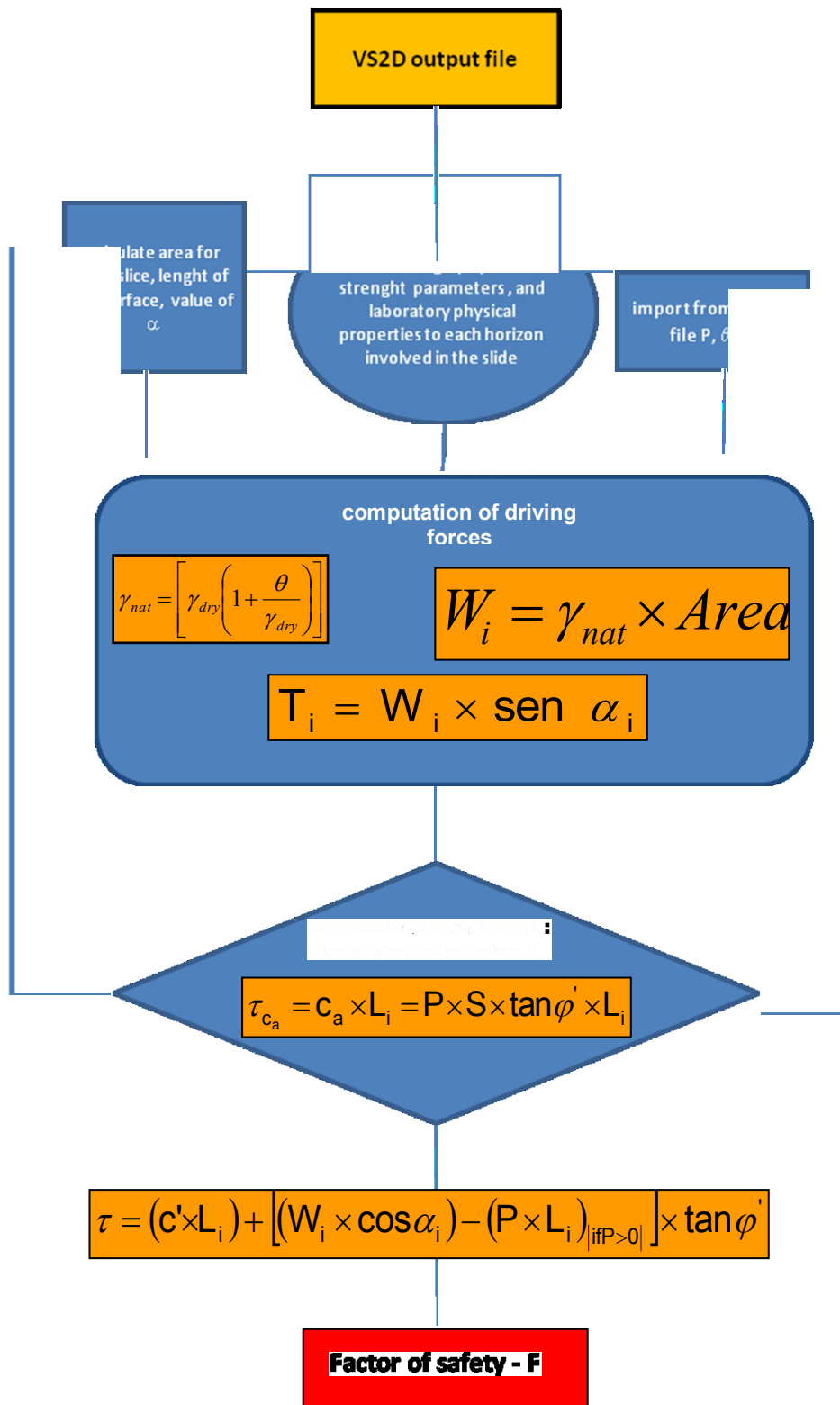


Figure 5.14: Flow diagram showing the logical path used to construct the hydro-mechanical model

Chapter 6

Conclusions

6.1 Relevance of the topics

The instability involving ash-fall pyroclastic soils mantling peri-Vesuvian hillslopes bordering the Campanian Plain is unique in and a very special type of shallow landslide if considered at the worldwide scale. This type of shallow landslide is also very relevant in Italy because it is the main source of risk for settlements in the foothills of the peri-Vesuvian hills. It is also, due to its catastrophic nature and complexity, of great significance to that part of the national scientific community that deals with susceptibility and hazard modeling.

This thesis is part of the huge and well-developed scenario of scientific research concerning the initiation phenomena of debris flow; research that started with a renewed energy after the landslides of 5th and 6th May of 1998. The aim was to improve the understanding of the triggering mechanisms.

The starting point was the awareness of the weak points of current systems that defend from natural instabilities that affect the territory, especially those related to “flow-like landslides” which cause damage, injury and fatalities every year. It was necessary to ask some question, such as: how well do we know the territory? How are we able to quantify the risks existing in it? What can we do to improve the defense system currently existing in order to reduce the possibility of landslides? Answering these questions means going beyond always acting only after a tragedy has occurred, The answers to the questions should permit us to understand the triggering mechanisms of initial landslides more fully, which is fundamental in order to identify potentially hazardous areas and to consider possible active defense on the slopes so that initial instability may be inhibited.

The significance of these problems led to focus the research on an innovative approach aimed at understanding the triggering mechanisms that would then permit the design of a specific model for the assessment of distributed landslide susceptibility .

Starting from the careful analysis of data and models known in the literature and from the field

evidence that the initial landslides have frequently decametric size, the objective of the research was focused on carrying out detailed investigations in triggering areas. Field surveys and laboratory analyses were executed considering three representative cases of initial landslides on the Sarno Mountain Range thus allowing the reconstruction of quantitative physical models and their hydro-mechanical modeling. The physical models of initial landslides can be considered a first attempt at quantitatively defining engineering-geological models of initial landslides on a detailed scale.

The results, if compared to the previous models known in literature, lead to a different interpretation of the triggering mechanism, thus highlighting the existence of hydrogeological conditions sufficient to determine the formation of an unsaturated / saturated throughflow within the pyroclastic cover and to justify the triggering of initial landslides close to natural and artificial morphological discontinuities.

On the basis of the engineering-geological models of three representative initial landslides, the numerical modeling of the hydrological processes within the pyroclastic mantle under non-saturated conditions and subsequent stability analysis, were carried out. Also, the clear relationship of cause – effect between rainfall and landslide occurrence provided a further element for the research activity which lead to the identification of the critical hydrological conditions, namely the intensity / duration hydrological threshold (Caine, 1980) for the initiation of landslides.

6.2 Concluding remarks of main results and open issues

The proposed quantitative models extend and elaborate on the conceptual ones known in literature and which regard the influence of topographical factors on the susceptibility to landslides involving ash-fall pyroclastic deposits on steep slopes, i.e. natural and anthropogenic conditions as predisposing factors to the initial failures.

Among the first factors, the abrupt increase of slope angle can be considered as being connected to the natural discontinuity of the bedrock such as rocky scarps, where pyroclastic cover undergoes a rapid thinning until there is the outcrop of the bedrock.

A similar condition is the knickpoint where slope angle increases more gently owing to reduced height of rocky scarps, determining a thinning of pyroclastic cover that still remains continuous. In general, considering the role of natural morphological factors, the geometry of pyroclastic soil

horizons is strongly linked to a rising slope angle, that would lead to a progressive reduction in the total thickness of the pyroclastic mantle and the pinching-out of pumiceous lapilli horizons (gravelly) up to values of slope angle and equal to about 50° . Above this value of slope angle, the pyroclastic soil thickness becomes negligible (De Vita et al., 2006a).

The hydrological modelling carried out by means of VS2DTI on the detailed physical models of the three initial landslides, permitted the understanding of the hydrological dynamics occurring within pyroclastic cover during rainfalls that determine its instability. From results of simulations at the failure time (Figures 5.5, 5.6 and 5.7), it is clear that water flow with relevant horizontal component and close to saturation conditions occur in a close range ($5\div 10$ m) around the restriction of the hydraulic section and particularly where C horizons pinch out. For the road cut condition too, the concentration of water flow with the increase of water content up to saturation occurs in a close range uphill from the free-to-air face. These observations are consistent with the small dimensions of initial landslides as observed in the field and with stability analysis itself. Considering hydraulic properties of pyroclastic soil horizons and particularly the high hydraulic conductivity contrast (pumiceous lapilli and the interposed paleosoil horizons), the existence of hydrogeological conditions leading to the formation of throughflow during intense and prolonged rainfalls and causing initial triggering has already been hypothesised (Crosta and Dal Negro, 2003; De Vita et alii, 2006b).

Such understandings can be considered very relevant for the comprehension of questions regarding the susceptibility of initial landslides because they reveal the crucial role carried out by small scale variations both of pyroclastic soil thickness (magnitude order of $1 \div 10^{-1}$ m) and morphology of slopes (magnitude order of $10^1 \div 1$ m), which, respectively, cannot be simplified as constant and assessed from ordinary topographic maps (1:5.000 scale). Appropriate scale of analysis for initial landslides triggering debris flows, especially if carried out only on topographic maps, is a challenging question owing to the possible false attribution of high susceptibility conditions to a specific landform. Consequently, the aforementioned aspects have to be considered for the application of distributed landslide susceptibility modelling.

The hydro-mechanical model defined by coupling results from hydrological modelling with those from mechanical analysis regarding the pyroclastic mantle covering Pizzo D'Alvano massif is quantitative as well. It does not take into account bedrock input such as buried springs to explain increase of pore pressure that would lead to failure which differs from findings assessed by other authors (Cascini et al., 2008; Cascini et al., 2010).

On the other hand, results from this model show that the front of unsaturated flow getting through the soil horizons constituting the pyroclastic mantle has the effect of concentrating up to saturation where pumiceous lapilli pinch out thus increasing pore pressures until they become positive. This phenomenon is observed, for all the main case studies taken into account, in areas of the slope where failure occurred.

Hydrological models of the slopes highlight that water flows firstly through the horizon with highest hydraulic conductivity (C horizon), and then, where draining section reduces or pinches out, water flow concentrates up to saturation. This type of shallow circulation was observed for each case study and it demonstrates that the contribution of springs from the bedrock can be neglected in attempting to explain the failure.

Hillslope hydrological modeling, carried out by means of VS2DTI with constant infiltration rates (5 mm/h; 10 mm/h; 20 mm/h and 40 mm/h) and considering normal pore pressure distribution within the pyroclastic mantle as the initial condition coupled with a stability modeling allowed the reconstruction of deterministic intensity/duration hydrological thresholds. These thresholds, even if conditioned by variability of shear strength parameters (c' and ϕ'), can be considered as an attempt to overcome or to test uncertainties of the classic empirical approach based on rain gauge data often recorded in distant positions from triggering zones and/or at lower altitudes that might influence their reliability, especially in mountainous areas and for short duration/high intensity rainfall events.

Some uncertainties regarding the proposed deterministic hydrological thresholds, exist since they depend on shear strength parameters characterizing ash fall pyroclastic deposits mantling the study area. They were determined by means of laboratory tests on soil samples not representative of macro-structures, (i.e. roots) and not very suitable to test the lower level of normal stress. On the basis of this assumption, further research should be focused on carrying out field measurements of shear strength aimed at determining the real value of apparent cohesion due to root strength.

Acknowledgments

I am very grateful to Professor De Vita, because he taught me lots of things during these three years. Thanks for giving me the chance to see U.S.A. and to do a very important research activity; thanks a lot, because it was the experience of my life.

Dr. Enrico Di Clemente technician in chief of the Engineering Geology and Geotechnics Laboratory at the Department of Earth Sciences of the University of Naples “Federico II” who directed laboratory analyses. During the long laboratory experience he taught me lots of things and he was always helpful, friendly and careful. His help was very precious to me, thanks!

I am very grateful to Dr. Baum for the welcome on my arrival in U.S.A, and he gave me precious advises every time I needed, I really appreciated it; I thank Dr. Jonathan Godt for being very helpful in research activities, thanks a lot.

I am very grateful to Dott. Iovine for accepting to revise my thesis and because he gave me precious advices.

I am very grateful to Luigi Ferranti because he supported me when PhD started, thanks.

I am very grateful to Dr. Osvaldo Nelson, Dr. Davide Villano and Dr. Simone De Simone who collaborated with us during their thesis degree to laborious field activities

I thank my mom, she is always precious to me, because she is infinitely lovely and patient, she is all for me; thanks to my sister for being kind every time I need it, and especially for supporting me in all my choices. Thanks dad because you always give me courage and you always believes in me, apart from everything.

...And thanks Marco, because you are always comprehensive and you always support my choices. Thanks...

References

- Amoozegar A. (1989) - A Compact Constant Head Permeameter For Measuring Saturated Hydraulic Conductivity Of The Vadose Zone. *Soil Science Society of America Journal*, **53**, pp. 1356-1361.
- Argand E. (1924) - La Tectonique de l'Asie. *Extrait du Compte-rendu du XIIIe Congrès géologique international 1922 (Liège)*, **1(5)**, pp. 171-372.
- Atterberg A. (1911) – Der Plastizität Der Tone. *International Mitteilungen für Botenkunde*, vol. 1, pp. 10-43.
- Bartorelli U. (1986) – Topografia (Seconda Edizione). *Pàtron Editore, Bologna (in Italian)*.
- Basile A., G. Mele and F. Terribile (2003) - Soil Hydraulic Behavior Of A Selected Benchmark Soil Involved In The Landslide Of Sarno 1998. *Geoderma*, **117 (3–4)**, pp. 331-346
- Baum R. (2000) – Computer Programs for Limit – Equilibrium Slope-Stability Analysis. Fellenius GS, BishopGS, and JanbuGS. U.S. Geological Survey. Open file report 00-107.
- Baum, R.L. and J.W. Godt, (2010) - Early warning of rainfall-induced shallow landslides and debris flows in the USA. *Landslides*, **7**, 259-272.
- Bilotta E. and V. Foresta (2002) – On The Measured Shear Strength Of Some Pyroclastic Soils Of Sarno Mountains. *Proc. 3th Int. Conf. on Unsaturated Soils, Recife (Brasil)*, **1**, pp. 495-500.
- Bilotta E., L. Cascini, V. Foresta, and G. Sorbino (2005) - Geotechnical characterization of pyroclastic soils involved in huge flowslides. *Geotechnical and Geological Engineering* **23**, pp. 365-402.
- Bishop A.W. (1955) - The Use of the Slip Circle in the Stability Analysis of Slopes. *Geotechnique*, **5 (1)**, pp. 7-17.
- Bovis J.M. (1985) – Earthflows in the Interior Plateau, southwest British Columbia. *Can. Geotech. Journal*, **22**: 313-334.
- Bower H. (1966) – Rapid field measurement of air entry value and hydraulic conductivity of soil as significant parameters in flow system analysis. *Water Resources Research*, vol. 2, n° 4, pp. 729-738.
- Brancaccio L., A. Cinque, F. Russo & D. Sgambati (2000) - Le frane del 5-6 maggio 1998 sul gruppo montuoso Pizzo d'Alvano (Campania): osservazioni geomorfologiche sulla loro distribuzione e sulla dinamica delle connesse colate. *Quaderni di Geologia Applicata*, **7(1)** pp. 5-36.
- Brooks R.H., A.T. Corey (1964) – Hydraulic properties of porous media. *Colorado State University, Hydrology Paper*, N° 3, March.
- Budetta P. & R. De Riso (2004) - The mobility of some debris flows in pyroclastic deposits of the northwestern Campanian region (southern Italy). *Bulletin of engineering geology and environment*, **63**, pp. 293-302.
- Caine N. (1980) - The rainfall intensity-duration control of shallow landslides and debris flows. *Geografiska Annaler* **62A**, pp. 23-27.
- Calcaterra D., M. Parise, B. Palma, and L. Pelella (2000) - The influence of meteoric events in triggering shallow landslides in pyroclastic deposits of Campania, Italy. *In: Landslides in research, theory and practice*, (Eds) Bromhead, E., Dixon, N., and Ibsen, M.L., *Proc. 8th Int. Symp. on Landslides, Cardiff, UK*, pp. 209–214.
- Campbell R.H. (1975) – Soil Slips, Debris Flows, and Rainstorms in the Santa Monica Mountains and vicinity, Southern California. *U.S. Geological Survey Professional paper* **851**, 51 pp.

- Carrara A., B. D'Elia, E. Semenza (1985) - Classificazione e nomenclatura dei fenomeni franosi. *Geol. Appl. Idrogeol.*, 20, 223-243(in Italian).
- Casagrande A. (1948) - Classification and Identification of Soils. *Transaction ASCE* vol. 113, p. 90.
- Casagrande A. (1971) – On liquefaction phenomena: report of a lecture. *Géotechnique*, 21, pp. 197-202.
- Cascini L. (2003) – La gestione scientifica dell'emergenza idrogeologica del maggio 1998. *Monografia, G.N.D.C.I., C.N.R. Edition. pp 376 (in Italian)*.
- Cascini L. (2004) - The Flowslides Of May 1998 In The Campania Region: The Scientific Emergency Management. *Rivista Italiana Di Geotecnica*, 2, pp. 11-44.
- Cascini L. and G. Sorbino (2004) – The contribution of soil suction measurements to the analysis of flowslide triggering. *Invited lecture, Proc. of the Int. workshop "Flows 2003-Occurrence and mechanisms of Flows in natural slopes and Earthfill"*, Sorrento, Patron Ed., pp. 77-86.
- Cascini L. and P. Versace (1986) - Eventi pluviometrici e movimenti franosi. *Atti XVI Convegno Nazionale di Geotecnica, Bologna*, 3, pp. 171-184 (in Italian).
- Cascini L. (2002) – Il rischio da frana in aree urbane dell'Appennino centro-meridionale. *Proc. 21th Italian Geotechnical conference, L'Aquila, Patron Editore, pp. 135-142 (in Italian)*.
- Cascini L. D. Guida, G. Romanzi, G. Nocera, G. Sorbino (2000) - A preliminary model for the landslides of May 1998 in Campania Region. *Proc. 2nd Intern. Symp. on Hard Soils Rocks: pp. 1623-1649, Balkema*.
- Cascini L. S Cuomo, M. Pastor, G. Sorbino (2010) – Modeling of rainfall-induced shallow landslides of the Flow type. *Journal of geotechnical and geoenvironmental engineering*, pp.85-98.
- Cascini L., S Ferlisi., G. Tagliaferro (2002) - Il contributo delle indagini storiche nella definizione del rischio da frana: un caso di studio. *Proc. 21th Italian Geotechnical Conference, L'Aquila, Patron Editore, pp. 135-142 (in Italian)*.
- Cascini L., S. Cuomo, D. Guida (2008) - Typical source areas of May 1998 flow-like mass movements in the Campania region, Southern Italy. *Engineering geology*. 96, pp. 107-125.
- Cascini L., S. Cuomo, G. Sorbino (2005) – Flow-like mass movements in pyroclastic soils: remarks on the modelling of triggering mechanisms. *Italian Geotechnical Journal*, 4, pp. 11-31 (in Italian).
- Cascini L. and G. Sorbino (2002) - Soil suction measurement over large areas: a case study. *Proc. 3rd Int. Conf. on Unsaturated Soils, Recife* 2, pp. 829-834.
- Cascini L., D. Guida, D. Romanzi, M. Nocera, G. Sorbino, (1998) - A preliminary model for the landslides of May 1998 in Campania Region. *II8 Int. Symp. on The Geotechnics of Hard Soil–Soft Rocks, Napoli*, vol. 3. pp. 1623– 1649
- Cascini L., G. Sorbino, and S. Cuomo (2003) - Modelling of flowslides triggering in pyroclastic soils. *Proc. Int. Conference on "Fast Slope Movements. Prediction and Prevention for Risk Mitigation"*, vol. 1. Patron Editore, Napoli, pp. 93-100.
- Celico P., S. Aquino, L. Esposito, V. Piscopo (2000) – Problematiche idrogeologiche connesse con i fenomeni di instabilità delle coltri piroclastiche della dorsale di pizzo D'Alvano. *Quaderni di geologia Applicata* 5(1), pp. 129-188 (in italian).
- Celico P. (1986) – Prospezioni idrogeologiche. *Liguori editore (In Italian)*.
- Celico P., P. De Vita, S. Fabbrocino, V. Piscopo, G. Galicchio, T. Gentile (2002) - Primi risultati dell'analisi dei debris flows nei versanti dei rilievi carbonatici perivesuviani. *Atti dei Convegni Lincei* 181 pp.. 114 – 133 (in italian).

- Celico P., P. De Vita, V. Piscopo (2001) – Primi risultati dell’analisi dei debris-flow nei versanti dei rilievi carbonatici peri-vesuviani: aspetti idrogeologici predisponenti e condizioni idrologiche critiche. Atti dei Convegni dei Lincei n. 181 “Il dissesto idrogeologico: Inventario e prospettive”, Accademia nazionale dei Lincei, 5 giugno 2001.
- Celico P., F.M. Guadagno., A. Vallario (1986) - Proposta di un modello interpretativo per lo studio delle frane nei terreni piroclastici. *Geologia Applicata e Idrogeologia*, **21**, 173-193 (in Italian).
- Celico P., Guadagno, F.M. (1998) - L’instabilità delle coltri piroclastiche delle dorsali carbonatiche in Campania: attuali conoscenze. *Quad. Geol. Appl.* **5**, pp. 129–188 (in Italian)
- Celico P., L. Esposito, V. Piscopo, S. Aquino, (2000) - Problematiche idrogeologiche connesse con i fenomeni di instabilità delle coltri piroclastiche della dorsale del Pizzo D’Alvano (Campania). *Quaderni di geologia applicata, Pitagora editrice*, **7(2)**, pp. 167–187 (in Italian).
- Channell J.E.T., B. D’Argenio, and F. Horváth (1979) – Adria, the african promontory in mesozoic Mediterranean Paleogeography. *Earth-Science Reviews*, 1979, Vol. 15, Issue 3, pp 213 - 292.
- Chirico G.B., P. Claps, F. Rossi, and P. Villani (2000) - Hydrologic conditions leading to debris-flow initiation in the Campanian volcanoclastic soil. *Mediterranean Storms. Proceedings of the EGS Plinius Conference*, pp. 473-484.
- Cinque A., E. Patacca, P. Scandone, M. Tozzi (1993) – Quaternary Kinematic evolution of the Southern Apennines. Relationship between surface geological features and deep lithospheric structures. *Annali di geofisica*, vol. XXXVI, N.2, pp 249-260.
- Corominas J. (1996) – The Reach Angle As A Mobility Index For Small Large Landslides. *Canadian Geotechnical Journal*, **33**, pp. 260-271.
- Crosta G.B., and P. Dal Negro (2003) – Observations and modelling of soil slip-debris flow initiation processes in piroclastica deposits: The Sarno 1998 event. *Natural Hazards Earth Syst. Sci.*, **3**, pp. 53-69.
- Crozier M.J., E.E. Vaughan J.M. Tippet (1990) – Relative instability of colluvium-filled bedrock depressions. *Earth Surface Proc. And Landforms*, **15**, pp. 329-339.
- Crozier MJ and RJ Eyles (1980) - Assessing the probability of rapid mass movement. In: *The New Zealand Institution of Engineers. Proceedings of Technical Groups (ed.): Proc. Third Australia - New Zealand Conference on Geomechanics, Wellington*, 6(Iss. 1 (G) Part 2), 2.47-2.51
- Cruden D.M. (1991) – A Simple Definition of a Landslide. *Bulletin of the International Association of Engineerin Geology*, **43**, pp. 27-29.
- Cruden, D.M., and D.J. Varnes (1996) - Landslide Types And Processes. In: *Turner, A.R., Schuster, R.L. (Eds.), Landslides: Investigation And Mitigation, Sp. Rep. 247. Transportation Research Board, National Research Council, National Academy Press, Washington, DC*, pp. 36–72.
- D’Argenio B, T. Pescatore, P. Scandone (1975) - Structural pattern of the Campania-Lucania Apennines. *Quaderni de “la ricerca scientifica, CNR”*, 1975; 90: 213-292 (in Italian).
- De Gennaro M., A. Langella, A. Colella & A. Buonodono (2000) - Caratterizzazione mineralogica delle vulcanoclastiti del Pizzo d’Alvano. *Quaderni di Geologia Applicata*, **7(1)**, pp 49-58 (in Italian)
- De Riso R, Budetta P, Calcaterra D, Santo A (1999) - Le colate rapide in terreni piroclastici del territorio campano. *Convegno “Previsione e prevenzione di movimenti franosi rapidi” Trento, Giugno 1999, Associazione Georisorse e Ambiente, Torino*, pp. 133–150 (in Italian).
- De Riso R. and E. Nota D’elogio (1973) - Sulla Franosità Della Zona Sud-Occidentale Della penisola Sorrentina. *Memorie e Note dell’Istituto di Geologia Applicata*, **12**, Napoli (In Italian).

- De Vita P. (2000) - Fenomeni di instabilità delle coperture piroclastiche dei Monti Lattari, di Sarno e di Salerno (Campania) ed analisi degli eventi pluviometrici determinanti. *Quaderni di Geologia Applicata* 7, pp. 213– 235 (2/2000) (in Italian).
- De Vita P. and P. Celico (2006) – Distribuzione Delle Coltri Piroclastiche Sui Versanti Carbonatici Perivesuviani E Suscettibilità A Franare. *Giornale di Geologia Applicata*, 3: 145-151 (in Italian).
- De Vita P. And P. Piscopo (2002) - Influences of hydrological and hydrogeological conditions on debris flows in peri-vesuvian hillslopes. *Natural Hazards and Earth System Sciences*, 2, pp. 1-9.
- De Vita P., D. Agrello and F. Ambrosino (2006a) - Landslide Susceptibility Assessment In Ash-Fall Pyroclastic Deposits Surrounding Mount Somma-Vesuvius. *Application Of Geophysical Surveys For Soil Thickness Mapping*. *Journal of Applied Geophysics*, 59, pp. 126-139.
- De Vita P., D. Agrello, F. Ambrosino, E. De Luzio (2003) - Caratterizzazione del sistema idrogeologico superficiale coltre piroclastica - substrato carbonatico nella dorsale dei Monti di Sarno. *Quaderni di Geologia Applicata, Serie AIGA* – pp. 49 – 69 (in Italian).
- De Vita P., P. Celico, M. Siniscalchi and R. Panza (2006b) – Distribution, Hydrogeological Features And Landslide Hazard Of Pyroclastic Soils On Carbonate Slopes In The Area Surrounding Mount Somma-Vesuvius. *Italian Journal of Engineering Geology and Environment*, 1, pp. 1-24.
- Del Prete M, F.M. Guadagno, A.B. Hawkins (1998) - Preliminary report on the landslides of 5 May 1998, Campania, southern Italy. *Bull Eng Geol Environ* 57, pp. 41–50
- Dewey J.F., M. L. Helman, S. D. Knott (1989) - Kinematics Of The Western Mediterranean. Geological Society Of London, Special Publication, 1989; 45, pp. 265-284.
- Di Crescenzo G. A. Santo (1999) - Analisi geomorfologica delle frane da scorrimento-colata rapida in depositi piroclastici della Penisola sorrentina. *Geografia Fisica e Dinamica Quaternaria*, 22, pp. 57-72.
- Di Crescenzo G. and A. Santo (2005) – Debris Slides-Rapid Earth Flow In The Carbonate Massifs Of The Campania Region (Southern Italy): Morphological And Morphometric Data For Evaluating Triggering Susceptibility. *Geomorphology*, 66, pp. 255-276.
- Di Gennaro A., G. Aronne, M. Buonanno and F. Terribile (1998) – Il progetto “Carta dei suoli della provincia di Napoli n scala di semi-dettaglio 1:50.000”. *Atti Convegno S.I.S.S., Napoli-Ischia 1-5 giugno 1998. (in Italian)*
- Eckersley D. (1990) – Instrumental laboratory flowslides. *Géotechnique*, 40, pp. 489-502.
- Esposito L. and E. Di Clemente (2003) - Proposta di una nuova procedura per la determinazione del limite di plasticità col cono penetrometrico. *Convegno internazionale di Geologia, Firenze 2004 (in Italian)*.
- Esposito L. And F.M. Guadagno (1998) - Some special geotechnical properties of pumice deposits. *Bullettin of Enginnering Geology and the Environment*, 57, pp 41-50.
- Fellenius W. (1927) - Erdstatische Berechnungen mit Reibung und Kohasion (Adha`sion) und unter Annahme kreiszylindrischer Gleitflä`chen. *Ernst & Sohn, Berlin*.
- Ferranti L. e J.S. Oldow, (2005) - Latest Miocene to quaternary horizontal and vertical displacement rates during simultaneous contraction and extension in the Southern Apennines orogen, Italy. *Terra nova*, 2005; Vol. 17, Num. 3, 2005 , pp. 209-214(6).
- Fiorillo F, F.M. Guadagno, S. Aquino, A. De Blasio (2001) - The December 1999 Cervinara landslides: further debris flows in the pyroclastic deposits of Campania (southern Italy). *Bull Eng Geol Environ* 60, pp. 171–184.

- Fiorillo F. And R.C. Wilson (2004) – Rainfall induced debris flows in pyroclastic deposits, Campania (southern Italy). *Engineering Geology* **75**, pp. 263–289.
- Fiorillo, F., F.M. Guadagno, S. Aquino, and A. De Blasio (2001) - The December 1999 Cervinara landslides: further debris flows in the pyroclastic deposits of Campania (southern Italy). *Bulletin of Engineering Geology and Environment*, **60**, pp. 171-184.
- Fisher R.V. (1985) - Pyroclastic rocks. *Springer*, 472 pp.
- Frattini P., G. B. Crosta, N. Fusi, P. Dal Negro (2004) - Shallow Landslides In Pyroclastic Soils: A Distributed Modeling Approach For Hazard Assessment. *Engineering Geology*, **73** pp. 277–295.
- Fredlund D.J. and A. Xing (1994) – Equations for the soil-water characteristic curve. *Canadian Geotechnical Journal*, **31**,(4) pp. 521-532.
- Fredlund D.J. and H. Rahardjo (1987) – Non-linearity of strength envelope for unsaturated soils. *In proceedings of the 6th International Conference on Expansive Soils, New Delhi, India, Vol. 1*, pp. 49-54.
- Fredlund D.J. and H. Rahardjo (1993) – Soil mechanics for unsaturated soils, Wiley, New York.
- Fredlund D.J., N.R. Morgestern, R.A. Widger (1978) – The shear strength of unsaturated soils. *Canadian Geotechnical Journal*, **15** (3), pp. 313-321.
- GeoSlope (1998) - International Ltd., Calgary, Alberta, Canada, SEEP/W manual.
- Godt J.W, and J.P. McKenna (2008) - Numerical modelling of rainfall thresholds for shallow landsliding in the Seattle, Washington, area. *Reviews in Engineering Geology, The Geological Society of America*, **20**, pp. 121-135.
- Godt, J.W., R.L. Baum and N. Lu (2009) - Landsliding in partially saturated materials. *Geophysical Research Letters*, **36**, pp. 1-5.
- Guadagno F.M, R. Forte, P. Revellino, F. Fiorillo, M. Focareta (2005) - Some aspects of the initiation of debris avalanches in the Campania Region: The role of morphological slope discontinuities and the development of failure. *Geomorphology* **66**, pp. 237–254.
- Guadagno F.M., (1991) - Debris Flow in the Campanian volcanoclastic soils (Southern Italy). *Proceedings International Conference on “Slope stability engineering developments and applications”*, Thomas Telford, London, pp. 125– 130.
- Guadagno F.M., S. Magaldi (2000) - Considerazioni sulle proprietà geotecniche dei suoli allofanici di copertura delle dorsali carbonatiche campane. *Quad. Geol. Appl.* **7**, pp. 143– 155.
- Guadagno F.M., S. Perriello Zampelli (2000) - Triggering mechanisms of the landslides that inundated Sarno, Quindici, Siano and Bracigliano (S. Italy) on May 5–6, 1998. *Proc. 8th Int. Symp. Landslides, Cardiff*, **2**, pp. 671–676.
- Guadagno F.M., S. Martino, G. Scarascia Mugnozza (2003) - Influence of man-made cuts on the stability of pyroclastic covers (Campania-Southern Italy): a numerical modelling approach. *Environ. Geol.* **43**, pp. 371–384.
- Guida D. (2003) – The role of the zero order basins in flowslide-debris flow occurrence and recurrence in Campania (Italy). *Proc. Int Conference on “fast slope Movements – Prediction and prevention for risk Mitigation”*, Pàtron Editore, Napoli, **1**, pp. 255-262.
- Guzzetti F, M. Cardinali, and P. Reichenbach (1994) - The AVI project: a bibliographical and archive inventory of landslides and floods in Italy. *Environ Manage* **18**, pp. 623–633.

- Hack J.T and J.C. Goodlett (1960) – Geomorphology and forest ecology of a mountain region in the Central Appalachians. *U.S. Geological Survey Professional Paper 347*, pp. 1-66.
- Heim A (1932) - Bergsturz und Menschenleben. *Zurich, Fretz und Wasmuth*. (English translation by Skermer NA, 1989, *Landslides and human lives*. BiTech Publishers, Vancouver BC).
- Horton R. E. (1940) - An Approach Toward a Physical Interpretation of Infiltration Capacity. *Soil Sci. Soc. Am. J.*, 5, pp. 399-417.
- Hsieh P.A., W. Wingle, and R.W. Healy (2000) - VS2DI: A Graphical Software Package for Simulating Fluid Flow and Solute or Energy Transport in Variably Saturated Porous Media. *U.S. Geological Survey. Water-Resources Investigations Report 9-4130*.
- Hungr O. & M. Jacob (2006) - Debris Flow Hazard And Related Phenomena. *Springer*.
- Hungr O., S.G. Evans, M.J. Bovis, and J.N. Hutchinson (2001) - A review of the classification of landslides of flow type. *Environmental and Engineering Geoscience*, 7, pp. 221-238.
- Hutchinson J.N. (1968) – Mass movement. In *Encyclopaedia of Geomorphology (Encyclopaedia of Earth Sciences Series III)*, R.W. Fairbridge (ed.), pp. 688-695.
- Hutchinson J.N. (1988) - General report: morphological and geotechnical parameters of landslides in relation to geology and hydrogeology. *Proc. 5th Int. Symp. On Landslides, Lausanne, I*, pp. 3-36.
- Hutchinson J.N. and R. Bhandari (1971) - Undrained loading, a fundamental mechanism of mudflows and other mass movements. *Géotechnique*, 21(4), pp. 353-358.
- Iverson R.M., M.E. Reid, and R.G. LaHusen, (1997) - Debris-flow mobilisation from landslides. *Annual Review of Earth Planetary Science*, 25, pp. 85-138.
- Jakob, M., and O. Hungr (2005). Debris-flow Hazards and Related Phenomena. *Springer Verlag*, 739 pp.
- Janbu N. (1973) – Slope stability computations. In *embankment-Dam Engineering: Casagrande Volume*, edited by R. C. Hirschfeld and J. S. Poulos, pp. 47-86, John Wiley, Hoboken, N.J.
- Johnson A.M. & P.H. Rahn (1970) – Mobilization of debris flows. *Z. Geomorphol. Suppl.* 9, pp. 168–186.
- Kirkby M.J. (1978) - Hillslope hydrology. *John Wiley & Sons*, 389 pp.
- Lappala E.G., R.W. Healy, E.P. Weeks (1987) – Documentation of computer program VS2D to solve the equations of fluid flow in variably saturated porous media. *U.S. Geological Survey. Water-Resources Investigations Report 83-4099*.
- Lirer L., R. Munno, P. Petrosino, A. Vinci, (1993) - Tephrostratigraphy of the AD 79 pyroclastic deposits in perivolcanic areas of Mt. Vesuvio (Italy). *J. Volcanol. Geotherm. Res.* 58, 133–149.
- Lirer L., T. Pescatore, B. Booth, G.P.L. Walker (1973) - Two Plinian pumice fall deposits from Somma-Vesuvius, Italy. *Geol. Soc. Amer. Bull.* 84, pp. 759–772.
- Lu N. and W. J. Likos (2002) – Unsaturated Soil Mechanics. (J. Wiley & Sons, Inc.).
- Lu N. and W. J. Likos (2004) – Rate of capillary rise in soils. *Journal of Geotechnical and Geoenvironmental engineering*, vol. 130 (6), pp. 646-655.
- Lu N., and W.J. Likos (2006) - Suction stress characteristic curve for unsaturated soil. *Journal of Geotechnical Geoenvironmental Engineering*, 123, pp. 131–142.
- Nicotera M.V. and R. Papa (2008) - Comportamento idraulico e meccanico della serie piroclastica di Monteforte Irpino. *Piattaforme Evolute di Telecomunicazioni e di Information Technology per l'Offerta di Servizi al settore ambiente PETIT-OSA*. Centro Specializzato Monitoraggio Frane, Aracne Editrice, pp. 272-280 (in Italian).

- Olivares L., L. Picarelli, L. Andreozzi, B. Avorio, E. Damiano, S. Lampitiello (2002) - Scenari di pericolosità di frana in terreni sciolti di natura piroclastica. *Proc. XXI Conv. Naz. di Geotecnica*, pp. 173-181. *L'Aquila (in Italian)*.
- Olivares L., L. Andreozzi, E. Damiano, B. Avolio, and L. Picarelli (2003) - Hydrologic response of a steep slope in unsaturated pyroclastic soils. *Proc. Int. Conference on "Fast Slope Movements Prediction and Prevention for Risk Mitigation"*. Patron Editore, Napoli, pp. 391–397.
- Patacca E., R. Sartori, and P. Scandone (1990) - Tyrrenian basin and Apenninic arcs: kinematic relation since late Tortonian times. *Memorie della Società Geologica Italiana*, 1990; 45: 425-451 (in Italian).
- Philip J.R. (1957) – The Theory Of Infiltration: The Infiltration Equation And Solution. *Soil Science*, 83, pp. 345-357.
- Picarelli L. and L. Olivares (2001) - Innesco e Formazione di colate di Fango in terreni sciolti di origine piroclastica. *Forum per il Rischio Idrogeologico in Campania, Napoli 22 Giugno 2001*, pp. 26–38 (in Italian).
- Picarelli L., L. Olivares, L. Andreozzi, E. Damiano and S. Lampitiello (2004) - A research on rainfall-induced flowslides in unsaturated soils of pyroclastic origin. In: *Lacerda Ehrlich Fontoura Sayao (Ed.), Landslides: Evaluation and Stabilization*, vol. 1, pp. 1497–1506.
- Pierson T.C. & J.E. Costa (1987) - A rheologic classification of subaerial sediment – water flows. *Geological society of America Rev. Eng. Geol.* 7, pp. 1–12.
- Rao S.M. (1995) - Mechanistic approach to the shear strength behavior of allophanic soils. *Eng Geol* 40, pp. 215–221.
- Raviolo P. (1993) – Il laboratorio geotecnico. *Editrice Controls (in Italian)*.
- Reid M.E. (1994) - A pore-pressure diffusion model for estimating landslide-inducing rainfall. *J. Geol.* 102, pp. 709– 717.
- Revellino P., O. Hungr, F.M. Guadagno and S.G. Evans, (2004) - Velocity and runout simulation of destructive debris flows and debris avalanches in pyroclastic deposits, Campania region, Italy. *Environmental Geology*, 45, pp. 295–311.
- Reynolds W.D. & D.E. Elrick (1986) – A method for simultaneous in-situ measurement in the vadose zone of field-saturated hydraulic conductivity, sorptivity, and the conductivity-pressure head relationship. *Ground Water Monit. Rev.* 6, pp. 84-95.
- Rodine JD. (1974) - Analysis of the mobilization of debris flows. *PhD thesis. Stanford Univ., Stanford, CA.* 226 pp.
- Rolandi G, P. Petrosino, J. Mac Geehin (2006) – The Interplinian Activity at Somma – Vesuvius in the Last 3500 Years, *Journal of Volcanology and Geothermal Research*, 82, pp. 19 – 52.
- Rolandi G. (2001) – Interventi Di ingegneria Naturalistica Nel Parco Nazionale del Vesuvio (a cura di C. Bifulco), pp 15 – 41 (in Italian).
- Rolandi G., A. Paone, M. Di Lascio, G. Stefani, (2007) - The 79 AD eruption of Somma: The relationship between the date of the eruption and the southeast tephra dispersion. *Journal of Volcanology and Geothermal Research*, 169, pp 87 – 98.
- Rolandi G., A.M. Barrella and A. Borrelli (1993) – The 1631 Eruption of Vesuvius. *Journal of Volcanology and Geothermal Research*, 58, pp. 183 – 201.
- Rolandi G., F Bertolini., G. Cozzolino, N. Esposito, D. Sannino (2000) - Sull'origine delle coltri piroclastiche presenti sul versante occidentale del Pizzo d'Alvano (Sarno – Campania). *Quaderni Di Geologia Applicata*, 7-1, 213-235 (in Italian).

- Rolandi G., G. Mastrolorenzo, A.M Barrella and A. Borrelli (1993b) – The Avellino plinian eruption of Somma-Vesuvius (3760 y B.P.) : the progressive evolution from magmatic to hydromagmatic style. *Journal of Volcanology and Geothermal Research*, **58**, pp. 67-88.
- Rolandi G., R. Munno, I. Postiglione (2004) - The A.D. 472 Eruption Of The Somma Volcano. *Journal of Volcanology and Geothermal Research*, **129**, pp. 291-319.
- Rolandi, G., Maraffi, S., Petrosino, P., Lirer, L. (1993a). The Ottaviano eruption of Somma-Vesuvius (8000 y B.P.): a magmatic alternating fall and flow-forming eruption. *J. Volcanol. Geotherm. Res.* **58**, pp. 43–65.
- Rosi M., C. Principe, R. Vecchi (1993) - The 1631 eruption of Vesuvius reconstructed from the review of chronicles and study of deposits. *J. Volcanol. Geotherm. Res.* **58**, pp. 151–182.
- Sanglerat G. (1972) – The Penetrometer and Soil Exploration. Developments in Geotechnical Engineering 1. *Elsevier Publishing: New York*.
- Sassa K. (1985) - The mechanism of debris flow. *Proceedings of XI International Conference on Soil Mechanics and Foundation Engineering, San Francisco. Balkema, Rotterdam, the Netherlands*, pp.1173-1176.
- Scotto di Santolo A. (2000) – Analisi Geotecnica dei fenomeni franosi nelle coltri piroclastiche della provincia di Napoli. *PhD Thesis, University of Federico II (in Italian)*.
- Sharpe C.F.S. (1938) – Landslides and Related Phenomena: A Study of Mass-Movements of Soils and Rock. *New York, Columbia University Press*.
- Sherwood P. T., M. D. A Riley (1970) - An investigation of a cone-penetrometer method for the determination of the liquid limit. *Géotechnique*; **20(2)**, pp. 203–208.
- Shoji S., R. Dahlgren and M. Nanzyo, (1993) - Morphology of volcanic ash soils. *In: Volcanic Ash Soils, Elsevier*, pp. 7-35.
- Skempton A.W. and J.N. Hutchinson (1969) - Stability of natural slopes and embankement foundations. *State of the art Report. 7th Int. Conf. Soil Mech. & Found. Engrg, Mexico, State of the art*, pp. 291-340.
- Soil Survey Staff (1998) - Soil taxonomy: a basic system of soil classification for making and interpreting soil surveys (2nd ed). Washington, DC: U.S. Department of Agriculture Soil Conservation Service).
- Sorbino G. (2005) - Numerical modelling of soil suction measurements in pyroclastic soils. *In: Tarantino Romero Cui (Ed.), Int. Symp. "Advanced experimental unsaturated soil mechanics". Taylor and Francis Group, London*, pp. 541-547.
- Sorbino G. and V. Foresta (2002) – Unsaturated Hydraulic Characteristic Of Pyroclastic Soils. *Proc. 3rd Int. Conf. on Unsaturated Soils, Recife (I)*, pp. 405-410.
- Takahashi T. (1978) –Mechanical characteristics of debris flow. *J. Hydraul. Div. Am. Soc. Civ. Eng.* **104**, pp. 1153–1169.
- Terribile F., A. Basile, R. De Mascellis, A. Di Gennaro, S. Vingiani (2000) - I suoli delle aree di crisi di Quindici e Sarno: proprieta` e comportamenti in relazione ai fenomeni franosi del 1998. *Quaderni di Geologia Applicata 7 (I)*, pp. 60– 79 (In Italian).
- Turner A.K., and R.L. Schuster (1996) - Landslides: investigation and mitigation. *National Academic Press*.
- Tzukamoto Y. and H. Minematsu (1987) – Hydrogeomorphological characteristics of a zero-order basin. *In proceeding, Symposium on Erosion and Sedimentation in the Pacific Rim. IAHS Publ. 165*, pp 61-70.

- Unesco (1972) - Annual Summary of Information Natural Disaster, *UNESCO, Paris*
- Us Corps Of Engineers (1960) - The Unified Classification System. *Waterways Exp. Est.*
- USDA (1998) - Keys to Soil Taxonomy. *USDA-Nat, Res. Cons. Service, 8th ed., 328.*
- Van Genuchten M. T. (1980) - A closed form equation for predicting the hydraulic conductivity of unsaturated soils. *Soil Science Society of America Journal, 44, pp. 892-898.*
- Van Genuchten, M. T., F.J. Leij and S.R. Jates (1991) - The Retc code for quantifying the hydraulic functions of unsaturated soils. *U.S. Department of Agriculture, Agricultural Research Service, Report IAG-DW12933934, Riverside, CA.*
- Van Wazer J.R., J.W. Lykons, K.Y. Kim and R.E. Colwell (1963) – Viscosity and flow measurement. *New York, Interscience, 405 pp.*
- Varnes D.J. (1978) – Slope movement Types and Processes. *In Special report 176: Landslides: Analysis and Control (R.L. Shuster and R.J.nKrizek, eds.), TRB, National Research Council, Washington, D.C., pp. 11-33.*
- Wang G. and Sassa K. (2001) – Factors affecting rainfall induced landslides in laboratory flume tests. *Géotechnique, 51, pp. 587-600.*
- Wang X. and C. H. Benson (2004) - Leak-Free Pressure Plate Extractor For Measuring the Soil Water Characteristic Curve. *Geotechnical Testing Journal, Vol. 27, 2, pp. 1-9.*
- Whitman, R. V., And W. A. Bailey (1967) - Use of Computers for Slope Stability Analysis. *Journal of the Soil Mechanics and Foundations Division, ASCE, Vol. 93, N° SM4, pp 475-498.*
- Wieczorek F. (1996) - Landslide types and processes. *In: Turner, A.R., Schuster, R.L. (Eds.), Landslides: Investigation and Mitigation, Sp. Rep. 247. Transportation Research Board, National Research Council, National Academy Press, Washington, DC, pp 76-90.*
- Wilson R.C and G. F. Wiezoreck (1995) - Rainfall thresholds for the initiation of debris flows at La Honda, California. *Env. & Eng. Geoscience, 1 (1), pp. 11-27.*
- WP/WLI 1990 – A Suggested Method for Reporting a Landslide. *Bulletin of the International Association of Engineering Geology, 41, pp. 5-12.*
- WP/WLI 1991 – A Suggested Method for a Landslide Summary. *Bulletin of the International Association of Engineering Geology, 43, pp. 101-110*
- WP/WLI (1993a) - A Suggested Method for Describing the activity of a Landslide. *Bulletin of the International Association of Engineering Geology, 47, pp. 53-57.*
- WP/WLI (1993b) – Multilingual landslide Glossary. *Bi-Tech Publisher, Richmond, British Columbia, Canada, 59 pp.*
- .Wroth C.P. and D.M. Wood (1978) - The Correlation of Index Properties with Some Basic Engineering Properties of Soils. *Canadian Geotechnical Journal, 15 (2), pp. 137-145.*
- Zangar (1952) –Theory and problems of water percolation. *Engineering Monogr. N° 8, Bureau Reclamation, U.S. Dep. Of Interior, Denver, Co.*
- Zilberbrand M. (2003) - Degassing Water Around Air Bubbles Entrapped in the Vadose Zone as a Mechanism of Carbonate Precipitation—A Hypothesis. *Journal of Sedimentary Research; July 2003; v. 73; no. 4; p. 491-497*